marine drugs

Marine Carbohydrate-Based Compounds with Medicinal Properties

Edited by

Irina M. Yermak and Viktoria Davydova

MDPI

Marine Carbohydrate-Based Compounds with Medicinal Properties

Marine Carbohydrate-Based Compounds with Medicinal Properties

Editors

Irina M. Yermak
Viktoria Davydova

MDPI

Editors
Irina M. Yermak
Far Eastern Branch,
Russian Academy of Sciences
Russia

Viktoria Davydova
Far Eastern Branch,
Russian Academy of Sciences
Russia

This is a reprint of articles from the Special Issue published online in the open access journal *Marine Drugs* (ISSN 1660-3397) (available at: https://www.mdpi.com/journal/marinedrugs/special_issues/Carbohydrate-Based_Medicinal).

For citation purposes, cite each article independently as indicated on the article page online and as indicated below:

LastName, A.A.; LastName, B.B.; LastName, C.C. Article Title. *Journal Name* **Year**, *Volume Number*, Page Range.

Contents

About the Editors

Irina M. Yermak

received her Dr. Sc. in chemistry. She is Principal scientist of G.B. Elykov Pacific Institute of Bioorganic Chemistry of the Russian Academy of Science. She worked in The Republic of Korea, in France, and in China as a visiting scientist. She has published more than 150 articles in reputable journals, has five patents and has written five book chapters. For the last 5 years, she has been the head of five projects, and under her leadership, eight researchers have received their Ph. Ds. She is an Expert of the Russian Science Foundation.

Viktoria Davydova

received her Ph. D at the Pacific Institute of Bioorganic Chemistry; specialization—bioorganic chemistry, chemistry of natural and biological active substances. Since 2013, Viktoriya Davydova has been a head of the Laboratory of Molecular Basis of Antibacterial Immunity in the Pacific Institute of Bioorganic Chemistry. The fields of her scientific interest are associated with the study of natural polysaccharides and their complexes, including complexes with endotoxins of Gram-negative bacteria, and physicochemical and biological properties of polyelectrolyte polysaccharide complexes.

Editorial

Current Trend of Marine Carbohydrate-Containing Compounds with Medicinal Properties

Irina M. Yermak * and Viktoria N. Davydova *

G.B. Elyakov Pacific Institute of Bioorganic Chemistry, Far Eastern Branch, Russian Academy of Sciences, 100 Let Vladivostoku Prosp., 159, 690022 Vladivostok, Russia

* Correspondence: imyer@mail.ru (I.M.Y.); vikdavidova@yandex.ru (V.N.D.)

Carbohydrates are most abundant biomolecules on Earth and, also, the most complex biomolecules in terms of structure. Marine carbohydrate-containing substances obtained from marine sources such as algae, microbes, and animals are usually biodegradable and biocompatible and exhibit biological properties that contribute to the discovery of a wide range of new bioactive substances with special pharmacological properties of interest to medicine. Carbohydrate-based compounds include glycans, glycoproteins, proteoglycans, glycolipids, and low-molecular and complex glycosides of differential origins. Marine glycans are remarkable molecules, playing a determinant role in biological processes. All cells, including human cells, have carbohydrates on their surfaces, known as the glycocalyx. The glycocalyx is a useful target for personalized medicine, including finding new biomarkers for diseases such as cancer and for patient stratification in clinical trials. The functional studies of carbohydrates concern molecular recognition such as carbohydrate–lectin or glycoside–enzyme interactions, cell recognition (normal and pathological), viral adhesion/penetration, and many other phenomena. Carbohydrate recognition plays a vital role in the activation and function of the immune system. The production and applications of marine carbohydrates as therapeutic agents are increasingly important topics of intensive research. A modern study of carbohydrates includes the development of glycotechnologies in the field of diagnosis and therapy of diseases and nutrients. The interest in the study of marine polysaccharides with therapeutic purposes relies on the possibility of developing novel approaches of less invasive and more personalized treatments. Many of these polysaccharides allow loading lower drug dosages, which may lead to a drastic reduction of the side effects caused by the drugs. The use of marine polysaccharides in the systems of drug delivery in tissue engineering and regenerative medicine is rapidly developing due to the numerous functional groups in their molecules, strong water absorption, favorable physicochemical properties, safety, low cost, wide distribution in nature, and biological activity. In addition, the structure of polysaccharides can be relatively easily modified in order to synthesize derivatives with desirable characteristics for drug delivery. Carbohydrate complexes are well-tolerated macroorganism systems and can be used in various fields, such as drug delivery systems; matrices for cell cultivation and enzyme immobilization; and materials for the reconstruction of bone, cartilage, cardiac, and dental tissues.

The Special Issue "Marine Carbohydrate-Based Compounds with Medicinal Properties" of the open access journal *Marine Drugs* (ISSN 1660-3397) ran from February 2020 to January 2021. In total, it consisted of 12 articles devoted to various aspects of marine carbohydrate-containing substances and the recent experimental studies carried out on their basis. In this Special Issue, we discussed the biological aspects and structural features of the various carbohydrate-based compounds of marine origin endowed with potential biomedical and biotechnological applications. The isolation of marine biologically active carbohydrate compounds and relevant studies on their structures and properties are important for the adding knowledge about molecular diversity in nature and the creation of medicines and other useful products.

Marine polysaccharides and their derivatives as soluble substances have promising prospects for medical use. Many microorganisms, including marine bacteria, secrete extracellular polysaccharides called exopolysaccharides (EPSs). EPSs have a lot of promise in cell therapy and tissue engineering. In the Special Issue, two articles were devoted to the study of EPSs isolated from marine bacteria. Since their natural tropism in targeting malignant tumors and their metastasis, EPSs have been recently considered as a vector to be combined with theranostic radionuclide pairs [1]. Antimetastatic properties in both murine and human osteosarcoma cell lines (POS-1 and KHOS) were evidenced by using exopolysaccharide derivatives, produced by the *Alteromonas infernus* bacterium [2]. Muñoz-Garcia et al. developed a strategy for further use as a therapeutic vector of EPS derivatives. First, the authors had to make sure that EPS might keep the ability of targeting cancer cells even when complexed with scandium (Sc). For this reason, in vitro studies concerning both the cell proliferation and cell viability of various tumor cell lines were realized. The cell index of human osteosarcoma (MNNG/HOS), human melanoma (A375), human lung cancer (A549), human glioblastoma (U251), and human breast cancer (MDA231) were monitored over a week using XCELLigence® technology. The tested complexes exhibited an antiproliferative effect; this effect was more effective compared to EPS alone. This increase of the antiproliferative properties was explained by a change in conformation of the EPS complexes due to their polyelectrolyte nature that was induced by complexation. The results, obtained by the authors, are very promising and reveal that EPS can be coupled to scandium for improving its biological effects and, also, suggest that no major structural modification occurs on the ligand [2].

The work of Gargouch et al. [3] demonstrated the biological activity of different molar mass exopolysaccharides (EPS) from *Porphyridium marinum* and its oligomers prepared by a high-pressure homogenizer. The analyses of the polymer compositions and viscosity measurements were conducted on all samples in order to propose hypotheses involving the activities caused by the intrinsic properties of the polymers. All EPS samples were tested for different biological activities, i.e., antibacterial, antifungal, and antibiofilm activities on *Candida albicans*, as well as for their effects on the viability of murine breast cancer cells. The results of these researchers showed the ability of EPS to suppress the proliferation of Gram (+) and Gram (−) bacteria, as well as the formation of a biofilm of *Candida albicans* in low concentrations. However, low molar masses were found to be more effective for antiproliferative activity against breast cancer cells. Depending on the biological activity tested, this study also disclosed that these biological activities could be due to their molar masses and their viscosity, as well as their composition (probably their content in sulfate and uronic acids). Thus, this study provided strong arguments to consider EPS from *P. marinum* as a natural source of antibacterial, antibiofilm, and anticancer products that are useful in pharmaceutical formulations and food industries as a natural preservative. Nevertheless, this study constituted a first step to evaluate the potential of EPS from *P. marinum* in a drug development approach.

Despite the numerous polysaccharide structures elucidated, the diversity of EPS seems largely underestimated, and the tools to predict their structures are still absent. The article by Drouillard et al. [4] concerned the structural elucidation of the polysaccharide secreted by *Vibrio alginolyticus* CNCM I-5035. *Vibrio alginolyticus* secretes an exopolysaccharide used as ingredient in the cosmetic industry under the trademark Epidermist. It is appreciated for its ability to improve the physical and chemical barrier functions of the skin by notably increasing the keratinocyte differentiation and epidermal renewal. Analyses of the native and alkali-treated polysaccharides, as well as the detailed characterization of purified di- and trisaccharides, demonstrated that the polysaccharide was composed of a repetition unit of three residues: D-galactose (D-Gal), D-*N*-acetylglucosamine (GlcNAc), and L-*N*-acetylguluronic acid, of which 30% (*m/m*) was acetylated in position 3. The complete structure of the polysaccharide was resolved giving the repetition unit: (→3)-α-D-Gal-(1→4)-α-L-GulNAcA/α-L-3OAc-GulNAcA-(1→4)-β-D-GlcNAc-(1→). This repetition unit was very similar to that found in the lipopolysaccharide extracted

from *Pseudoalteromonas nigrifaciens* KMM161 [5]. The structure of the polysaccharide investigated by Drouillard et al. was the third exopolysaccharide structure secreted by a *V. alginolyticus* strain [6]. The composition of the repetition unit determined, as well as the sequence of residues, had no similarities, suggesting that the biosynthetic pathways of these polysaccharides probably have no common ancestor. The structural diversity found in the *V. alginolyticus* strains was also true for all the strains of the *Vibrio* genus. The Carbohydrate Structure Database [7] has entries describing polysaccharides—including secreted polysaccharides or lipopolysaccharides—of the genus *Vibrio*. The structural diversity of the polysaccharides suggests a very high plasticity of the polysaccharide biosynthesis pathway of the strains belonging to the genus *Vibrio*.

Due to of their substantial diversity and rich composition of biologically active compounds, algae are of considerable interest to the pharmaceutical industries and medicine. The structures and biological activities of polysaccharides from brown, red, and green algae were discussed in several papers of the Special Issue. The structure and immunostimulatory effect of two sulfated and pyruvate galactans from green alga *Caulerpa cupressoides* var. *flabellata* were studied by Barboza et al. [8]. According to NMR spectroscopy, both galactans were composed primarily of 3)-β-D-Galp-(1→3) units. Pyruvate groups were also found, forming five-membered cyclic ketals as 4,6-*O*-(1′carboxy)-ethylidene-β-D-Galp residues. Some galactose residues were sulfated at C-2. One of these sulfated polysaccharides (SP) had some galactose units sulfated at C-4. An analysis of the effects of these SP on the macrophages resulted in the production of nitrogen oxide (NO), reactive oxygen species(ROS) and proinflamatory cytokines, which indicated that sulfation at the C-4 position is not essential for the immunomodulatory activity of these galactans. The immunostimulating activity of *C. cupressoides* galactans showed their practical potential in the development of new biomedical products.

A protective effect on colitis in mice induced by dextran sulfate sodium (DSS) of the sulfate *Ulva* polysaccharide with low molecular weight (LMW-ulvan), prepared using the enzymatic method, was studied by Li et al. [9]. MW-ulvan had a molecular weight of 2.56 kDa and contained (1→3,4)-linked Rha, (1→4)-linked Xyl, and (1→4)-linked GlcA, with small amounts of (1→4)-linked Rha residues; the sulfate substitution was at the C-3 of Rha. MW-ulvan reduced the inflammatory infiltration and damage, which can be attributed to the enhancement of the antioxidant defense system in mice. It was also suggested that the improvement of LMW-ulvan in DSS-induced colitis might be closely related to its protective effect on the intestinal mucosal barrier by increasing the expression of tight junction proteins. Thus, LMW-ulvan could further inhibit the abnormal immune response in the intestinal mucosa, thus ameliorating the mucosal barrier function and intestinal mucosal permeability. These results indicated that LMW-ulvan may be a promising application for inflammatory bowel disease.

The work of Vigors et al. [10] was devoted to the study of the effect of an algal polysaccharide extract that was used in the diet of pigs on the productivity of animals—in particular, the immune and microbial profile of their gastrointestinal tract. The authors used algae extracts to improve the performance and digestive health in postweaning pigs. The weaning process is a stressful event in the animal's life, characterized by intestinal and immune dysfunctions that result in impaired feed intake, health, and growth. Previously, this group of authors showed that feeding extracts such as laminarin (LAM) and fucoidan in the immediate postweaning period inhibit multiple beneficial physiological adaptations in the gastrointestinal tract that can improve pig performance during this difficult time [11]. In this regard, the authors continued their work and studied the effects of feeding with seaweed extracts enriched with laminarin (LAM) and fucoidan (FUC) on the performance indicators of the animals, gut microbiological profile, and transcriptome profiles up to 35 days after weaning. While neither extract had beneficial effects on the animal performance, the LAM supplementation had a positive influence on the intestinal health through alterations in the gastrointestinal microbiome and increased butyrate production.

The brown algae also synthesized alginates that are widely used in the food and pharmaceutical industries. Alginate oligosaccharide (AOS) is an oligomer of alginate, which has the characteristics of low relative molecular weight, good solubility, high safety, and high stability. The alginate lyase has unique advantages in the preparation of alginate oligosaccharides and processing of brown algae. Alginate lysis is adopted to catalytically degrade alginate into AOS by β-elimination under relatively mild and controllable conditions. The gene Alg2951, encoding a PL7 family alginate lyase with exo/endo-type activity, was cloned from a novel marine bacterium *Alteromonas portus* HB161718T and then expressed in *Escherichia coli* by Huang et al. [12]. The recombinant Alg2951 in the culture supernatant reached an activity of 63.6 U/mL, with a molecular weight of approximately 60 kDa. The results showed that Alg2951 was a cold-adapted PL7 alginate lyase with a significant preference toward polyG. Moreover, Alg2951 was shown to be a NaCl- and KCl-activated enzyme with exolytic and endolytic activity. Meanwhile, it specifically degraded polyG and sodium alginate but had almost no activity on polyM. The authors suggested that Alg2951 could catalyze the hydrolysis of sodium alginate to produce monosaccharides and trisaccharides. The enzymatic hydrolysates displayed good antioxidant activity by assays of the scavenging abilities towards radicals (hydroxyl and ABTS+) and the reducing power. Due to its cold-adapted and dual exo/endo-type properties, Alg2951 can be a potential enzymatic tool for industrial production.

The ability to synthesise acid polysaccharides as carrageenans (CRGs) and agar is a most interesting property of red seaweeds. Intensive studies have shown that CRGs can be regarded not only as foodstuff ingredients but, also, as drugs because of a wide spectrum of biological and physiological activities [13]. The inhibitory effects of carrageenans (CRGs) on lipopolysaccharides (LPS) induced inflammation in a mouse model of endotoxemia and, in the complex therapy of patients with enteric infections of *Salmonella* etiology, were appreciated by Yermak et al. [14]. CRGs were able to increase the synthesis of anti-inflammatory interleukin 10 (IL-10) in vitro, and, at low concentrations, their activity in the mixture with LPS was higher. The protective effect of different structural types of CRGs against *Escherichia coli* LPS was studied in vivo by monitoring the biochemical and pathomorphological parameters that respond most adequately to any acting stressor, including bacterial endotoxin. Less-sulfated κ- and κ/β-CRGs and the food supplement "Carrageenan-FE" increased the nonspecific resistance of mice to *E. coli* LPS at the expense of the inhibition of the processes of thymus involution, adrenals hypertrophy, thyroid atrophy, hypercorticoidism, glycogenolysis, and lactate acidosis. The authors suggested that the nonspecific resistance of the organism to *E. coli* LPS induced by CRG may be due to both the immunomodulatory effect of CRGs and their influence on the macromolecular structure of LPS. Additionally, in the current study, the estimation of the therapeutic action of "Carrageenan-FE" in a complex therapy of patients with enteric infections of *Salmonella* etiology was evaluated. "Carrageenan-FE" restored the system of hemostasis and corrected some biochemical indicators and parameters in the immune systems of the patients. These results allow to hope for a practical application of CRGs for lowering the endotoxemia level in patients under the development of the infectious process caused by Gram-negative bacteria.

One of the well-known polysaccharides is chitosan. In this Special Issue, the medico-biological properties of chitosan and its derivatives were discussed in three articles. The mechanism of healing of burn wounds under the action of a chitosan (CS) hydrogel containing gentamicin (GT) was systematically explored by Yan et al. [15]. The wound dressing based on the chitosan–gentamicin conjugate had antibacterial properties and good cytocompatibility and hemocompatibility. The wound healing experiment showed a synergic effect between CS and GT and the highest recovery rates in the late phase of trauma healing. The animals in the CS–GT group had the thickest dermis, dense dermal mesenchyme, and spindle-shaped fibroblasts, indicating optimal tissue repair. A further analysis showed that the CS–GT hydrogel promoted the synthesis of total proteins in the

granulation tissue of the skin, led to the facilitation of collagen fibrogenesis, decreased the expression of inflammatory cytokines, and, ultimately, accelerated wound healing.

Lan et al. [16] evaluated the effects of the dietary supplementation of chitosan oligosaccharides (COS) on the intestinal integrity, oxidative status, and the inflammation response with a hydrogen peroxide (H_2O_2) challenge. A dietary COS supplementation decreased the duodenum and ileum mucosal IL-6 level and jejunum mucosal tumour necrosis factor-α (TNF-α) level, inhibited the expression of IL-6 in the jejunum and ileum and TNF-α in the jejunum and ileum, and increased the duodenum and ileum mucosal IL-10 levels. The results of this research group suggested that COS can maintain the integrity of the intestine during oxidative stress by modulating the oxidative status of the bowel and release of inflammatory cytokines. These results suggested that COS could maintain the intestinal integrity under oxidative stress by modulating the intestinal oxidative status and release of inflammatory cytokines. Dietary COS supplementation may be an effective nutritional strategy to alleviate the detrimental effects of oxidative stress.

Complexes on the basis of carbohydrates are often prepared to improve their functional properties. This approach allows easily adapting complex characteristics for specific medical applications. The immunotropic activity of polyelectrolyte complexes (PEC) of chitosan with polysaccharides of red seaweed–κ-carrageenan (κ-CRG) of various compositions was assessed in comparison with the initial polysaccharides in comparable doses [17]. The highest activity of CS and κ-CRG, as well as their soluble PEC, was observed in a histamine-induced exudative inflammation directly related to the activation of phagocytic cells, i.e., macrophages and neutrophils. The ability of PEC to scavenge NO depends on the content of the κ-CRG in the PEC. The ability of the PEC to induce the synthesis of proinflammatory (TNF-α) and anti-inflammatory (IL-10) cytokines in peripheral blood mononuclear cells was determined by the activity of the initial κ-CRG, regardless of their composition.

Glyceroglycolipids are widely distributed in plants, microalgae, and cyanobacteria and present bioactivities and pharmacological activities and can be widely used in the pharmaceutical industry. A study by Xu and Miao [18] provided further insights into the glyceroglycolipid metabolism, as well as the scientific basis for glyceroglycolipid synthesis optimization and cyanobacteria glyceroglycolipids utilization via metabolic engineering. The authors showed that there are 12 differentially expressed transcriptional regulators that could be potential candidates related to glyceroglycolipid regulation, according to a transcriptome analysis. The transcriptome analysis also suggested post-transcriptional or post-translational regulations in glyceroglycolipid synthesis.

Thus, this Special Issue covered a series of experimental studies recently carried out in the field of marine carbohydrate-containing compounds. In their publications, scientists from Ireland, Russia, France, China, the Republic of Korea, and Brazil discussed new results obtained from the isolation and study of marine polysaccharides and their derivatives and complexes. The wide spectrum of biological activities of these compounds, such as immunomodulatory, antibacterial, anticancer, anti-inflammatory, antibiofilm, and antioxidant, obtained in experiments in vitro and in vivo showed the prospects for their practical use in medicine (their practical potential in the development of new biomedical products).

As guest editors, we are thankful to all the scientists from the diverse research institutes and universities who contributed to the success of the Special Issue "Marine Carbohydrate-Based Compounds with Medicinal Properties".

References

1. Heymann, D.; Ruiz-Velasco, C.; Chesneau, J.; Ratiskol, J.; Sinquin, C.; Colliec-Jouault, S. Anti-Metastatic Properties of a Marine Bacterial Exopolysaccharide-Based Derivative Designed to Mimic Glycosaminoglycans. *Molecules* **2016**, *21*, 309. [CrossRef] [PubMed]
2. Muñoz-Garcia, J.; Mazza, M.; Alliot, C.; Sinquin, C.; Colliec-Jouault, S.; Heymann, D.; Huclier-Markai, S. Antiproliferative Properties of Scandium Exopolysaccharide Complexes on Several Cancer Cell Lines. *Mar. Drugs* **2021**, *19*, 174. [CrossRef] [PubMed]
3. Gargouch, N.; Elleuch, F.; Karkouch, I.; Tabbene, O.; Pichon, C.; Gardarin, C.; Rihouey, C.; Picton, L.; Abdelkafi, S.; Fendri, I.; et al. Potential of Exopolysaccharide from *Porphyridium marinum* to Contend with Bacterial Proliferation, Biofilm Formation, and Breast Cancer. *Mar. Drugs* **2021**, *19*, 66. [CrossRef] [PubMed]
4. Drouillard, S.; Chambon, R.; Jeacomine, I.; Buon, L.; Boisset, C.; Courtois, A.; Thollas, B.; Morvan, P.Y.; Vallée, R.; Helbert, W. Structure of the Polysaccharide Secreted by *Vibrio alginolyticus* CNCM I-5035 (Epidermist 4.0TM). *Mar. Drugs* **2020**, *18*, 509. [CrossRef] [PubMed]
5. Gorshkova, R.P.; Nazarenko, E.L.; Zubkov, V.A.; Ivanova, E.P.; Gorshkova, N.M.; Isakov, V.V. Structure of O-Specific Polysaccharide from *Pseudoalteromonas nigrifaciens* Strain KMM 161. *Biokhimiya* **2002**, *67*, 810–814.
6. Drouillard, S.; Jeacomine, I.; Buon, L.; Boisset, C.; Courtois, A.; Thollas, B.; Morvan, P.Y.; Vallée, R.; Helbert, W. Structure of the Exopolysaccharide Secreted by a Marine Strain *Vibrio alginolyticus*. *Mar. Drugs* **2018**, *16*, 164. [CrossRef] [PubMed]
7. Toukach, P.V.; Egorova, K.S. Carbohydrate Structure Database Merged from Bacterial, Archaeal, Plant and Fungal Parts. *Nucleic Acids Res.* **2016**, *44*, D1229–D1236. [CrossRef] [PubMed]
8. Barbosa, J.; Sabry, D.A.; Silva, C.H.F.; Gomes, D.L.; Santana-Filho, A.P.; Sassaki, G.L.; Rocha, H.A.O. Immunostimulatory Effect of Sulfated Galactans from the Green Seaweed *Caulerpa cupressoides* var. flabellata. *Mar. Drugs* **2020**, *18*, 234. [CrossRef] [PubMed]
9. Li, Y.; Ye, H.; Wang, T.; Wang, P.; Liu, R.; Li, Y.; Tian, Y.; Zhang, J. Characterization of Low Molecular Weight Sulfate *Ulva* Polysaccharide and its Protective Effect Against IBD in Mice. *Mar. Drugs* **2020**, *18*, 499. [CrossRef] [PubMed]
10. Vigors, S.; O'Doherty, J.; Rattigan, R.; Sweeney, T. Effect of Supplementing Seaweed Extracts to Pigs until d35 Post-Weaning on Performance and Aspects of Intestinal Health. *Mar. Drugs* **2021**, *19*, 183. [CrossRef] [PubMed]
11. Rattigan, R.; Sweeney, T.; Vigors, S.; Thornton, K.; Rajauria, G.; O'Doherty, J.V. The Effect of Increasing Inclusion Levels of a Fucoidan-Rich Extract Derived from *Ascophyllum nodosum* on Growth Performance and Aspects of Intestinal Health of Pigs Post-Weaning. *Mar. Drugs* **2019**, *17*, 680. [CrossRef] [PubMed]
12. Huang, H.; Li, S.; Bao, S.; Mo, K.; Sun, D.; Hu, Y. Expression and Characterization of a Cold-Adapted Alginate Lyase with Exo/Endo-Type Activity from a Novel Marine Bacterium *Alteromonas portus* HB161718T. *Mar. Drugs* **2021**, *19*, 155. [CrossRef] [PubMed]
13. Pereira, L. Biological and Therapeutic Properties of the Seaweed Polysaccharides. *Int. Biol. Rev.* **2018**, *2*. [CrossRef]
14. Yermak, I.M.; Volod'ko, A.V.; Khasina, E.I.; Davydova, V.N.; Chusovitin, E.A.; Goroshko, D.L.; Kravchenko, A.O.; Solov'eva, T.F.; Maleev, V.V. Inhibitory Effects of Carrageenans on Endotoxin-Induced Inflammation. *Mar. Drugs* **2020**, *18*, 248. [CrossRef] [PubMed]
15. Yan, T.; Kong, S.; Ouyang, Q.; Li, C.; Hou, T.; Chen, Y.; Li, S. Chitosan-Gentamicin Conjugate Hydrogel Promoting Skin Scald Repair. *Mar. Drugs* **2020**, *18*, 233. [CrossRef] [PubMed]
16. Lan, R.; Chang, Q.; Wei, L.; Zhao, Z. The Protect Effects of Chitosan Oligosaccharides on Intestinal Integrity by Regulating Oxidative Status and Inflammation under Oxidative Stress. *Mar. Drugs* **2021**, *19*, 57. [CrossRef]
17. Davydova, V.N.; Sorokina, I.V.; Volod'ko, A.V.; Sokolova, E.V.; Borisova, M.S.; Yermak, I.M. The Comparative Immunotropic Activity of Carrageenan, Chitosan and their Complexes. *Mar. Drugs* **2020**, *18*, 458. [CrossRef] [PubMed]
18. Xu, X.; Miao, X. Glyceroglycolipid Metabolism Regulations under Phosphate Starvation Revealed by Transcriptome Analysis in *Synechococcus elongatus* PCC 7942. *Mar. Drugs* **2020**, *18*, 360. [CrossRef] [PubMed]

Article

Effect of Supplementing Seaweed Extracts to Pigs until d35 Post-Weaning on Performance and Aspects of Intestinal Health

Stafford Vigors [1], John O'Doherty [1,*], Ruth Rattigan [1] and Torres Sweeney [2]

[1] School of Agriculture and Food Science, University College Dublin, Belfield, Dublin 4, Ireland; staffordvigors1@ucd.ie (S.V.); ruth.rattigan@ucdconnect.ie (R.R.)
[2] School of Veterinary Medicine, University College Dublin, Belfield, Dublin 4, Ireland; torres.sweeney@ucd.ie
[*] Correspondence: john.vodoherty@ucd.ie; Tel.: +3531-716-7128

Abstract: The objective of this study was to examine the effects of feeding laminarin (LAM) and fucoidan (FUC) enriched seaweed extracts up to d35 post-weaning on measures of animal performance, intestinal microbial and transcriptome profiles. 75 pigs were assigned to one of three groups: (1) basal diet; (2) basal diet + 250 ppm fucoidan; (3) basal diet + 300 ppm laminarin with 7 replicates per treatment group. Measures of performance were collected weekly and animals sacrificed on d35 post-weaning for the sampling of gastrointestinal tissue and digesta. Animal performance was similar between the basal group and the groups supplemented with FUC and LAM ($P > 0.05$). Pigs fed the basal diet had higher alpha diversity compared to both the LAM and FUC supplemented pigs ($P < 0.05$). Supplementation with LAM and FUC increased the production of butyric acid compared to basal fed pigs ($P < 0.05$). At genus level pigs fed the LAM supplemented diet had the greatest abundance of *Faecalbacterium*, *Roseburia* and the lowest *Campylobacter* of the three experimental treatments ($P < 0.05$). While neither extract had beneficial effects on animal performance, LAM supplementation had a positive influence on intestinal health through alterations in the gastrointestinal microbiome and increased butyrate production.

Keywords: laminarin; fucoidan; gastrointestinal tract; microbiome; transcriptome; swine; post-weaning; antibiotic alternatives

1. Introduction

The weaning process is a stressful event in the pig's life, characterized by intestinal and immune dysfunctions that result in impaired feed intake, health and growth [1]. The post-weaning growth check is characterized by an increased proliferation of pathogenic bacteria, in particular β-hemolytic enterotoxigenic *E. coli* serotypes, causing post-weaning diarrhea [2]. Antibiotic growth promoters are an effective means to reduce pathogenic bacteria such as *E. coli* and enhance growth rates in the immediate post-weaning period. However, the use of antibiotics as growth promoters was banned in the EU in 2006 (EC regulation no. 1831/2003). Since the ban on antibiotics, pharmacological doses of zinc oxide (ZnO) are used to reduce the incidence of diarrhea and improve performance in the post-weaning period. However, mounting concerns over the accumulation of ZnO in soils and a link between ZnO usage and antibiotic resistance have meant a phasing out of its usage by 2022 (Regulation (EU) 2019/61 on Veterinary Medicines and Regulation (EU) 2019/4 on Medicated Feed). This legislation also adds further restrictions to the use of antibiotics for prophylaxis or metaphylaxis. Therefore, there has been a focus on finding more natural means to improve performance and digestive health in pigs during the post-weaning period.

This search for natural alternatives has focused on a wide variety of substances such as organic acids, yeast derivatives, glucans, mannans, herbs and spices amongst many others [3]. One alternative that has been explored is the use of seaweed extracts such as laminarin (LAM) and fucoidan (FUC) as an alternative to antibiotics and ZnO [4]. The

7

extract LAM is a β-glucan composed of β-1-3-D-glucan with β-1-6 branch chains that vary with species in distribution and length, while FUC represents a class of fucose-enriched sulfated polysaccharides extracted from the extracellular matrix of brown algae, with L-fucose 4-sulfate as the major component [4].

The feeding of seaweed extracts, such as laminarin and fucoidan, in the immediate post-weaning period illicits multiple beneficial physiological adaptions in the gastrointestinal tract, that can improve pig performance during this challenging time. A number of studies have examined the effects of feeding laminarin and fucoidan for 14 days post-weaning [5–7]. In the study of Rattigan et al. [5], pigs were offered 3 levels of a laminarin rich extract to identify the most appropriate inclusion level. The 300 ppm laminarin supplemented group exhibited the greatest beneficial effects with improvements in animal performance with accompanying positive alterations in small intestinal morphology, microbial populations and gene expression profiles. Based on these positive findings, a more detailed analysis of the microbiome was conducted by Vigors et al. [7], where increased abundance of *Prevotella* and reductions in the family *Enterobacteriaceae* were reported in the laminarin supplemented group. In addition, while pigs supplemented with 250 ppm fucoidan did not see any improvement in performance, they had improved faecal scores and increased concentrations of total volatile fatty acids in the colon but had alterations in gene expression and microbial profiles which potentially could have negative connotations for animal health in the longer term [8]. Hence, in this experiment, the feeding of the experimental diets was continued past d14 until d35 to assess the longer-term effects on animal performance and intestinal health. This strategy will establish whether the feeding of LAM continues to be beneficial until d35 or beneficial effects are limited to the immediate post-weaning period. Therefore, the objective of this research was to examine the effects of feeding seaweed extracts (SWE) up to d35 post-weaning on animal performance with a focus on immune and microbial profiles in the gastrointestinal tract.

2. Results

2.1. Characterization of Seaweed Extracts

The LAM extract was obtained from *Laminaria Digitata* and contained 653.2 g of laminarin per kg DM, 190 g/kg fucoidan per kg DM, 5 g/kg phlorotannin per kg DM, 51 g/kg mannitol per kg DM, 40 g/kg alginates per kg DM (Table 1).

Table 1. Biochemical composition of the extracts obtained following extraction and purification.

Component	LAM	FUC
Laminarin	653.2	25.9
Fucoidan	190	441
Phlorotannin	5	135
Mannitol	51	43.8
Alginates	40	34.8

(g/kg dry weight extract)

The FUC rich extract was obtained from *Ascophyllum nodosum* and contained 441 g of fucoidan per kg DM, 25.9 g laminarin/kg DM, 135g alginates/kg DM, 43.8 g mannitol/kg DM, 34.8 g phlorotannin's/kg DM.

2.2. Animal Performance

The average body weights of the pigs on the SWE diets were the same as the control group at the end of the experimental period ($P > 0.05$; Table 2). While no significant effects of dietary supplementation with either LAM or FUC were identified for measures of ADFI or ADG compared to the control group ($P > 0.05$), pigs fed the FUC supplemented diet had lower G:F ratio compared to the control ($P < 0.05$; Table 2).

Table 2. The effect of supplementation with either laminarin or fucoidan on animal performance.

	Basal	**FUC250**	**Lam300**	**SEM**	**P Value**
Weight d0	8.42	8.38	8.36	0.10	0.877
Weight d14	10.95	11.17	11.19	0.49	0.931
Weight d35	23.46	21.72	22.60	0.96	0.454
ADFI *	0.91	0.94	0.88	0.04	0.537
ADG	0.60	0.50	0.54	0.03	0.071
G:F	0.67 [a]	0.54 [b]	0.63 [ab]	0.04	0.045

*ADFI: average daily feed intake; ADG: average daily gain; G:F: gain to feed ratio; [a,b] values with different superscripts differ significantly ($P < 0.05$); A total of seven replicates were used per treatment group (replicate = pen, 3/pigs/pen).

2.3. Volatile Fatty Acids

Pigs on the LAM diet had the highest concentrations of total volatile fatty acid (VFA) and butyrate compared to the FUC supplemented group and the basal group ($P < 0.05$; Table 3).

Table 3. The effect of supplementation with either laminarin or fucoidan on volatile fatty acids (VFAs) produced in colonic digesta on d35 post-weaning.

	Basal	**FUC250**	**Lam300**	**SEM**	**P Value**
VFA (mmol/l digesta)					
Total	154.76 [ab]	149.89 [a]	172.45 [b]	9.19	0.041
Acetate	119.75	109.64	127.43	7.80	0.214
Propionate	26.20	26.87	27.68	2.82	0.919
Butyrate	7.36 [a]	11.83 [b]	15.52 [c]	1.54	0.003
Valerate	0.77	0.83	0.93	0.13	0.724
Isobutyrate	0.30	0.34	0.41	0.05	0.356
Isovalerate	0.38	0.39	0.50	0.08	0.479
Ace:Pro	4.97	4.26	4.95	0.61	0.666
Protein Derived SCFA	1.46	1.56	1.83	0.22	0.481

Ace:Pro: Acetate to propionate ratio, Seven replicates per treatment used; [a,b,c,] values with different superscripts differ significantly ($P < 0.05$); A total of seven replicates were used per treatment group (replicate = pig).

2.4. Differential Abundance Analysis of Bacterial Taxa in Colonic Digesta and Alpha Diversity Analysis

Next-generation sequencing of the 16S rRNA gene using the Illumina Miseq platform was conducted to examine the impact of feeding the experimental diets on the intestinal microbiome. This analysis assessed the impact on measures of diversity (Table 4) and differential abundance analysis that was conducted at the taxonomic levels of Phylum, Family and Genus. The analysis of all taxa is presented in the Supplementary Tables (S1–S3) while significant data are presented in Table 5.

Table 4. Effects of laminarin and fucoidan supplementation on measures of alpha diversity in colonic digesta.

	Basal	**FUC**	**LAM300**	**SEM**	**P Value**
Observed	179.00 [a]	158.71 [b]	158.14 [b]	4.51	0.016
Chao1	179.94 [a]	159.84 [b]	158.70 [b]	4.55	0.018
ACE	180.06 [a]	159.88 [b]	158.99 [b]	4.55	0.018
Shannon	4.49 [a]	4.07 [b]	4.29 [b]	0.05	0.047
Fisher	39.61 [a]	33.96 [b]	33.84 [b]	1.17	0.016
Simpson	0.98	0.96	0.97	0.01	0.095

[a,b] values with different superscripts differ significantly ($P < 0.05$); A total of seven replicates were used per treatment group (replicate = pig).

Table 5. Assessment of microbial composition in colonic digesta.

	Basal *	**FUC250**	**LAM300**	**SEM**	**Adj*P***
Phylum					
Bacteroidetes	65.76	55.59	60.23	3.01	0.140
Firmicutes	20.29 [a]	18.14 [a]	27.98 [b]	1.81	0.005
Proteobacteria	11.08 [a]	22.47 [b]	3.39 [c]	1.32	0.001
Spirochaetes	1.21 [a]	2.48 [a]	5.70 [b]	0.61	0.001
Family					
Ruminococcaceae	8.61 [a]	5.11 [b]	10.65 [a]	1.07	0.011
Campylobacteraceae	4.74 [a]	17.67 [b]	0.21 [c]	0.97	0.001
Spirochaetaceae	1.23 [a]	2.47 [a]	5.91 [b]	0.61	0.003
Genus					
Faecalibacterium	7.11 [a]	3.03 [b]	8.39 [a]	0.94	0.005
Alloprevotella	6.78 [a]	2.17 [b]	1.72 [b]	0.79	0.001
Campylobacter	4.75 [a]	17.72 [b]	0.21 [c]	0.97	0.001
Roseburia	4.26 [a]	6.01 [ab]	7.52 [b]	0.98	0.007
Treponema	1.23 [a]	2.47 [a]	5.89 [b]	0.61	0.001

[a,b,c] values with different superscripts differ significantly ($P < 0.05$); * A total of seven replicates were used per treatment group (replicate = pig).

Pigs fed the basal diet had the highest alpha diversity of the three experimental groups based on Observed, Chao1, ACE, Shannon and Fisher measures of alpha diversity ($P < 0.05$). The LAM and FUC supplemented pigs had similar levels of alpha diversity.

Phylum: Pigs on the LAM supplemented diets had increased abundance of Firmicutes and Spirochaetes compared to pigs fed the basal and FUC supplemented diets ($P < 0.05$). Pigs fed the FUC supplemented diet had the highest abundance of Proteobacteria compared to both the basal and LAM diets ($P < 0.05$) with pigs fed a LAM supplemented diet having lower abundance of Proteobacteria compared to the basal diet ($P < 0.05$).

Family: Pigs on the LAM supplemented diets had lower *Campylobacteraceae* and increased *Spirochaetaceae* compared to the other two groups ($P < 0.05$) and increased *Ruminococcaceae* compared to the FUC supplemented group ($P < 0.05$).

Genus: Pigs on the FUC supplemented diet had lower *Faecalbacterium* and higher *Campylobacter* compared to pigs on both the LAM and basal diets ($P < 0.05$). Pigs on the LAM supplemented diet had lower *Campylobacter* compared to the other two diets ($P < 0.05$). Pigs on the basal diet had increased *Alloprevotella* compared to pigs fed the SWE supplemented diets. LAM supplementation increased *Roseburia* compared to the pigs fed the control diet ($P < 0.05$), while also increasing *Treponema* compared to pigs fed both the basal and the pigs fed the diet supplemented with FUC ($P < 0.05$).

2.5. Differential Expression Analysis of Genes Related to Nutrient Absorption and the Intestinal Immune Response

The Nanostring nCounter technology was employed to examine the effect of LAM and FUC supplementation on the expression of genes related to intestinal health and functionality. The expression profile of 32 genes in the small intestine were measured, as described in the materials and methods. All gene expression data is presented in Supplementary Tables S4–S6 while significant data is presented in Table 6.

2.5.1. Differential Expression Analysis of Digestive Enzyme and Nutrient Transporter gene expression

Duodenum: FUC supplementation increased the expression of *SLC6A19* compared to LAM supplementation, while FUC supplementation increased the expression of *CNDP1* compared to both LAM supplementation and the basal group ($P < 0.05$). Pigs fed the basal diet had increased expression of *SLC16A10* compared to both LAM and FUC supplementation.

Jejunum: LAM supplementation increased the expression of *MCT1/SLC16A1* compared to FUC supplementation and the basal group ($P < 0.05$).

Table 6. Effect of laminarin or fucoidan inclusion on the gene expression of nutrient transporters and immune markers in the duodenum, jejunum and ileum.

	Basal	**FUC250**	**Lam300**	**SEM**	***P* Value**
	Nutrient transporters and digestive enzymes				
Duodenum					
SLC6A19	2557.15 [ab]	2839.39 [b]	1954.65 [a]	217.85	0.030
CNDP1	320.60 [a]	472.57 [b]	301.63 [a]	48.77	0.045
SLC16A10	568.63 [a]	418.27 [b]	443.36 [b]	41.29	0.042
Jejunum					
SLC16A1	1182.78 [a]	1587.81 [b]	1230.59 [a]	79.36	0.004
Ileum					
SLC2A2	2108.30 [a]	436.09 [b]	1438.96 [ab]	420.96	0.038
GCG	4530.86 [a]	1351.68 [b]	2844.24 [ab]	812.76	0.041
FABP2	21949.73 [a]	4078.26 [b]	12809.36 [ab]	4594.29	0.042
SLC5A1	16134.62 [a]	3930.36 [b]	9226.85 [ab]	3156.59	0.042
SI	46058.26 [a]	12573.66 [b]	25949.67 [ab]	8748.13	0.043
CNDP1	310.73 [a]	161.77 [b]	160.23 [b]	46.13	0.048
OCLN	2464.03 [a]	786.38 [b]	1782.07 [ab]	442.92	0.048
	Markers of immune response and intestinal integrity				
Jejunum					
CXCL8	1042.45 [a]	1815.05 [b]	1121.75 [a]	194.7	0.022
MUC1	41.70 [a]	45.81 [a]	26.89 [b]	3.61	0.004
OCLN	5209.83 [a]	3788.43[b]	4300.55 [ab]	329.86	0.022
Ileum					
TGFB1	240.40 [a]	325.40 [b]	235.21 [a]	23.64	0.029
TNF	79.88 [a]	136.30 [b]	85.51 [a]	15.26	0.037
CLDN5	115.14 [a]	66.00 [b]	83.2 [ab]	13.14	0.046
CLDN3	2281.14 [a]	694.20 [b]	1501.2 [ab]	416.79	0.047
OCLN	2464.03 [a]	786.38 [b]	1782.07 [ab]	442.92	0.048

[a,b] values with different superscripts differ significantly ($P < 0.05$); A total of seven replicates were used per treatment group (replicate = pig).

Ileum: FUC supplementation decreased the expression of *SLC2A2*, *GCG*, *FABP2*, *SLC5A1* and *SI* compared to the basal group ($P < 0.05$). Pigs fed the basal diet had increased expression of *CNDP1* compared to the FUC and LAM supplemented groups ($P < 0.05$).

2.5.2. Differential Expression of Markers of Immune Response and Intestinal Integrity

Jejunum: Pigs on the FUC supplemented diet had increased expression of *CXCL8* compared to both LAM supplementation and the basal diet ($P < 0.05$). Pigs on the LAM supplemented diet had reduced *MUC1* compared to the basal and LAM supplemented diet ($P < 0.05$). Pigs on the basal diet had higher expression of *OCLN* compared to pigs fed the FUC and LAM supplemented diets ($P < 0.05$).

Ileum: pigs fed the FUC supplemented diet had increased expression of *TGFB1* and *TNF* compared to the control and LAM groups ($P < 0.05$). Supplementation with FUC decreased expression of *CLDN5*, *CLDN3* and *OCLN* compared to the basal diet ($P < 0.05$).

3. Discussion

While supplementation with LAM was previously shown to be effective in improving pig performance from weaning until day 14 post-weaning [5], the results of this study suggest that, under good sanitary conditions, there is no additional benefit on performance to continued supplementation with either LAM or FUC supplementation up to day 35 post-weaning. It is important to note, however, that pigs fed the LAM supplemented diet had increased colonic butyrate production and positive alterations in the colonic microbiome characterized by reduced *Campylobacter* and increases in the genus *Roseburia* and *Faecalbacterium*. Such effects could contribute to a better host immune response to any potential environmental/pathogen challenge during this time period.

There were substantial differences in the microbiome profile between the three experimental groups. There was a contrasting effect between the two SWE supplemented treatments, particularly in relation to changes in the phylum Proteobacteria. The pigs fed the LAM supplemented diet had a decrease in this phylum, while pigs fed the FUC supplemented diet had an increase in the abundance of this phyla compared to pigs fed the basal diet. These differences were supported at both family and genus taxonomic levels with differences in the family *Campylobacteraceae* and the genus *Campylobacter*. The magnitude of the differences was interesting as pigs fed LAM had 23 times lower *Campylobacter* compared to pigs fed the basal diet, while pigs fed the FUC supplemented diet had 4 times higher *Campylobacter* compared to pigs fed the control diet. *Campylobacter* is a major foodborne pathogen often solely linked to infections from broilers through *C. jejuni*, however, *C. coli* is implicated with infections originating from swine [9]. A potential anti-bacterial effect following the addition of LAM is potentially of major benefit to the pig industry [10]. While *Campylobacter* is often considered to form part of the commensal flora of pigs and cause no negative impact on animal performance, there is some debate as high counts of *Campylobacter* are often observed in conjunction with other bacteria during incidences of diarrhea [11]. From either the aspect of reducing a zoonotic pathogen or improving intestinal health, the observed effects on *Campylobacter* by the addition of LAM can be considered a positive finding while the large increase in *Campylobacter* following the addition of FUC is likely to have negative connotations.

Coinciding with the lowest abundance of Proteobacteria in this study, pigs fed the LAM supplemented diet had the greatest abundance of the phylum Firmicutes. This increase was predominantly related to increases in the *Ruminococcaceae* and the *Lachnospiraceae* families. At genus level this coincided with differences in *Faecalbacterium* and *Roseburia*. Within the genus *Faecalbacterium* only one species has been identified in the literature, which is *Faecalbacterium prausnitzi*, implying that this change at genus level relates to a change in abundance of this species. This genus has been associated with increased intestinal health based on a low incidence of post-weaning diarrhea in pigs [12]. In humans, *Faecalbacterium prausnitzi* is used as an indicator of intestinal health and is also considered to be a very promising probiotic for human use [13,14]. The end products of carbohydrate fermentation by *Faecalbacterium prausnitzi* are formate, lactate and substantial quantities of butyrate [15]. Further corroborating the potential improved gut health in pigs fed LAM are an increase in the genus *Roseburia*. *Roseburia* is a member of the Firmicutes phylum and is associated with the production of butyrate [8]. Therefore, the increase in *Faecalbacterium and Roseburia* could be associated with the increase in butyric acid identified in pigs from this study fed the LAM supplemented diet. Butyrate is produced from bacterial fermentation to provide energy to colonocytes. It also has functions as a cellular mediator, regulating multiple functions of gut cells and beyond, including gene expression, cell differentiation, gut tissue development, immune modulation, oxidative stress reduction and diarrhea control [16]. These changes suggest an improvement in gut health in pigs fed the LAM supplemented diet.

In contrast to the clear beneficial effects of supplementation with LAM on members of the Firmicutes and Proteobacteria phyla, the increase in abundance of the Spirochaetes phylum are less clear. Within this phylum associated changes were identified with increases in the family *Spirochaetaceae* and the genus *Treponema* were also identified, with pigs fed the LAM supplemented diet having greater abundance than both the two other experimental groups. The genus contains both pathogenic as well as commensal bacteria [17]. Pathogenic bacteria include *Treponema pallidum*, and others such as *T. denticola* (Tde), *T. putidum* (Tpu) *T. pedis* (Tpe), *T. brennaborense* (Tbr), and *T. paraluiscuniculi* (Tpar) which are the causative agents of various disease in both humans and animals [18]. Porcine intestinal Spirochaetes form a diverse group of organisms including the beta-hemolytic *Serpulina/Treponema hyodysenteriae* which is the main etiological agent of swine dysentery [19]. While the classification of OTUs at species level is unreliable, in this study, species classified as part of the genus Treponema include *berlinense*, *bryantii*, *succinifaciens*, *suis* and *porcinum*.

While data related to these species is limited, *Treponema porcinum*, *Treponema succinifaciens*, *Treponema berlinense* and *Treponema bryantii* are associated with improved feed efficiency in pigs [20,21]. Further analysis such as shotgun metagenomics will need to be conducted to better understand the impact of changes in this genus have on the function of the microbiome. However, based on the other positive effects on gut health in pigs fed the LAM supplemented diet and the lack of negative impacts on gut health, it seems the changes in the Spirochaetes phylum are not negatively impacting the pigs.

Pigs fed both the LAM and the FUC supplemented diets had reduced bacterial diversity based on the Observed, Chao1, ACE and Fisher measures of alpha diversity. While there are conflicting opinions in the literature, lower bacterial diversity is generally considered to have negative connotations as greater microbial diversity is directly associated with ecosystem stability [22]. For example, in humans, reductions in diversity is associated with a range of health issues and diseases [23]. Therefore, while a reduced diversity in the pigs fed the FUC supplemented agrees with the changes in the microbiome and performance for this group, the reduction in diversity in pigs fed the LAM supplemented diet is surprising. The changes in the microbiome in this group particularly in the reduction in *Campylobacter* suggest improved gut health and therefore, it is unlikely that a reduction in diversity is having a negative influence in this group of pigs.

In relation to the gene expression data in this study, there are contrasting effects between the diets supplemented with the seaweed extracts. In relation to supplementation with LAM only minor changes in gene expression were identified relative to the control while more substantial changes were identified in pigs fed the FUC supplemented diet relative to pigs fed the control diet. However, there was region specific differences. In the duodenum, pigs fed the FUC supplemented diet had increased expression of SLC6A19 and CNDP1 compared to pigs fed the basal and also the pigs fed the diet supplemented with LAM. The two SWE supplemented groups had reduced expression of SLC16A10 compared to pigs fed the basal non-supplemented diet. These three transporters are all involved in the transport of amino acids [24]. This suggests there is increased availability and transport of amino acids in the duodenum of pigs fed the diets containing seaweed extracts compared to pigs fed the control. However, nutrient transporters are regulated by dietary substrate levels meaning the increased expression of protein transporters is a response to an increase in nutrient availability in the duodenum which can be impacted by a number of factors such as feed intake, but also may be a response to changes in intestinal architecture such as reductions in villus height [25]. A further influence of the SWE on nutrient transport was identified in the jejunum with pigs fed the FUC supplemented diets having increased expression of MCT1/SLC16A. SLC16A1 is responsible for the transport of monocarboxylates such as L-lactate and ketone bodies and also with the transport of butyrate [26,27]. These data, while speculative suggest an increased bacterial fermentation in the jejunum with the addition of FUC leading to increased production of butyrate and subsequent absorption with MCT1. While the influence of bacterial fermentation in small intestine is not as pronounced as the large intestine, the production and utilisation of butyrate in the small intestine and in particular the jejunum, as is the case in this study is important in the modulation of balance between apoptosis and proliferation [28]. In contrast to the upregulation of expression of genes related to nutrient digestion and absorption in the duodenum and jejunum, in the ileum, FUC supplementation led to a reduction in the expression of SLC2A2, GCG, FABP2, SGLT1 and SI in the ileum. Similar, results were identified where the feeding of a similar level of FUC in the post-weaning period had a similar influence on nutrient transporters suggesting that the addition of FUC has an impact in nutrient availability [6]. In the study of Rattigan et al. [6] the authors attributed the reduction in gene expression to the presence of alginates and fucoidan in the extract. Both FUC and alginates have been attributed with increasing the viscosity of digestive contents, reducing the flow of digesta and reducing the mixing of digestive contents leading to lower rates of nutrient breakdown [29,30]. The impact of these contrasting effects in different regions of the small intestine are difficult to quantify particularly due to the fact ileal digestibility's

was not measured. Unfortunately, the material required to conduct an analysis of nutrient digestibility was unavailable due to the volume of digesta in the digestive tract at the time of slaughter. Further research will be required to further understand the impacts of these extracts and nutrient breakdown and absorption.

Significant effects were identified between experimental groups in both the expression of targets related to barrier function and the expression of cytokines. Pigs fed the FUC supplemented diet had reductions in the expression of *OCLN* in both the jejunum and ileum compared to pigs fed the basal diet, while a tendency towards reduced expression was also identified in the duodenum. In agreement with these data is a reduction in the expression of *CLDN3* and *CLDN5* in the ileum compared to pigs fed the control diet. Proteins in the claudin and occludin families are a main component of tight junctions and form a seal that modulates paracellular transport in the intestinal epithelium [31]. Reduced expression of claudins such as 3 and 5 is associated with intestinal inflammatory disorders [32]. This is in agreement with effect identified on the expression of IL8/CXCL8 in the jejunum and the increased expression of *TGFB1* and *TNF* in the ileum of pigs fed the diet supplemented with FUC compared to pigs fed the basal unsupplemented diet. For the pigs fed the FUC supplemented diet the changes in gene expression are likely indicators of detrimental effects of the extract on gut health with increased markers of inflammation and reduced gene expression of targets associated with barrier function. In conjunction with the changes in the microbiome in the large intestine these data are possible explanations for the reduction in performance of pigs fed FUC. The pigs fed LAM had reductions in the expression of *MUC1* compared to pigs fed the basal and also pigs fed the diet supplanted with LAM. MUC1 provides a barrier against potential pathogens while also modulating the expression of inflammatory cytokines [33]. Therefore, the increase in expression of this gene is surprising as pigs fed the diet supplemented with LAM had no increases in inflammation, a healthier microbial profile and improved performance. Further research will need to be conducted to establish the reasons for this increase in expression such as a quantification of protein abundance as changes in expression are not always a true reflection of the production of the associated protein.

The aim of this study was to determine if the continued supplementation of two SWEs past the initial post-weaning period continues to be beneficial to performance. It is interesting to note that while SWE supplementation past the immediate post-weaning period up to d 35 in this study did not result in improved performance in healthy pigs under good sanitary experimental conditions, there was evidence to suggest that LAM supplementation had positive effects on gut health. This is significant as previous studies have identified that SWE supplementation can provide substantial performance and health benefits when the pigs become challenged. Heim at al [34] identified that SWE supplemented pigs had lower faecal scores and better performance than basal fed pigs following an ETEC challenge. Rattigan et al. [6] identified that LAM supplementation improves performance when pigs are housed in unsanitary conditions. While the mode of action is not completely understood, the evidence would suggest that bioactives in the SWE can influence both the host immune cells and gut microbiome cells. For instance, bioactives such as laminarin, can be internalized by intestinal epithelial cells and gut associated lymphoid cells [35]. This internalization upregulates the expression of pattern recognition receptors, increasing protective cytokine expression and induces protection against infectious challenge [36]. Hence, this effect would not be evident until the pigs undergo some type of environmental or pathogenic challenge.

4. Materials and Methods

All experimental procedures described in this work were approved under the University College Dublin Animal Research Ethics Committee (AREC-17-19-O'Doherty, 11 May 2017) and were conducted in accordance with Irish legislation (SI no. 543/2012) and the EU directive 2010/63/EU for animal experimentation.

4.1. Experimental Design and Animal Management

72 weaned pigs (progeny of Landrace boars × (Large White × Landrace) sows) were sourced from sows from the same farrowing house. Blocking of piglets was done on the basis of initial live weight (8.4 kg, sd 1.05 kg), sex, litter of birth and pigs were assigned to one of three groups: 1) basal diet; 2) basal diet + 250 ppm fucoidan rich extract (FUC); 3) basal diet + 300 ppm of a laminarin (LAM) rich extract with a total of 8 replicates per treatment.

The pigs were penned in groups of three and housed on fully slatted floors (1.68 × 1.22 m) with the initial temperature set at 30 °C and subsequently reduced each week by 2 °C with the humidity maintained at 65%. Pig weights were recorded on day 0 (weaning) and subsequently on days 7, 14, 21, 28 and 35. Feed and water were available ad libitum from four-space feeders and nipple drinkers, respectively, throughout the experiment.

4.2. Preperation of Experimental Diets and Characterisation of Extracts

Pigs in this experiment were offered one of three diets: (1) basal diet; (2) basal diet + 250 ppm FUC; (3) basal diet + 300 ppm LAM. The basal diet contained 15.3 MJ/kg digestible energy, 190 g/kg crude protein and 13.5 g/kg total lysine. The basal diet was comprised of wheat (34%), extruded full fat soya (17%), flaked wheat (13%) soya bean meal (48% crude protein) (10.5%), flaked maize (7%) whey powder (5%), provisoy (soya protein concentrate) (6.5%), soya oil (3%) with the remainder compromised of mineral and vitamin supplements (Table 7). Lysine was used a reference for calculation of the other amino acid requirements (NRC, 2012). The extraction procedures and methodology were described in previous publications but are further outlined below [5,6,37].

A laminarin-rich extract (BioAtlantis Ltd., Clash Industrial Estate, Tralee, Ireland) was obtained from *Laminaria Digitata* using a hydrothermal-assisted extraction and pre-optimized conditions for maximum yield of laminarin as described previously [38,39]. Briefly, dried and milled seaweed was suspended of 0.1N HCl maintaining a solid to liquid ratio of 1:21 (g/mL). The mixture was thoroughly agitated to ensure uniformity and then subjected to a temperature of 100 °C for 30 min. The subsequent crude extract was partially purified to increase the relative polysaccharide content and to remove or reduce other constituents; proteins, polyphenols, mannitol and alginate. This was achieved through mixing the crude extract with pure ethanol (to remove polyphenols) followed by water (to remove protein) and calcium chloride (to remove alginates).

A fucoidan-rich extract (BioAtlantis Ltd., Clash Industrial Estate, Tralee, Ireland) was obtained from *Ascophyllum nodosum* using a hydrothermal-assisted extraction and pre-optimized conditions for maximum yield of fucoidan [39]. The crude extract was partially purified to increase the relative polysaccharide content and to remove or reduce other constituents such as proteins, polyphenols, mannitol and alginate. This was achieved through mixing the crude extract with pure ethanol (to remove polyphenols) followed by water (to remove protein) and calcium chloride (to remove alginates). Fractions were separated based on molecular weight by employing a molecular weight cut-off centrifugal concentrator (100 KDa cut-off).

4.3. Post Slaughter Sample Collection

On d35 following slaughter, tissue sections of 1cm^2 were cut from the duodenum, jejunum and ileum and washed using sterile PBS (Oxoid). The overlying smooth muscle was removed before storage in 5 mL RNAlater solution (Applied Biosystems, Dublin, Ireland) overnight at 4 °C which was subsequently removed before long term storage at −80 °C. Colonic digesta was removed and stored in sterile containers (Sarstedt, Wexford, Ireland) and frozen (−20 °C) for subsequent 16s rRNA sequencing and VFA analyses.

Table 7. Ingredient and chemical composition of basal diet *.

Ingredient (g/kg)	
Wheat	380.0
Barley	233.0
Soya bean meal	170.0
Full fat soya	120.0
Whey powder	50.0
Dicalcium phosphate	13.0
Soya oil	10.0
Calcium carbonate (Limestone)	11.0
Lysine HCL	4.0
Vitamins and minerals	3.0
Salt	3.0
DL-methionine	1.5
L-threonine	1.5
Chemical analysis	
DM	866.1
Crude protein (N × 6.25)	190
Digestible energy (MJ/kg) [†]	14.95
Ash	48.4
Neutral detergent fibre	114.00
Lysine [†]	13.5
Methionine and cysteine [†]	7.4
Threonine [†]	7.9
Tryptophan [†]	2.6
Calcium [†]	7.2
Phosphorous [†]	6.0

* Treatments were as follows: (1) basal diet; (2) basal diet; basal diet + 250 parts per million (ppm) fucoidan; (3) basal diet + 300 ppm of a laminarin rich extract basal diet; [†] Values calculated based on tabulated nutritional composition [40]. The basal diet was formulated to provide: Cu, 100; Fe, 140; Mn, 47; Zn, 120; I, 0.6; Se, 0.3; retinol, 1.8; cholecalciferol, 0.025; α-tocopherol, 67; phytylmenaquinone, 4; cyanocobalamin, 0.01; riboflavin, 2; nicotinic acid, 12; pantothenic acid, 10; choline chloride, 250; thiamine, 2; pyridoxine, 0.015 (mg/kg diet). Celite was also included at 300 mg/kg.

4.4. Volatile Fatty Acid Analysis

The VFA concentrations in the digesta were determined using gas liquid chromatography (GLC) as reported by Clarke et al. [41]. 1 g of digesta was mixed with distilled water (2.5 × sample weight) and centrifuged at 1400 g for 10 min (Sorvall GLC-2B laboratory centrifuge, DuPont, Wilmington, DE, USA). One mL of the subsequent supernatant and 1 mL of internal standard (0.05% 3-methyl-n-valeric acid in 0.15 M oxalic acid dihydrate) were mixed with 3 mL of distilled water. The reaction mixture was centrifuged at 500 g for 10 min, and the supernatant was filtered through 0.45 PTFE syringe filter into a chromatographic sample vial. An injection volume of 1 μL was injected into a Varian 3800 GC equipped with a EC™ 1000 Grace column (15 m × 0.53 mm I.D) with 1.20 μm film thickness. The temperature was set at 75–95 °C increasing by 3 °C/min, 95–200 increasing by 20 °C per minute, which was held for 0.50 min. The detector and injector temperature were 280 °C and 240 °C, respectively, while the total analysis time was 12.42 min.

4.5. Microbiological Analyses

4.5.1. Microbial DNA Extraction

The extraction of microbial genomic DNA was conducted using a QIAamp DNA stool kit (Qiagen, West Sussex, UK) according to standard protocols. After DNA extraction DNA was evaluated using the Nanodrop spectrophotometer (Thermo Scientific, Wilmington, DE, USA).

4.5.2. Illumina Sequencing

The V3–V4 hypervariable region of the bacterial 16S rRNA gene was performed on an Illumina MiSeq platform according to their standard protocols (Eurofins, Wolverhampton, UK). The V3–V4 region was PCR-amplified with universal primers taking in adapters including nucleotide sequences for forward and reverse index primers. Amplicon purification was conducted with AMPure XP beads (Beckman Coulter, Indianapolis, IN, USA) and prepared for index PCR using Nextera XT index primers (Illumina, San Diego, CA, USA). The purification step was repeated on the indexed samples using AMPure XP beads and assessed using a fragment analyzer (Agilent, Santa Clara, CA, USA). Following this step a pool was made using equal quantities from each experimental sample. The library was then analysed using the Bioanalyzer 7500 DNA kit (Agilent) and sequenced using the V3–V4 chemistry (2 × 300 bp paired-end reads).

4.6. Bioinformatic and Statistical Analyses

Quantitative Insights into Microbial Ecology (Qiime) was used to examine the sequencing data [42]. Sequencing primers were removed using the cutadapt package and the resulting paired end reads were merged using the paired-end reads function within Qiime using the standard criteria. Demultiplexing of paired end raw reads was through the split libraries function and quality filtering was conducted utilizing default QIIME parameters. Only reads that contained no ambiguous characters, no non-exact barcode matches, a sequence length > 225 nucleotides and a read-quality score of >27 were retained. The uclust function in Qiime was used to pick OTUs based on a sequence similarity of 97%. Singletons were removed, as only OTUs that were present at the level of at least two reads in more than one sample were retained while chimeric sequences were removed using ChimeraSlayer [43,44]. The GreenGenes database assigned OTUs to different taxonomic levels. A combination of the mormalized OTU table, experimental phenotypic data and the phylogenetic tree were combined to produce the phyloseq object for further analysis (http://www.r-project.org; version 3.5.0, accessed on 25 March). This phyloseq R package was used to examine measures of richness and diversity using the Observed, Chao1, ACE, Shannon, Fisher and Simpson measures as described by Maurer et al. [45]. The PROC GLIMMIX procedure of Statistical Analysis Software (SAS) 9.4 (SAS Institute, Cary, NC, USA) was used to examine differences between experimental treatments at phylum, family and genus level with pig being the experimental unit and *P*-values presented using a Benjamini–Hochberg (BH) correction.

4.7. Nanostring nCounter Analysis

Tissue from the duodenum, jejunum and ileum were used for analysis of gene expression profiles using the Nanostring nCounter Analysis System (Nanostring Technologies, Seattle, Washington, USA). Gene lists contained six positive and eight negative controls, eight reference targets and thirty-two target genes. A single multiplexed hybridisation reaction, as originally described by Geiss et al. [46] was used to analyse all target genes. Samples were initially standardized to 20 ng/μL using a Qubit fluorometer (Thermo Fisher Scientific). A master mix was created by combining 70 μL of hybridisation buffer and the reporter codeset, as per the manufacturer instructions. For the hybridization reaction each tube contained the master mix (8 μL), the sample (5 μL) (total RNA concentration 100 ng) and capture probeset (2 μL). Each reaction tube was inverted to mix and spun down before incubation at 65 °C for 20 h in a Bio-rad thermocycler.

The Nanostring nCounter prep station liquid handling robot which was used for post-hybridisation processing. This involved the removal of excess unbound probes and immobilisation of samples onto the internal surface of the sample cartridge to allow imaging to be conducted using the digital analyser, which collects data by taking images of the immobilised fluorescent reporters in the sample cartridge with a CCD camera through a microscope objective lens.

The analysis and normalisation of the raw Nanostring data were performed using the nSolver Analysis Software v4.0 (Nanostring Technologies) which was used for initial data normalisation and analysis. The background threshold value was estimated using the average count of the negative control probes in every reaction plus 2 standard deviations to which all samples were adjusted [47]. Gene targets with raw counts below the threshold in more than two thirds of samples were excluded from the analysis. Raw counts were normalised using a combination of positive control normalisation and codeset content normalisation. The former accounts for errors such as pipetting errors, lot-to-lot variation in nCounter preparation plates and nCounter cartridges, while the latter uses reference/housekeeping genes to account for variability in the quantity and quality of sample RNA.

4.8. Analysis of Performance and Gene Expression Data

The univariate procedure of SAS 9.4 (SAS Institute, Cary, NC, USA) was used to check performance, gene expression and VFA data for normality. Experimental data were analysed as a complete randomized design using the mixed procedure of SAS with the fixed effect of treatment. The initial weight was used as a covariate for the performance data with pen being the experimental unit. For all other data, the pig was the experimental unit. The probability level that denoted significance was $P < 0.05$, while P-values between 0.05 and 0.1 are considered numerical tendencies. Data are presented as least-square means with their standard errors of the mean.

5. Conclusions

In conclusion, while it was hypothesized that both LAM and FUC extracts would have a beneficial impact on performance and intestinal health out to day 35 post-weaning, only the supplementation of LAM was beneficial on intestinal health, with no identifiable effect on performance. Further research will need to be conducted to assess the long-term impact of the feeding the LAM extract in unsanitary/challenge conditions, but also for inclusion in human studies due to its positive impact on the intestinal microbiome.

Conflicts of Interest: The authors declare no conflict of interest.

References

1. Campbell, J.M.; Crenshaw, J.D.; Polo, J. The biological stress of early weaned piglets. *J. Anim. Sci. Biotechnol.* **2013**, *4*, 19. [CrossRef]
2. Pluske, J.R. Feed- and feed additives-related aspects of gut health and development in weaning pigs. *J. Anim. Sci. Biotechnol.* **2013**, *4*, 1–7. [CrossRef] [PubMed]
3. Gallois, M.; Rothkötter, H.J.; Bailey, M.; Stokes, C.R.; Oswald, I.P. Natural alternatives to in-feed antibiotics in pig production: Can immunomodulators play a role? *Animal* **2009**, *3*, 1644–1661. [CrossRef]
4. Sweeney, T.; O'Doherty, J.V. Marine macroalgal extracts to maintain gut homeostasis in the weaning piglet. *Domest. Anim. Endocrin.* **2016**, *56*, S84–S89. [CrossRef]
5. Rattigan, R.; Sweeney, T.; Maher, S.; Thornton, K.; Rajauria, G.; O'Doherty, J.V. Laminarin-rich extract improves growth performance, small intestinal morphology, gene expression of nutrient transporters and the large intestinal microbial composition of piglets during the critical post-weaning period. *Br. J. Nutr.* **2020**, *123*, 255–263. [CrossRef] [PubMed]
6. Rattigan, R.; Sweeney, T.; Vigors, S.; Thornton, K.; Rajauria, G.; O'Doherty, A.J.V. The Effect of Increasing Inclusion Levels of a Fucoidan-Rich Extract Derived from Ascophyllum nodosum on Growth Performance and Aspects of Intestinal Health of Pigs Post-Weaning. *Mar. Drugs* **2019**, *17*, 680. [CrossRef] [PubMed]
7. Vigors, S.; O'Doherty, J.V.; Rattigan, R.; McDonnell, M.J.; Rajauria, G.; Sweeney, T. Effect of a Laminarin Rich Macroalgal Extract on the Caecal and Colonic Microbiota in the Post-Weaned Pig. *Mar. Drugs* **2020**, *18*, 157. [CrossRef]
8. Louis, P.; Young, P.; Holtrop, G.; Flint, H.J. Diversity of human colonic butyrate-producing bacteria revealed by analysis of the butyryl-CoA:acetate CoA-transferase gene. *Environ. Microbiol.* **2010**, *12*, 304–314. [CrossRef] [PubMed]
9. Thakur, S.; Gebreyes, W.A. *Campylobacter coli* in Swine Production: Antimicrobial Resistance Mechanisms and Molecular Epidemiology. *J. Clin. Microbiol.* **2005**, *43*, 5705–5714. [CrossRef]
10. Li, Y.; Wang, X.; Wang, X.-Q.; Wang, J.; Zhao, J. Life-long dynamics of the swine gut microbiome and their implications in probiotics development and food safety. *Gut Microbes* **2020**, *11*, 1824–1832. [CrossRef]
11. Fosse, J.; Seegers, H.; Magras, C. Prevalence and risk factors for bacterial food-borne zoonotic hazards in slaughter pigs: A review. *Zoonoses Public Health* **2009**, *56*, 429–454. [CrossRef]
12. Massacci, F.R.; Berri, M.; Lemonnier, G.; Guettier, E.; Blanc, F.; Jardet, D.; Rossignol, M.N.; Mercat, M.-J.; Doré, J.; Lepage, P.; et al. Late weaning is associated with increased microbial diversity and Faecalibacterium prausnitzii abundance in the fecal microbiota of piglets. *Anim. Microbiome* **2020**, *2*, 2. [CrossRef] [PubMed]
13. Miquel, S.; Martin, R.; Rossi, O.; Bermudez-Humaran, L.; Chatel, J.; Sokol, H.; Thomas, M.; Wells, J.; Langella, P. Faecalibacterium prausnitzii and human intestinal health. *Curr. Opin. Microbiol.* **2013**, *16*, 255–261. [CrossRef]
14. Sokol, H.; Pigneur, B.; Watterlot, L.; Lakhdari, O.; Bermúdez-Humarán, L.G.; Gratadoux, J.-J.; Blugeon, S.; Bridonneau, C.; Furet, J.-P.; Corthier, G. Faecalibacterium prausnitzii is an anti-inflammatory commensal bacterium identified by gut microbiota analysis of Crohn disease patients. *Proc. Natl. Acad. Sci. USA* **2008**, *105*, 16731–16736. [CrossRef]
15. Duncan, S.H.; Louis, P.; Flint, H.J. Lactate-Utilizing Bacteria, Isolated from Human Feces, That Produce Butyrate as a Major Fermentation Product. *Appl. Environ. Microb.* **2004**, *70*, 5810–5817. [CrossRef]
16. Bedford, A.; Gong, J. Implications of butyrate and its derivatives for gut health and animal production. *Anim. Nutr.* **2018**, *4*, 151–159. [CrossRef]
17. Norris, S.; Paster, B.; Moter, A.; Göbel, U. The Genus Treponema. In *The Prokaryotes*; Springer: New York, NY, USA, 2006; pp. 211–234. [CrossRef]
18. Buyuktimkin, B.; Zafar, H.; Saier, M.H., Jr. Comparative genomics of the transportome of Ten Treponema species. *Microb. Pathog.* **2019**, *132*, 87–99. [CrossRef] [PubMed]
19. Neef, N.A.; Lysons, R.J.; Trott, D.J.; Hampson, D.J.; Jones, P.W.; Morgan, J.H. Pathogenicity of porcine intestinal spirochetes in gnotobiotic pigs. *Infect. Immun.* **1994**, *62*, 2395–2403. [CrossRef] [PubMed]
20. McCormack, U.M.; Curião, T.; Buzoianu, S.G.; Prieto, M.L.; Ryan, T.; Varley, P.; Crispie, F.; Magowan, E.; Metzler-Zebeli, B.U.; Berry, D.; et al. Exploring a possible link between the intestinal microbiota and feed efficiency in pigs. *Appl. Environ. Microb.* **2017**, *83*, e00380-17. [CrossRef] [PubMed]
21. Quan, J.; Wu, Z.; Ye, Y.; Peng, L.; Wu, J.; Ruan, D.; Qiu, Y.; Ding, R.; Wang, X.; Zheng, E.; et al. Metagenomic Characterization of Intestinal Regions in Pigs With Contrasting Feed Efficiency. *Front. Microbiol.* **2020**, *11*. [CrossRef] [PubMed]
22. Panizzon, J.P.; Pilz Júnior, H.L.; Knaak, N.; Ramos, R.C.; Ziegler, D.R.; Fiuza, L.M. Microbial Diversity: Relevance and Relationship Between Environmental Conservation And Human Health. *Braz. Arch. Biol. Technol.* **2015**, *58*, 137–145. [CrossRef]
23. Valdes, A.M.; Walter, J.; Segal, E.; Spector, T.D. Role of the gut microbiota in nutrition and health. *BMJ* **2018**, *361*, k2179. [CrossRef] [PubMed]
24. Bröer, S.; Fairweather, S. Amino Acid Transport Across the Mammalian Intestine. *Compr. Physiol.* **2011**, *9*, 343–373.
25. Diamond, J.M.; Karasov, W.H. Adaptive regulation of intestinal nutrient transporters. *Proc. Natl. Acad. Sci. USA* **1987**, *84*, 2242–2245. [CrossRef]
26. Park, S.J.; Smith, C.P.; Wilbur, R.R.; Cain, C.P.; Kallu, S.R.; Valasapalli, S.; Sahoo, A.; Guda, M.R.; Tsung, A.J.; Velpula, K.K. An overview of MCT1 and MCT4 in GBM: Small molecule transporters with large implications. *Am. J. Cancer Res.* **2018**, *8*, 1967–1976.

27. Saksena, S.; Theegala, S.; Bansal, N.; Gill, R.K.; Tyagi, S.; Alrefai, W.A.; Ramaswamy, K.; Dudeja, P.K. Mechanisms underlying modulation of monocarboxylate transporter 1 (MCT1) by somatostatin in human intestinal epithelial cells. *Am. J. Physiol. Gastrointest. Liver Physiol.* **2009**, *297*, G878–G885. [CrossRef] [PubMed]
28. Zhong, X.; Zhang, Z.; Wang, S.; Cao, L.; Zhou, L.; Sun, A.; Zhong, Z.; Nabben, M. Microbial-Driven Butyrate Regulates Jejunal Homeostasis in Piglets During the Weaning Stage. *Front. Microbiol.* **2019**, *9*. [CrossRef]
29. Hoebler, C.; Guillon, F.; Darcy-Vrillon, B.; Vaugelade, P.; Lahaye, M.; Worthington, E.; Duée, P.-H.; Barry, J.-L. Supplementation of pig diet with algal fibre changes the chemical and physicochemical characteristics of digesta. *J. Sci. Food Agric.* **2000**, *80*, 1357–1364. [CrossRef]
30. Jiménez-Escrig, A.; Sánchez-Muniz, F.J. Dietary fibre from edible seaweeds: Chemical structure, physicochemical properties and effects on cholesterol metabolism. *Nutr. Res.* **2000**, *20*, 585–598. [CrossRef]
31. Ozden, O.; Black, B.L.; Ashwell, C.M.; Tipsmark, C.K.; Borski, R.J.; Grubb, B.J. Developmental profile of claudin-3, -5, and -16 proteins in the epithelium of chick intestine. *Anat. Rec.* **2010**, *293*, 1175–1183. [CrossRef]
32. Garcia-Hernandez, V.; Quiros, M.; Nusrat, A. Intestinal epithelial claudins: Expression and regulation in homeostasis and inflammation. *Ann. N. Y. Acad. Sci.* **2017**, *1397*, 66–79. [CrossRef]
33. McGuckin, M.A.; Lindén, S.K.; Sutton, P.; Florin, T.H. Mucin dynamics and enteric pathogens. *Nat. Rev. Microbiol.* **2011**, *9*, 265–278. [CrossRef]
34. Heim, G.; Walsh, A.M.; Sweeney, T.; Doyle, D.N.; O'Shea, C.J.; Ryan, M.T.; O'Doherty, J.V. Effect of seaweed-derived laminarin and fucoidan and zinc oxide on gut morphology, nutrient transporters, nutrient digestibility, growth performance and selected microbial populations in weaned pigs. *Br. J. Nutr.* **2014**, *111*, 1577–1585. [CrossRef] [PubMed]
35. Rice, P.J.; Adams, E.L.; Ozment-Skelton, T.; Gonzalez, A.J.; Goldman, M.P.; Lockhart, B.E.; Barker, L.A.; Breuel, K.F.; DePonti, W.K.; Kalbfleisch, J.H.; et al. Oral Delivery and Gastrointestinal Absorption of Soluble Glucans Stimulate Increased Resistance to Infectious Challenge. *J. Pharmacol. Exp. Ther.* **2005**, *314*, 1079. [CrossRef]
36. Leonard, S.G.; Sweeney, T.; Bahar, B.; O'Doherty, J.V. Effect of maternal seaweed extract supplementation on suckling piglet growth, humoral immunity, selected microflora, and immune response after an ex vivo lipopolysaccharide challenge. *J. Anim. Sci.* **2012**, *90*, 505–514. [CrossRef] [PubMed]
37. Garcia-Vaquero, M.; O'Doherty, J.V.; Tiwari, B.K.; Sweeney, T.; Rajauria, G. Enhancing the Extraction of Polysaccharides and Antioxidants from Macroalgae Using Sequential Hydrothermal-Assisted Extraction Followed by Ultrasound and Thermal Technologies. *Mar. Drugs* **2019**, *17*, 457. [CrossRef]
38. Rajauria, G.; Ravindran, R.; Garcia-Vaquero, M.; Rai, D.K.; Sweeney, T.; O'Doherty, J. Molecular characteristics and antioxidant activity of laminarin extracted from the seaweed species Laminaria hyperborea, using hydrothermal-assisted extraction and a multi-step purification procedure. *Food Hydrocoll.* **2021**, *112*, 106332. [CrossRef]
39. Garcia-Vaquero, M.; Rajauria, G.; Tiwari, B.; Sweeney, T.; O'Doherty, J. Extraction and yield optimisation of fucose, glucans and associated antioxidant activities from Laminaria digitata by applying response surface methodology to high intensity ultrasound-assisted extraction. *Mar. Drugs* **2018**, *16*, 257. [CrossRef] [PubMed]
40. Sauvant, D.; Perez, J.M.; Tran, G. *Table of Composition and Nutritional Value of Feed Materials. Pigs, Poultry, Cattle, Sheep, Goats, Rabbits, Horses, Fish*; Wageningen Academic Publishers: Wageningen, The Netherlands, 2004.
41. Clarke, L.C.; Sweeney, T.; Curley, E.; Duffy, S.K.; Rajauria, G.; O'Doherty, J.V. The variation in chemical composition of barley feed with or without enzyme supplementation influences nutrient digestibility and subsequently affects performance in piglets. *J. Anim. Physiol Anim. Nutr.* **2018**, *102*, 799–809. [CrossRef]
42. Caporaso, J.G.; Kuczynski, J.; Stombaugh, J.; Bittinger, K.; Bushman, F.D.; Costello, E.K.; Fierer, N.; Peña, A.G.; Goodrich, J.K.; Gordon, J.I.; et al. QIIME allows analysis of high-throughput community sequencing data. *Nat. Methods* **2010**, *7*, 335–336. [CrossRef] [PubMed]
43. Haas, B.J.; Gevers, D.; Earl, A.M.; Feldgarden, M.; Ward, D.V.; Giannoukos, G.; Ciulla, D.; Tabbaa, D.; Highlander, S.K.; Sodergren, E.; et al. Chimeric 16S rRNA sequence formation and detection in Sanger and 454-pyrosequenced PCR amplicons. *Genome Res.* **2011**, *21*, 494–504. [CrossRef] [PubMed]
44. DeSantis, T.Z.; Hugenholtz, P.; Larsen, N.; Rojas, M.; Brodie, E.L.; Keller, K.; Huber, T.; Dalevi, D.; Hu, P.; Andersen, G.L. Greengenes, a chimera-checked 16S rRNA gene database and workbench compatible with ARB. *Appl. Environ. Microb.* **2006**, *72*, 5069–5072. [CrossRef] [PubMed]
45. Maurer, B.A.; McGill, B.J. Measurement of species diversity. In *Biological Diversity: Frontiers Measurement Assessment*; Oxford University Press: New York, NY, USA, 2011; pp. 55–65.
46. Geiss, G.K.; Bumgarner, R.E.; Birditt, B.; Dahl, T.; Dowidar, N.; Dunaway, D.L.; Fell, H.P.; Ferree, S.; George, R.D.; Grogan, T.; et al. Direct multiplexed measurement of gene expression with color-coded probe pairs. *Nat. Biotechnol.* **2008**, *26*, 317. [CrossRef] [PubMed]
47. Vigors, S.; Doherty, J.V.O.; Ryan, M.; Sweeney, T. Analysis of the basal colonic innate immune response of pigs divergent in feed efficiency and following an ex vivo lipopolysaccharide challenge. *Physiol. Genom.* **2019**, *51*, 443–448. [CrossRef] [PubMed]

MDPI

Article

Antiproliferative Properties of Scandium Exopolysaccharide Complexes on Several Cancer Cell Lines

Javier Muñoz-Garcia [1,†], Mattia Mazza [2,3,†], Cyrille Alliot [2,4], Corinne Sinquin [5], Sylvia Colliec-Jouault [5], Dominique Heymann [1,6] and Sandrine Huclier-Markai [2,3,*]

1 Institut de Cancérologie de l'Ouest, Université de Nantes, Blvd Jacques Monod, F-44805 Saint-Herblain, France; javier.munoz@ico.unicancer.fr (J.M.-G.); dominique.heymann@univ-nantes.fr (D.H.)

2 GIP ARRONAX, 1 rue Aronnax, CEDEX 3, F-44817 Nantes, France; mattia.mazza@subatech.in2p3.fr (M.M.); alliot@arronax-nantes.fr (C.A.)

3 Laboratoire SUBATECH, 4 rue Alfred Kastler, BP 20722, CEDEX 3, F-44307 Nantes, France

4 Centre de Recherche en Cancérologie et Immunologie Nantes Angers, INSERM, U892, 8 quai Moncousu, CEDEX 1, F-44007 Nantes, France

5 IFREMER, Institut Français de Recherche pour L'exploitation de la mer, rue de l'Ile d'Yeu, BP21105, CEDEX 3, F-44311 Nantes, France; corinne.sinquin@ifremer.fr (C.S.); Sylvia.Colliec.Jouault@ifremer.fr (S.C.-J.)

6 Department of Oncology and Metabolism, Medical School, University of Sheffield, Sheffield S10 2TN, UK

* Correspondence: sandrine.huclier@subatech.in2p3.fr; Tel.: +33-(0)51-85-85-37 or +33-(0)28-21-25-23

† These author contributed equally to this work.

Abstract: Antimetastatic properties on both murine and human osteosarcoma cell lines (POS-1 and KHOS) have been evidenced using exopolysaccharide (EPS) derivatives, produced by *Alteromonas infernus* bacterium. These derivatives had no significant effect on the cell cycle neither a pro-apoptotic effect on osteosarcoma cells. Based on this observation, these EPSs could be employed as new drug delivery systems for therapeutic uses. A theranostic approach, i.e., combination of a predictive biomarker with a therapeutic agent, has been developed notably by combining with true pair of theranostic radionuclides, such as scandium ^{47}Sc/^{44}Sc. However, it is crucial to ensure that, once complexation is done, the biological properties of the vector remain intact, allowing the molecular tropism of the ligand to recognize its molecular target. It is important to assess if the biological properties of EPS evidenced on osteosarcoma cell lines remain when scandium is complexed to the polymers and can be extended to other cancer cell types. Scandium-EPS complexes were thus tested in vitro on human cell lines: MNNG/HOS osteosarcoma, A375 melanoma, A549 lung adenocarcinoma, U251 glioma, MDA231 breast cancer, and Caco2 colon cancer cells. An xCELLigence Real Cell Time Analysis (RTCA) technology assay was used to monitor for 160 h, the proliferation kinetics of the different cell lines. The tested complexes exhibited an anti-proliferative effect, this effect was more effective compared to EPS alone. This increase of the antiproliferative properties was explained by a change in conformation of EPS complexes due to their polyelectrolyte nature that was induced by complexation. Alterations of both growth factor-receptor signaling, and transmembrane protein interactions could be the principal cause of the antiproliferative effect. These results are very promising and reveal that EPS can be coupled to scandium for improving its biological effects and also suggesting that no major structural modification occurs on the ligand.

Keywords: exopolysaccharides; scandium; theranostic; cancer cell lines; proliferation

1. Introduction

The key role of glycosaminoglycans (GAGs), natural polysaccharides found in mammalian tissue, has been recognized in the regulation of cell properties and functions. They are now considered as pharmacological targets to treat several diseases and notably metastatic cancers. GAGs play a central role in the organization of the extracellular matrix (ECM) through their binding to various molecules (ECM components, cell-surface receptors,

21

growth factors and cytokines). Nowadays, several therapeutic strategies are developed with the aim of restoring cell function due to a degradation of endogenous GAGs either in protecting endogenous GAGs or in using exogenous GAGs or GAG-mimetics [1–4].

Unfractionated heparin and its low-molecular-weight (LMW) derivatives are widely used to prevent or treat venous thromboembolism, which is a common complication in cancer patients. Clinical trials have shown that cancer patients treated with heparins have improved, with a decrease in cancer progression and a longer survival time [5,6], which may be explained by heparin's functional interference with critical biological steps of metastasis spread [7]. Despite their therapeutic potential, side-effects induced by their anticoagulant properties (e.g., hemorrhagic complications and heparin-induced thrombocythemia) may occur, limiting thus a long-term treatment. Heparin could present also a contamination with prion proteins or oversulfated chondroitin sulfate [8]. Heparin's use in therapy is sometimes limited due to this hazard profile. As a result, the number of studies on heparin mimetic molecules has increased in recent years. Polysaccharides may be a new source of heparin-like molecules among the possible drug candidates. Traditional algal or modern bacterial polysaccharides may be used as a substitute for mammalian GAGs [9]. Furthermore, preliminary animal studies have shown that polysaccharides extracted from eukaryotes and prokaryotes living in the marine environment could reveal a better benefit/risk ratio [9]. Algal polysaccharides like fucoidans–especially low-molecular-weight fucoidan preparations–have previously been shown to have heparin-like properties with low hemorrhagic risks [10]. As soluble molecules or polymers, marine polysaccharides derived from bacteria have a lot of promise in cell therapy and tissue engineering. When compared to other polysaccharides from eukaryotes, they can be produced in bioreactors under completely regulated conditions [11].

Among these marine polysaccharides, an exopolysaccharide (EPS) of interest was isolated from the culture broth of a hydrothermal bacterium called *Alteromonas infernus*. A monosulfated nonasaccharide composed of six neutral hexoses and three hexuronic acids, including one galacturonic acid unit bearing one sulfate group, makes up the repeating unit of this EPS. It presents a high molecular weight ($>10^6$ g mol^{-1}) and a low sulfate content ($<10\%$) [12–14]. When compared to heparin, this native EPS had a very poor anticoagulant effect. To improve its biological activities and provide a GAG mimetic compound, native EPS has been modified first by radical depolymerization, then by oversulfation to create EPS derivatives [15,16]. In the following, EPS-DR denotes native EPS that has undergone radical depolymerization, whereas EPS-DRS denotes EPS that has been further over-sulfated. These two chemical modifications allow for a decrease in molecular weight while increasing sulfate content [17]. The anticoagulant efficacy of this LMW highly sulfated EPS derivative is increased over that of its native precursor, but it is still 10 and 5 times less potent than unfractionated and LMW heparin, respectively. Following the oversulfation stage, an oversulfated EPS structure (EPS-DRS) has been suggested, with three additional sulfate groups on both glucose and galactose constitutive of the repeating unit (unpublished data). It is made up of three hexose units that have been oversulfated and have been reported elsewhere [15–17].

In vitro studies on bone remodeling have displayed different levels of bone resorption regulation by EPS-DRS, most of them leading to pro-resorptive effects [15]. These results have brought to consider those compounds to be tested on osteosarcoma, characterized by high potency to induce lung metastasis [18]. EPS-DRS of different sizes have been tested against two osteosarcoma cell lines (mouse POS-1 and human HOS) revealing that an EPS derivative of 15 kDa could effectively inhibit both migration and invasiveness of osteosarcoma cells in vitro, while it could be very efficient at inhibiting the establishment of lung metastases in vivo [19].

Since their natural tropism in targeting malignant tumor and their metastasis, EPS have been recently considered as vector to be combined with theranostic radionuclide pairs. Through the possibility of doing therapy and diagnostic at the same time, theranostic compounds represent new innovative clinical tools to be employed in a perspective of "per-

sonalized/precision" medicine [20]. More precisely, a theranostic pair [44]Sc/[47]Sc could be both employed for Positron Emission Tomography (PET) imaging to detect primary and secondary tumors, as well as for Targeted RadioTherapy in order to bombard tumor tissues with gamma radiations [21]. Complexation between EPS and scandium has already been assessed and quantified in a previous work [22]. The EPS derivatives selected for this study are a highly sulfated one, called DRS (M_w = 27 kDa) and a lower-sulfated one, called DR (with M_w = 16 kDa). The complexation properties of these two EPS with scandium were higher than the ones on glucuronic and galacturonic acids, even though Sc-EPS complexes appear to be less stable ($K_{ScEPS-DR}$ = 9.14; $K_{ScEPS-DRS}$ = 7.69) than scandium complexes with 1,4,7,10-Tetraazacyclododecane-1,4,7,10-tetraacetic acid (DOTA) and diethylenetriaminepentaacetic acid (DTPA), classically used in radiopharmaceutical drugs.

For further use as a therapeutic vector, it is important to ensure that EPS may keep the ability of targeting cancer cells even when complexed with scandium. For this reason, in vitro studies concerning both cell proliferation and cell viability of various tumor cell lines were realized here to evaluate if there is a synergetic effect of Sc-EPS complexes on different cancer cell lines, compared to the EPS alone and scandium alone. To this aim, the cell index of human osteosarcoma (MNNG/HOS), human melanoma (A375), human lung cancer (A549), human glioblastoma (U251), and human breast cancer (MDA231) were monitored over a week using XCELLigence® technology. XCELLigence measures the electric impedance of cell assessed. This impedance is directly related to the cell adhesion process and, consequently, to cell proliferation and/or cell death. Moreover, the effect of the metal-to-ligand ration of the EPS-Sc complexes was assessed and, a heparin was used as a reference system for these EPS.

2. Results

2.1. Human MNNG/HOS Osteosarcoma Cell Line

2.1.1. Effect of Scandium Alone on Cell Proliferation and Viability

Figure 1 shows the effect of scandium alone on MNNG/HOS osteosarcoma cell proliferation as well as cell viability. Concerning the cell index (CI) measured by xCELLigence RTCA, the software employed transformed the CI of all wells at all time points to the normalized cell index (NCI), which was considered the CI value of individual wells at the same time point (base-time). This transformation made the NCI more comparable between the wells [23].
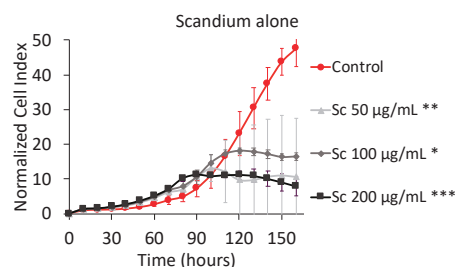
Figure 1. Normalized cell index plot of MNNG/HOS cells after 160 h of contact with Sc^{3+} at 50 µg mL^{-1} (**), 100 µg mL^{-1} (*), and 200 µg mL^{-1} (***) * = p value $\leq$ 0.0001, ** = p value $\leq$ 0.005, *** = p value $\leq$ 0.05.

The NCI plot shown in Figure 1 depicts two different kinds of curves. The ascending bi-exponential curve of the control is due to the fact that, in its well, the space to grow up was not saturated yet. The saturation was reflected by a plateau. Normally, two scenarios can occur once the plateau is set: (1) the plateau continues until starting a definitive descending evolution characteristic of damaged cells that are not attached to the surface of the well; (2) the plateau continues until starting a momentary decrease followed by a brief rise, that is characteristic of the replacement of damaged cells by new healthy cells.

The curves for scandium concentrations at 50 and 100 µg mL^{-1} showed a plateau that reflected no more MNNG/HOS cells proliferation but the detachment from the well was not observed yet. For the scandium concentration at 200 µg mL^{-1}, the detachment of cells slightly began at 140 h. Unfortunately, the time frame of 160 h was not sufficient to see if the decrease was definitive or kept oscillating. The MTT assay confirmed that the concentration of 200 µg mL^{-1} displayed a reduction of cell viability of around 25% after 160 h. For lower concentrations (i.e., 50 µg mL^{-1} and 100 µg mL^{-1}), an increase of cell viability was noticed.

2.1.2. Effect of EPS and Heparin Alone

The effect of both EPS-DR and -DRS and heparin on cell proliferation and cell viability is showed in Figure 2. It is noticed that NCI plot of EPS-DRS is very different from the ones of heparin and EPS-DR. For EPS-DRS, a second round of xCELLigence experiment was performed, leading to a higher number of MNNG/HOS cells (i.e., 5000 cells) compared to the first one (i.e., 3000 cells). This is why the control of EPS-DRS reached the peak of proliferation sooner than the two other ones, while for heparin and EPS-DR cells were still proliferating. This allowed evidencing the effect of the not modulated by the addition of heparin whatever the concentration considered. It was noticed that for 50 µg mL^{-1} of EPS-DR, the lowest sulfated EPS of this study, 100% viability was reached compared to the control.
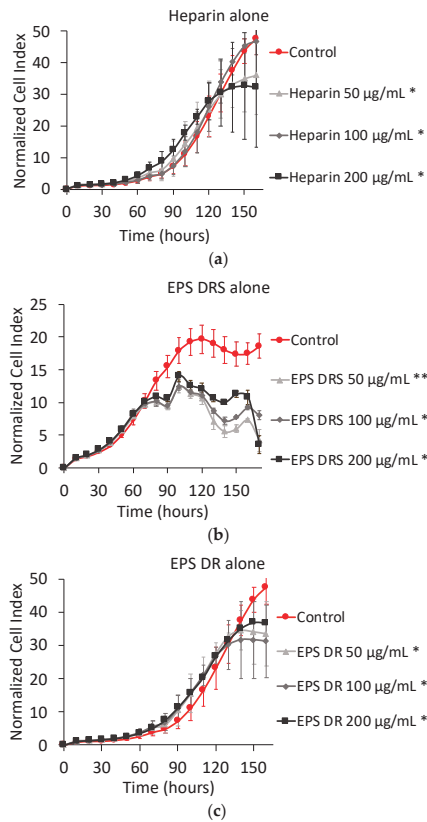
Figure 2. To the left, normalized cell index plot of MNNG/HOS cells after 160 of contact with (**a**) heparin alone at 50 µg mL^{-1} (*), 100 µg mL^{-1} (*), and 200 µg mL^{-1} (*); (**b**) EPS DRS alone at 50 µg mL^{-1} (**), 100 µg mL^{-1} (*), and 200 µg mL^{-1} (*); (**c**) EPS-DR alone at 50 µg mL^{-1} (*), 100 µg mL^{-1} (*), and 200 µg mL^{-1} (*).

2.1.3. Effect of Polysaccharide:Scandium Complexes

Heparin:Scandium (Hep:Sc) Complex

Figure 3 shows the NCI plot from xCELLigence RTCA of MNNG/HOS cells after 160 h of contact. The Hep:Sc complexes were prepared for four different metal-to-ligand ratios. For a metal-to-ligand ratio of 1:0.5 (Figure 3a), with a total concentration of heparin of 50 μg mL^{-1}, there was no effect on cell proliferation. After 100 h of contact, for the same metal-to-ligand ratio but with higher concentrations of heparin (i.e., 100 and 200 μg mL^{-1} respectively), there was a significant decrease of the cell proliferation rates.

Figure 3. Normalized cell index Plot of MNNG/HOS cells after 160 h of contact with different stoichiometric ratios L:M: (**a**) heparin:scandium (Hep:Sc) 1:0.5 at 50 μg mL^{-1} (*), 100 μg mL^{-1}, and 200 μg mL^{-1}; (**b**) Hep:Sc 1:1 at 50 μg mL^{-1} (*), 100 μg mL^{-1} (*), and 200 μg mL^{-1} (*); (**c**) Hep:Sc 1:2 at 50 μg mL^{-1}, 100 μg mL^{-1} (**), and 200 μg mL^{-1}; (**d**) Hep:Sc 1:4 at 50 μg mL^{-1} (*), 100 μg mL^{-1} (*), and 200 μg mL^{-1} (*).* = *p* value ≤ 0.0001, ** = *p* value ≤ 0.005.

With a metal-to-ligand ratio Hep:Sc of 1:1 (Figure 3b), the decrease in cell proliferation was well displayed and dose-dependent. For metal-to-ligand ratio of Hep:Sc of 1:2 (Figure 3c), there was no further exponential growth after 90 h of contact for all the concentrations of heparin considered. Finally, for a metal-to-ligand ratio of Hep:Sc of 1:4 (Figure 3d), there were the same proliferation rates between the control and treated cells until 100 h of incubation followed by a temporary decrease of cell proliferation.

If those results are compared to the ones obtained on cell viability, the metal-to-ligand ratio ratios of 1:0.5 and 1:4 exhibited higher percentages of cell viability. In contrast, for a constant metal-to-ligand ratio of 1:1, a significant decrease of almost 40% is observed when increasing the total concentration of heparin. The only drop on cell viability is observed for a metal-to-ligand ratio of 1:2 and for a concentration of heparin of 200 μg mL^{-1}; at these conditions, there is no more viable cells present in the well after 160 of contact.

EPS-DRS:Scandium (EPS-DRS:Sc) Complex

Figure 4 shows the NCI plot of MNNG/HOS cells after 160 h of contact with four metal-to-ligand ratio of EPS-DRS:Sc complex. Regarding the four metal-to-ligand ratio of the EPS-DRS:Sc complexes, the shape are very close to each other, meaning that neither the metal to ligand ratio, nor the total concentration of EPS-DRS play a key role in the cell

proliferation. Only one difference could be noticed, a slight reduction of cell proliferation, in the range 10–15 to 5–10 of NCI. For an EPS-DRS concentration of 200 µg mL^{-1}, the cell proliferation decreases suddenly after 150 h, after than a plateau has been reached. This has been noticed for the four metal-to-ligand ratios considered. This seems stopping the oscillating kinetics to very low and stable NCI values, comparable to those of heparin complexes (see Figure 3). No significant changes in cell viability for the four metal-to-ligand ratios considered, was observed, even at for the concentration of 200 µg mL^{-1} in EPS-DRS.

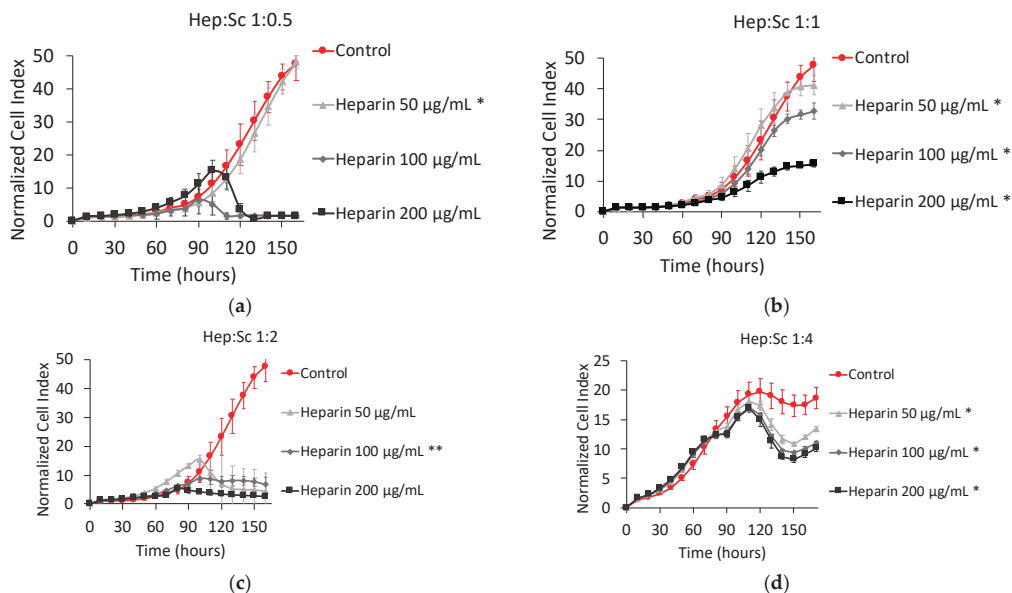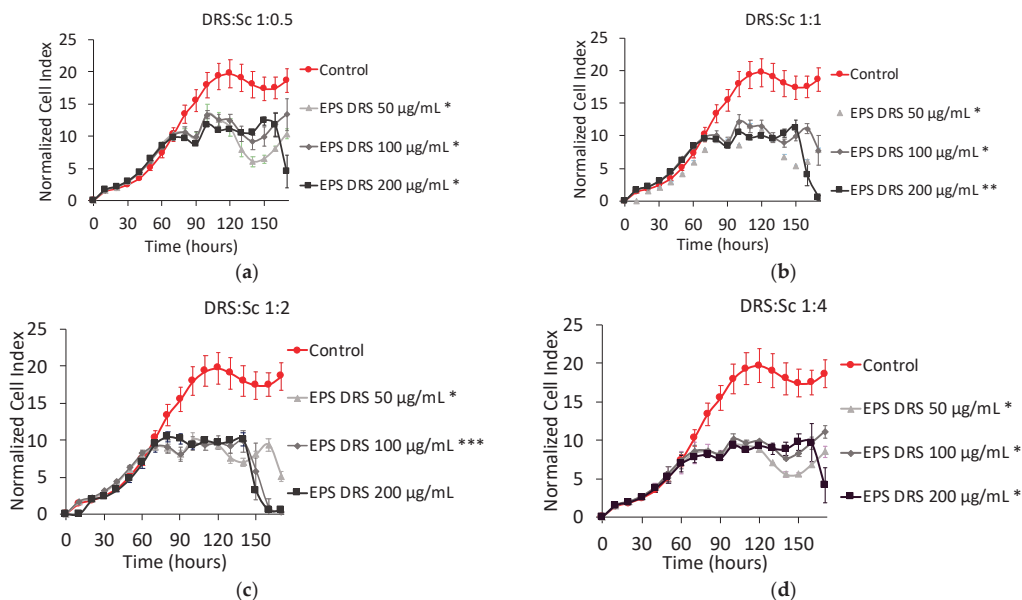**Figure 4.** Normalized cell index plot of MNNG/HOS cells after 160 h of contact with different stoichiometric ratios L:M: (**a**) EPS-DRS:Sc 1:0.5 at 50 µg mL^{-1} (*), 100 µg mL^{-1} (*), and 200 µg mL^{-1} (*); (**b**) EPS-DRS:Sc 1:1 at 50 µg mL^{-1} (*), 100 µg mL^{-1} (*), and 200 µg mL^{-1} (**); (**c**) EPS-DRS:Sc 1:2 at 50 µg mL^{-1} (*), 100 µg mL^{-1} (***), and 200 µg mL^{-1}; (**d**) EPS-DRS:Sc 1:4 at 50 µg mL^{-1} (*), 100 µg mL^{-1} (*), and 200 µg mL^{-1} (*).* = p value $\leq$ 0.0001, ** = p value $\leq$ 0.005, *** = p value $\leq$ 0.05.

EPS-DR:Scandium (EPS-DR:Sc) Complex

Figure 5 shows the NCI plot on MNNG/HOS cells after 160 h of contact with four metal-to-ligand ratios of EPS-DR:Sc complex. For the ratios EPS-DR:Sc 1:1 and 1:2, the cell proliferation profiles are quite similar. For the metal-to-ligand ratio of 1:1, after 100 h of contact, a peak of proliferation was reached at very low NCI for all the EPS-DR concentrations considered. Then, there was a plateau that tended to zero NCI for the highest concentration of EPS-DR. For the ratios EPS-DR:Sc 1:1 and 1:2, the standard deviation of all the curves appeared very high. Likewise, even for metal-to-ligand ratio of 1:0.5 and 1:4, similar curves were obtained, that could be quite well superimposed with the control. For these two metal-to-ligand ratios, the cell proliferation started oscillating after 120 h.

The cell proliferation profiles were compared to the cell viability results. For metal-to-ligand ratio of 1:0.5 and 1:4, there was a high percentage of cell viability after 160 h of contact whereas for metal-to-ligand ratio of 1:1, there was a significant decrease when increasing the concentration of EPS-DR. This behavior was very similar to the one observed on Hep:Sc complexes.
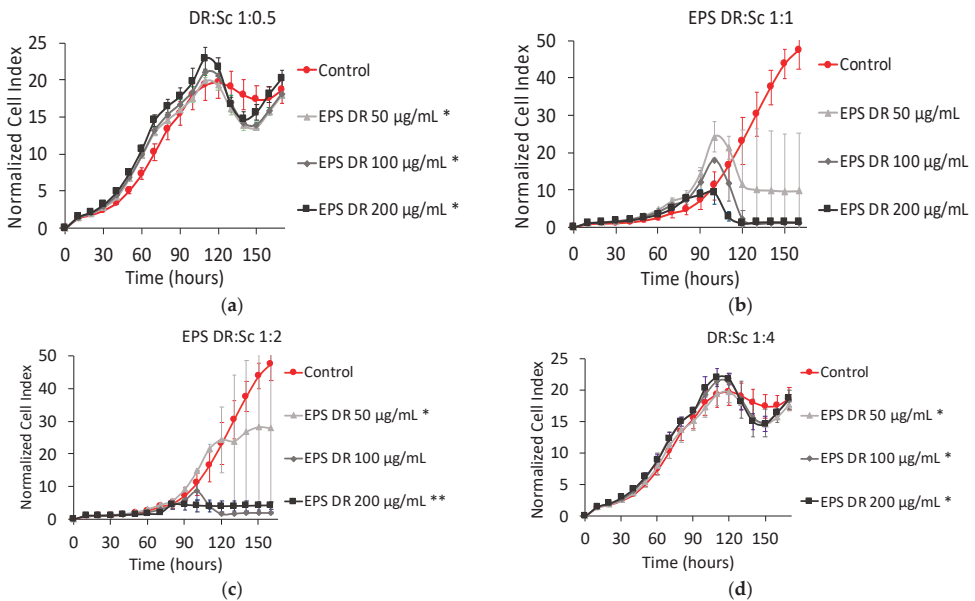
Figure 5. Normalized cell index plot of MNNG/HOS cells after 160 h of contact with different stoichiometric ratios L:M: (**a**) EPS-DR:Sc 1:0.5 at 50 µg mL^{-1} (*), 100 µg mL^{-1} (*), and 200 µg mL^{-1} (*); (**b**) EPS-DR:Sc 1:1 at 50 µg mL^{-1}, 100 µg mL^{-1}, and 200 µg mL^{-1}; (**c**) EPS-DR:Sc 1:2 at 50 µg mL^{-1} (*), 100 µg mL^{-1}, and 200 µg mL^{-1} (**); (**d**) EPS-DR:Sc 1:4 at 50 µg mL^{-1} (*), 100 µg mL^{-1} (*), and 200 µg mL^{-1} (*). * = *p* value $\leq$ 0.0001, ** = *p* value $\leq$ 0.005.

2.2. Human A375 Melanoma Cells

Effect of Scandium and Polysaccharides Alone

Figure 6 shows the effect on cell proliferation of scandium, as well as the three polysaccharides alone. All the compounds reduced the cell proliferation after 95 h of contact. The effect of scandium alone was comparable to that of heparin or EPS-DR alone. Nevertheless, the EPS-DRS alone, that had the higher sulfate content, displayed a more traditional profile of detaching cells.

Figure 6. Normalized cell index plot of human A375 melanoma cells after 95 h of contact with (**a**) scandium at concentration of 100 µg mL^{-1} (*) and (**b**) polysaccharides alone at concentration of 100 µg mL^{-1}: heparin (*), EPS-DRS (*), EPS-DR (*). * = *p* value $\leq$ 0.0001.

2.3. Effect of Polysaccharide:Scandium Complexes

For both EPS considered in this work, i.e., EPS-DR and -DRS, scandium-polysaccharide complexes were more efficient in reducing the cell proliferation than the EPS themselves as shown in Figure 7. For Hep:Sc (Figure 7a) and EPS-DRS:Sc (Figure 7b) complexes, at increasing metal-to-ligand ratio, a more important decrease in cell proliferation was observed. The same trend could be observed for EPS-DR:Sc complexes (Figure 7c). The best conditions for reducing the cell proliferation were reached for a metal-to-ratio of 1:2, leading to a cell proliferation reduction of approximately 55–88%.

Figure 7. Normalized cell index plot of human A375 melanoma cells after 95 h of contact with different scandium-polysaccharide complexes at concentration of 100 $\mu g\ mL^{-1}$ and various stoichiometric ratios: (**a**) Hep:Sc 1:0.5 (*), 1:1 (*), 1:2 (*), heparin alone (*); (**b**) EPS-DRS:Sc 1:0.5 (*), 1:1 (*), 1:2 (**), EPS-DRS alone (*); (**c**) EPS-DR:Sc 1:0.5 (*), 1:1 (*), 1:2 (*), EPS-DR alone (*). * = p value $\leq$ 0.0001, ** = p value $\leq$ 0.005.

2.4. Human A549 Lung Cancer Cells

2.4.1. Effect of Scandium and Polysaccharides Alone

From Figure 8a, scandium seemed having no impact on the proliferation of lung cancer cells after 95 h of contact. By contrast, among the polysaccharides considered in this work, only EPS-DRS seemed to slow down the kinetic of the cell proliferation. By comparison to EPS-DR, containing lower sulfate content, it could be assumed so far that the sulfate content of the macromolecule played a role on the cell proliferation, at least for the cell line A549.

2.4.2. Effect of Polysaccharide:Scandium Complexes

As shown in Figure 9a–c, the cell proliferation curves obtained when the cells contacted EPS-DR:Sc and Hep:Sc complexes, exhibited quite similar kinetic behaviors.

Only the metal-to-ligand ratio of 1:2 had an impact on the cell proliferation. This effect was more pronounced with EPS-DRS:Sc (Figure 9b) but for this one, there was no influence of the metal-to-ligand ratio.

Figure 8. Normalized cell index plot of human A549 lung cancer cells after 95 h of contact with (**a**) scandium at concentration of 100 μg mL^{-1} (*) and (**b**) polysaccharides alone at concentration of 100 μg mL^{-1}: heparin (*), EPS-DRS (*), EPS-DR (*). * = p value ≤ 0.0001.

Figure 9. Normalized cell index plot of human A549 lung cancer cells after 95 h of contact with different scandium-polysaccharide complexes at concentration of 100 μg mL^{-1} and various stoichiometric ratios: (**a**) Hep:Sc 1:0.5 (*), 1:1 (*), 1:2 (*), heparin alone(*); (**b**) EPS-DR:Sc 1:0.5 (*), 1:1 (*), 1:2 (*), EPS-DRS alone (*); (**c**) EPS-DRS:Sc 1:0.5 (*), 1:1 (*), 1:2 (*), EPS-DR alone (*). * = p value ≤ 0.0001.

2.5. Human U251 Glioblastoma Cells

Scandium alone induced a slight decrease of U251 cell proliferation (Figure 10a). Among the three polysaccharides, only heparin and EPS-DRS (Figure 10b), the most sulfated polysaccharides, slowed down the proliferation of approximately 45% compared to the untreated control group.

When considering the scandium complexes (Figure 10c–e), in particular, Hep:Sc and EPS-DR:Sc complexes showed a less efficient reduction in the proliferation of glioblastoma cells compared to the polysaccharide themselves. As observed for the other cell lines tested, there was an exception for the metal-to-ligand ratio 1:2 that influenced the kinetics. Additionally, EPS-DRS:Sc complexes were rather more efficient than DRS alone but this

activity was not correlated to the metal-to-ligand ratio as has been evidenced by the other cell lines tested above.
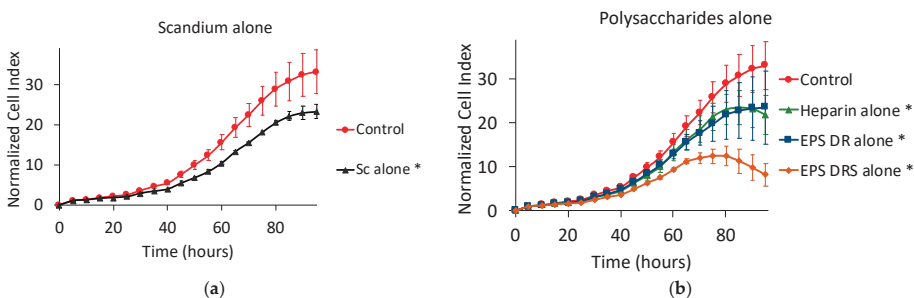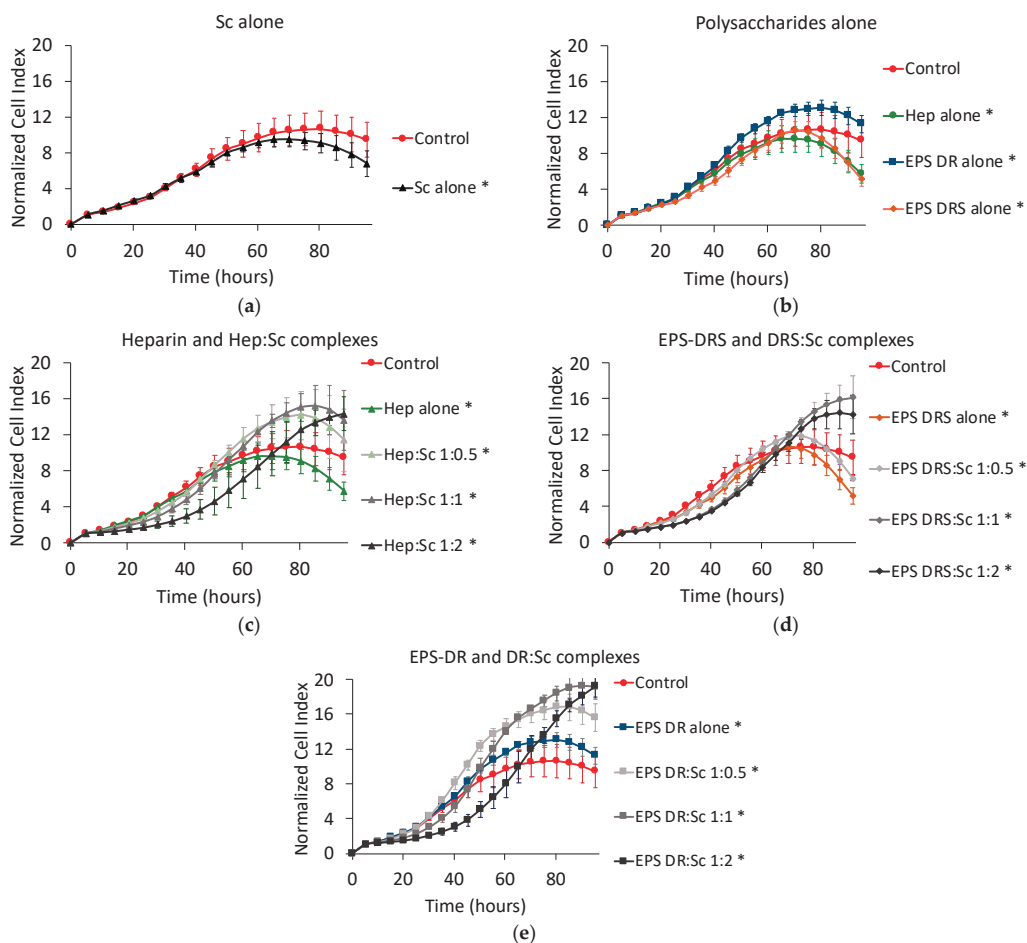

Figure 10. Normalized cell index plot of human U251 glioblastoma cells after 95 h of contact with (**a**) scandium at concentration of 100 μg mL^{-1} (*) and (**b**) polysaccharides alone at concentration of 100 μg mL^{-1}: heparin (*), EPS-DRS (*), EPS-DR (*)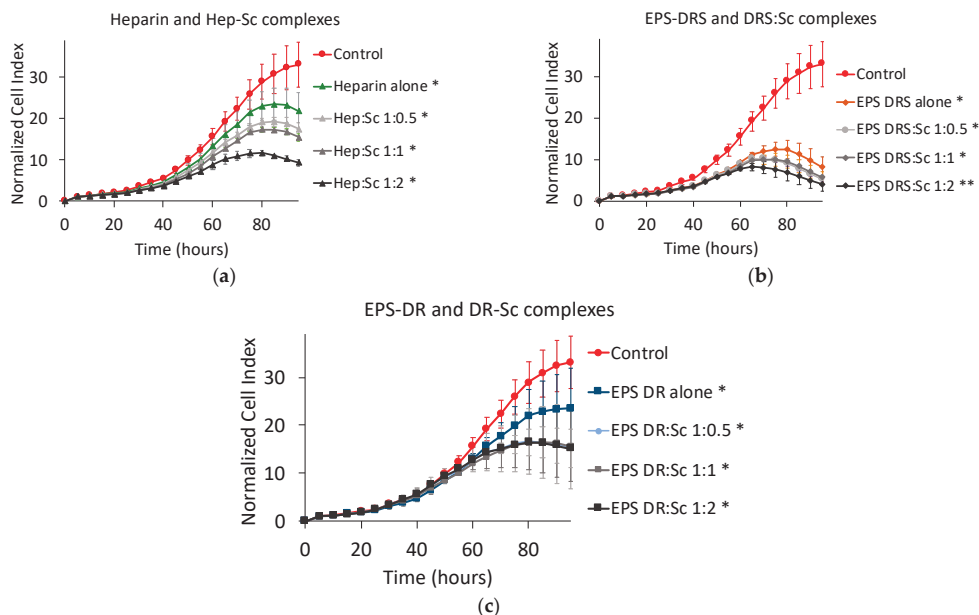. Normalized cell index plot of U251 cells after 95 h of contact with different scandium-polysaccharide complexes at concentration of 100 μg mL^{-1} and various stoichiometric ratios: (**c**) Hep:Sc 1:0.5 (*), 1:1 (*), 1:2 (*), heparin alone(*); (**d**) EPS-DRS:Sc 1:0.5 (*), 1:1 (*), 1:2 (*), EPS-DRS alone (*); (**e**) EPS-DR:Sc 1:0.5 (*), 1:1 (*), 1:2 (*), EPS-DR alone (*). * = *p* value ≤ 0.0001.

2.6. Human MDA231 Breast Cancer Cells

Scandium alone slightly decreased the cell proliferation of breast cancer cell, as shown in Figure 11a. Among the polysaccharides alone, only EPS-DRS demonstrated highly reducing the kinetics of proliferation (Figure 11b).

Hep:Sc and EPS-DR:Sc complexes were more efficient than the respective polysaccharides alone only at the stoichiometric ratio L:M 1:1 (Figure 11c–e), but standard deviations were very high for all the curves. EPS-DRS:Sc complexes exhibited the same effect of the polysaccharide alone (Figure 11d).
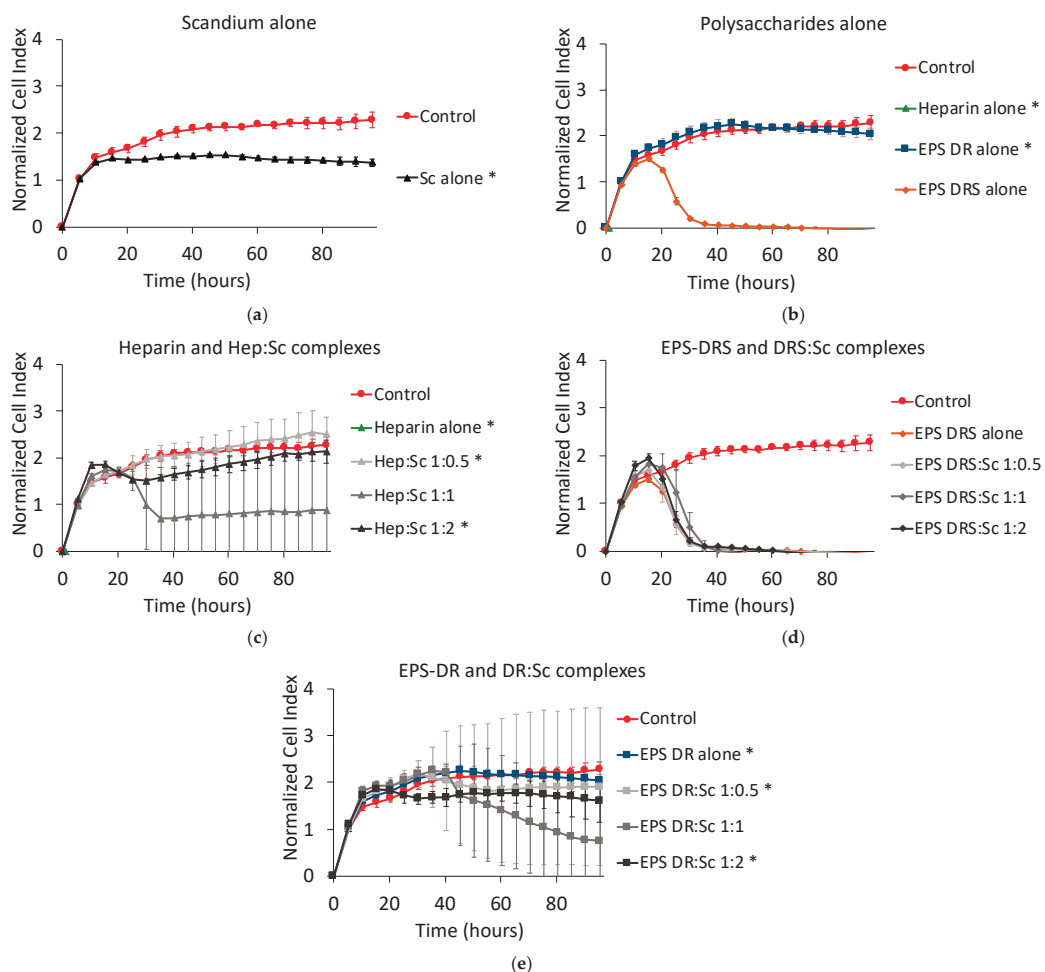
Figure 11. Normalized cell index plot of human MDA231 breast cancer cells after 95 h of contact with (**a**) scandium at concentration of 100 µg mL^{-1} (*) and (**b**) polysaccharides alone at concentration of 100 µg mL^{-1}: heparin (*), EPS-DRS, EPS-DR (*). Normalized cell index plot of MDA231 cells after 95 h of contact with different scandium-polysaccharide complexes at concentration of 100 µg mL^{-1} and various stoichiometric ratios: (**c**) Hep:Sc 1:0.5 (*), 1:1, 1:2 (*), heparin alone (*); (**d**) EPS-DRS:Sc 1:0.5, 1:1, 1:2, EPS-DRS alone; (**e**) EPS-DR:Sc 1:0.5 (*), 1:1, 1:2 (*), EPS-DR alone (*). * = p value $\leq$ 0.0001.

2.7. Human Caco2 Colon Cancer Cells

For this cell line, the contact time was prolonged to 140 h to display significant effects of compounds. Scandium alone did not have any effect on cell proliferation of colon cancer cells, as shown in Figure 12a. Once again, only EPS-DRS demonstrated significantly reducing the kinetics of proliferation (Figure 12b).
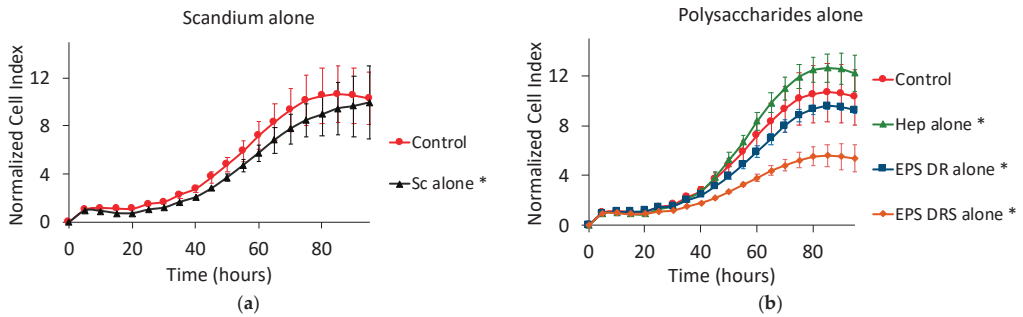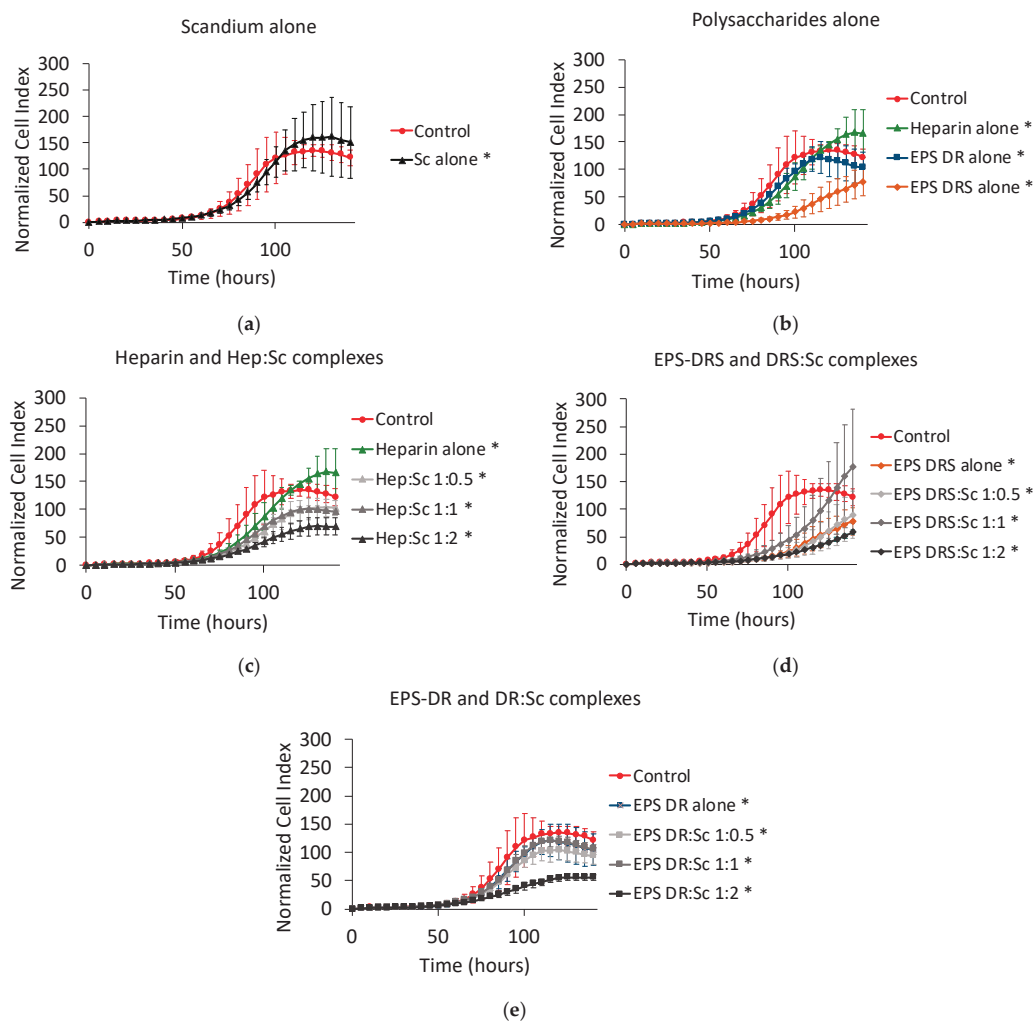
Figure 12. Normalized cell index plot of human Caco2 colon cancer cells after 140 h of contact with (**a**) scandium at concentration of 100 μg mL^{-1} (*) and (**b**) polysaccharides alone at 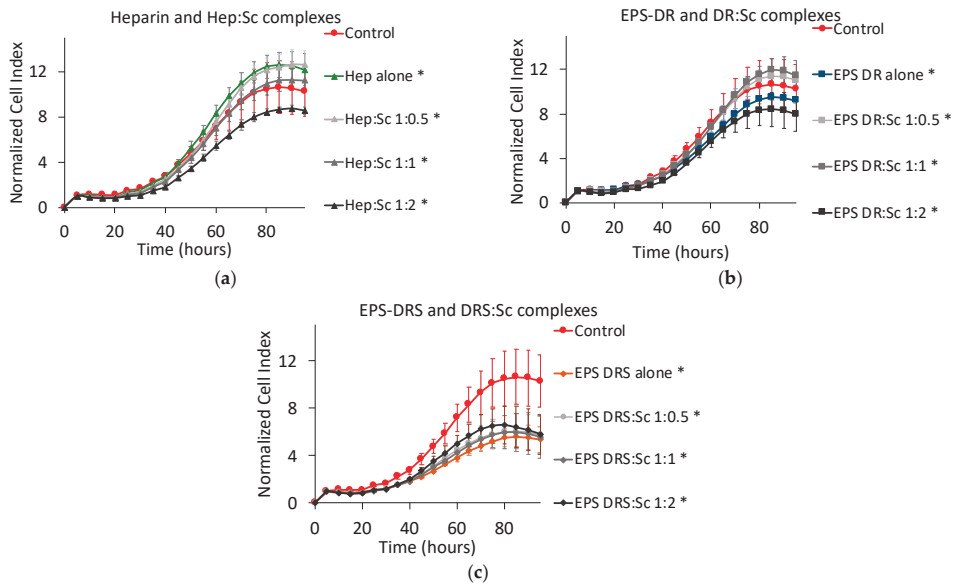concentration of 100 μg mL^{-1}: heparin (*), EPS-DRS (*), EPS-DR (*). Normalized cell index plot of Caco2 colon cancer cells after 140 h of contact with different scandium-polysaccharide complexes at concentration of 100 μg mL^{-1} and various stoichiometric ratios: (**c**) Hep:Sc 1:0.5 (*), 1:1 (*), 1:2 (*), heparin alone (*); (**d**) EPS-DRS:Sc 1:0.5 (*), 1:1 (*), 1:2 (*), EPS-DRS alone (*); (**e**) EPS-DR:Sc 1:0.5 (*), 1:1 (*), 1:2 (*), EPS-DR alone (*). * = *p* value ≤ 0.0001.

Hep:Sc and EPS-DR:Sc complexes were more efficient than the respective polysaccharides alone only at the stoichiometric ratio of 1:2 (Figure 12c,e). EPS-DRS:Sc complexes exhibited the same effect of the polysaccharide alone (Figure 12d), except at the ratio 1:1.

Table 1 summarizes the effect of Hep:Sc and EPS:Sc complexes for different metal-to-ligand ratio and different concentrations on human osteosarcoma, melanoma, lung cancer, glioblastoma and breast cancer cell lines.

Table 1. Summary of the effect of Hep:Sc and EPS:Sc complexes for different metal-to-ligand ratio and different concentrations on MNNG/HOS, A375, A549, U251, MDA231 and Caco3. + = low anti-proliferative effect, ++ = medium anti-proliferative effect, +++ = high anti-proliferative effect, − = low proliferative effect, − − = medium proliferative effect, − − − = high proliferative effect, NT = not tested.

Complex	Ratio	Total Conc. of GAGs	Total Conc. of Sc	Effect on Cell Proliferation					
				MNNG/HOS	A375	A549	U251	MDA231	Caco2
	M:L	µg mL⁻¹	µg mL⁻¹	Osteosarcoma	Melanoma	Lung	Glioblastoma	Breast Cancer	Colon Cancer
Hep:Sc	1:0.5	50	0.36	No effect			NT		
		100	0.71	+ + +	+ +	−	−	No effect	+
		200	1.42	+ + +			NT		
	1:1	50	0.71	+			NT		
		100	1.42	+ +	+ +	No effect	− −	+ +	+
		200	2.83	+ + +			NT		
	1:2	50	1.42	+ + +					
		100	2.83	+ + +	+ + +	+	− −	No effect	+ +
		200	5.66	+ + +					
	1:4	50	2.83	+ +			NT		
		100	5.66	+ +					
		200	11.32	+ +					
EPS-DRS:Sc	1:0.5	50	0.40	+ +					
		100	0.79	+	+ + +	+ +	+	+ + +	+
		200	1.58	+			NT		
	1:1	50	0.79	+ +			NT		
		100	1.58	+ +	+ + +	+ +	− −	+ + +	−
		200	3.16	+ + +			NT		
	1:2	50	1.58	+ + +					
		100	3.16	+ + +	+++	+ +	−	+ + +	+ +
		200	6.31	+ + +					
	1:4	50	3.16	+ + +			NT		
		100	6.31	+ +					
		200	12.62	+ + +					
EPS-DR:Sc	1:0.5	50	0.24	No effect					
		100	0.48	No effect	+ +	−	− −	No effect	+
		200	0.95	No effect			NT		
	1:1	50	0.48	+ + +			NT		
		100	0.95	+ + +	+ +	−	− − −	+ +	+
		200	1.90	+ + +			NT		
	1:2	50	0.95	+ +					
		100	1.90	+ + +	+ +	+	− − −	+	+ +
		200	3.79	+ + +					
	1:4	50	1.90	No effect			NT		
		100	3.79	No effect					
		200	7.58	No effect					

3. Discussion

3.1. Effect of Scandium Alone

Published data are quite scarce on scandium, which seems not having a major biological role. The food chain contains trace amounts of this metal, so the average daily intake per person is less than 0.1 μg [24]. To the best of our knowledge, the toxicity of scandium has not been reported. The major risk of scandium exposure could be aerosols and gasses that can be inhaled within a working environment (for instance rare-earth mining plants). A long-term exposure by inhalations may cause lung embolism. Kawai et al. [24] have reported that low concentrations of scandium can determine an overproduction of antibiotic when added to certain *Streptomyces* cultures.

In our study, a biological effect has been highlighted on the different cancer cell lines (osteosarcoma, lung, glioblastoma, melanoma, breast). The literature found on the evaluation of scandium has described an absorption and prolonged retention of scandium in some tissues [25], especially with accumulation in the liver, spleen and bone [26] or in the bone [27]. A complete biodistribution with $^{46}Sc^{3+}$ [28] has been performed. From the best of our knowledge, there is no reported data on in vitro cytotoxicity studies of scandium with osteosarcoma cells. Only one study from Herath and Evans [29] described the effect of scandium oxide (Sc_2O_3), that is a solid compound, on a commercial human osteoblast-like cell line (TE85 HOS). Scandium oxide showed a lower cell proliferation after 3 weeks of contact compared to the control. TE85 HOS represent the parental cells from which the MNNG/HOS cells were derivated after chemical transformation with 0.01 μg mL^{-1} MNNG (a carcinogenic nitrosamine). TE85 HOS parental cell line is not tumorigenic in mouse in contrast to MNNG/HOS. Herath and Evans [29] also demonstrated by cell viability studies, that Sc_2O_3 did not affect cell viability.

3.2. Effect of Heparin and EPS Alone

It is already known that GAG participate in the regulation of several cellular events, such as cell adhesion, proliferation and migration [4]. Actually, GAGs are heterogeneous macromolecules characterized by a high diversity of disaccharide units that forms the primary structure. Major differences include types of uronic acid and hexosamine, number and position of *O*-sulfated and *N*-sulfated groups, resulting in GAGs with different chemical and biological properties [30]. Among GAGs, heparin has already showed a significant antiproliferative effect on various cell types [31–33]. Studies have demonstrated that high contents in heparin structure of iduronic acid (IdoA) and N-sulfated glucosamine (GLcN) are fundamental to inhibit cell proliferation [31]. The degree of sulfation has also revealed to be a critical factor in the inhibition of cell proliferation [31]. Nikitovic et al. [34] have proved a strong inhibition of cell proliferation of both normal and transformed osteoblasts by heparin already at low concentrations. In our study, heparin reduced, the cell proliferation in a dose-dependent manner after 160 h, as shown in Figure 2a. This time, however, is not enough to observe the drop of NCI like in EPS-DRS. The higher degree of sulfation could be the cause of such drop. These results agree with the previous in vitro studies relating the effect of these EPS on cell proliferation of MNNG/HOS cells [19] and osteoblastic cells [15].

It has been shown that high concentrations of GAGs interrupted growth factor-receptor signaling in osteoblasts-like Saos-2 cells by sequestering growth factors (e.g., FGF2) and preventing their interaction with cell-surface receptors [35]. This biological effect could be realized also with EPS, explaining the slowdown in cell proliferation kinetics.

Cell viability after 160 h of contact with the polysaccharides alone has been also assessed using MTT assays (results are not showed in this paper), and it resulted high for the polysaccharide concentrations considered. Considering the fact that the cell viability measured through the MTT assays, reflects mitochondrial metabolism as biochemical marker of cell viability, it could be reasonable to think that the slowdown or drop of cell proliferation is not imputable to the blockade of this biochemical process. EPS, as GAG mimetics, interact with cell transmembrane proteins such as selectins and integrins,

responsible of cell adhesion and cell-cell interactions [36]. Since the decrease in proliferation kinetics reflects the detaching of cells from the gold biosensors in the well, it could be possible that the loss of adhesion could be derivate from the lack of normal functioning of these cell transmembrane proteins and not from an internal cell damage like the stop of metabolism.

In the literature there have been evidences on the role of heparin in lung cancer [37,38]. Low molecular weight heparins (LMWH) were found to have positive effects in decreasing the proliferation of metastasis through its anticoagulant and non-anticoagulant properties (inhibition of P- and L-selectins). The effects on cell proliferation on primary tumors are more contested since heparin and other GAGs do not seem to effectively reduce it [3,39]. By contrast, in the present study, an increase of proliferation of human lung cancer cells was clearly evidenced with heparin at the concentration of 100 µg mL^{-1} in Figure 11b, whereas EPS-DR and -DRS displayed a more moderate slowdown of the kinetics. It was evidenced also that the sulfation degree played a role on this proliferation kinetics. This increase of anti-proliferative effect with an increasing the degree of sulfation is in agreement with the results of Wright et al. [31].

LMWH have also been tested in the past on human melanoma cells displaying valid anti-proliferative effects [40]. Additional experiments on melanoma models have demonstrated a clear antimetastatic effect, attributable to the non-anticoagulant properties of heparin. The antimetastatic mechanism of that seems to reside in the inhibition of P- and L-selectins with consequent lack of cell-cell interactions [40]. In the present case, the different polysaccharides considered alone exhibited an anti-proliferative effect on the cell growth kinetics of human melanoma cells, revealing also that the degree of sulfation of these polysaccharides play a positive modulation on the proliferation by reducing it. These results agree with those showing another GAG [41], from animal environment, showing also a significant decrease in the proliferation of melanoma cells.

By contrast, the role of certain GAGs, such as chondroitin sulfate, is controversial in the pathogenesis of glioblastoma and breast cancer, since they seem enhance the tumor invasion [42,43]. The same stimulating effect on cell proliferation has been shown by heparin on colon cancer [44]. From the results presented in Figures 10b and 12b, heparin and both EPS-DR and -DRS presented a slight effect in reducing the proliferation of glioblastoma and colon cancer cells. Schnoor et al. [45] have also demonstrated in vitro that heparin can cause a decrease of glioblastoma cell growth. Concerning breast cancer cell, no significant effect on the decrease of proliferation is showed, except for EPS-DRS. Comparing the effect of these three polysaccharides of interest, EPS DRS revealed to be the most efficient in reducing the proliferation kinetics of all the four cell lines tested, especially on MNNG/HOS cells where the effect is dose dependent.

3.3. Synergic Effect of Complexes

Polysaccharide-scandium complexes (EPS-DR:Sc, EPS-DRS:Sc and Hep:Sc) are more efficient than their respective polysaccharides alone in reducing the cell proliferation. That was the case for all the cell lines tested, thus revealing that the complexation with scandium does not prevent the biological activity of these polysaccharides. There is a synergetic effect by combining these polysaccharides with scandium, since the anti-proliferative effect has risen.

3.3.1. Heparin:Sc (Hep:Sc)

On MNNG/HOS cell line, as shown in Figure 3, the complex Hep:Sc with a 1:0.5 metal-to-ligand ratio appears the most efficient complex in reducing the NCI to almost zero, followed by the metal-to-ligand ratio 1:2 of Hep:Sc. Both complexes exhibit a dose–response effect; in particular for the complex Hep:Sc with a 1:1 metal-to-ligand ratio. From a clinical point of view, the change in concentration of this complex would allow controlling its therapeutic window, revealing a good candidate for the elaboration of a new therapeutic

strategy. The effect of the other complex seems to appear, instead, as an on-off effect, more difficult to control.

For the highest concentration for all the complexes tested on MNNG/HOS cells, the profile of their proliferation kinetics was quite different. The complexation with scandium and in particular, the different ratios seem to induce different effects. This could reside in a different polymer conformation assumed by heparin at different ratios of metal. From our previous work, the effect of added counterions on polysaccharide conformation has been assessed revealing how hydrodynamic volume and gyration radius of this polyelectrolyte is influenced by the ionic strength, so by the opposite charges provided by the presence of metal ions. If the conformation of the polysaccharide changes, the way it interacts with its macromolecular targets would change as well, resulting in a different modulation of the biological effect [45].

Considering a fixed concentration of Hep:Sc complexes of 100 µg mL^{-1}, the increase of the metal to ligand ratio had an important effect also on human melanoma and colon cancer cell line. After 95 h of contact for melanoma cells (140 h for colon cancer cells), the ratio 1:2 seems to exhibit the most pronounced anti-proliferative effect, whereas the decrease in cell proliferation is clearly dependent on the L:M ratio. The change in conformation mediated by the complexation would positively modulate the biological effect. By contrast, the proliferation kinetic on human lung cancer, glioblastoma and breast cancer cells did not seem to be impacted by the complex. This behavior indicates that heparin is not efficient as anti-proliferative agent on primary tumors generated from these three human cancer cell lines.

3.3.2. EPS-DRS:Sc and EPS-DR:Sc

Considering the effect of EPS-DR:Sc complexes on human osteosarcoma, melanoma cells, and colon cancer cells, the metal-to-ligand ratio of 1:1 and 1:2 revealed to have a significant impact on cell proliferation. One explanation of these two different kinetics may be related to the fact that complexation with scandium at these ratio lead into a change of conformation, this may inhibit cell proliferation for contact time superior to 90 h and at high concentrations of EPS. For metal-to-ligand ratio of 1:0.5 and 1:4, that are comparable, they show a very similar effect compared to EPS DR alone.

The same EPS-DR:Sc complexes did not display the same effect on human lung cancer, glioblastoma and breast cancer cell lines meaning that the slowdown in cell proliferation is not related to this specific kind of tumor. This seems in agreement with the fact that the biological effect normally influences only the formation of metastasis.

Glioblastoma appears to be not much sensitive to these GAG mimetics since even EPS-DRS:Sc did not show significant results in decreasing the proliferation kinetics. By the contrary, EPS-DRS:Sc revealed a great slowdown in the cell proliferation of human lung cancer, breast cancer, melanoma and colon cancer cell lines that was ratio dependent. The higher sulfate content of DRS may enhance the anticoagulant properties, resulting in a much stronger interaction with P- and L-selectins due the possibility to allow more electrostatic interactions with those proteins. Moreover, the possible change in conformation would act in a synergic way allowing a positive modulation of the anti-proliferative effect.

From cell assays, EPS-DRS:Sc with a 1:2 metal-to-ligand ratio, came out to be the best polysaccharide-scandium complex in reducing the cell proliferation of human osteosarcoma, human melanoma, human lung cancer, human breast cancer and colon cancer cells. These results confirm the importance of the degree of sulfation which positively enhances the cytostatic effect of these exopolysaccharides alone or complexed.

4. Materials and Methods

4.1. Molecules Assessed

Heparin sodium salt (M_w = 18,320 Da, S% = 10%) from porcine intestinal mucosa H4784 and scandium chloride hexahydrate were purchased from Sigma-Aldrich (Saint Quentin Fallavier, France). EPS derivatives DR (M_w = 16,440 Da, S% = 3%) and DRS

(M_w = 27,360 Da, S% = 15%) were kindly provided by LEMMMB laboratory of IFREMER (Nantes). Polysaccharide solutions (heparin, EPS-DR and EPS-DRS alone) were prepared at high concentration stock solutions (2×10^{-4} mol L^{-1}) in Milli-Q water; scandium alone solution was prepared at high concentration stock solution (10^{-1} mol L^{-1}) in Milli-Q water. For each of the three polysaccharides, a set of complexes with four stoichiometric metal-to-ligand ratio (1:0.5, 1:1, 1:2, 1:4) has been prepared by mixing different aliquots of the previous prepared stock solutions. Higher stoichiometric ratios have been excluded to avoid cytotoxic effects related to high ionic strengths.

Complexation between scandium and polysaccharides has been previously checked and displayed using Free-Ion Selective Radiotracer Extraction (FISRE) as described somewhere else [45]. FISRE was used to determine the stability constants of a complex L:M, at tracer level, using a cationic exchange resin Chelex 100, poured into the solutions. These solutions contained fixed 10^{-4} mol L^{-1} Sc^{3+} and varying ligand concentration from 10^{-9} to 10^{-3} mol L^{-1}. The resulting suspensions were daily monitored and adjusted to pH = 6. The separation of the solid and liquid phases was done by sedimentation. Aliquots of the supernatant from 0.4 to 1 mL were taken for ICP-AES analysis (ICP spectometer iCAP 6000 of Thermo Scientific, Illkirch, France).

M:L ratio has been established by preparing solutions where the concentration in mol/L of the metal was, from 0.5 to 4 times the one of ligand. After preparation, all 16 compounds (Sc alone, heparin alone and the four complexes Hep:Sc, EPS-DRS alone and the four complexes EPS-DRS:Sc, DR alone and the four complexes DR:Sc) were filtered with a 13 μm syringe filter before being frozen to prevent bacteria contamination. Fresh dilutions at 200, 100 and 50 μg/mL of each compound were obtained right before the experiments adding cell culture medium to aliquots from stock solutions.

4.2. Proliferation Assay

Human MNNG/HOS osteosarcoma cell line, A375 melanoma, A549 lung cancer, U251 glioblastoma, MDA231 breast cancer and Caco2 colon cancer cell lines were purchased from the American Tissue Cell Collection (ATTC, Molsheim, France). Human MNNG/HOS osteosarcoma cell line (ATCC) was cultured with DMEM high glucose, pyruvate, non-glutamine from Gibco (Thermo-Fisher), supplemented with glutamine (Thermo-Fisher) and 10% of fetal bovine serum (FBS, Thermo-Fisher). Human A375 melanoma cell line (ATCC) was cultured with DMEM 4.5 g/L high glucose, pyruvate, non-glutamine from Gibco (Thermo-Fisher), supplemented with glutamine (Thermo-Fisher) and 5% of fetal bovine serum (FBS, Thermo-Fisher). Human A549 lung cancer cell line (ATCC) was cultured with DEMEM/F12 (Sigma Aldrich), supplemented with glutamine (Thermo-Fisher) and 5% of fetal bovine serum (FBS, Thermo-Fisher). Human U251 glioblastoma cell line (ATCC) was cultured with DMEM 4.5 high glucose, pyruvate, non-glutamine from Gibco (Thermo-Fisher), supplemented with glutamine (Thermo-Fisher) and 5% of fetal bovine serum (FBS, Thermo-Fisher). Human MDA231 breast cancer cell line (ATCC) was cultured with L-15 media from Gibco (Thermo-Fisher), supplemented with glutamine (Thermo-Fisher) and 5% of fetal bovine serum (FBS, Thermo-Fisher). Human Caco2 colon cancer cell line (ATCC) was cultured with DMEM 4.5 g/L high glucose, pyruvate, non-glutamine from Gibco (Thermo-Fisher), supplemented with glutamine (Thermo-Fisher) and 5% of fetal bovine serum (FBS, Thermo-Fisher).

Cells were incubated at 37 °C with humidity saturated controlled atmosphere and 5% CO_2. At confluence, cells are detached using Trypsin (Thermo-Fisher) and washed to neutralize the enzyme. MNNG/HOS cells were seeded in triplicate at 5000 cells per well (50 μL) with 50 μL of culture medium (to measure the background) for 4 h, the time necessary for cell seeding, in an E-Plate view 96 (Chem Agilent, Santa Clara, CA, USA) before adding 100 μL of compound at the three concentrations (50, 100 and 200 μg mL^{-1} for MNNG/HOS cells, 100 μg mL^{-1} for A375, A549, U251 cells). The choice of these concentrations provided a wide range to study a possible dose dependent response. Proliferation curves are normalized respect the time point of drug incorporation. The plate was

monitored for 160 h (MNNG/HOS cells), 140 h (Caco2 cells) and 95 h (A375, A549, U251, MDA231 cells) using a RTCA instruments (Agilent and ACEA, Santa Clara, CA, USA). Experiments have been done in triplicates and repeated twice. Statistical tests have been conducted using Regression Data Analysis Tool in Excel®.

4.3. Viability Assay

MNNG/HOS cells were seeded in triplicate at 3000 cells par well (50 µL) with 50 µL of culture medium for 4 h in an E-Plate view 96 (Chem Agilent) before adding 100 µL of compound at the three concentrations (50, 100 and 200 µg mL^{-1}). The choice of these concentrations provided a wide range to study a possible dose dependent response. The plate was left 160 h: the volume of each well was reduced to 100 µL before adding 10 µL of 5 mg/mL MTT (Sigma-Aldrich) and incubating for at least 3 h at 37 °C and 5% CO_2. After this time, the liquid was removed and 200 µL of DMSO was added to each well to dissolve the formed formazan crystals before proceeding to the colorimetric quantification with a multi-well spectrophotometer (Victor 3x from PerkinElmer, Villebon-sur-Yvette, France) at the wavelength of 500–600 nm.

5. Conclusions

This in vitro study has demonstrated the biological effects of these unconventional exopolysaccharides. EPS derivatives (-DR or -DRS). EPS derivatives can slowdown cell proliferation kinetic, confirming their anti-proliferative effect on human osteosarcoma cells without significantly influencing the cell viability. Close results have been found also on human melanoma cells, while human glioblastoma cells have not been affected by those EPS derivatives. The anti-proliferative effect on other cell lines (i.e., human osteosarcoma, melanoma, breast cancer and lung cancer) is effective with polysaccharides but even more enhanced when EPS derivatives, and heparin, are complexed to scandium, in which the impact on the NCI is dose–response. The degree of complexation is represented by the different metal-to-ligand ratio. Different behaviors in the decrease of the proliferation kinetic have been evidenced depending on the metal-to-ligand ratio, that could be related to a conformation change of the polysaccharide when complexed with scandium. EPS-DRS:Sc with a 1:2 metal-to-ligand ratio has been shown to be the most effective compound in displaying a cytostatic effect. Our group has evidenced in a previous work [45] that the rheological behavior of EPS derivatives and heparin, notably the conformation, is influenced by the ionic strength of solvent, as well as at different concentrations of scandium. Thus, it is assumed that the change in conformation could modulate positively or negatively the antiproliferative effect. Concerning the cause of the antiproliferative or cytostatic effect, a damage in the cellular metabolism does not seem to be implicated since the cells remain viable, at least in the time frame of our study. The most probable explanation would be that an inhibition of growth factor-receptor signaling, as well as an interference of cell-cell adhesion mediated by specific transmembrane proteins.

These results are very encouraging in a theranostic perspective because of the intrinsic tropism of these EPS derivatives for cancer cells is maintained, even after the complexation. Additionally, the anti-proliferative effect on certain cell lines could be modulated by the degree of complexation. In the near future, the influence of the degree of complexation will be performed to investigate which are the best metal-to-ligand ratio in terms of efficacy. Besides, xCELLigence assay with EPS derivatives could be extended to other cell lines known to be sensible to GAG properties, while testing new assays to target other cellular mechanisms involved in cellular toxicity. Moreover, the biological effects of these EPS will be tested on normal cells as well in order to guarantee no cytostatic effect on healthy cells. The efficacy of these compounds will be evaluated with the PET tracer of $^{44m/44}$Sc.

Author Contributions: Conceptualization, S.H.-M., D.H., and S.C.-J.; methodology, D.H., J.M.-G., M.M. and S.C.-J.; software, J.M.-G.; validation, D.H., S.H.-M. and S.C.-J.; formal analysis, J.M.-G., M.M.; investigation, J.M.-G., M.M.; resources, C.S., S.C.-J.; data curation, M.M., J.M.-G.; writing—original draft preparation, M.M.; writing—review and editing, D.H., J.M.-G., S.C.-J., S.H.-M., C.A.;

visualization, D.H., S.H.-M.; supervision, D.H., S.H.-M.; project administration, S.H.-M.; funding acquisition, S.H.-M. All authors have read and agreed to the published version of the manuscript.

Institutional Review Board Statement: Not applicable.

Informed Consent Statement: Not applicable.

Data Availability Statement: Data available in a publicly accessible repository. The data presented in this study are openly available at [10.3390/md19030174].

Conflicts of Interest: The authors declare no conflict of interest.

Abbreviations

CI	cell index
EPS	exopolysaccharides
GAG	glycosaminoglycanes
LMW	low molecular weight
LMWH	Low molecular weight heparins
NCI	normalized cell index
RTCA	Real Cell Time Analysis

References

1. Borsig, L. Antimetastatic activities of heparins and modified heparins. Experimental evidence. *Thromb. Res.* **2010**, *125*, S66–S71. [CrossRef]
2. Yip, G.W.; Smollich, M.; Götte, M. Therapeutic value of glycosaminoglycans in cancer. *Mol. Cancer Ther.* **2006**, *5*, 2139–2148. [CrossRef]
3. Belting, M. Glycosaminoglycans in cancer treatment. *Thromb. Res.* **2014**, *133*, S95–S101. [CrossRef]
4. Afratis, N.; Gialeli, C.; Nikitovic, D.; Tsegenidis, T.; Karousou, E.; Theocharis, A.D.; Pavão, M.S.; Tzanakakis, G.N.; Karamanos, N.K. Glycosaminoglycans: Key players in cancer cell biology and treatment: GAG Targeting in Cancer Cell Biology. *FEBS J.* **2012**, *279*, 1177–1197. [CrossRef] [PubMed]
5. Lyman, G.H. Thromboprophylaxis with low-molecular-weight heparin in medical patients with cancer. *Cancer* **2009**, *115*, 5637–5650. [CrossRef]
6. Debourdeau, P.; Elalamy, I.; De Raignac, A.; Méria, P.; Gornet, J.M.; Amah, Y.; Korte, W.; Marty, M.; Farge, D. Long-term use of daily subcutaneous low molecular weight heparin in cancer patients with venous thromboembolism: Why hesitate any longer? *Support. Care Cancer* **2008**, *16*, 1333–1341. [CrossRef] [PubMed]
7. Bendas, G.; Borsig, L. Cancer Cell Adhesion and Metastasis: Selectins, Integrins, and the Inhibitory Potential of Heparins. *Int. J. Cell Biol.* **2012**, *2012*, 1–10. [CrossRef] [PubMed]
8. Köwitsch, A.; Zhou, G.; Groth, T. Medical application of glycosaminoglycans: A review: Medical Application of Glycosaminoglycans. *J. Tissue Eng. Regen. Med.* **2018**, *12*, e23–e41. [CrossRef]
9. Senni, K.; Pereira, J.; Gueniche, F.; Delbarre-Ladrat, C.; Sinquin, C.; Ratiskol, J.; Godeau, G.; Fischer, A.-M.; Helley, D.; Colliec-Jouault, S. Marine Polysaccharides: A Source of Bioactive Molecules for Cell Therapy and Tissue Engineering. *Mar. Drugs* **2011**, *9*, 1664–1681. [CrossRef]
10. Jouault, S.C.; Mauray, S.; Theveniaux, J.; Sternberg, C.; Vidal, B.; Fischer, A.M.; Millet, J. Antithrombotic and Anticoagulant Activities of a Low Molecular Weight Fucoidan by the Subcutaneous Route. *Thromb. Haemost.* **1999**, *81*, 391–395. [CrossRef]
11. Guezennec, J. Deep-sea hydrothermal vents: A new source of innovative bacterial exopolysaccharides of biotechnological interest? *J. Ind. Microbiol. Biotechnol.* **2002**, *29*, 204–208. [CrossRef]
12. Colliec-Jouault, S.; Zanchetta, P.; Helley, D.; Ratiskol, J.; Sinquin, C.; Fischer, A.M.; Guezennec, J. Les polysaccharides microbiens d'origine marine et leur potentiel en thérapeutique humaine. *Pathol. Biol.* **2004**, *52*, 127–130. [CrossRef]
13. Roger, O.; Kervarec, N.; Ratiskol, J.; Colliec-Jouault, S.; Chevolot, L. Structural studies of the main exopolysaccharide produced by the deep-sea bacterium Alteromonas infernus. *Carbohydr. Res.* **2004**, *339*, 2371–2380. [CrossRef]
14. Raguénès, G.H.C.; Peres, A.; Ruimy, R.; Pignet, P.; Christen, R.; Loäec, M.; Rougeaux, H.; Barbier, G.; Guezennec, J.G. Alteromonas infernus sp. nov., a new polysaccharide-producing bacterium isolated from a deep-sea hydrothermal vent. *J. Appl. Microbiol.* **1997**, *82*, 422–430. [CrossRef]

15. Ruiz-Velasco, C.; Baud'Huin, M.; Sinquin, C.; Maillasson, M.; Heymann, D.; Colliec-Jouault, S.; Padrines, M. Effects of a sulfated exopolysaccharide produced by Altermonas infernus on bone biology. *Glycobiology* **2011**, *21*, 781–795. [CrossRef]

16. Chopin, N.; Sinquin, C.; Ratiskol, J.; Zykwinska, A.; Weiss, P.; Cérantola, S.; Le Bideau, J.; Colliec-Jouault, S. A Direct Sulfation Process of a Marine Polysaccharide in Ionic Liquid. *BioMed Res. Int.* **2015**, *2015*, 50865. [CrossRef] [PubMed]

17. Jouault, S.C.; Chevolot, L.; Helley, D.; Ratiskol, J.; Bros, A.; Sinquin, C.; Roger, O.; Fischer, A.-M. Characterization, chemical modifications and in vitro anticoagulant properties of an exopolysaccharide produced by Alteromonas infernus. *Biochim. Biophys. Acta* **2001**, *1528*, 141–151. [CrossRef]

18. Bruland, Ø.S.; Pihl, A. On the current management of osteosarcoma. A critical evaluation and a proposal for a modified treatment strategy. *Eur. J. Cancer* **1997**, *33*, 1725–1731. [CrossRef]

19. Heymann, D.; Ruiz-Velasco, C.; Chesneau, J.; Ratiskol, J.; Sinquin, C.; Colliec-Jouault, S. Anti-Metastatic Properties of a Marine Bacterial Exopolysaccharide-Based Derivative Designed to Mimic Glycosaminoglycans. *Molecules* **2016**, *21*, 309. [CrossRef] [PubMed]

20. Cutter, G.R.; Liu, Y. Personalized medicine: The return of the house call? *Neurol. Clin. Pract.* **2012**, *2*, 343–351. [CrossRef]

21. Huclier-Markai, S.; Alliot, C.; Sebti, J.; Brunel, B.; Aupiais, J. A comparative thermodynamic study of the formation of scandium complexes with DTPA and DOTA. *RSC Adv.* **2015**, *5*, 99606–99617. [CrossRef]

22. Mazza, M.; Alliot, C.; Sinquin, C.; Colliec-Jouault, S.; Reiller, P.E.; Huclier-Markai, S. Marine Exopolysaccharide Complexed With Scandium Aimed as Theranostic Agents. *Molecules* **2021**, *26*, 1143. [CrossRef]

23. Zhang, J.D. Introduction to the Data Analysis of the Roche XCELLigence—System with RTCA Package. 11. Available online: www.bioconductor.org\T1\guilsinglrightinst\T1\guilsinglrightdoc (accessed on 22 March 2021).

24. Permyakiv, E. *Metalloproteomics*; Wiley: Hoboken, NJ, USA, 2009.

25. Byrd, B.L.; Watson, E.E.; Cloutier, R.J.; Hayes, R.L. Effect of Stable Scandium on the Long-term Whole Body Retention of Intravenously Administered 46Sc Citrate in the Rat. *Health Phys.* **1975**, *29*, 375–379. [CrossRef] [PubMed]

26. Hirano, S.; Suzuki, K.T. Exposure, Metabolism, and Toxicity of Rare Earths and Related Compounds. *Environ. Health Perspect.* **1996**, *104*, 11.

27. Rosoff, B.; Siegel, E.; Williams, G.L.; Spencer, H. Distribution and excretion of radioactive rare-earth compounds in mice. *Int. J. Appl. Radiat. Isot.* **1963**, *14*, 129–135. [CrossRef]

28. Moghaddam-Banaem, L.; Jalilian, A.R.; Pourjavid, M.; Bahrami-Samani, A.; Mazidi, M.; Ghannadi-Maragheh, M. Preparation and Quality Control of Scandium-46 Bleomycin as a Possible Therapeutic Agent. *Iran. J. Nucl. Med.* **2012**, *20*, 6.

29. Herath, H.M.T.U.; Silvio, L.D.; Evans, J.R.G. Scandia—A potential biomaterial? *J. Mater. Sci. Mater. Electron.* **2005**, *16*, 1061–1065. [CrossRef]

30. Lima, M.; Rudd, T.; Yates, E. New Applications of Heparin and Other Glycosaminoglycans. *Molecules* **2017**, *22*, 749. [CrossRef]

31. Wright, T.C.; Castellot, J.J.; Petitou, M.; Lormeau, J.C.; Choay, J.; Karnovsky, M.J. Structural Determinants of Heparin's Growth Inhibitory Activity: Interdependence of oligosaccharide size and charge. *J. Biol. Chem.* **1989**, *264*, 1534–1542. [CrossRef]

32. Volpi, N.; Bolognani, L.; Conte, A.; Petrini, M. Effects of Chondroitin Sulfates with Different Structures on Leukemia Cells: U-937 Cell Proliferation and Differentiation. *Leuk. Res.* **1993**, *17*, 789–798. [CrossRef]

33. Syrokou, A.; Tzanakakis, G.; Tsegenidis, T.; Hjerpe, A.; Karamanos, N.K.; Potten, C.; Darzynkiewicz, Z.; Sasaki, K. Effects of glycosaminoglycans on proliferation of epithelial and fibroblast human malignant mesothelioma cells: A structure-function relationship. *Cell Prolif.* **1999**, *32*, 85–99. [CrossRef] [PubMed]

34. Nikitovic, D.; Zafiropoulos, A.; Tzanakakis, G.N.; Karamanos, N.K.; Tsatsakis, A.M. Effects of glycosaminoglycans on cell proliferation of normal osteoblasts and human osteosarcoma cells depend on their type and fine chemical compositions. *Anticancer. Res.* **2005**, *25*, 2851–2856.

35. Hausser, H.-J.; Brenner, R.E. Low doses and high doses of heparin have different effects on osteoblast-like Saos-2 cells in vitro. *J. Cell. Biochem.* **2004**, *91*, 1062–1073. [CrossRef] [PubMed]

36. Stevenson, J.L.; Varki, A.; Borsig, L. Heparin attenuates metastasis mainly due to inhibition of P- and L-selectin, but non-anticoagulant heparins can have additional effects. *Thromb. Res.* **2007**, *120*, S107–S111. [CrossRef]

37. Abu Arab, W.; Kotb, R.; Sirois, M.; Rousseau, É. The Role of Heparin in Lung Cancer. *J. Neoplasms* **2017**, *1*, 14–28. [CrossRef]

38. Kucukoner, M.; Isikdogan, A.; Kaplan, M.; Inal, A.; Zinciroglu, S.; Cit, M.; Cil, T.; Karadayi, B.; Dirie, A.; Yildiz, I. Can LMWH Improve the Outcome for Patients with Inoperable Stage III Non-Small Cell Lung Cancer? *Contemp. Oncol.* **2012**, *16*, 416. [CrossRef]

39. Morla, S. Glycosaminoglycans and Glycosaminoglycan Mimetics in Cancer and Inflammation. *Int. J. Mol. Sci.* **2019**, *20*, 1963. [CrossRef]

40. Bereczky, B.; Gilly, R.; Rásó, E.; Vágó, Á.; Tímár, J.; Tóvári, J. Selective antimetastatic effect of heparins in preclinical human melanoma models is based on inhibition of migration and microvascular arrest. *Clin. Exp. Metastasis* **2005**, *22*, 69–76. [CrossRef]

41. Ahn, M.Y.; Kim, B.J.; Kim, H.J.; Jin, J.M.; Yoon, H.J.; Hwang, J.S.; Park, K.-K. Anti-cancer effect of dung beetle glycosaminoglycans on melanoma. *BMC Cancer* **2019**, *19*, 1–12. [CrossRef]

42. Logun, M.T.; Wynens, K.E.; Simchick, G.; Zhao, W.; Mao, L.; Zhao, Q.; Mukherjee, S.; Brat, D.J.; Karumbaiah, L. Surfen-mediated blockade of extratumoral chondroitin sulfate glycosaminoglycans inhibits glioblastoma invasion. *FASEB J.* **2019**, *33*, 11973–11992. [CrossRef]

43. Gomes, A.M.; Stelling, M.P.; Pavão, M.S.G. Heparan Sulfate and Heparanase as Modulators of Breast Cancer Progression. *BioMed Res. Int.* **2013**, *2013*, 852093. [CrossRef] [PubMed]
44. Chatzinikolaou, G.; Nikitovic, D.; Asimakopoulou, A.; Tsatsakis, A.; Karamanos, N.K.; Tzanakakis, G.N. Heparin—A unique stimulator of human colon cancer cells' growth. *IUBMB Life* **2008**, *60*, 333–340. [CrossRef] [PubMed]
45. Schnoor, R.; Maas, S.L.N.; Broekman, M.L.D. Heparin in malignant glioma: Review of preclinical studies and clinical results. *J. Neuro Oncol.* **2015**, *124*, 151–156. [CrossRef] [PubMed]

Article

Expression and Characterization of a Cold-Adapted Alginate Lyase with Exo/Endo-Type Activity from a Novel Marine Bacterium *Alteromonas portus* HB161718[T]

Huiqin Huang [1,2,*], Shuang Li [1,3], Shixiang Bao [1,2], Kunlian Mo [1,2], Dongmei Sun [3] and Yonghua Hu [1,2,4,*]

1   Institute of Tropical Bioscience and Biotechnology, Hainan Institute for Tropical Agricultural Resources, CATAS, Haikou 571101, China; lishuangyouxiang@126.com (S.L.); baoshixiang@itbb.org.cn (S.B.); mokunlian@163.com (K.M.)
2   Hainan Provincial Key Laboratory for Functional Components Research and Utilization of Marine Bioresources, Haikou 571101, China
3   College of Life Science and Technology, Heilongjiang Bayi Agricultural University, Daqing 163000, China; sdmlzw@126.com
4   Laboratory for Marine Biology and Biotechnology, Pilot National Laboratory for Marine Science and Technology, Qingdao 266071, China
*   Correspondence: huanghuiqin@itbb.org.cn (H.H.); huyonghua@itbb.org.cn (Y.H.); Tel.: +86-898-66890695 (H.H.); +86-898-66890671 (Y.H.)

Abstract: The alginate lyases have unique advantages in the preparation of alginate oligosaccharides and processing of brown algae. Herein, a gene *alg2951* encoding a PL7 family alginate lyase with exo/endo-type activity was cloned from a novel marine bacterium *Alteromonas portus* HB161718[T] and then expressed in *Escherichia coli*. The recombinant Alg2951 in the culture supernatant reached the activity of 63.6 U/mL, with a molecular weight of approximate 60 kDa. Alg2951 exhibited the maximum activity at 25 °C and pH 8.0, was relatively stable at temperatures lower than 30 °C, and showed a special preference to poly-guluronic acid (polyG) as well. Both NaCl and KCl had the most promotion effect on the enzyme activity of Alg2951 at 0.2 M, increasing by 21.6 and 19.1 times, respectively. The TCL (Thin Layer Chromatography) and ESI-MS (Electrospray Ionization Mass Spectrometry) analyses suggested that Alg2951 could catalyze the hydrolysis of sodium alginate to produce monosaccharides and trisaccharides. Furthermore, the enzymatic hydrolysates displayed good antioxidant activity by assays of the scavenging abilities towards radicals (hydroxyl and ABTS+) and the reducing power. Due to its cold-adapted and dual exo/endo-type properties, Alg2951 can be a potential enzymatic tool for industrial production.

Keywords: alginate lyase; cold-adapted; exo/endo-type; *Alteromonas portus*; oligosaccharide; antioxidant activity

1. Introduction

Alginate is derived from the cell wall and intercellular substance of brown seaweed, accounting for approximately 22–44% (w/w) of seaweed biomass [1]. It is a kind of linear, water-soluble, and acidic polysaccharide composed of one or both of β-D-mannuronic acid (M) and its C-5 epimer α-L-guluronic acid (G) [2]. The M and G subunits form polyguluronic acid (poly-α-L-guluronate, polyG), polymannuronic acid (poly-β-D-mannuronate, polyM), and mixed random polymer (polyGM) in three types of block structures by α/β-1,4 glycosidic bonds [3]. Alginate is widely used in the field of food and pharmaceutical industry owing to its high viscosity and gelling properties. Further, it has attracted attention as a promising marine biomass for the production of biofuels and chemicals in biorefinery applications [4].

Alginate oligosaccharide (AOS) is an oligomer of alginate, which has the characteristics of low relative molecular weight, good solubility, high safety, and high stability. It is

reported that AOS has potential applications in agricultural, health product, and medical industries, since it exhibits significant pharmacological, physiological, and biological activities, including antioxidant, immunomodulation, antibacterial, antitumor, anticoagulation, and plant growth-promoting activities [5–7].

Alginate lyase is adopted to catalytically degrade alginate into AOS by *β*-elimination under relatively mild and controllable conditions. According to the substrate specificity, alginate lyases can be classified into three groups: polyM-specific lyase (EC 4.2.2.3), polyG-specific lyases (EC 4.2.2.11), and polyMG-specific lyases (EC 4.2.2) that can degrade polyG, polyM, and polyMG blocks of alginate, respectively [8]. Alginate lyases can be classified into endo- and exo-lytic fashions, according to the mode of degradation of alginate. Endolytic enzymes can cleave the glycosidic bonds inside the alginate with unsaturated oligosaccharides as the main products, while exotype ones can degrade oligomeric alginates and alginate polymers into monomers [9,10]. Furthermore, on the basis of their amino acid sequence similarities, the enzymes are generally grouped into seven polysaccharide lyases (PL) families in the Carbohydrate-Active Enzymes (CAZy) database—that is, PL-5, -6, -7, -14, -15, -17, and -18 [11,12]. Alginate lyases from the PL7 family have been widely studied, e.g., NitAly from *Nitratiruptor* sp. SB155-2 [13], lyA from *Isoptericola halotolerans* NJ-05 [14], Aly1281 from *Pseudoalteromonas carrageenovora* ASY5 [15], and MtAl138 from *Microbulbifer thermotolerans* DAU221 [16]. Alginate lyases are widely derived from marine algae; mollusks; and microorganisms (including bacteria, fungi, and viruses), among which marine bacteria are the most common resources. Many kinds of alginate lyase-secreting bacteria have been reported from marine bacteria, such as *Pseudoalteromona*, *Alteromonas*, *Microbulbifer*, *Zobellia*, *Vibrio*, and *Bacillus* [9,17–19].

In our previous study, a novel alginate lyase-producing strain, *Alteromonas portus*, was obtained from marine sand sample and taxonomically studied [17]. In this work, a gene *alg2951*, encoding alginate lyase Alg2951, was studied for a cloning, expression, and degradation product analysis. The results showed that Alg2951 was a cold-adapted PL7 alginate lyase with significant preference toward polyG. Moreover, Alg2951 was shown to be a NaCl- and KCl-activated enzyme with exolytic and endolytic activity, which released 4-deoxy-L-erythro-5-hexoseulose uronic acid (DEH) and trisaccharide from sodium alginate. In addition, the antioxidant capacity of the obtained AOS was investigated.

2. Results

2.1. Screening and Identification of Strain HB161718[T]

Based on the screening results by the plate assay and activity determination, strain HB161718[T] from coastal sand collected from Tanmen Port in Hainan, China showed a significant activity of alginate lyase. Two types of gellation reactions, white-halo and white-ring zone, were observed on the plate, which showed that two types of alginate lyases, polyM-specific and polyG-specfic iyases, were incubated (Figure S1). On a marine agar 2216 (Difco Laboratories, Detroit, MI, USA.) plate, the colonies were creamy, circular, smooth, and 1 to 2 mm in diameter after incubating at 30 °C for three days. Cells were Gram-stain-negative, rod-shaped with a width of approx. 0.8–1.1 μm and a length of 1.2–2.0 μm, and motile with a single polar flagellum (Figure S2). The 16S rRNA gene sequence (1455 bp) of strain HB161718[T] was sequenced (GenBank No. MG994978), and the phylogenetic analysis showed a close relationship to members of the genus *Alteromonas*. The results of the phenotypic, phylogenetic, and genotypic analyses clearly indicated that the alginate lyase-excreting isolate HB161718[T] was classified as a novel *Alteromonas* species, for which the name *Alteromonas portus* sp. nov. is proposed. The type strain is HB161718[T] (= CGMCC 1.13585[T] = JCM 32687[T]) [17].

2.2. Genome Sequencing and Bioinformatics Analysis of Alginate Lyase Alg2951

The draft genome of *Alteromonas portus* HB161718[T] comprises 32 contigs and 4,543,354 bp in length (GenBank No. SWCO00000000), with a depth coverage of 449×. The scaffold average length and *N50* are 141,979 bp and 453,001 bp, respectively. Genes (3,948) were

detected with 3,834 coding DNA sequences, and the DNA G+C content was 44.1%. A total of 143 proteins were matched with the CAZy database, including 39 glycoside hydrolases (GHs), 49 glycosyl transferases (GTs), 34 carbohydrate esterases (CEs), 10 polysaccharide lyases (PLs), and 11 auxiliary activities (AAs). Further analyses revealed that four of the putative PLs, Alg1687 (PL 17, accession number: WP136782264.1), Alg1691 (PL7, accession number: WP136781786.1), Alg2951 (PL7, accession number: WP136782863.1), and Alg3615 (PL7, accession number: WP136783496.1), were involved in alginate degradation.

The open reading frame (ORF) of the *alg2951* gene consists of 1,608 bp and encodes a 535-amino acid protein. The online analysis results showed that Alg2951 had a calculated molecular weight (Mw) of 60.66 kDa and the theoretical isoelectric point (pI) value of 5.13. It contained an alginate lyase domain of the PL7 family, and the N-terminal 25–43th amino acids were predicted to be a transmembrane region. To further confirm the attribution of Alg2951, a phylogenetic tree was constructed according to the amino acid sequences of Alg2951 and other reported alginate lyases. As shown in Figure 1, Alg2951 was clearly located in the same clade with the PL7 family alginate lyases and formed a distinct branch. Furthermore, Alg2951 showed the highest similarity (59.9%) with the PL7 alginate lyase (from *Pseudoalteromonas* sp. SM0524). The results of the sequence alignment and phylogenetic analysis imply that Alg2951 belongs to the PL7 family and is a novel member.
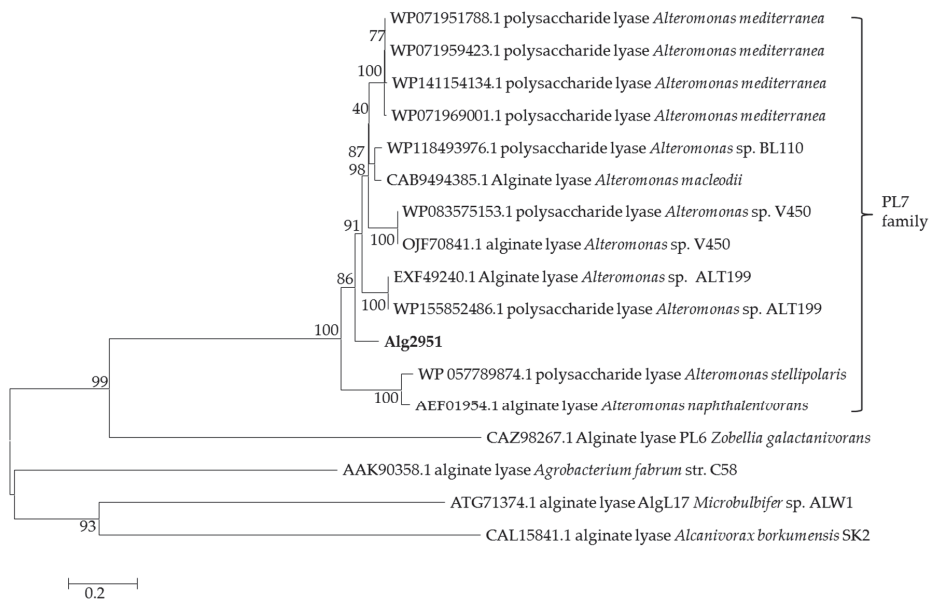
Figure 1. The neighbor-joining phylogenetic tree generated based on the amino acid sequences of the reported alginate lyases by the neighbor-joining method. Bootstrap values of 1000 trials were presented in the branching points.

Furthermore, a multiple sequence alignment was carried out between Alg2951 and eight well-characterized alginate lyases of the PL7 family (Figure 2). The eight alginate lyases included alginate lyase from *Corynebacterium* sp. ALY-1 (Accession: BAA83339.1), *Flavobacterium* sp. UMI-01 (Accession: BAP05660.1), *Klebsiella pneumoniae* (Accession: AAA25049.1), *Persicobacter* sp. CCB-QB2 (Accession: WP_053404615.1), *Pseudomonas aeruginosa* PAO1 (Accession: AAG04556.1), *Sphingomonas* sp. A1 (Accession: BAD16656.1), *Zobellia galactanivorans* Dsij[T] (Accession: CAZ98266.1), and *Zobellia galactanivorans* Dsij[T] (Accession: CAZ95239.1). The results showed that Alg2951 contained the typical conserved motifs of the PL7 family, such as "RS/TELRE", "QIH", and "YFKAG", which were re-

lated to the substrate combination and catalytic activity. These amino acids were verified by site-directed mutagenesis to bind the alginate substrate or to determine the catalytic activity [20]. For the PL7 family of alginate lyases, the conserved domain of the second region "QIH" means that it was more inclined to degrade polyG, while "QVH" meant that it was more inclined to use polyM as the substrate [21,22]. Thus, Alg2951 may be also a polyG-preferred alginate lyase.
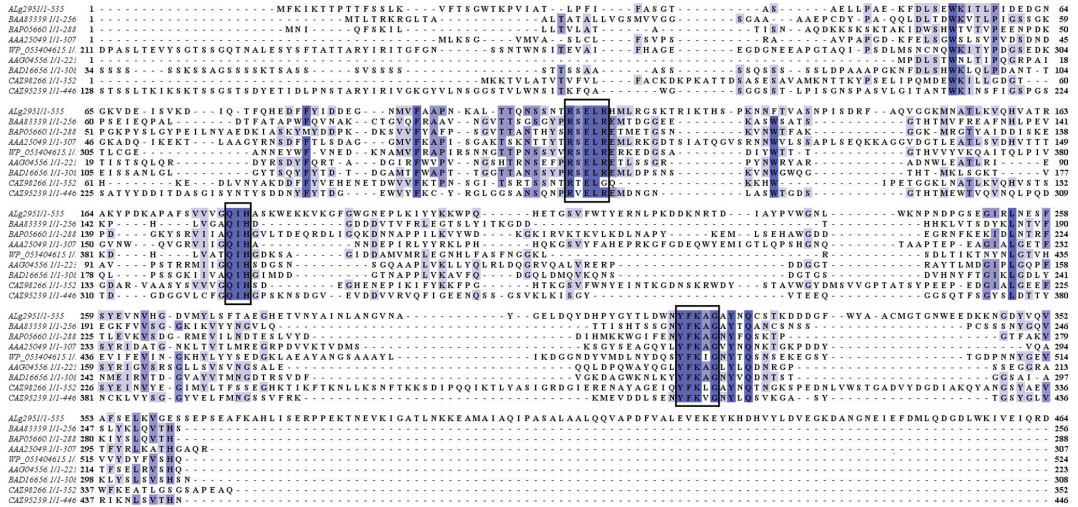
Figure 2. Multiple sequence alignments of Alg2951 and eight well-characterized alginate lyases of the PL7 family. The conserved amino acid regions are marked in the black boxes.

2.3. Expression, Purification, and Activity Detection of the Recombinant Alg2951 (rAlg2951)

To detect the enzyme activity of Alg2951, it was expressed in *Escherichia coli* with His-tag and purified by NTA-Ni Sepharose affinity chromatography. The results of the SDS-PAGE analysis showed that the purified protein appeared as a main band that was close to the predicted Mw of 60.66 kDa (Figure 3a). The alginate lyase activity of Alg2951 was tested by the plate assay and ultraviolet absorption method. The results of the plate assay showed that transparent circles were formed (Figure 3b), which suggested that the recombinant protein had alginate lyase activity. The size of the enzymolysis circle reflecteed the strength of the enzyme activity. Taking the empty vector-induced group and the noninduced group as controls, it was determined that the enzyme activity was produced by the induced recombinant protein, and the activity of Alg2951 was higher than that before purification.

The substrate specificity of Alg2951 was detected by measuring the increased absorbance at 235 nm of the unsaturated uronic acids that were generated from the oligomers via a β-elimination reaction. According to the results of the substrate specificity assay, the recombinant enzyme exhibited a higher activity with alginate and polyG than with polyM (Figure S3), and its ability to degrade polyM was only 2.1% of polyG. The result indicates that Alg2951 prefers to depolymerize polyG and is a member of polyG lyase, which is consistent with the previous prediction that Alg2951 is a polyG alginate lyase. Obviously, the recombinant enzyme could significantly act on polyG and sodium alginate. The preference of Alg2951 suggested it could be used for the production of guluronate oligosaccharides from polyG blocks and th epreparation of polyM blocks from sodium alginates via degrading the polyG and polyMG blocks [23,24]. Similar results were reported for alginate lyase from *Streptomyces* sp. A5 [25] and *Pseudomonas* sp. KS-408 [8], which were only specific for polyM or polyG. Meanwhile, some reported alginate lyases

possessed a broad substrate specificity, showing activity towards sodium alginate, polyG, and polyM [26,27].

Figure 3. (**a**) SDS-PAGE analysis of the recombinant Alg2951 expression and purification. Lane M, protein marker; lane 1, recombinant protein; lane 2, induced supernatant; and lane 3, the purified Alg2951. (**b**) Detection of alginate lyase activity. (1) Empty vector control, (2) noninduced control, (3) the induced group protein, and (4) the purified protein.
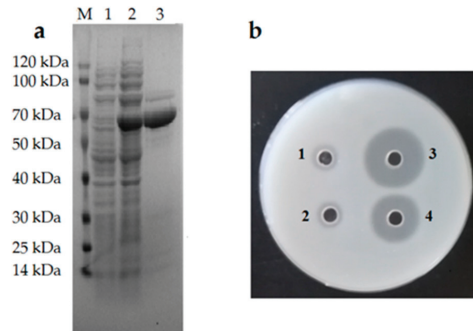
2.4. Temperature and pH Properties of the rAlg2951

The enzymatic properties of the purified recombinant Alg2951 were investigated. As shown in Figure 4a, Alg2951 exhibited a maximum enzyme activity at 25 °C. At the temperature range of 15–40 °C, Alg2951 manifested over 60% of the highest activity and 45.2% of the highest activity at remained 4 °C, while there was almost no detectable activity at 60 °C. These results suggest that Alg2951 has cold-adapted characteristics. The thermostability of Alg2951 was determined at a temperature ranging from 4 to 60 °C (Figure 4b). Alg2951 was relatively stable at temperatures lower than 30 °C; approximately 100% of the activity was maintained after incubation at less than 30 °C for 0.5 h. As the temperature rose above 30 °C, the activity declined dramatically; approximately 66.5% of the Alg2951 activity remained after being incubated at 40 °C for 0.5 h and was rapidly inactivated as the temperature increased, and the vast majority of the activity was lost above 50 °C. These results indicate that the thermostability of Alg2951 is quite low, further supporting that Alg2951 is a cold-adapted enzyme.

As shown in Figure 4c, the activity of Alg2951 was the highest at pH 8.0 but below 40% of the maximum activity when the pH value was lower than 7.0 or higher than 9.0. The activity of Alg2951 was stable at pH 8.0 but only retained about 40% of the activity at pH 7.0 and pH 9.0 (Figure 4d). Obviously, the pH has a great influence on the enzyme activity, and the acidic environment has more significant influence. It retained over 25% of the initial activity after being incubated at a pH range of 9.0–10.0, while only below 6.2% activity remained under pH 6.0.

Most of the reported alginate lyases showed their highest activity at about 40 °C [27–30]. In accordance with the other cold-adapted enzymes studied, the cold-adapted alginate lyases generally have lower optimal temperatures, higher low-temperature catalytic activities, and lower thermal stability than the mesophilic homologs [31]. The cold-adapted alginate lyase performed their optimal catalytic activities at less than 35 °C, generally unstable at temperatures higher than 30 °C, and commonly performed more than 50% of the highest activity at 20 °C [31,32]. Compared with the cold-adapted alginate lyases before [33], Alg2951 showed higher activity at 20 °C and possessed better thermostability at temperatures lower than 30 °C. During the catalytic process of cold-adapted alginate lyases, contamination, consumption energy, and inactivation difficulty can be reduced. Therefore, Alg2951 provides a new catalytic tool for potential industrial applications.
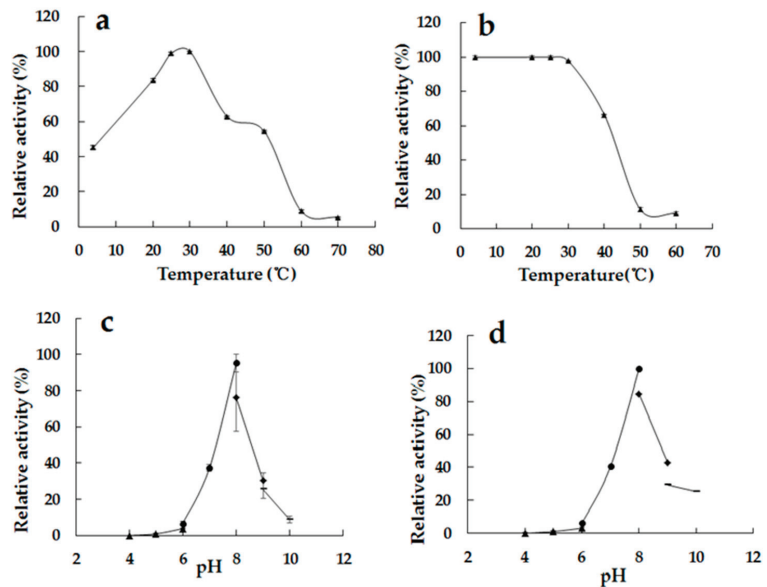
Figure 4. The biochemical characteristics of Alg2951. (**a**) Effect of different temperatures on the activity of Alg2951 (4–70 °C). (**b**) Effect of different temperatures on the stability of Alg2951 (4–60 °C). (**c**) Effect of different pH levels on the activity 2951. (pH 4–10). (**d**) Effect of different pH levels on the stability of Alg2951 (pH 4–10). The highest activity was taken as 100%. Data are given as the means ± standard deviation, *n* =3.

2.5. Effects of Ions and Compounds on the Activity of the Recombinant Alg2951

As shown in Figure 5a, the effects of metal ions and compounds (1 mM and 10 mM) on the activity of Alg2951 were detected. At 1 mM, K^+, Na^+, and Mg^{2+} displayed a slightly promoted effect on the enzyme activity. However, Mn^{2+} showed some inhibitory effect with 88.3% of the relative activity, followed by Fe^{2+} and Ba^{2+} with 79.0% and 73.3%, respectively. Zn^{2+} and the chelating agent ethylenediamine tetraacetic acid (EDTA) significantly inhibited the Alg2951 activity, resulting in an enzymatic activity below 35%. The addition of the surface-active agent SDS directly led to the loss of enzyme activity. Moreover, it was found that Na^+ and K^+ at 10 mM greatly increased the activity of Alg2951, reaching 1.4 and 4.0 times of the control group, respectively. Therefore, in the subsequent experiments, the effects of NaCl and KCl at different concentrations on the activity of Alg2951 were further studied.

In addition, as shown in Figure 5b, in the range of the KCl addition from 10 to 800 mM, the enzyme activity was greatly promoted. At a concentration of 0.2 M, the highest enzyme activity was 19.1 times that in the absence of KCl. NaCl had the same promotion effect on the enzyme activity, and the highest activity was even higher than that of the KCl group, reaching 21.6 times of that of the control group at 0.2 M (Figure 5c). Thus, an appropriate amount of KCl and NaCl can greatly promote the enzyme activity of Alg2951 and boost oligosaccharide production.

Lots of salt-activated alginate lyases were reported, the activities of which were increased by cations such as K^+, Na^+, Mg^{2+}, and Mn^{2+} [34–36]. In this work, Alg2951 was also a salt-activated alginate lyase, the activities of which could be increased by 21.6 and 19.1 times at 0.2-M NaCl and KCl, respectively. The powerful promoting effect of salt increases the feasibility of utilizing this alginate lyase for industrial applications.
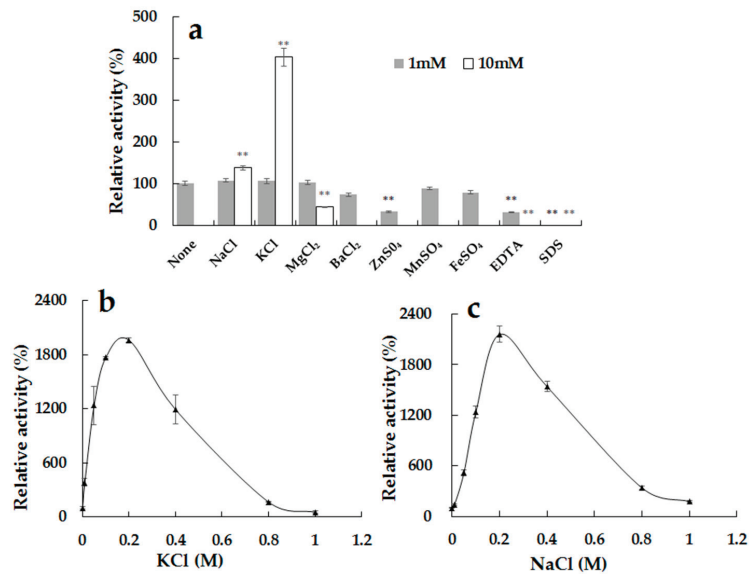
Figure 5. (**a**) Effects of metal ions, ethylenediamine tetraacetic acid (EDTA), and SDS on the activity of Alg2951. ** $p < 0.01$. (**b**) Effect of KCl on the activity of Alg2951. (**c**) Effect of NaCl on the activity of Alg2951. The reaction in the original alginate solution containing no extra substance was taken as 100%. Data are shown as the means ± standard deviation, $n = 3$.

2.6. Analysis of the Degradation Product

As shown in Figure 6a, the TLC result showed that the alginate degradation products hydrolyzed for 30 min at 25 °C by Alg2951 (the results performed for 60, 90, and 150 min had the same spots, and data were not shown). The results showed that the main reaction products of alginate were monosaccharide and trisaccharide. The final degradation product of Alg2951 for the alginate polymer was also analyzed by ESI-MS in negative-ion mode (Figure 6b). The peak at 175.02 m/z (ΔDP1 − H)$^-$ corresponded to the molecular mass of the unsaturated alginate monosaccharides and its conversion products DEH. The peak at 549.18 m/z (ΔDP3 + Na − H)$^-$ corresponded to the molecular masses of unsaturated alginate trisaccharide. The esults of the TLC and MS revealed that the Alg2951-mediated degradation of alginate produced DEH and trisaccharide. Taking into account the dominance of monosaccharides and trisaccharides in the hydrolysate, it could be inferred that Alg2951 had high efficiency exo- and endo-activity on the alginate. The product distribution of Alg2951 was similar to the other enzymes, which also exhibited dual endo-/exo-type activity. For example, PL17 family enzyme Alg17B from a marine strain BP-2 degraded alginate to produce oligosaccharides with DP of 2–6, and the main product was a monosaccharide [37], the PL17 family enzyme AlgSH17 from *Microbulbifer* sp. SH-1 also degraded alginate to produce a monosaccharide with small amounts of oligosaccharides with DP 2–6 [38], and the PL15 family alginate lyase from *Sphingomonas* sp. MJ-3 possessed endolytic and exolytic activity and generated both oligomers and monomers [10].
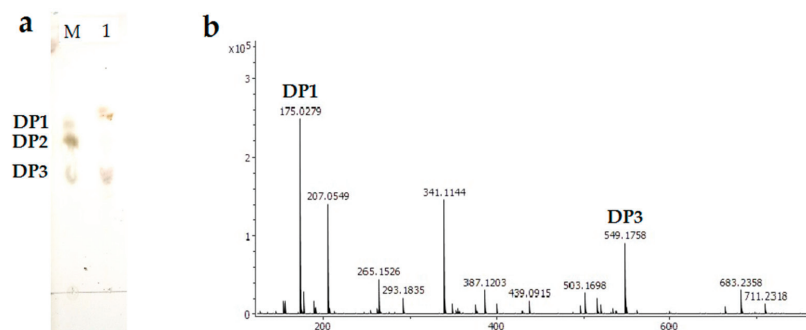
Figure 6. Degradation product analysis of alginate by purified Alg2951 with TLC (**a**) and ESI-MS (**b**). Lane M, the purified monomeric sugar, dimer, and trimer standards and Lane 1, the degradation products performed for 150 min. The DP1 and DP3 peaks represent a monosaccharide and trisaccharide, respectively. DP1 monosaccharide *m/z* 175 and DP3 (trisaccharide *m/z* 527 + Na$^+$ − H: *m/z* 549).

In most cases, the endo-type alginate lyases degrade alginate to produce unsaturated alginate oligosaccharides (AOS), while the exo-type alginate lyases degrade alginate or AOS to produce unsaturated monosaccharides, with the final product of 4-deoxy-L-erythro-5-hexoseulose uronic acid (DEH) by nonreductive conversion [39]. In bacteria, DEH can be converted into 2-keto-3-deoxygluconate (KDG) by a reductase, which is metabolized through the Entner-Doudoroff (ED) pathway [40]. There have been many exo-type alginate lyases reported so far—for example, AlgL17 from *Microbulbifer* sp. ALW1 [41], Atu3025 from *Agrobacterium tumefaciens* [39], Alg17C from *Saccharophagus degradans* 2–40 [42], and AlyFRB from *Falsirhodobacter* sp. alg1 [43]. In recent years, exo-type alginate lyase has received widespread attention, because the unsaturated monosaccharide produced by the degradation of alginate can be easily converted into DEH, a promising material for the production of bioethanol and chemicals [44]. Our results provided a new resource of DEH and trisaccharide.

2.7. Antioxidant Activity of the Hydrolysates from rAlg2951-Treated Sodium Alginate

Assays of reducing power and scavenging hydroxyl and ABTS radicals were used to assess the antioxidant activity. As shown in Figure 7a, AOS exhibited a concentration-dependent ability to scavenge hydroxyl radicals and showed a maximum activity of $92.34 \pm 0.32\%$ when applied at a concentration of 60.0 mg/mL. The activity was less at low concentrations of AOS, but high activity appeared at high concentrations (>50 mg/mL), stronger than the positive control ascorbic acid (Vc). The IC$_{50}$ value of scavenging hydroxyl was 30.93 mg/mL, which was significantly higher than that reported by Yang et al. (4.3 mg/mL) [38] and Zhang et al. (8.7 mg/mL) [15]. The ABTS radical is also used as a substrate to evaluate the free-radical scavenging ability of an antioxidant. In the present work, the oligosaccharide samples were able to scavenge the ABTS free radical even at low concentrations. As shown in Figure 7b, 15-mg/mL AOS exhibited an optimal ABTS radical scavenging activity of $82.2 \pm 0.3\%$; moreover, 10-mg/mL Vc exhibited an optimal activity of $80.3 \pm 0.4\%$. The IC$_{50}$ value of the ABTS radical was 2.17 mg/mL, which was lower than that of hydrolysates produced by alginate lyase Aly1281 (5.65 mg/mL) [15] and slightly higher than the hydrolysis by alginate lyase AlgL17 (1.85 mg/mL) [41]. It is reported that there is a direct relationship between the antioxidant activity and reducing power. The Fe^{3+} reduction ability is an important index of electron-donating activity [45]. In the reducing power assay (Figure 7c), at a concentration of 1–5 mg/mL, the reducing effects of AOS increased from 0.525 to 1.194 at 700 nm with increasing the enzyme concentration. The reducing power improved with the increased concentration of the samples, displaying a linear correlation, which indicated the ability of AOS to reduce ferric ions to ferrous

ions. Moreover, at the concentration of 5–20 mg/mL, the reducing power tended to be stable, showing a weak upward trend. In summary, the hydrolysis by Alg2951 resulted in mainly low-molecular-weight AOS (monosaccharides and trisaccharide), which present good scavenging activities of up to >92% and >82% toward hydroxyl and ABTS radicals, respectively. The disadvantage is that the hydroxyl radical scavenging effect can reach the ideal level when the AOS concentration is higher than 50 mg/mL, while only 47.7% at the concentration of 30 mg/mL. The AOS produced by the enzymatic hydrolysis of Alg2951 shows antioxidant activities and has great potential in the high-value processing of seaweed resources.
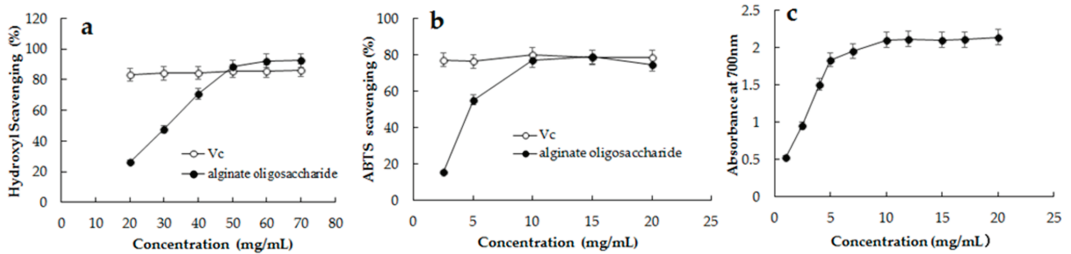
Figure 7. Antioxidant activities of the hydrolysis products from Alg2951-treated sodium alginate. (**a**) Scavenging effect on the hydroxyl radicals. (**b**) Scavenging effect on the ABTS radical. (**c**) Reducing ability. Data represent the mean ± standard deviation of triplicate measurements. Vc is the positive control.

3. Materials and Methods

3.1. Materials, Strains, and Plasmids

Sodium alginate derived from brown seaweed was purchased from Sangon (Shanghai, China). PolyM and polyG (purity > 90%) were purchased from Qingdao BZ Oligo Biotech Co., Ltd. (Qingdao, China). Other chemicals and reagents used in this study were of analytical grade, except that ethanol used to precipitate oligosaccharide was of chromatographic grade. *Escherichia coli* DH5α and BL21 (DE3) were from TransGen Biotech Co., Ltd. (Beijing, China). The pET28a (+) plasmid was used as the expression vector.

3.2. Screening and Identification of Strain HB161718[T]

Sediment samples were collected from Tanmen Port in Hainan, China (110°37′38′′ E, 19°14′13′′ N) in March 2017 and then spread on modified MA, which contained 5-g sodium alginate per liter additionally. Alginate lyase-excreting activity was tested by plate assay using 1-M calcium chloride as the enzyme-producing indicator [46]. Furthermore, the activity of alginate lyase was determined by the ultraviolet absorption method [47]. One unit of enzyme activity was defined as an increase of 0.1 in absorbance per min at 235 nm. Based on the combined phylogenetic relatedness and phenotypic and genotypic features, strain HB161718[T] was identified by polyphasic taxonomy [17].

3.3. Genome Sequencing and Bioinformatics Analysis of the Alginate Lyase

Genomic DNA was extracted using the bacterial genomic DNA fast extraction kit (Tiangen Biotech, Beijing, China). The draft genome sequence of strain HB161718[T] was sequenced by the Illumina HiSeq 2500 platform (2 × 150 paired-ends). The de novo genome assembly was performed using SPAdes version 3.5.0. Protein-coding sequences were predicted with Glimmer version 3.02 software, and polysaccharide lyases were predicted using the CAZy (Carbohydrate-Active Enzymes) database [48].

The open reading frame (ORF) of the DNA sequence was translated into the corresponding amino acid sequence using ORF finder (https://www.ncbi.nlm.nih.gov/orffinder/ (accessed on 10 May 2020)). The protein domain predictionwas performed by Simple Modular Architecture Research Tool (SMART) (http://web.expasy.org/protparam/ (accessed on 10 May 2020)). The signal peptide was analyzed using the SignalP-5.0 server

(http://www.cbs.dtu.dk/services/SignalP/ (accessed on 12 May 2020)) [49]. Domain analysis was performed in the SMART Database (http://smart.enbl-heidelberg.de/ (accessed on 12 May 2020)). The theoretical isoelectronic point (pI) and molecular weight (Mw) were predicted online (http://web.expasy.org/protparam/ (accessed on 12 May 2020)). The neighbor-joining phylogenetic tree was generated based on the reported alginate lyases using MEGA version 7.0 [50]. Multiple sequence alignment was performed among the characterized PL7 family alginate lyases using Clustal X (version 2.1) and obtained using Jalview V2.10.5.

3.4. Cloning, Expression, Purification, and Activity Detection of the Alginate Lyase Alg2951

The *alg2951* gene from the genomic DNA of strain HB161718[T] was used to design the primers for PCR amplification. The primers for cloning the *alg2951* gene (the forward primer: 5′-GGATCCATGTTTAAAATAAAAACAACGCCT-3′ and the reverse primer: 5′-AAGCTTATGTTTCCATTCTTCGCTTAG-3′, with the restriction sites of *BamHI* and *HindIII* in the forward and reverse primers underlined, respectively), were designed using primer premier 6 with reference to the *alg2951* gene sequence. The alginate lyase gene was then subcloned into the pET 28a (+) expression vector for heterologous expression. The recombinant *E. coli* BL21 (DE3) harboring the pET 28a (+)/*alg2951* was cultured in LB medium containing 100-μg ampicillin/mL and induced by adding 0.05-mM IPTG at 16 °C for 21 h. After expression, the cells were harvested by centrifugation and sonicated in lysis buffer. The recombinant protein included in the cell homogenate was purified by an NTA-Ni Spharose column and then analyzed by 12% sodium dodecyl sulfate polyacrylamide gel electrophoresis (SDS-PAGE).

The purified alginate lyase activity was tested by plate assay [46] and determined by the ultraviolet absorption method [47]. The enzyme activity assays of sodium alginate, polyM, and polyG were defined for investigating the substrate specificity. PolyM, polyG, and sodium alginate were dissolved, respectively, in 50-mM Na_2HPO_4-NaH_2PO_4 buffer (pH 7.0) with 3-mg/mL working concentration and used as the sole substrate in the test. The reactions were initiated by adding the appropriate enzyme and stopped by heating in boiling water for 10 min. The amount of yielded unsaturated uronic acid was monitored by recording the absorbance of the reaction mixture at 235 nm, using sodium alginate as the reference (100%).

3.5. Effects of Temperature and pH Properties Activity and Stability

To determine the optimal temperature, the enzyme activity was measured at various temperatures (4 °C, 25 °C, and 20–70 °C at 10 °C increments) and pH 8.0. To test the thermal stability, the enzyme was preincubated at various temperatures and pH 8.0 for 30 min. To determine the optimal pH, the enzyme activity was measured at various pHs (pH 4.0–10.0 at 1.0 increments) at 25 °C. To test the pH stability, the enzyme was preincubated at various pHs, 4 °C for 1 h. The alginate solution as a substrate was prepared in 10-mM buffers with different pH levels (Na_2HPO_4-NaH_2PO_4, pH 3.0–8.0; Tris-HCl, pH 8.0–9.0; and glycine-NaOH, pH 9.0–10.0). After each treatment, the enzyme activity was monitored by measuring the absorbance at 235 nm. All reactions were performed in triplicate.

3.6. Effects of Metal Ions and Compounds on Alg2951 Activity

To determine the metal ions and compounds, the enzyme activity was measured at 1-mM and 10-mM NaCl, KCl, $MgCl_2$, $BaCl_2$, $ZnSO_4$, $MnSO_4$, $FeSO_4$, ethylenediamine tetraacetic acid (EDTA), and sodium dodecyl sulfate (SDS), respectively, under the optimum temperature and pH conditions. The enzyme activity without the treatment or addition of extra substances was defined as 100%. All reactions were performed in triplicate.

3.7. Analysis of Alg2951 Reaction Products

To elucidate the mode of action of Alg2951 toward the alginate, alginate degradation was performed with 10-g/L sodium alginate in 50-mM phosphate buffer (pH 8.0) as a

substrate. The reaction was initiated by the addition of purified Alg2951 (5 U) in a 1-mL reaction volume and performed at the optimal temperature of 25 °C for 30, 60, 90, and 150 min. The reaction solution was then inactivated by heating in boiling water for 10 min, and the polysaccharide was precipitated overnight with three times the volume of chromatography grade absolute ethanol. After centrifugation at 10,000 rpm for 15 min at 4 °C, the supernatant was freeze-dried with a vacuum freezer dryer and applied for TLC and ESI-MS analyses of the degraded products of Alg2951. In the TLC analysis of the oligosaccharide product, a TLC plate (Silica Gel 60 F 254, Merck, Darmstadt, Germany) was used. The solvent system was 1-butanol/acetic acid/water (2:2:1, *v/v*). The chromatography plate was sprayed with 5% (*v/v*) sulfuric acid in ethanol and then heated at 110 °C for 5 min to visualize spots of oligosaccharide. The monomeric sugar, dimer, and trimer standards were used as markers in TLC chromatography. The molecular mass of the main products obtained from the reaction of alginate with Alg2951 for 10 h was further determined via electrospray ionization mass spectrometry (ESI-MS). A total of 2-μL degradation product was loop-injected into the ESI-MS instrument (Bruker Daltonik GmbH, Bremen, Germany) and operated in negative-ion mode with the following settings: calibration dynamics, 2; capillary voltage, 4.00 kV; cone voltage, 20.00 V; source temperature, 150 °C; desolvation temperature, 350 °C; cone gas flow rate, 50 L/h; and desolvation gas flow, 500 L/h [51].

3.8. Antioxidant Activity of the Alginate Degradation Products of Alg2951

The freeze-dried AOS powder degraded at 25 °C for 30 min was applied for the antioxidant activity determination as described above. The assay of the ferric-reducing power of the AOS was carried out in accordance with the method described before [51,52]. The absorbance of the mixture was measured at 700 nm using distilled water as the blank. Hydroxyl radical scavenging activity was determined by using the hydroxyl free-radical scavenging capacity assay kit (Solarbio, Beijing, China), and the absorbance was measured at 536 nm. Total antioxidant activity was determined by using the total antioxidant capacity assay kit with a rapid ABTS method (Solarbio, Beijing, China), and the absorbance was measured at 414 nm. Distilled water and Vc were set as the blank and positive control, respectively. Antioxidant abilities were measured with reference to the procedures of the manuals [41].

4. Conclusions

In this work, alginate lyase Alg2951 was cloned from a novel marine bacterium *Alteromonas portus* HB161718[T], expressed extracellularly, and characterized. The cold-adapted Alg2951 performed its highest activity at 25 °C and performed more than 60% activity at 15–40 °C and was relatively stable at temperatures lower than 30 °C as well. Furthermore, it was a PL7 alginate lyase and could be powerfully promoted by sodium and potassium salts at a concentration of 0.2 M. Meanwhile, it specifically degraded polyG and sodium alginate but had almost no activity on polyM. The TLC and ESI-MS analyses indicated that it could hydrolyze sodium alginate to produce DEH and trisaccharide in an exolytic and endolytic manner. Moreover, the degradation products of alginate by Alg2951 exhibited good antioxidant activities by detecting the scavenging hydroxyl, ABTS radicals ability, and reducing power. This study hopefully provides a potential tool for pharmaceutical and industrial applications.

Conflicts of Interest: The authors declare no conflict of interest.

References

1. Sharma, S.; Horn, S.J. Enzymatic saccharification of brown seaweed for production of fermentable sugars. *Bioresour. Technol.* **2016**, *213*, 155–161. [CrossRef] [PubMed]
2. Pawar, S.N.; Edgar, K.J. Alginate derivatization: A review of chemistry, properties and applications. *Biomaterials* **2012**, *33*, 3279–3305. [CrossRef]
3. Zhu, B.W.; Yin, H. Alginate lyase: Review of major sources and classification, properties, structure-function analysis and applications. *Bioengineered* **2015**, *6*, 125–131. [CrossRef] [PubMed]
4. Lee, K.Y.; Mooney, D.J. Alginate: Properties and biomedical applications. *Prog. Polym. Sci.* **2012**, *37*, 106–126. [CrossRef] [PubMed]
5. Tusi, S.K.; Khalaj, L.; Ashabi, G.; Kiaei, M.; Khodagholi, F. Alginate oligosaccharide protects against endoplasmic reticulum-and mitochondrialmediated apoptotic cell death and oxidative stress. *Biomaterials* **2011**, *32*, 5438–5458. [CrossRef]
6. Zhang, Y.H.; Yin, H.; Zhao, X.M.; Wang, W.X.; Du, Y.G.; He, A.L.; Sun, K.G. The promoting effects of alginate oligosaccharides on root development in *Oryza sativa* L. mediated by auxin signaling. *Carbohydr. Polym.* **2014**, *113*, 446–454. [CrossRef]
7. Liu, J.; Yang, S.; Li, X.; Yan, Q.; Reaney, M.J.T.; Jiang, Z. Alginate oligosaccharides: Production, biological activities, and potential applications. *Compr. Rev. Food Sci. Food Saf.* **2019**, *6*, 1859–1881. [CrossRef]
8. Kam, N.; Park, Y.J.; Lee, E.Y.; Kim, H.S. Molecular identification of a polyM-specific alginate lyase from *Pseudomonas* sp. strain KS-408 for degradation of glycosidic linkages between two mannuronates or mannuronate and gulronate in alginate. *Can. J. Microbiol.* **2011**, *57*, 1032–1041. [CrossRef]
9. Chen, X.L.; Dong, S.; Xu, F.; Dong, F.; Li, P.Y.; Zhang, X.Y.; Zhou, B.C.; Zhang, Y.Z.; Xie, B.B. Characterization of a new cold-adapted and salt-activated polysaccharide lyase family 7 alginate lyase from *Pseudoalteromonas* sp. SM0524. *Front. Microbiol.* **2016**, *7*, 1120–1128. [CrossRef]
10. Park, H.H.; Kam, N.; Lee, E.Y.; Kim, H.S. Cloning and characterization of a novel oligoalginate lyase from a newly isolated bacterium *Sphingomonas* sp. MJ-3. *Mar. Biotechnol.* **2012**, *14*, 189–202. [CrossRef]
11. Cantarel, B.L.; Coutinho, P.M.; Rancurel, C.; Bernard, T.; Lombard, V.; Henrissat, B. The carbohydrate-aactive enZymes database (CAZy): An expertre source for glycogenomics. *Nucleic Acids Res.* **2009**, *37*, D233–D238. [CrossRef]
12. Li, F.L.; Lu, M.; Ji, S.Q.; Wang, B. Biochemical and structural characterization of alginate lyases: An update. *Curr. Biotechnol.* **2015**, *4*, 223–239.
13. Inoue, A.; Anraku, M.; Nakagawa, S.; Ojima, T. Discovery of a novel alginate lyase from *Nitratiruptor* sp. SB155-2 thriving at deep-sea hydrothermal vents and identification of the residues responsible for its heat stability. *J. Bio. Chem.* **2016**, *291*, 15551–15563. [CrossRef]
14. Zhu, B.W.; Ning, L.M.; Jiang, Y.C.; Ge, L. Biochemical characterization and degradation pattern of a novel endo-type bifunctional alginate lyase AlyA from marine bacterium *Isopericola halotolerans*. *Mar. Drugs* **2018**, *16*, 258. [CrossRef]
15. Zhang, Y.H.; Shao, Y.; Jiao, C.; Yang, Q.M.; Weng, H.F.; Xiao, A.F. Characterization and application of an alginate lyase, Aly1281 from marine bacterium *Pseudoalteromonas carrageenovora* ASY5. *Mar. Drugs* **2020**, *18*, 95. [CrossRef] [PubMed]
16. Jeong, H.R.; Yoo, J.S.; Choi, Y.L.; Jang, Y.S.; Lee, Y.S. Characterization of an organic solvent-tolerant polysaccharide lyase from *Microbulbifer thermotolerans* DAU221. *Int. J. Biol. Macromol.* **2021**, *169*, 452–462. [CrossRef] [PubMed]
17. Huang, H.Q.; Mo, K.L.; Li, S.; Sun, D.M.; Zhu, J.; Zou, X.X.; Hu, Y.H.; Bao, S.X. *Alteromonas portus* sp. nov.; an alginate lyase–excreting marine bacterium. *Int. J. Syst. Evol. Microb.* **2020**, *70*, 1516–1521. [CrossRef] [PubMed]
18. Huang, H.Q.; Mo, K.L.; Hu, Y.H.; Liu, M.; Zhu, J.; Zou, X.X.; Bao, S.X. *Microbulbifer harenosus* sp. nov.; an alginate-degrading bacterium isolated from coastal sand. *Int. J. Syst. Evol. Microb.* **2020**, *70*, 1639–1643. [CrossRef] [PubMed]
19. Thomas, F.; Lundqvist, L.; Jam, M.; Jeudy, A.; Barbeyron, T.; Sandström, C.; Michel, G.; Czjzek, M. Comparative characterization of two marine alginate lyases from *Zobellia galactanivorans* reveals distinct modes of action and exquisite adaptation to their natural substrate. *J. Biol. Chem.* **2013**, *288*, 23021–23037. [CrossRef]

20. Zhu, B.W.; Sun, Y.; Ni, F.; Ning, L.M.; Yao, Z. Characterization of a new endo-type alginate lyase from *Vibrio* sp. NJU-03. *Int. J. Biol. Macromol.* **2018**, *108*, 1140–1147. [CrossRef]
21. Uchimura, K.; Miyazaki, M.; Nogi, Y.; Kobayashi, T.; Horikoshi, K. Cloning and sequencing of alginate lyase genes from deep-sea strains of *Vibrio* and *Agarivorans* and characterization of a new *Vibrio* enzyme. *Mar. Biotechnol.* **2010**, *12*, 526–533. [CrossRef] [PubMed]
22. Yamasaki, M.; Ogura, K.; Hashimoto, W.; Mikami, B.; Murata, K. A structural basis for depolymerization of alginate by polysaccharide lyase family-7. *J. Mol. Biol.* **2005**, *352*, 11–21. [CrossRef]
23. Huang, L.S.X.; Zhou, J.G.; Li, X.; Peng, Q.; Lu, H.; Du, Y.G. Characterization of a new alginate lyase from newly isolated *Flavobacterium* sp. S20. *J. Ind. Microbiol. Biotechnol.* **2013**, *40*, 113–122. [CrossRef] [PubMed]
24. Ochi, Y.; Takeuchi, T.; Murata, K.; Kawabata, Y.; Kusakabe, I. A simple method for preparation of poly-mannuronate using poly-guluronate lyase. *Biosci. Biotech. Biochem.* **1995**, *59*, 1560–1561. [CrossRef]
25. Cao, L.; Xie, L.; Xue, X.; Tan, H.; Liu, Y.; Zhou, S. Purification and characterization of alginate lyase from *Streptomyces* species strain A5 isolated from banana rhizosphere. *J. Agr. Food Chem.* **2007**, *55*, 5113–5117. [CrossRef] [PubMed]
26. Swift, S.M.; Hudgens, J.W.; Heselpoth, R.D.; Bales, P.M.; Nelson, D.C. Characterization of AlgMsp, an alginate lyase from *Microbulbifer* sp. 6532A. *PLoS ONE* **2014**, *9*, e112939. [CrossRef] [PubMed]
27. Li, S.Y.; Yang, X.M.; Bao, M.M.; Wu, F.; Yu, W.G.; Han, F. Family 13 carbohydrate-binding module of alginate lyase from *Agarivorans* sp. L11 enhances its catalytic efficiency and thermostability, and alters its substrate preference and product distribution. *FEMS Microbiol. Lett.* **2015**, *362*, fnv054. [CrossRef]
28. Mochizuki, S.; Nishiyama, R.; Inoue, A.; Ojima, T. A novel aldo-keto reductase, HdRed, from the pacific abalone *Haliotis discus hannai*, which reduces alginate-derived 4-deoxy-l-erythro-5-hexoseulose uronic acid to 2-keto-3-deoxy-d-gluconate. *J. Biol. Chem.* **2015**, *290*, 30962–30974. [CrossRef]
29. Kim, H.T.; Ko, H.J.; Kim, N.; Kim, D.; Lee, D.; Choi, I.G.; Woo, H.C.; Kim, M.D.; Kim, K.H. Characterization of a recombinant endo-type alginate lyase (Alg7D) from *Saccharophagus degradans*. *Biotechnol. Lett.* **2012**, *34*, 1087–1092. [CrossRef]
30. Zhu, B.W.; Ni, F.; Ning, L.M.; Sun, Y.; Yao, Z. Cloning and characterization of a new pH-stable alginate lyase with high salt tolerance from marine *Vibrio* sp. NJ-04. *Int. J. Biol. Macromol.* **2018**, *115*, 1063–1070. [CrossRef]
31. Li, S.Y.; Yang, X.M.; Zhang, L.; Yu, W.G.; Han, F. Cloning, expression, and characterization of a cold-adapted and surfactant-stable alginate lyase from marine bacterium *Agarivorans* sp. L11. *J. Microbiol. Biotechnol.* **2015**, *25*, 681–686. [CrossRef]
32. Xiao, L.; Feng, H.; Yang, Z.; Lu, X.Z.; Yu, W.G. A novel alginate lyase with high activity on acetylated alginate of *Pseudomonas aeruginosa* FRD1 from *Pseudomonas* sp. QD03. *World J. Microbiol. Biotechnol.* **2006**, *22*, 81–88. [CrossRef]
33. Wang, Z.P.; Cao, M.; Li, B.; Ji, X.F.; Zhang, X.Y.; Zhang, Y.Q.; Wang, H.Y. Cloning, secretory expression and characterization of a unique pH-stable and cold-adapted alginate lyase. *Mar. Drugs* **2020**, *18*, 189. [CrossRef] [PubMed]
34. Dou, W.F.; Wei, D.; Li, H.; Li, H.; Rahman, M.M.; Shi, J.S.; Xu, Z.H.; Ma, Y.H. Purification and characterisation of a bifunctional alginate lyase from novel *Isoptericola halotolerans* CGMCC 5336. *Carbohydr. Polym.* **2013**, *98*, 1476–1482. [CrossRef] [PubMed]
35. Chen, P.; Zhu, Y.M.; Men, Y.; Zeng, Y.; Sun, Y.X. Purification and characterization of a novel alginate lyase from the marine bacterium *Bacillus* sp. Alg07. *Mar. Drugs* **2018**, *16*, 86. [CrossRef] [PubMed]
36. Li, S.Y.; Wang, L.N.; Chen, X.H.; Zhao, W.W.; Sun, M.; Han, Y.T. Cloning, expression, and biochemical characterization of two new oligoalginate lyases with synergistic degradation capability. *Mar. Biotechnol.* **2018**, *20*, 75–86. [CrossRef]
37. Huang, G.; Wen, S.; Liao, S.; Wang, Q.; Pan, S.; Zhang, R.; Lei, F.; Liao, W.; Feng, J.; Huang, S. Characterization of a bifunctional alginate lyase as a new member of the polysaccharide lyase family 17 from a marine strain BP-2. *Biotechnol. Lett.* **2019**, *41*, 1187–1200. [CrossRef]
38. Yang, J.; Cui, D.; Ma, S.; Chen, W.; Chen, D.; Shen, H. Characterization of a novel PL 17 family alginate lyase with exolytic and endolytic cleavage activity from marine bacterium *Microbulbifer* sp. SH-1. *Int. J. Bio. Macro.* **2021**, *169*, 551–563. [CrossRef] [PubMed]
39. Ochiai, A.; Yamasaki, M.; Mikami, B.; Hashimoto, W.; Murata, K. Crystal structure of exotype alginate lyase Atu3025 from *Agrobacterium tumefaciens*. *J. Biol. Chem.* **2010**, *285*, 24519–24528. [CrossRef] [PubMed]
40. Kersters, K.; De Ley, J. The occurrence of the Entner–Doudoroff pathway in bacteria. *Antonie Van Leeuwenhoek* **1968**, *34*, 393–408. [CrossRef] [PubMed]
41. Jiang, Z.D.; Guo, Y.X.; Wang, X.X.; Lie, H.B.; Ni, H.; Li, L.J.; Xiao, A.F.; Zhu, Y.B. Molecular cloning and characterization of AlgL17, a new exo-oligoalginate lyase from *Microbulbifer* sp. ALW1. *Protein Expr. Purif.* **2019**, *161*, 17–27. [CrossRef]
42. Kim, H.T.; Chung, J.H.; Wang, D.; Lee, J.; Woo, H.C.; Choi, I.; Kim, K.H. Depolymerization of alginate into a monomeric sugar acid using Alg17C, an exo-oligoalginate lyase cloned from *Saccharophagus degradans* 2–40. *Appl. Microbiol. Biotechnol.* **2012**, *93*, 2233–2239. [CrossRef] [PubMed]
43. Mori, T.; Takahashi, M.; Tanaka, R.; Miyake, H.; Shibata, T.; Chow, S.; Kuroda, K.; Ueda, M.; Takeyama, H. *Falsirhodobacter* sp. alg1 harbors single homologs of endo and exo-type alginate lyases efficient for alginate depolymerization. *PLoS ONE* **2016**, *11*, e155537. [CrossRef] [PubMed]
44. Nakata, S.; Murata, K.; Hashimoto1, W.; Kawai, S. Uncovering the reactive nature of 4-deoxy-l-erythro-5-hexoseulose uronate for the utilization of alginate, a promising marine biopolymer. *Sci. Rep.* **2019**, *9*, 17147–17157. [CrossRef] [PubMed]
45. Liu, J.; Xu, J.; Zhang, X.; Zhou, F.; Lyu, P.; Zhao, Y. Ding, Preparation, composition analysis and antioxidant activities of konjac oligo–glucomannan. *Carbohyd. Polym.* **2015**, *130*, 398–404. [CrossRef] [PubMed]

46. Hisano, T.; Nishimura, M.; Yamashita, T.; Imanaka, T.; Muramatsu, T.; Kimura, A.; Murata, K. A simple method for determination of substrate specificity of alginate lyases. *J. Fermen. Bioeng.* **1994**, *78*, 182–184. [CrossRef]
47. Budi, S.W.; van Tuinen, D.; Arnould, C.; Dumas-Gaudot, E.; Gianinazzi-Pearson, V.; Gianinazzi, S. Hydrolytic enzyme activity of *Paenibacillus* sp. strain B2 and effects of the antagonistic bacterium on cell integrity of two soil-borne pathogenic fungi. *Appl. Soil. Ecol.* **2000**, *15*, 191–199. [CrossRef]
48. Lombard, V.; Golaconda Ramulu, H.; Drula, E.; Coutinho, P.M.; Henrissat, B. The carbohydrate-active enzymes database (CAZy) in 2013. *Nucleic Acids Res.* **2013**, *42*, D490–D495. [CrossRef] [PubMed]
49. Nielsen, H. Predicting secretory proteins with SignalP. *Methods Mol. Biol.* **2017**, *1611*, 59–73.
50. Kumar, S.; Stecher, G.; Li, M.; Knyaz, C.; Tamura, K. MEGA X: Molecular evolutionary genetics analysis across computing platforms. *Mol. Biol. Evol.* **2018**, *35*, 1547–1549. [CrossRef]
51. Zhu, B.; Hu, F.; Yuan, H.; Sun, Y.; Yao, Z. Biochemical characterization and degradation pattern of a unique pH-stable polyM-specific alginate lyase from newly isolated *Serratia marcescens* NJ-07. *Mar. Drugs* **2018**, *16*, 129. [CrossRef] [PubMed]
52. Gülçin, İ.; Bursal, E.; Şehitoğlu, M.H.; Bilsel, M.; Gören, A.C. Polyphenol contents and antioxidant activity of lyophilized aqueous extract of propolis from Erzurum, Turkey. *Food Chem. Toxicol.* **2010**, *48*, 2227–2238. [CrossRef] [PubMed]

Article

Potential of Exopolysaccharide from *Porphyridium marinum* to Contend with Bacterial Proliferation, Biofilm Formation, and Breast Cancer

Nesrine Gargouch [1,2], Fatma Elleuch [3,4], Ines Karkouch [5], Olfa Tabbene [5], Chantal Pichon [3], Christine Gardarin [1], Christophe Rihouey [6], Luc Picton [6], Slim Abdelkafi [4], Imen Fendri [2] and Céline Laroche [1,*]

[1] Institut Pascal, CNRS, SIGMA Clermont, Université Clermont Auvergne, F-63000 Clermont-Ferrand, France; nesrinekarkouch@hotmail.fr (N.G.); christine.gardarin@uca.fr (C.G.)

[2] Laboratoire de Biotechnologie Végétale Appliquée à l'Amélioration des Cultures, Faculty of Sciences of Sfax, University of Sfax, Sfax 3000, Tunisia; imenfendri@fss.usf.tn

[3] Centre de Biophysique Moléculaire, CNRS-UPR 4301, 45071 Orléans, France; fatmaelleuch@ymail.com (F.E.); chantalpichon@cnrs-orleans.fr (C.P.)

[4] Unité de Biotechnologie des Algues, Biological Engineering Department, National School of Engineers of Sfax, University of Sfax, Sfax 3038, Tunisia; slimabdelkafi@enis.tn

[5] Laboratory of Bioactive Substances, Biotechnology Center of Borj-Cedria (CBBC), BP-901, Hammam-Lif 2050, Tunisia; karkouch_ines@yahoo.fr (I.K.); olfa.tabbene@cbbc.rnrt.tn (O.T.)

[6] Normandie University, UNIROUEN, INSA Rouen, CNRS, PBS, 76000 Rouen, France; christophe.rihouey@univ-rouen.fr (C.R.); luc.picton@univ-rouen.fr (L.P.)

[*] Correspondence: celine.laroche@uca.fr; Tel.: +33-473-40-74-19

Abstract: Exopolysaccharide (EPS) from marine microalgae are promising sources of a new generation of drugs. However, lot of them remain to be discovered and tested. In this study, EPS produced by *Porphyridium marinum* and its oligomers prepared by High Pressure Homogenizer have been tested for different biological activities, i.e., antibacterial, anti-fungal and antibiofilm activities on *Candida albicans*, as well as for their effects on the viability of murine breast cancer cells. Results have shown that all EPS samples present some biological activity. For antibacterial and antibiofilm activities, the native EPS exhibited a better efficiency with Minimum Inhibitory Concentration (MIC) from 62.5 μg/mL to 1000 μg/mL depending on the bacterial strain. For *Candida albicans*, the biofilm formation was reduced by about 90% by using only a 31.3 μg/mL concentration. Concerning breast cancer cells, lower molar masses fractions appeared to be more efficient, with a reduction of viability of up to 55%. Finally, analyses of polymers composition and viscosity measurements were conducted on all samples, in order to propose hypotheses involving the activities caused by the intrinsic properties of polymers.

Keywords: *Porphyridium marinum*; exopolysaccharide; high pressure homogenizer; antibacterial activity; anti-biofilm activity; anti-cancer activity

1. Introduction

In recent years, several studies have been conducted on bioactive molecules extracted from microalgal strains such as carbohydrate polymers, proteins, lipids and pigments whose biological and physicochemical properties can be used in the food, cosmetics, medical and pharmacological industries [1,2]. Among these microalgae, red microalgae, especially the genus *Porphyridium* and *Rhodella*, have attracted interest for their richness in sulfated exopolysaccharides (EPS). The molar masses of EPS in these genera is in a range of $2–7 \times 10^6$ Da [3]. These anionic sulfated PS contain glucuronic acid and several major neutral sugars such as xylose, galactose and glucose [3,4]. Nevertheless, the structures of these exopolymers have not yet been elucidated except for some oligosaccharidic sequences [5]. These polymers have many potential activities, including antiviral, anti-tumor

57

and antioxidant activities. All of these activities were reported to be linked to these poly-mers' physicochemical characteristics such as the degree of sulfation, molecular weight and their rheological behavior [2,4]. However, studies on their antibacterial, anti-fungal and antibiofilm activities remain scarce.

The red microalga *Porphyridium marinum* was studied only for its production of exopolysaccharides and the antiparasitic activity these exopolysaccharides cause for honey bee infection through microsporidia *Nosema ceranae* [6,7]. In this study, EPS produced by *P. marinum* and its oligomers prepared by High Pressure Homogenizer (HPH) were evaluated for several biological activities. These activities were (i) their ability to inhibit the multiplication of Gram (+) and (−) bacterial strains, (ii) the multiplication and biofilm formation of *Candida albicans* yeast and (iii) the proliferation of breast cancer cells. The HPH technique consists of continuously forcing a liquid flow at low velocity using a volumetric pump through a restriction between a seat and a valve, the size of which can be imposed in order to control pressure drop. This technique is a green and non-thermal technology, unlike the most widely used namely chemical and thermal (microwave) methods that are limited by their efficiencies and their toxicities by using chemicals products such as trifluoroacetic acid and sulfuric acid. Moreover, HPH is less costly than enzymatic methods which are simple but often limited by the commercial availability of enzymes, their cost and their sensitivity to denaturation. Furthermore, it is a versatile tool that is commonly used in food and pharmaceutical industries for making emulsions, solid dispersions or cell lyses [8]. Finally, analyses of polymers composition and viscosity measurements were conducted on all EPS fractions, in order to match the activities with the intrinsic properties of polymers and to propose hypotheses on the action mechanism.

2. Results

2.1. Production of Different Molar Masses Exopolysaccharides by HPH

High Pressure Homogenization, which has been shown to be effective in reducing the molar masses of polysaccharides [9,10], has been applied to EPS produced by the red microalga *P. marinum* in order to obtain lower molar masses exopolysaccharides and therefore to decrease their viscosity. EPS obtained from *P. marinum* were submitted to up to five cycles of HPH at a pressure of 2.7 kbar and three exopolysaccharide fractions were recovered, such as untreated EPS (EPS-0C), EPS after two HPH passes (EPS-2C) and EPS after five HPH passes (EPS-5C).

The number and weight average molar masses (respectively Mn and Mw), gyration (Rg) radius, hydrodynamic (Rh) and intrinsic viscosities ([η]) of samples have been determined by Steric Exclusion Chromatography coupled to multi-angle laser light scattering, viscometry and a differential refractive index (SEC/MALLS/Visco/DRI) and are reported in Table 1.

Table 1. Macromolecular characterization of *P. marinum* EPS samples.

Samples	% Recovery	M_n (kDa)	M_w (kDa)	Rg (nm)	Rh (nm)	[η] mL/g
EPS-0C	8.5	890 (±35%)	1400 (± 40%)	150 (± 5%)	67 (± 5.1)	1480 (± 1%)
EPS-2C	73	400 (± 0.7%)	550 (± 2%)	43 (± 2%)	26 (± 0.5)	230 (± 0.4%)
EPS-5C	72	340 (± 0.6%)	550 (± 4%)	41 (± 3%)	21 (± 0.6)	155 (± 0.5%)

M_w: Weight-average molar mass estimated by SEC-MALLS-DRI. M_n: Number-average molar mass estimated by SEC MALLS-DRI. Rg: Gyration radii. Rh: Hydrodynamic radii. [η]: Intrinsic viscosity.

M_w and M_n of the native exopolysaccharides were about 1400 and 900 kDa, respectively. Nevertheless, due to an important retention of exopolysaccharide during the filtration (on a 0.45 μm filter), these value are characteristic of less than 10% (Table 1) of the initial mass of the sample before filtration. This low amount of analyzed sample is indicative of the large level of uncertainty on the molar mass determination. However, these values of molar masses seem to be congruent with the results previously reported by Soanen et al. [7] for EPS from *P. marinum* (1800 kDa, recovery rate of 30%). This large loss

could be explained by the presence of very large aggregated structures, as we observed high values of hydrodynamic and gyration radii (67 and 150 nm, respectively), but also by the fact that the elution was disperse (i.e., elution on a large volume, thus corresponding to variations in Rg and Rh, but with a quite constant molar mass). Such comportment has also been observed by other authors while analyzing molar masses for microalgae EPS. The work of [11] on *Porphyridium* sp. EPS could be cited in this context, who also suggested the presence of aggregates, as well as a more recent study on *Porphyridium cruentum* [12]. Such large aggregates can be the consequence of hydrophobic associations (the presence of esterified sugar or amphiphilic proteins), hydrogen bonds or complexes between polysaccharides and/or proteins. Besides, we have demonstrated in a previous study on *Flintiella sanguinaria* EPS [13] that large aggregates were present. Conformation analysis in dilute solution with a chaotropic salt (KSCN) led to a partial disaggregation of it, suggesting intermolecular interactions by hydrogen or hydrophobic interactions due to the presence of methyl and acetyl groups on the polysaccharide backbone. However, a protease treatment also confirmed that proteins significantly contribute to this associative structure, but mainly by intramolecular interactions. Thus, even if we have not explored this interaction mechanism more in depth in the present study, the presence of such large aggregates is very likely. In contrast to EPS-0C, the filtration losses of the EPS fractions obtained after two or five passes in the HPH are considerably reduced (about 70% of the samples have been analyzed, see Table 1), leading to more significant values of the polymer physicochemical characteristics. This can be attributed to the decrease in molar masses, even if some smaller aggregates can still remain. As expected, the molar masses of the treated EPS were substantially reduced from 1400 to 550 kDa for M_w together with the size (Rh from 67 to 21 nm, Rg from 150 to 41 nm) and [η] from about 1500 to 150 mL/g). Therefore, the HPH treatment was clearly effective to reduce both molar masses, hydrodynamic and gyration radius of polymers by a factor of 2.5, 3 and 3.5, respectively. However, the difference between the 2nd and 5th passage appears to not be really significant.

2.2. Structural and Physico-Chemical Characterization of EPS Samples

The purity of the native EPS (EPS-0C) was first evaluated, showing that our sample was constituted of 62% sugars. Additionally, 9% ± 0.04 of proteins were found to be present in the polysaccharide extract. This percentage is consistent with those generally found in the literature for EPS from red microalgae [2]. Some authors have even suggested that these proteins could be covalently bound to the polysaccharidic moiety [14]. No further purification was then applied to the sample.

Biological activity of polysaccharides is often attributed to the presence of sulfate groups and uronic acids in their structure. The composition of the 3 samples was analyzed by colorimetric assays, HPAEC-PAD and FTIR. As shown in Table 2, no modification of the global composition was noticed since all samples were composed of around 22% of uronic acids, and 9% of sulfate groups. The HPAEC chromatograms are provided as Supplementary Materials.

Concerning monosaccharides composition, the exopolysaccharides of *P. marinum* consisted mainly of xylose, galactose and glucose as previously reported by Soanen et al. [7]. Only slight differences were noticed between treated and untreated samples, which were considered to not be significant. This result is in accordance with the fact that no additional purification step was included after HPH treatment, so all monosaccharides present in the native sample remained in the treated ones. Differences between uronic acids content obtained by colorimetric assay (22% in weight) and HPAEC (~5% molar ratio glucuronic acid) could be attributed to the presence of an unidentified peak in HPAEC corresponding to another acidic monosaccharide. This hypothesis is supported by the fact that methylated glucuronic acid (2-*O*-Me-GlcA) has been described for *Porphyridium cruentum* [15], and more recently, [16] have observed the presence of a methylated uronic acid in the EPS from *Porphyridium sordidum*. Moreover, this peak has been already observed by authors while analyzing the EPS from *Flintiella sanguinaria* (another red marine microalgae). During

this study, it was concluded that this peak should correspond to a methylated and/or acetylated glucuronic acid. This hypothesis was formulated because the analysis of the desubstituted sample (specific treatment to release methyl and acetyl groups for their quantification), led to the disappearance of this peak and increase in the area of glucuronic acid peak. However, the lack of commercial standards prevented its formal identification and quantification [13].

Table 2. Uronic acids, sulfate content and monosaccharide composition of the different polysaccharidic samples.

	EPS Samples		
	EPS-0C	EPS-2C	EPS-5C
Uronic acids (%)	22 ± 0.1	22 ± 0.1	21 ± 0.2
Sulfates (%)	9.2 ± 0.3	8.7 ± 0.8	9.2 ± 0.7
Xylose (%)	47	47	44
Galactose (%)	25	25	29
Glucose (%)	20	19	20
Fucose (%)	1	1	1
Arabinose (%)	2	2	1
Glucuronic acid (%)	5	5	4

Uronic acids and sulfates content were determined by colorimetric assays and expressed as Eq.GlcA and Eq.SO$_4$, respectively. Values are the average of at least 3 independent assays. Monosaccharide composition was obtained by HPAEC and results expressed as molar ratios.

Finally, infrared spectrum analysis indicated that the HPH-depolymerized products had the same footprint as the native exopolysaccharide (Figure 1).
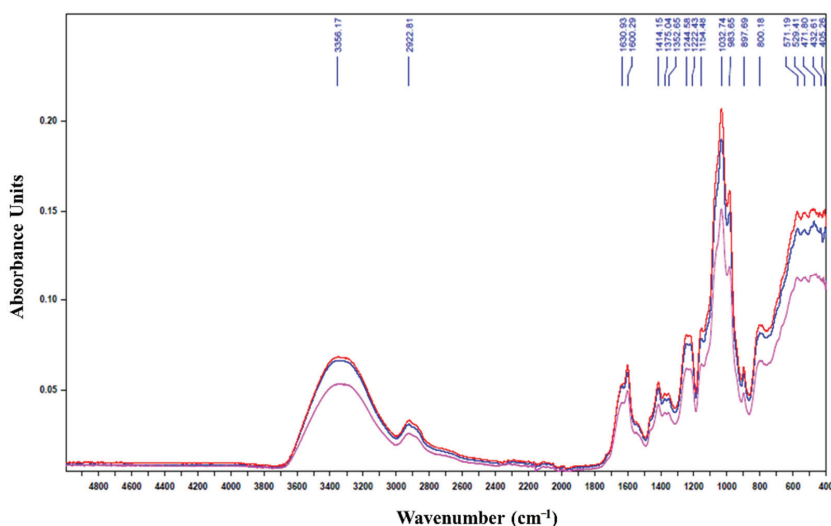
Figure 1. Infrared spectrum of exopolysaccharide (EPS) before and after passage in the high pressure homogenizer. Blue: EPS-0C, Red: EPS-2C, Pink: EPS-5C.

No difference was noticed in the absorption bands detected between 1630 and 1414 cm^{-1} which are characteristic of the asymmetric vibrations of the protonated and deprotonated carboxylic groups linked to the presence of uronic acids [17,18]. The 1222.43 cm^{-1} band characteristic of the S=O sulfate groups [19] of the red microalgae EPS was retained for the two treated polysaccharides: EPS-2C and EPS-5C. Also, the absorption bands detected at 897.69 cm^{-1}, characteristic of the deformation of the β-C$_1$ anomeric bonds [20,21],

were well preserved during the depolymerization. The bands observed at 1154 cm^{-1} are characteristic of the glycosidic structure (C-O-C). In fact, the presence of these bands despite the depolymerization by HPH shows that only certain glycosidic bonds have been affected and altered. These results confirm the still high molar masses of EPS-2C and EPS-5C determined by SEC/MALLS (Table 1). These findings are consistent with those observed by [22] while extracting fucoidans from the seaweed *Nemacystus decipients* by several cycles of HPH.

Apart from functional groups, the viscosity of polymers has been suggested to play a role in some biological activities. As an example, it has been demonstrated by Sun et al. [23] that by decreasing the average molar masses of the polymer, the viscosity was considerably reduced (in agreement with our results, see Table 1) and consequently the antioxidant activity gradually improved. Thus, the rheological behavior of the various exopolysaccharide extracts (EPS-0C, EPS-2C and EPS-5C) was explored in flow mode by plotting the viscosity curves as a function of the shear rate (Figure 2). The different samples were prepared at the same concentration (1 mg/mL) for a comparative study but also at some active concentrations that will be highlighted later in this paper (125 and 62.5 μg/mL for EPS-0C, 125 and 2500 μg/mL for EPS-2C as well as 250 and 2500 μg/mL for EPS-5C).

As shown in Figure 2A, the EPS-0C at the highest concentration, (i.e., 1000 μg/mL) evidences a non-Newtonian and shear-thinning behavior that means the decrease of the viscosity of the solution with the increase of the shear rate. Moreover, the absence of a Newtonian plateau at low shear rates could be indicative of a yield stress behavior in agreement with a connected structure of the fluid. This result could be correlated to the high aggregation tendency showed in a diluted regime (SEC/MALLS/Visco/DRI measurements). Some papers described rheological behavior of microalgae EPS, including from *Porphyridium* species (*P. cruentum* [12], *P. sordidum* and *P. purpureum* [24]), but all were conducted at greater concentrations than in the present study (0.125% or more), leading to difficulties in comparing viscosity values. However, they also observed a shear thinning behavior [12,23,25,26]. At lower concentrations (for 125 μg/mL and 62.5 μg/mL), EPS-0C presents a quite Newtonian profile. Thus, the viscosity was found to be considerably decreased from 44.22 mPa.s (1000 μg/mL) to 2.95 mPa.s (125 μg/mL) and 1.62 mPa.s (62.5 μg/mL) at a shear rate of 10 s^{-1} (Figure 2A). This result is in agreement with Balti et al.'s [27] study, who observed a decrease in viscosity from 18.7 to 4.6 mPa.s when the sugar concentrations decreased from 1.74 to 0.48 g/L at a shear rate equal to 15 s^{-1}. On the other hand, the viscosities of EPS-2C and EPS-5C solutions have shown a linear relationship with the shear rate typical of Newtonian fluids (Figure 2B,C). Thus, decreasing the molar masses of EPS by HPH led to a significant impact on viscosity which decreased from 44.22 mPa.s for EPS-0C to 1.12 mPa.s (just slightly higher than water viscosity) for EPS-5C for a shear rate equal to 10 s^{-1}. As for molar masses determination, no more effect between two and five passages has been detected with this rheological study. Partial depolymerization of EPS from *Porphyridium* sp. has been shown to strongly affect viscosity, with, for the lower molecular weight samples, a comportment typical of Newtonian fluids [23]. Villay et al. [8] showed the same effect on other types of polysaccharides (guar gum, hydroxyethylcellulose (HEC), sodium carboxymethylcellulose (Na-CMC), sodium alginate (Na-alginate) and gum Arabic) treated with HPH. The effect of number of treatment cycles was similar for all the polysaccharides. The first treatment always had the strongest impact on viscosity reduction. Then, no effect on the zero-shear viscosity "η_s" was observed after 2 and 3 cycles. Finally, a slight decrease of η_s was observed between cycles 4 and 6. At last, only a slight difference in viscosities of the treated samples could be detected as a function of concentration according to the expected dilute regime of concentration. These results were in accordance with the intrinsic viscosity (η) measurements (Table 1) which decreased significantly after depolymerization from 1480 to 155 mL/g (Table 1).
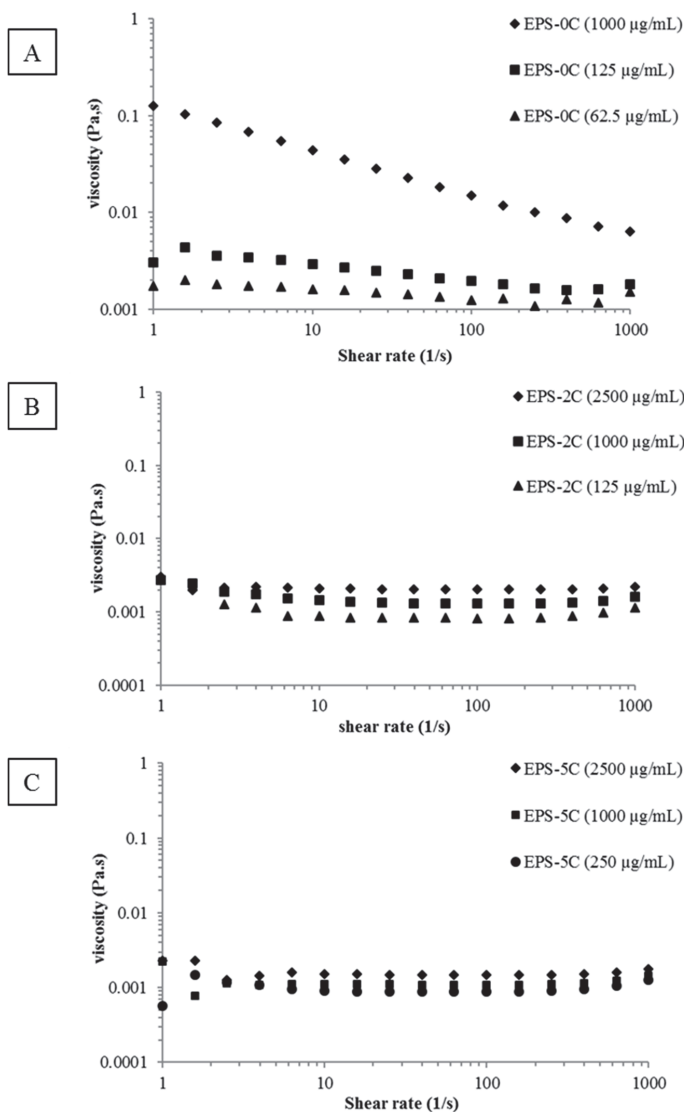
Figure 2. Shear flow behavior of EPS samples as a function of concentrations. (**A**): Native EPS (EPS-0C) at 1000 μg/mL (♦), 125 μg/mL (■) and 62.5 μg/mL (▲); (**B**): EPS-2C at 2500 μg/mL (♦), 1000 μg/mL (■) and 125 μg/mL (▲); (**C**): EPS-5C at 2500 μg/mL (♦), 1000 μg/mL (■) and 250 μg/mL (●).

2.3. Biological Activities

2.3.1. Antibacterial and Anti-*Candida Albicans* Activities

The three EPS fractions were screened for their ability to inhibit the growth of four bacterial strains (*Staphylococcus aureus* ATCC 29213, methicillin resistant *Staphylococcus aureus* (SMR), *Escherichia coli* ATCC 25922 and *Salmonella* Enteritidis ATCC 13076) and the yeast *Candida albicans* ATCC 10231.

All 3 EPS samples showed an antibacterial activity against the different bacterial strains tested. However, no antifungal activity against *Candida albicans* was detected. The most active was the native EPS that exhibited antibacterial activity against *E. coli* and *Salmonella* (Gram (−)) at MIC (Minimum Inhibitory Concentration) of 62.5 µg/mL and 125 µg/mL, respectively. This extract has also shown growth inhibition of Gram (+) bacteria at MIC 125 µg/mL for *S. aureus* and 1000 µg/mL for SMR. EPS-2C inhibited Gram (−) bacteria at a concentration of 2500 µg/mL and exhibited activity against *S. aureus* at a MIC of 1250 µg/mL. Finally, EPS-5C showed an antibacterial activity against *E. coli* and *S. aureus* at a concentration of 2500 µg/mL (Table 3). The MIC value of the different EPS samples was higher than that of the reference antibiotics Cefazolin and Amphotericin B that were used as positive controls. Even if the antimicrobial potential of these conventional antimicrobial agents was higher than that of EPS, the later could represent a natural and safer molecule without secondary effects.

Table 3. Antibacterial and anti-*Candida albicans* activities of *P. marinum* EPS samples.

Strains	MIC (µg/mL)				
	EPS-0C	**EPS-2C**	**EPS-5C**	**Cefazolin**	**Amphotericin B**
Gram (−) Bacteria					
Escherichia coli ATCC 25922	62.5	2500	2500	8	-
Salmonella Enteritidis	125	2500	-	4	-
Gram (+) Bacteria					
Staphylococcus aureus ATCC 29213	125	1250	2500	1	-
Staphylococcus Methicilin Resistant (SMR)	1000	-	-	512	-
Yeast					
Candida albicans ATCC 10231	-	-	-	-	0.125

MIC: Minimal Inhibitory Concentration. (-): Not determined. Cefazolin and Amphotericin B were used as positive controls.

These antibacterial activities were also demonstrated by the appearance of an inhibition zone on agar medium using the well diffusion method at MIC concentrations obtained previously (Figure 3). According to this test, it clearly appeared that the various exopolysaccharide fractions have an inhibitory effect on the growth of the bacteria, manifested by the formation of an inhibition zone around the wells. This area depended on the sensitivity of the bacterial strain to the EPS extract and its concentration. Indeed, *Escherichia coli* ATCC 25922 was found to be the most sensitive Gram (−) bacterium to EPS-0C with a MIC of 62.5 µg/mL while *Staphylococcus aureus* ATCC 29213 was the most sensitive Gram (+) bacterium to EPS-0C with a MIC equal to 125 µg/mL. This sensitivity was revealed by an inhibition zone which was the most extensive in comparison with those of the other polysaccharide extracts (Figure 3), which were active only at concentrations greater than or equal to 1000 µg/mL. Thus, the native EPS (EPS-0C) seemed to be the most active compared to other exopolysaccharide extracts (EPS-2C and EPS-5C).
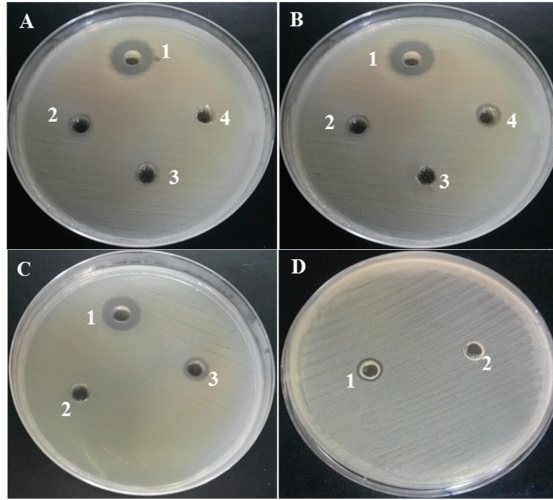
Figure 3. Zones of inhibition of the different bacterial strains affected by the exopolysaccharide extracts. (**A**): Activity against *E. coli*, 1: EPS-0C, 2: EPS-2C, 3: EPS-5C, 4: water, (**B**): Activity against *S. aureus*, 1: EPS-0C, 2: EPS -5C, 3: water, 4: EPS-2C, (**C**): Activity against *Salmonella*, 1: EPS-0C, 2: water, 3: EPS-2C, (**D**): Activity against SMR, 1: EPS-0C, 2: water.

2.3.2. Inhibition of Biofilm Formation by *Candida Albicans* ATCC 10231

P. marinum EPS extracts were tested for their ability to inhibit *Candida albicans* biofilm formation by the 96-well plate crystal violet test. The three fractions (EPS-0C, EPS-2C and EPS-5C) were revealed to be active against the formation of *Candida albicans* biofilm (Figure 4) without affecting the planktonic growth of this yeast, as no mortality had been observed previously (Table 3).
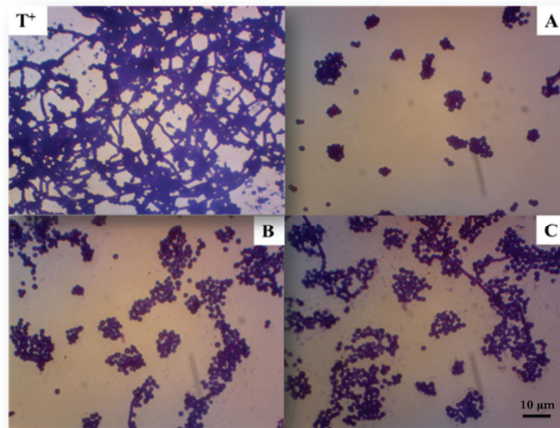
Figure 4. Representative reverse microscopy images of the biofilm formed by *C. albicans* ATCC 10231 in absence (positive control: T$^+$) or in the presence of exopolysaccharides at active concentrations. (**A**): EPS-0C at 31.3 μg/mL; (**B**): EPS-2C at 125 μg/mL and (**C**): EPS-5C at 250 μg/mL. The assay was performed on a 96-well plate for 24 h at 37 °C and the adherent biofilm cells were stained by crystal-violet.

Based on this observation, active EPS do not appear to target cell viability; they instead represent compounds whose mechanism of action would be the inhibition of the virulent form of *C. albicans*, in particular the transition from the yeast form to the mycelial form. As shown on Figure 5, the native polymer EPS-0C was the most active compared to other fractions (EPS-2C and EPS-5C). In fact, it has shown an inhibition of 90 ± 1% at a concentration equal to 31.3 µg/mL, not significantly different from the efficiency of farnesol, used as a positive control, which inhibits 91% of *C. albicans* biofilm formation at 31.3 µg/mL concentration. However, EPS-2C inhibited the formation of biofilm by up to 78 ± 2% at 125 µg/mL and EPS-5C had an activity of 83 ± 3% at a concentration of 250 µg/mL.
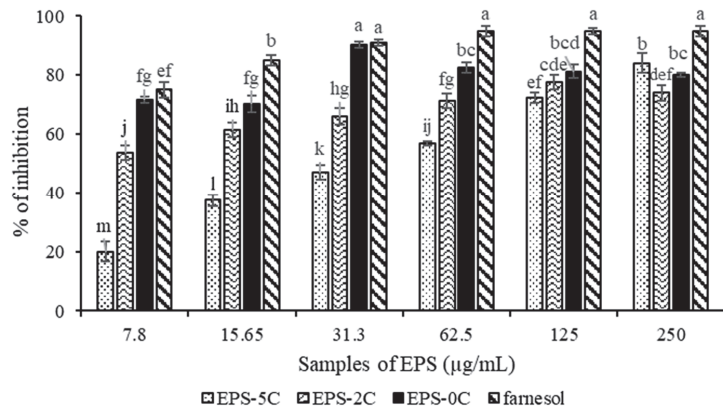
Figure 5. Percentage of inhibition of *Candida albicans* biofilm formation by different molar masses EPS from *P. marinum* (EPS-0C, EPS-2C and EPS-5C) and at different concentrations between 7.8 and 250 µg/mL. Farnesol was used as a positive control. Results were expressed as mean ± standard deviations of triplicate determinations. Different lowercase letters stand for significantly different values (Duncan multiple range test, $p < 0.05$).

2.3.3. T1 Mammary Carcinoma Cells Sensitivity towards EPS Samples

The results of the in vitro test of the different EPS fractions on a murine breast carcinoma 4T1 cell lines have shown an antiproliferative activity on cancer cells mainly for EPS-2C and EPS-5C fractions (Figure 6). Indeed, the EPS-0C extract at the concentration of 2 mg/mL showed no significant inhibition of cancer cells with a percentage of viability equal to 85 ± 0.8%, which was found to not be significantly different from the viability obtained at the lower concentration (>90%). This result highlights the fact that the native EPS has no activity on carcinoma cells proliferation. In contrast, the antiproliferative activity was improved with the EPS-2C and EPS-5C exopolysaccharides having lower molar masses, as they were found to reduce the cell viability by 51 ± 0.75% and 45 ± 0.82%, respectively at a concentration of 2 mg/mL. As shown on Figure 6, EPS-2C and EPS-5C inhibited the proliferation of cancer cells in a concentration-dependent manner. In fact, the more the concentration (from 0.0625 to 2 mg/mL) increased, the more the antiproliferative activity of cancer cells increased, but with no statistically different behavior between the 2 samples.

Cytotoxicity of EPS samples was assayed on mammalian cell line Vero. Viability of cells was evaluated for each sample and at different concentrations (up to 5 mg/mL). Results showed that on the whole range of concentrations tested (between 9.75 to 5000 µg/mL), and for the 3 extracts (EPS-0C, EPS-2C and EPS-5C), no significant difference in viability was observed, and that it was almost 100% in all cases. As the CC50 (The 50% cytotoxic concentration, defined as the sample concentration able to reduce the cell viability by 50% when compared to an untreated control) of the samples were evaluated to be >5 mg/mL,

and that no cytotoxic effect was observed for these samples in the range of concentrations used for the XTT test, the decrease in cell viability of carcinoma cells (about 50%) observed for 2 mg/mL concentrations could not be attributed to a cytotoxicity of the extracts and thus confirmed the antiproliferative effect.
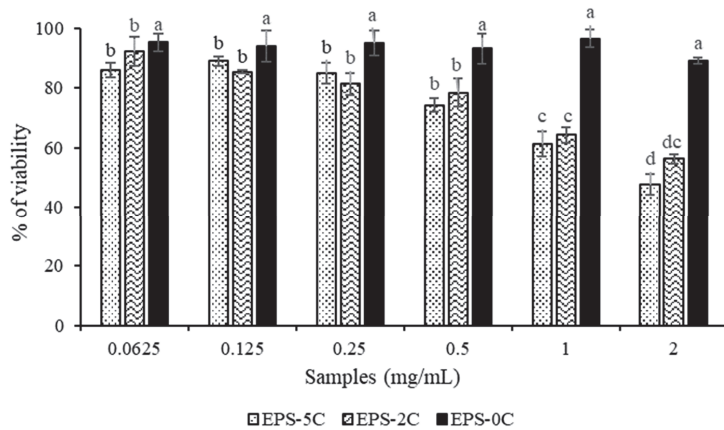
Figure 6. Percentage of viability of murine mammary carcinoma cells 4T1 under the action of EPS samples from *P. marinum* (EPS-0C, EPS-2C and EPS-5C), at concentrations between 0.0625 and 2 mg/mL. Results were expressed as mean ± standard deviations of triplicate determinations. Different lowercase letters stand for significantly different values (Duncan multiple range test, $p < 0.05$).

3. Discussion

EPS from red microalgae showed several biological activities [28–33] that were generally linked to their molecular weight, rheological behavior [23,34] and their content in sulfate groups and uronic acids. In our study, we evaluated the global and monosaccharide composition, the FTIR footprint, the amount of uronic acids and sulfate groups and the molecular masses of our samples. These results are in accordance with other studies on *P. marinum* EPS [6,7]. EPS from microalgae are complex molecules (much more complex than polysaccharides from other sources), making their complete characterization really challenging. Only a few numbers of EPS coming from microalgae have been studied for glycosidic linkages and none of these studies have led to a complete and defined structure [2]. The cause of this poor knowledge of EPS structures is linked to the fact that these heteropolymers often contains 5 to 10 different monosaccharides, numerous non-sugar substituents such as sulfate, methyl, acetyl and/or pyruvyl groups, and they apparently lack a repeating unit. In a drug development approach, it is mandatory to have fully characterized molecules at the molecular level, including resolution of the glycosidic linkages. However, methods that are classically applied successfully to polysaccharides from other sources (NMR, MALDI-TOF, GC-MS/EI) actually fail to resolve the structure of EPS from microalgae [2]. Even if the elucidation of this complete structure is still lacking, we intended to highlight a potential relationship between structure, physico-chemical properties and activities.

Many researchers have reported that minor changes in molar masses, or viscosity can have positive effects on antitumor activity. In this study, we demonstrate that EPS-2C and EPS-5C show an anti-proliferative activity against breast cancer cells at a high concentration of 2 mg/mL (Figure 6). This activity could be attributed to their lower molar masses and therefore to their low viscosity, thereby increasing their absorption and permeation ability. By further decreasing the molar masses of EPS from *P. marinum*, it could then be expected to increase this anti-proliferative effect. In 2009, Gardeva et al. [34] reported the anti-tumor

activity of *Porphyridum cruentum* exopolysaccharide. They discovered that this sulfated polymer strongly inhibited proliferation of Graffi myeloid tumors in vitro and in vivo. These authors hypothesized that the anticancer activity of the exopolysaccharide extracted from *Porphyridium cruentum* could be associated with its immunostimulatory action as well as its direct cytotoxic properties. In 2012 [35], the anti-tumor and immunomodulatory activities of *P. cruentum* exopolysaccharides of different molar masses were evaluated on the mouse model carrying the S180 tumor in vivo and on the activation of peritoneal macrophages in vitro. The degraded EPSs showed a net immunomodulation dependent on their molar masses as well as the administered concentration. The smallest fragment of 6.53 kDa had the strongest immuno-reinforcing activity, which was in agreement with the results obtained in our study. Other studies have confirmed that many types of polysaccharides, such as lentinan, *Spirulina maxima* polysaccharide and *Chondrus ocellatus* λ-carrageenan, exhibited significant antitumor activity for low molar masses samples [36–38]. In general, the antitumor effects of polysaccharides involve several mechanisms such as modification of the biochemical character of the cell membrane, induction of differentiation and apoptosis of tumor cells and regulation of cell signaling pathways. Nevertheless, immunomodulation is generally considered to be the most important mechanism [39]. It will then be interesting to test lower molar masses samples for antitumoral activity, and to evaluate the immunomodulatory effect to go further in the comprehension of the mechanism.

Bacteria are very common microorganisms in the pathogenic state. The best known and encountered bacteria in the medical sector is *Staphylococcus aureus* which is involved in nosocomial infections [40], but which can also be responsible for food poisoning just like *Escherichia coli* and *Salmonella* [41,42]. However, some bacteria also have developed an increased resistance to clinical antibiotics like methicillin, rendering it ineffective [43]. *Candida albicans* is the most common microorganism among fungal infections, causing high mortality and morbidity especially in immunocompromised patients [44]. The formation of the biofilm represents the virulent form of the pathogen contributing to the pathogenesis of candidiasis. The formation of the *Candida albicans* biofilm is favored by the passage from the unicellular yeast form (blastopore) to the mycelial form (hyphe and pseudohyphe) [45,46], with the ability to strongly adhere to biological surfaces or inert surfaces of medical devices [47]. Biofilm formation leads to high levels of resistance to most conventional antifungal agents, mainly fluconazole and amphotericin B, which have several limitations in terms of efficacy, toxicity, drug interaction and high cost. Thus, the search for alternative strategies and the development of new and more effective antifungal and antibacterial agents is necessary for better therapeutic management. For these reasons, EPS fractions from *P. marinum* were also tested for their antimicrobial and antibiofilm activities. It was found that the native EPS as well as the depolymerized EPS (EPS-2C and EPS-5C) provided an antibacterial and antibiofilm activity with different efficiency levels (Table 3, Figure 5). Our EPS can thus be considered as a powerful inhibitor of bacterial multiplication compared to other exopolysaccharides extracted from other microalgae. De Jesus Raposo et al. [48] indicated that the EPS produced by *Porphyridium cruentum* exhibited antibacterial activity against Gram (+) (*S. aureus*) and Gram (−) bacteria (*E. coli* and *S.* Enteritidis). Indeed at 1% (*w/v*), it clearly inhibited *S.* Enteritidis, reducing CFU to 19%. However, the concentration used in the present study was much lower. The most active fraction was the native EPS at low concentrations that were not showing high viscosity (31.3 µg/mL for the inhibition of the biofilm of *Candida albicans* 110231, 62.5 µg/mL for *anti-Escherichia coli* ATCC 25922 multiplication and 125 µg/mL for anti-*Salmonella* Enteritidis ATCC 13076 and anti-*Staphylococcus aureus* ATCC 29213 growth). Very few polysaccharides from microalgae were described as negatively impacting biofilm formation. The only available study has shown that the cell-bound polysaccharide from *Navicula phyllepta* specifically inhibited biofilm formation from the bacteria *Flavobacterium* sp., while it stimulated biofilm development by *Roseobacter*, and *Shewanella* genera [49]. In comparison with the literature, the efficiency of EPS-0C to inhibit biofilm formation by *C. albicans* observed in this study was greater

(>90%), and this for much lower applied doses (31.3 µg/mL). However, the active dose of EPS-2C and 5C was found to be greater than for EPS-0C, showing that decreasing the molar mass has a negative impact on their efficiency.

The native EPS was also active against *Staphylococcus aureus* methicillin resistant at a concentration equal to 1000 µg/mL (Table 3) showing a significant viscosity (Figure 2A). Therefore, in addition to the functional groups (sulfate and uronic acids, see Table 2) present on EPS-0C, the role of viscosity cannot be excluded from its inhibiting properties on the multiplication of SMR. The rheological behavior of the EPS-2C and EPS-5C fractions was always the same regardless of the applied concentration (2500 µg/mL, 1000 µg/mL or 125 µg/mL) (Figure 2B,C). At these concentrations, these samples have a low viscosity and exhibit a Newtonian behavior. Therefore, the biological activity of these EPSs against bacterial strains and the inhibition of *Candida albicans* biofilm formation could be attributed to their chemical composition, probably primarily to the sulfate and uronic acids groups, as several studies have relied on biological activity with the presence of sulfate groups [33,48,50,51]. Nevertheless, the sulfation degree may not be the only parameter to be considered to explain the biological activity of polysaccharides. Their position and therefore their "accessibility" can improve or not improve the biological activity of the EPS, as demonstrated by [6]. Moreover, several different mechanisms may exist, as non-sulfated polysaccharides (such as chitosan) have exhibited significant efficiency as an antibacterial and antibiofilm agent. For example, Costa et al. [52] have shown that the highest percentage inhibition of biofilm formation by *C. albicans* (66.94%) was obtained for high molar masses chitosan at 0.5 mg/mL and the lowest inhibition percentage (37.97%) was obtained for the low molar masses at 0.75 mg/mL, which was in agreement with our results. Cobrado et al. [53] also showed that low molar masses chitosan (107 kDa) was able to reduce *C. albicans* biofilm formation up to 41% at a 2.5 mg/mL concentration. For antibacterial activities, results are sometimes controversial, with depending on studies, greater efficiency on Gram (+) bacteria [54,55] or on Gram (−) ones [56,57]. In fact, the antimicrobial activities of chitosan would be greatly dependent on its physical characteristics, most notably weight average molar masses (Mw) and degree of deacetylation (DD) (for a review, see [58]). Therefore, the antimicrobial mechanisms and structure-function relationships of polysaccharides remain to be elucidated.

4. Materials and Methods

4.1. Extraction of Exopolysaccharides

The exopolysaccharide was recovered from a culture of red microalga *Porphyridium marinum*, obtained from Culture Collection of Algae and Protozoa (http://www.ccap.ac.uk/). Cultivation was conducted in 2 L Erlenmeyer flask, containing 1 L of Pm medium [7], under continuous light at 150 µmole photons/m^2/s, stirring at 110 rpm and at a temperature of 20 °C. The medium was inoculated with 100 mL of a subculture. As previously described [7], synthesis and accumulation of EPS occurred after nitrogen deprivation and entry in a stationary phase. Culture was stopped after 30 days, centrifuged (10,000× *g*, 30 min, 20 °C), and the supernatant was desalted and concentrated using a tangential filtration cassette (Vivaflow 200, Sartorius, Göttingen, Germany) having a cutoff threshold of 100 kDa [7]. Finally, the resulting EPS solution was lyophilized before storage at room temperature.

4.2. Preparation of Different-MW Exopolysaccharides

The exopolysaccharide of *P. marinum* was treated using a High Pressure Homogenizer (HPH, 2.7 kbars, TS HAIVA, Constant Systems LTD, Daventry, UK) to obtain polysaccharide fractions of different molar masses. A polysaccharide stock solution was prepared at a concentration of 2 g/L. Up to five successive cycles were used to obtain 3 samples which were subsequently recovered and lyophilized. The corresponding degraded samples are labeled as follows, according to the number of cycles in the HPH:

- EPS-0C for the undegraded sample,
- EPS-2C for the polysaccharide after two cycles,
- EPS-5C for the polysaccharide after five cycles.

4.3. Exopolysaccharides Characterization

4.3.1. Total Sugars, Neutral Sugars, Uronic Acids, Sulfate and Proteins Content

Total sugar content of samples was evaluated by the resorcinol method using glucose as standard [59]. Uronic acids and neutral sugar contents of EPS extracts were assayed with meta-hydroxyldiphenyl (m-HDP) and resorcinol as described by, respectively, [60] and [59] using glucose and glucuronic acid as standards. In these assays, glycosidic linkages are broken during high temperature sulfuric acid treatment and dehydration of sugar units leads to furfural compounds formation. These latter interact by condensation with phenolic compounds (resorcinol or m-HDP depending on the assay), giving colored compounds that can be measured respectively at 450 or 520 nm. Briefly, for the m-HDP assay, 200 μL of sample are mixed with 1 mL of a 0.12 M borax ($Na_2B_4O_7$,$10H_2O$) prepared in 96% (w/v) sulfuric acid. After a 1 h incubation at 90 °C, 200 μL of m-HDP solution are added and absorbance measured at 520 nm. The m-HDP solution is prepared just before assay by diluting 102 μL of m-HDP stock solution (100 mg of m-HDP solubilized in 1 mL DMSO, kept at 4 °C) with 5 mL of 80% (w/v) sulfuric acid. The results were expressed in mg/g of D-glucuronic acid equivalent (GlcAEq). For resorcinol assay, 200 μL of sample are mixed with 200 μL of a 6 g/L resorcinol solution and 1 mL of 80% (w/v) sulfuric acid. After 30 min at 90 °C, followed by 30 min at room temperature, 1.4 mL of water are added and absorbance at 450 nm is measured. The results directly expressed in mg/g of D-glucose equivalent (GlcEq) correspond to the total sugars amount. As the uronic acids interfere with the assay, a glucuronic acid standard curve was performed following the same procedure, and the corrective formula described by [61] was applied, in order to access the neutral sugars amount.

Sulfur content was determined by the turbidimetric method [62] using K_2SO_4 as a standard. Results were expressed in mg/g of SO_4 equivalent. Briefly, 120 mg of samples were hydrolyzed with 3 mL of 2 M chlorhydric acid for 2 h at 100 °C. After centrifugation (10,000× g, 30 min), 1 mL of supernatant is added to 9 mL of milliQ water, 1 mL of 0.5 M HCl, and 0.5 mL of $BaCl_2$/gelatin reagent (150 mg of gelatin dissolved in 50 mL of water at 70 °C, kept 16 h at 4 °C, and finally mixed with 0.5 g of $BaCl_2$). After 30 min incubation at room temperature, sulfate groups released during the hydrolysis of polysaccharides form a precipitate of barium sulfate, which can be detected at 550 nm. Protein content was evaluated by the Lowry method [63] using bovine serum albumin (BSA) as a standard.

4.3.2. Monosaccharide Composition of EPS

The identification and quantification of the constitutive monosaccharides of *P. marinum* EPS was conducted by high performance anion exchange chromatography (HPAEC) on an ICS 3000 (Dionex, Sunnyvale, CA, USA). Exopolysaccharides were hydrolyzed with 2 M TFA at 120 °C for 1 h 30 min, neutralized with 35% ammonia and then centrifuged at 14,000× g for 15 min. The recovered supernatant was filtered at 0.22 μm before injection. The elution was carried out with a pre-column and a CarboPac PA1 column (4 × 50 mm and 4 × 250 mm, respectively) whose stationary phase is an anion exchange resin. Samples were eluted isocratically with 18 mM NaOH for 25 min, followed by a linear gradient between 0 and 0.5 M sodium acetate in 200 mM NaOH for 20 min to elute acidic monosaccharides. Run was followed by 15 min washing with 200 mM NaOH. The eluent flow rate was kept constant at 1 mL/min. A range of external standards (Fucose, Arabinose, Galactose, Glucose, Rhamnose, Xylose, Mannose, Fructose, Ribose, Galactosamine, Glucosamine, N-AcetylGlucosamine, N-AcetylGalactosamine, Galacturonic acid and Glucuronic acid) with concentrations ranging from 0.001 to 0.01g/L, and then the addition of internal standards in the samples enabled qualitative and quantitative analysis of the composition of polysaccharides.

4.3.3. Molar Masses Determination

Molar masses and polydispersity index of EPS were analyzed by a size exclusion chromatography coupled to a multiangle laser light scattering detector, a viscometric detector and a differential refractive index detector (SEC/MALLS/Visco/DRI). The polysaccharide solutions were prepared at 0.5 mg/mL (dilute regime) in the chromatographic eluent (i.e., LiNO$_3$ at 0.1 M, filtered on 0.1 µm) under soft magnetic agitation at 60 °C during 4 h and then filtrated on a 0.45 µm filter unit (regenerated cellulose). An automatic sample injector (SIL 20A, Shimadzu, Kyoto, Japan) equipped with a 500 µL injection loop was used for injection. The solvent was driven by a pump (LC 10Ai, Shimadzu, Kyoto, Japan) at a flow rate of 0.5 mL/min. The sample was first drawn into a pre-column (Shodex OHPAK SB-G) before being directed to two standard steric exclusion columns (Shodex OHPAK SB 804 and 806 HQ). At the outlet of the column, the compounds were quantified by a differential refractometer (DRI 10A, Shimadzu, Kyoto, Japan), a multi-angle laser light scattering detector (Dawn® heleos, Wyatt technology Corp., Santa Barbara, CA, USA) equipped with a K5 cell of 50 µL, a red source (Ga-As 690 nm) of 5 mW, 18 measurement diodes and a viscosity detector (Viscostar 2, Wyatt Technology Corp., Goleta, CA, USA). The data obtained was processed with the Astra 6.1.1 software which provided the weight and number average molar masses (M_n and M_w, respectively) and also the gyration (Rg) radius and both intrinsic viscosities ([η]) and hydrodynamic (Rh) based on the viscosity detector.

4.3.4. Infrared Spectrometry Footprint (FTIR)

Infrared measurements were made using a VERTEX 70 (Bruker, Billerica, MA, USA) spectrometer. The samples were analyzed on an ATR A225 diamond module. IR spectra (50 scans) were obtained at room temperature (referenced against air) over the 500–4000 cm^{-1} range. The spectra were analyzed with the OPUS 7.2 software.

4.3.5. Shear Flow Behavior of EPS Samples

The shear flow behavior of samples (viscosity measurements as function of shear rate) was determined using an AR-G2 rheometer (TA Instruments Ltd., Hertfordshire, UK). Measurements were conducted using a steel cone-plate (40 mm radius, 2°, gap 50 µm) geometry. The temperature was set at 30 °C, with a circulating bath or a Peltier system depending on geometry. The viscosity measurements were made over a shear rate range of 1 to 10^3 s^{-1}.

4.4. Biological Activities

4.4.1. Antibacterial Activity

Four bacterial strains: *Staphylococcus aureus* ATCC 29213, methicillin-resistant *Staphylococcus aureus* (SMR), *Escherichia coli* ATCC 25922 and *Salmonella* Enteritidis ATCC 13076, were used as indicator strains for the determination of the antibacterial activity. Exopolysaccharides samples were tested for antibacterial activity by using the well diffusion method and the minimum inhibitory concentration (MIC) using the microdilution method on sterile 96-well plate [64]. Briefly, on Petri dishes containing solid Luria broth (LB) medium previously inoculated with the bacterial inoculum, 6 mm wells were dug in the medium and then sealed with a thin layer of liquefied soft agar to limit the diffusion of the sample under the solid medium. Samples with 50 µL of exopolysaccharides were placed in each well. Sterile distilled water was used as a negative control. The diameters of the inhibition zones were measured after 18 h of incubation at 30 °C.

To determine the MIC, bacterial strains were grown in LB medium at 30 °C. 10^5 CFU/mL of each bacterial suspension were incubated for 24 h at 30 °C in the presence of the test sample at concentrations ranging from 7.81 to 1000 µg/mL. Wells containing the bacterial strain alone were used as a positive control, while wells containing only the culture medium were considered as a negative control. MIC values were determined for the lowest concentration of the extract, showing complete inhibition of bacterial cell growth.

4.4.2. Anti-Candida Albicans Activity

Detection of antifungal activity against *Candida albicans* 10231 was performed using the microdilution method on a 96-well plate, as previously described by Grieco et al. [65]. Briefly, a culture of *C. albicans* (30 °C in WB medium) is diluted in the same growth medium to reach 10^5 UFC/mL and the suspension is introduced in each well, with different concentrations of samples between 7.81 and 1000 μg/mL and the plate is incubated 24 h at 37 °C. Two controls were included. The negative control corresponds to the growth medium, and the positive control contains *C. albicans* in the growth medium. MIC values were determined as the lowest concentration of the extract showing complete inhibition of *Candida* cell growth.

4.4.3. Inhibition of Biofilm Formation

Biofilm quantification was performed using the crystal violet staining assay on a 96-well polystyrene plate, as demonstrated by Jin et al. [66]. Indeed, a suspension of *Candida albicans* with a final concentration of 10^5 CFU/mL was prepared in the RPMI 1640 culture medium (R8758, Sigma-Aldrich, St. Quentin Fallavier Cedex, France). Fifty microliters of *C. albicans* inoculum was distributed into each well of the microplate in the presence of different exopolysaccharides samples, with concentrations ranging from 7.81 to 1000 μg/mL to have a final volume of 100 μL. The plate was then incubated at 37 °C for 24 h. After incubation, crystal violet staining was performed to demonstrate the inhibitory effect of biofilm formation. Briefly, the culture medium was removed and each well was washed twice with PBS buffer (pH = 7.4; 0.1 M). For biofilm fixation, 100 μL of 99% methanol was added. The biofilm was then stained with 0.05% crystal violet for 15 min at room temperature. The excess was removed by two washes with ultra pure water. Purple coloration appeared after the addition of 100 μL of 33% acetic acid and was detected at 630 nm. The percentage of biofilm inhibition was determined by the equation below:

$$\% \text{ inhibition} = [100 - ((A_{\text{Sample}} - A_{\text{blank}})/(A_{\text{Control}} - A_{\text{blank}}))] \times 100 \qquad (1)$$

with A_{Blank} and A_{Control} corresponding to the absorbance of RPMI medium and untreated biofilm at 630 nm, respectively.

4.4.4. Cytotoxicity Evaluation

Cytotoxicity EPS samples were tested on mammalian cell line Vero using MTT method according to Medjeldi et al. [67], measuring absorbance at 540 nm. The percentage of cytotoxic effect was calculated using the following equation:

$$[(A_{\text{Control}} - A_{\text{Sample}})/(A_{\text{Control}})] \times 100. \qquad (2)$$

The 50% cytotoxic concentration (CC50), defined as the sample concentration able to reduce the cell viability by 50% when compared to an untreated control, was determined by linear regression analysis from a dose-response curve.

4.4.5. Antiproliferative Effect of Different M_W-EPS on Breast Cancer Cells

The exopolysaccharides samples were tested for their ability to inhibit the proliferation of the 4T1 murin breast carcinoma cells. The antiproliferative activity was determined by the XTT test as described in the Cell Proliferation Kit II (Sigma, 11465015001 Roche, St. Quentin Fallavier, France).

The results were expressed as a percentage of viability via the following formula:

$$\% \text{ Viability} = (A_{\text{test}}/A_{\text{control}}) \times 100 \qquad (3)$$

A_{Control}: Absorbance of untreated cells at 450 nm.

4.5. Statistical Analyses

Data were collected from three independent experiments assayed in triplicate and expressed as the mean ± standard deviation (SD). The statistical significance was analyzed by one-way ANOVA with STATISTICA. 5 software. The post-hoc test of Duncan multiple range was used to perform comparisons. Results were considered as statistically significant with a $p < 0.05$.

5. Conclusions

The present study demonstrated the biological activity of different molar masses exopolysaccharides from *Porphyridium marinum*. Interestingly, our findings clearly revealed the potentiality of native exopolysaccharide EPS-0C to inhibit the proliferation of Gram (+) and Gram (−) bacteria, as well as the formation of biofilm of *Candida albicans* at low concentration. However, the low molar masses exopolysaccharides EPS-2C and EPS-5C were found to be more effective for antiproliferative activity against breast cancer cells. Depending on the biological activity tested, this study also disclosed that these biological activities could be due to their molar masses, their viscosity as well as their composition (probably their content in sulfate and uronic acids). Thus, this study provides strong arguments to consider exopolysaccharides from *Porphyridium marinum* as a natural source of antibacterial, antibiofilm and anticancer products that are useful in pharmaceutical formulations and food industries as a natural preservative. Nevertheless, this study constitutes a first step to evaluate the potential of EPS from *P. marinum* in a drug development approach.

Supplementary Materials: The following are available online at https://www.mdpi.com/1660-3397/19/2/66/s1, Figure S1: HPAEC chromatograms of native (a: EPS-0C) and depolymerized EPS (b: EPS-2C, c: EPS-5C).

Author Contributions: Conceptualization: N.G., I.F. and C.L.; Investigation: N.G., I.K., F.E., C.G. and C.R.; Supervision: C.P., S.A., O.T., I.F. and C.L.; Validation: I.F. and C.L.; Writing—original draft: N.G. and C.L.; Writing—review & editing: I.K., C.R., L.P., I.F., N.G. and C.L. All authors have read and agreed to the published version of the manuscript.

Institutional Review Board Statement: Not applicable.

Informed Consent Statement: Not applicable.

Data Availability Statement: Data is contained within the article or Supplementary Materials.

Conflicts of Interest: The authors declare no conflict of interest.

References

1. Gargouch, N.; Karkouch, I.; Elleuch, J.; Elkahoui, S.; Michaud, P.; Abdelkafi, S.; Laroche, C.; Fendri, I. Enhanced B-phycoerythrin production by the red microalga *Porphyridium marinum*: A powerful agent in industrial applications. *Int. J. Biol. Macromol.* **2018**, *120*, 2106–2114. [CrossRef] [PubMed]
2. Delattre, C.; Pierre, G.; Laroche, C.; Michaud, P. Production, extraction and characterization of microalgal and cyanobacterial exopolysaccharides. *Biotechnol. Adv.* **2016**, *34*, 1159–1179. [CrossRef] [PubMed]
3. Li, S.; Ji, L.; Shi, Q.; Wu, H.; Fan, J. Advances in the production of bioactive substances from marine unicellular microalgae *Porphyridium* sp. *Bioresour. Technol.* **2019**, *292*, 122048. [CrossRef]
4. Gaignard, C.; Gargouch, N.; Dubessay, P.; Delattre, C.; Pierre, G.; Laroche, C.; Fendri, I.; Abdelkafi, S.; Michaud, P. New horizons in culture and valorization of red microalgae. *Biotechnol. Adv.* **2019**, *37*, 193–222. [CrossRef] [PubMed]
5. Geresh, S.; Arad, S.; Levy-Ontman, O.; Zhang, W. Isolation and characterization of poly- and oligosaccharides from the red microalga *Porphyridium sp. Carbohydr. Res.* **2009**, *344*, 343–349. [CrossRef]
6. Roussel, M.; Villay, A.; Delbac, F.; Michaud, P.; Laroche, C.; Roriz, D.; El Alaoui, H.; Diogon, M. Antimicrosporidian activity of sulphated polysaccharides from algae and their potential to control honeybee nosemosis. *Carbohydr. Polym.* **2015**, *133*, 213–220. [CrossRef]
7. Soanen, N.; Da Silva, E.; Gardarin, C.; Michaud, P.; Laroche, C. Improvement of exopolysaccharide production by *Porphyridium marinum*. *Bioresour. Technol.* **2016**, *213*, 231–238. [CrossRef]
8. Villay, A.; de Filippis, F.L.; Picton, L.; LeCerf, D.; Vial, C.; Michaud, P. Comparison of polysaccharide degradations by dynamic high-pressure homogenization. *Food Hydrocoll.* **2012**, *27*, 278–286. [CrossRef]

9. Porto, B.C.; Cristianini, M. Effect of dynamic high pressure on emulsifying and encapsulant properties of cashew tree gum. *Carbohydr. Polym.* **2018**, *186*, 350–357. [CrossRef]
10. Fenoradosoa, T.A.; Laroche, C.; Delattre, C.; Dulong, V.; Lecerf, D.; Picton, L.; Michaud, P. Rheological behavior and non-enzymatic degradation of a sulphated galactan from *Halymenia durvillei* (Halymeniales, Rhodophyta). *Appl. Biochem. Biotechnol.* **2012**, *167*, 1303–1313. [CrossRef]
11. Geresh, S.; Adin, I.; Yarmolinsky, E.; Karpasas, M. Characterization of the extracellular polysaccharide of *Porphyridium* sp.: Molecular weight determination and rheological properties. *Carbohyd. Polym.* **2002**, *50*, 183–189. [CrossRef]
12. Bernaerts, T.M.M.; Kyomugasho, C.; Van Looveren, N.; Gheysen, L.; Foubert, I.; Hendrickx, M.E.; Van Loey, A.M. Molecular and rheological characterization of different cell wall fractions of *Porphyridium cruentum*. *Carbohydr. Polym.* **2018**, *195*, 542–550. [CrossRef] [PubMed]
13. Gaignard, C.; Macao, V.; Gardarin, C.; Rihouey, C.; Picton, L.; Michaud, P.; Laroche, C. The red microalga *Flintiella sanguinaria* as a new exopolysaccharide producer. *J. Appl. Phycol.* **2018**, *30*, 2803–2814. [CrossRef]
14. Capek, P.; Matulováa, M.; Combourieu, B. The extracellular proteoglycan produced by *Rhodella grisea*. *Int. J. Biol. Macromol.* **2008**, *43*, 390–393. [CrossRef] [PubMed]
15. Percival, E.; Foyle, A.R. The extracellular polysaccharides of *Porphyridium cruentum* and *Porphyridium aerugineum*. *Carbohydr. Res.* **1979**, *72*, 165–176. [CrossRef]
16. Medina-Cabrera, E.V.; Rühmann, B.; Schmid, J.; Sieber, V. Characterization and comparison of *Porphyridium sordidum* and *Porphyridium purpureum* concerning growth characteristics and polysaccharide production. *Algal Res.* **2020**, *49*, 101931. [CrossRef]
17. Monsoor, M.A.; Kalapathy, U.; Proctor, A. Determination of polygalacturonic acid content in pectin extracts by diffuse reflectance Fourier transform infrared spectroscopy. *Food Chem.* **2001**, *74*, 233–238. [CrossRef]
18. Gómez-Ordóñez, E.; Rupérez, P. FTIR-ATR spectroscopy as a tool for polysaccharide identification in edible brown and red seaweeds. *Food Hydrocoll.* **2011**, *25*, 1514–1520. [CrossRef]
19. Chopin, T.; Kerin, B.F.; Mazerolle, R. Phyccolloid chemistry as taxonomic indicator of phylogeny in the Gigartinales, Rhodophyceae: A review and current developments using fourrier transform infrared diffuse reflectance spectroscopy. *Phycol. Res.* **1999**, *47*, 167–188. [CrossRef]
20. Deng, J.; Shi, J.J.; Li, X.Z.; Liu, H.M. Soluble polysaccharides isolation and characterization from rabbit eye blueberry (*Vaccinium ashei*) fruits. *Bioresources* **2013**, *8*, 405–419.
21. Tomar, S.; Adaganti, S.Y. Production of ethanol using Calliandra shrub by hydrothermal pretreatment method. *Int. J. Curr. Eng. Tech.* **2013**, *3*, 1921–1924.
22. Li, G.Y.; Luo, Z.C.; Yuan, F.; Yu, X.B. Combined process of high-pressure homogenization and hydrothermal extraction for the extraction of fucoidan with good antioxidant properties from *Nemacystus decipients*. *Food Bioprod. Process.* **2017**, *106*, 35–42. [CrossRef]
23. Sun, L.; Wang, C.; Shi, Q.; Ma, C. Preparation of different molecular weight polysaccharides from *Porphyridium cruentum* and their antioxidant activities. *Int. J. Biol. Macromol.* **2009**, *45*, 42–47. [CrossRef] [PubMed]
24. Medina-Cabrera, E.V.; Gansbiller, M.; Rühmann, B.; Schmid, J.; Sieber, V. Rheological characterization of *Porphyridium sordidum* and *Porphyridium purpureum* exopolysaccharides. *Carbohydr. Polym.* **2021**, *253*, 117237. [CrossRef]
25. Geresh, S.; Arad, S.M. The extracellular polysaccharides of the red microalgae: Chemistry and rheology. *Bioresour. Technol.* **1991**, *38*, 195–201. [CrossRef]
26. Eteshola, E.; Karpasas, M.; Arad, S.M.; Gottlieb, M. Red microalga exopolysaccharides: 2. Study of the rheology, morphology and thermal gelation of aqueous preparations. *Acta Polym.* **1998**, *49*, 549–556. [CrossRef]
27. Balti, R.; Balc'h, R.L.; Brodu, N.; Gilbert, M.; Le Gouic, B.; Le Gall, S.; Sinquin, C.; Massé, A. Concentration and purification of *Porphyridium cruentum* exopolysaccharides by membrane filtration at various cross-flow velocities. *Process Biochem.* **2018**, *74*, 175–184. [CrossRef]
28. Matsui, S.M.; Muizzudin, N.; Arad, S.M.; Marenus, K. Sulfated polysaccharides from red microalgae anti-inflammatory properties in vitro and *in vivo*. *Appl. Biochem. Biotechnol.* **2003**, *104*, 13–22. [CrossRef]
29. Tannin-Spitz, T.; Bergman, M.; Van-Moppes, D.; Grossman, S.; Arad, S.M. Antioxidant activity of the polysaccharide of the red microalga *Porphyridium* sp. *J. Appl. Phycol.* **2005**, *17*, 215–222. [CrossRef]
30. Jiao, G.; Yu, G.; Zhang, J.; Ewart, H.S. Chemical structures and bioactivities of sulphated polysaccharides from marine algae. *Mar. Drugs* **2011**, *9*, 196–223. [CrossRef]
31. Guzmán-Murillo, M.A.; Ascencio, F. Anti-adhesive activity of sulphated exopolysaccharides of microalgae on attachment of the red sore disease-associated bacteria and *Helicobacter pylori* to tissue culture cells. *Lett. Appl. Microbiol.* **2000**, *30*, 473–478. [CrossRef] [PubMed]
32. Huheihel, M.; Ishanu, V.; Tal, J.; Arad, S.M. Activity of *Porphyridium* sp. polysaccharide against herpes simplex viruses in vitro and in vivo. *J. Biochem. Biophys. Methods* **2002**, *48*, 189–200. [CrossRef]
33. Arad, S.M.; Levy-Ontman, O. Red microalgal cell-wall polysaccharides: Biotechnological aspects. *Curr. Opin. Biotech.* **2010**, *21*, 358–364. [CrossRef] [PubMed]
34. Gardeva, E.; Toshkova, R.; Minkova, K.; Gigova, L. Cancer Protective Action of Polysaccharide, Derived from Red Microalga *Porphyridium cruentum*—A Biological Background. *Biotechnol. Biotech. Equip.* **2009**, *23*, 783–787. [CrossRef]

35. Sun, L.; Wang, L.; Zhou, Y. Immunomodulation and antitumor activities of different molecular-weight polysaccharides from *Porphyridium cruentum*. *Carbohydr. Polym.* **2012**, *87*, 1206–1210. [CrossRef]
36. Chen, D.; Wu, X.Z.; Wen, Z.Y. Sulfated polysaccharides and immune response: Promoter or inhibitor? *Panminerva Med.* **2008**, 177–183.
37. Zhou, G.F.; Sheng, W.X.; Yao, W.D.; Wang, C.H. Effect of low molecular λ-carrageenan from *Chondrus ocellatus* on antitumor H-22 activity of 5-Fu. *Pharmacol. Res.* **2006**, *53*, 129–134. [CrossRef]
38. Zhu, X.L.; Chen, A.F.; Lin, Z.B. *Ganoderma lucidum* polysaccharides enhance the function of immunological effector cells in immunosuppressed mice. *J. Ethnopharmacol.* **2007**, *111*, 219–226. [CrossRef]
39. Zhou, G.; Sun, Y.; Xin, H.; Zhang, Y.; Li, Z.; Xu, Z. In vivo antitumor and immunomodulation activities of different molecular weight lambda-carrageenans from *Chondrus ocellatus*. *Pharmacol. Res.* **2004**, *50*, 47–53. [CrossRef]
40. Valaperta, R.; Tejada, M.R.; Frigerio, M.; Moroni, A.; Ciulla, E.; Cioffi, S.; Capelli, P.; Costa, E. *Staphylococcus aureus* nosocomial infections: The role of a rapid and low-cost characterization for the establishment of a surveillance system. *New Microbiol.* **2010**, *33*, 223–232.
41. Zeaki, N.; Johler, S.; Skandamis, P.N.; Schelin, J. The Role of Regulatory Mechanisms and Environmental Parameters in Staphylococcal Food Poisoning and Resulting Challenges to Risk Assessment. *Front. Microbiol.* **2019**, *10*, 1307. [CrossRef] [PubMed]
42. Mostafa, A.A.; Al-Askar, A.A.; Almaary, K.S.; Dawoud, T.M.; Sholkamy, E.N.; Bakri, M.M. Antimicrobial activity of some plant extracts against bacterial strains causing food poisoning diseases. *Saudi J. Biol. Sci.* **2018**, *25*, 361–366. [CrossRef] [PubMed]
43. Tabbene, O.; Slimene, I.B.; Bouabdallah, F.; Mangoni, M.L.; Urdaci, M.; Limam, F. Production of Anti-Methicillin-Resistant *Staphylococcus* Activity from *Bacillus subtilis* sp. Strain B38 Newly Isolated from Soil. *Appl. Biochem. Biotechnol.* **2009**, *157*, 407–419. [CrossRef] [PubMed]
44. Lin, M.Y.; Yuan, Z.L.; Hu, D.D.; Hu, G.H.; Zhang, R.L.; Zhong, H.; Yan, L.; Jiang, Y.Y.; Su, J.; Wang, Y. Effect of loureirin A against *Candida albicans* biofilms. *Chin. J. Nat. Med.* **2019**, *17*, 616–623. [CrossRef]
45. Vale-Silva, L.A.; Buchta, V.; Valentova, E. Effect of sub-inhibitory concentration of some established and experimental antifungal compounds on the germ tube formation in *Candida albicans*. *Folia Microbiol.* **2007**, *52*, 39–43. [CrossRef] [PubMed]
46. Ariyachet, C.; Solis, N.V.; Liu, Y.; Prasadarao, N.V.; Filler, S.G.; McBride, A.E. SR-Like RNA-binding protein Slr1 affects *Candida albicans* filamentation and virulence. *Infect. Immun.* **2013**, *81*, 267–1276. [CrossRef]
47. Borghi, E.; Morace, G.; Borgo, F.; Rajendran, R.; Sherry, L.; Nile, C.; Ramage, G. New strategic insights into managing fungal biofilms. *Front. Microbiol.* **2015**, *6*, 1077. [CrossRef]
48. de Jesus Raposo, M.F.; de Morais, A.M.; de Morais, R.M. Influence of sulphate on the composition and antibacterial and antiviral properties of the exopolysaccharide from *Porphyridium cruentum*. *Life Sci.* **2014**, *101*, 56–63. [CrossRef]
49. Doghri, I.; Lavaud, J.; Dufour, A.; Bazire, A.; Lanneluc, I.; Sablé, S. Cell-bound exopolysaccharides from an axenic culture of the intertidal mudflat Navicula phyllepta diatom affect biofilm formation by benthic bacteria. *J. Appl. Phycol.* **2017**, *29*, 165–177. [CrossRef]
50. Vijayabaskar, P.; Vaseela, N.; Thirumaran, G. Potential antibacterial and antioxidant properties of a sulfated polysaccharide from the brown marine algae *Sargassum swartzii*. *Chin. J. Nat. Med.* **2012**, *10*, 421–428. [CrossRef]
51. Amorim, R.; Rodrigues, J.; Holanda, M.; Quinderé, A.; Paula, R.; Melo, V.M.M.; Benevides, N.M.B. Antimicrobial effect of a crude sulfated polysaccharide from the red seaweed *Gracilaria ornate*. *Braz. Arch. Biol. Technol.* **2012**, *55*, 171–181. [CrossRef]
52. Costa, E.; Silva, S.; Tavaria, F.; Pintado, M. Antimicrobial and Antibiofilm Activity of Chitosan on the Oral Pathogen *Candida albicans*. *Pathogens* **2014**, *3*, 908–919. [CrossRef] [PubMed]
53. Cobrado, L.; Silva-Dias, A.; Azevedo, M.M.; Pina-Vaz, C.; Rodrigues, A.G. In vivo antibiofilm effect of cerium, chitosan and hamamelitannin against usual agents of catheter-related bloodstream infections. *J. Antimicrob. Chemother.* **2013**, *68*, 126–130. [CrossRef] [PubMed]
54. No, H.K.; Park, N.Y.; Lee, S.H.; Meyers, S.P. Antibacterial activity of chitosans and chitosan oligomers with different molecular weights. *Int. J. Food Microbiol.* **2002**, *74*, 65–72. [CrossRef]
55. Silva, L.P.; Britto, D.; Seleghim, M.H.R.; Assis, O.B.G. In vitro activity of water-soluble quaternary chitosan chloride salt against. *E coli. World J. Microbiol. Biotechnol.* **2010**, *26*, 2089–2092. [CrossRef]
56. Laroche, C.; Delattre, C.; Mati-Baouche, N.; Salah, R.; Ursu, A.V.; Moulti-Mati, F.; Michaud, P.; Pierre, G. Bioactivity of Chitosan and Its Derivatives. *Curr. Org. Chem.* **2018**, *22*, 641–667. [CrossRef]
57. Rabea, E.I.; Badawy, M.E.T.; Stevens, C.V.; Smagghe, G.; Steurbaut, W. Chitosan as antimicrobial agent: Applications and mode of action. *Biomacromolecules* **2003**, *4*, 1457–1465. [CrossRef]
58. Liu, X.F.; Guan, Y.L.; Yang, D.Z.; Li, Z.; Yao, K.D. Antibacterial action of chitosan and carboxymethylated chitosan. *J. Appl. Polym. Sci.* **2001**, *79*, 1324–1335.
59. Monsigny, M.; Petit, C.; Roche, A.C. Colorimetric determination of neutral sugars by a resorcinol sulfuric acid micromethod. *Anal. Biochem.* **1988**, *175*, 525–530. [CrossRef]
60. Blumenkrantz, N.; Asboe-Hansen, G. New method for quantitative determination of uronic acids. *Anal. Biochem.* **1973**, *54*, 484–489. [CrossRef]
61. Montreuil, J.; Spick, G.; Chosson, A.; Segard, E.; Scheppler, N. Methods of study of the structure of glycoproteins. *J. Pharm. Belg.* **1963**, *18*, 529–546. [PubMed]

62. Dodgson, K.S.; Price, R.G. A note on the determination of the ester sulphate content of sulphated polysaccharides. *Biochem. J.* **1962**, *84*, 106–110. [CrossRef] [PubMed]
63. Lowry, O.H.; Rosenbrough, N.J.; Farr, A.L.; Randall, R.J. Protein measurement with the folin phenol reagent. *J. Biol. Chem.* **1951**, *193*, 265–269. [CrossRef]
64. Azaiez, S.; Ben Slimene, I.; Karkouch, I.; Essid, R.; Jallouli, S.; Djebali, N.; Elkahoui, S.; Limam, F.; Tabbene, O. Biological control of the soft rot bacterium *Pectobacterium carotovorum* by Bacillus amyloliquefaciens strain Ar10 producing glycolipid-like compounds. *Microbiol. Res.* **2018**, *217*, 23–33. [CrossRef]
65. Grieco, P.; Carotenuto, A.; Auriemma, L.; Limatola, A.; Di Maro, S.; Merlino, F.; Mangoni, M.L.; Luca, V.; Di Grazia, A.; Campiglia, P.; et al. Novel α-MSH peptide analogues with broad spectrum antimicrobial activity. *PLoS ONE* **2013**, *8*, e61614. [CrossRef]
66. Jin, Y.; Yip, H.K.; Samaranayake, Y.H.; Yau, J.Y.; Samaranayake, L.P. Biofilm-forming ability of *Candida albicans* is unlikely to contribute to high levels of oral yeast carriage in cases of human immunodeficiency virus infection. *J. Clin. Microbiol.* **2003**, *41*, 2961–2967. [CrossRef]
67. Medjeldi, S.; Bouslama, L.; Benabdallah, A.; Essid, R.; Haou, S.; Elkahoui, S. Biological activities, and phytocompounds of northwest Algeria *Ajuga iva* (L) extracts: Partial identification of the antibacterial fraction. *Microb. Pathog.* **2018**, *121*, 173–178. [CrossRef]

Article

The Protect Effects of Chitosan Oligosaccharides on Intestinal Integrity by Regulating Oxidative Status and Inflammation under Oxidative Stress

Ruixia Lan, Qingqing Chang, Linlin Wei and Zhihui Zhao *

College of Coastal Agriculture Sciences, Guangdong Ocean University, Zhanjiang 524088, China;
Lanrx@gdou.edu.cn (R.L.); changqingqing@outlook.com (Q.C.); wllgdhy@163.com (L.W.)
* Correspondence: zhzhao@gdou.edu.cn; Tel.: +86-1356-050-3527

Abstract: The aim of this study was to evaluate the effects of the dietary supplementation of chitosan oligosaccharides (COS) on intestinal integrity, oxidative status, and the inflammation response with hydrogen peroxide (H_2O_2) challenge. In total, 30 rats were randomly assigned to three groups with 10 replications: CON group, basal diet; AS group, basal diet + 0.1% H_2O_2 in drinking water; ASC group, basal diet + 200 mg/kg COS + 0.1% H_2O_2 in drinking water. The results indicated that COS upregulated ($p < 0.05$) villus height (VH) of the small intestine, duodenum, and ileum; mucosal glutathione peroxidase activity; jejunum and ileum mucosal total antioxidant capacity; duodenum and ileum mucosal interleukin (IL)-6 level; jejunum mucosal tumor necrosis factor (TNF)-α level; duodenum and ileum mucosal IL-10 level; the mRNA expression level of zonula occludens (ZO)-1 in the jejunum and ileum, claudin in the duodenum, nuclear factor-erythroid 2-like 2 in the jejunum, and heme oxygenase-1 in the duodenum and ileum; and the protein expression of ZO-1 and claudin in jejunum; however, it downregulated ($p < 0.05$) serum diamine oxidase activity and D-lactate level; small intestine mucosal malondialdehyde content; duodenum and ileum mucosal IL-6 level; jejunum mucosal TNF-α level; and the mRNA expression of IL-6 in the duodenum and jejunum, and TNF-α in the jejunum and ileum. These results suggested COS could maintain intestinal integrity under oxidative stress by modulating the intestinal oxidative status and release of inflammatory cytokines.

Keywords: chitosan oligosaccharides; inflammation cytokines; intestine; oxidative status; oxidative stress

1. Introduction

The pernicious effects of oxidative stress on intestinal function have been widely studied [1,2]. Studies have demonstrated oxidative stress was one of the vital factors contributing to intestinal injury and disfunction [3,4]. Oxidative stress was frequently related to increases in interleukin (IL)-1β, IL-6, and tumor necrosis factor (TNF)-α [3,5], and undermined intestinal function [6]. Both oxidative stress and inflammation could disturb intestinal function by over-production of reactive oxygen species (ROS) and pro-inflammatory cytokines [2,7]. Impaired intestinal integrity, accompanied with intestinal permeability and histological changes [8–10], promote the transportation of toxic luminal substances, which may contribute to intestinal disease and even death [10–12]. The intestine predominantly responds to virous stressors, especially oxidative stress and inflammation [3,13–15]. Hence, alleviating intestinal oxidative stress and inflammation are important in maintaining intestinal function. Therefore, an ideal candidate, which has free-radical scavenging activity, and antioxidant and anti-inflammation capacities, is urgently needed to maintain intestinal function under oxidative stress.

Chitosan oligosaccharides (COS) are the degraded products of chitosan; compared to chitosan, COS are non-toxic, non-allergenic, less viscous, and entirely soluble in water [16]. COS also have multiple properties, including free-radical scavenging, and antioxidant,

anti-inflammatory, antibacterial, and immune-enhancing activities, which capture much attention, and they are widely used in biomedical medicine and agriculture science [17]. Qiao et al. [18] reported COS could relieve sepsis by virtue of their antioxidation property and anti-inflammatory effect. Liu et al. [19] demonstrated COS could remit oxidative damage in umbilical vein endothelial cells. Lan et al. [20] demonstrated COS remitted H_2O_2-induced oxidative stress in the liver, kidney and spleen by alleviating oxidative and inflammation stress. Furthermore, COS also have positive effects on intestinal health [21,22]. It is believed that intestinal oxidative stress and the inflammation response are highly related to intestinal integrity and function. COS captured attention due to antioxidant and anti-inflammatory activities. Therefore, this study was done to evaluate the effects of dietary COS supplementation on intestinal integrity, oxidative status, and the inflammatory response with H_2O_2 challenge.

2. Results

2.1. Intestinal Mucosal Morphology

Figure 1 and Table 1 show intestinal morphology indices. Compared with the CON group, the villus height (VH) and VH to crypt depth (CD) ratio of the small intestine were decreased ($p < 0.05$) in the AS group (basal diet + 0.1% H_2O_2 in drinking water). Compared with the AS group, COS increased the VH of the small intestine, and the VH:CD of the duodenum and jejunum.
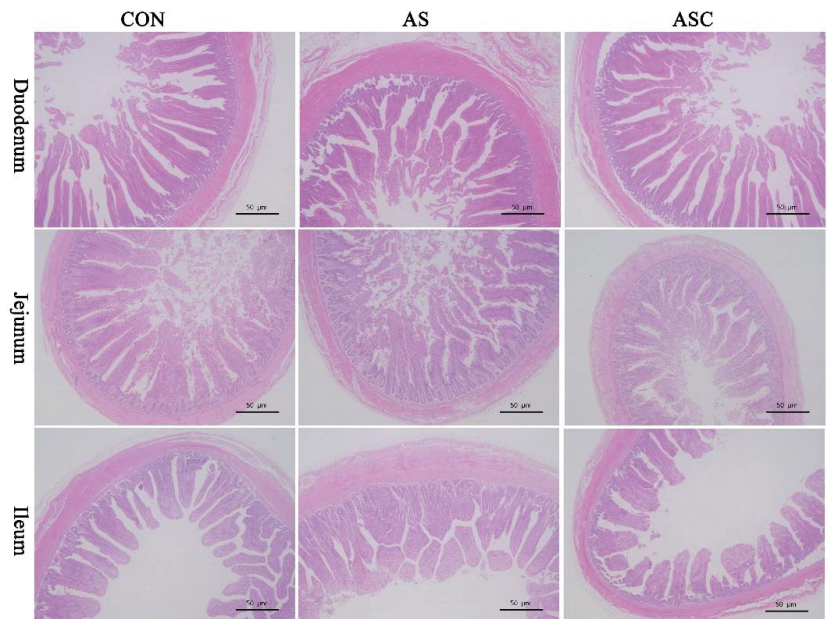

Figure 1. Effects of chitosan oligosaccharides on intestinal morphology when challenged with hydrogen peroxide. CON group, basal diet; AS group, basal diet + 0.1% hydrogen peroxide (H_2O_2) in drinking water; ASC group, basal diet + 200 mg/kg COS + 0.1% H_2O_2 in drinking water. Scale label: 50 μm.

Table 1. Effects of chitosan oligosaccharides on intestinal mucosal morphology when challenged with hydrogen peroxide.

Items [1]	CON	AS	ASC	SEM [2]	*p*-Value
		Duodenum			
VH (μm)	277.71 [a]	219.07 [b]	258.72 [c]	5.70	<0.0001
CD (μm)	104.32	97.34	104.08	2.48	0.1265
VH:CD	2.67 [a]	2.26 [b]	2.50 [a]	0.06	0.0021
		Jejunum			
VH (μm)	209.73 [a]	157.59 [b]	190.96 [a]	6.86	0.0010
CD (μm)	84.68	79.47	81.85	3.41	0.5751
VH:CD	2.48 [a]	2.00 [b]	2.34 [a]	0.05	0.0002
		Ileum			
VH (μm)	170.16 [a]	116.56 [b]	150.19 [a]	7.26	0.0013
CD (μm)	67.69	61.19	65.81	2.41	0.1969
VH:CD	2.52 [a]	1.91 [b]	2.29 [ab]	0.13	0.0221

[1] COS, chitosan oligosaccharide; CON group, basal diet; AS group, basal diet + 0.1% hydrogen peroxide (H_2O_2) in drinking water; ASC group, basal diet + 200 mg/kg COS + 0.1% H_2O_2 in drinking water; VH, villus height; CD, crypt depth. [2] SEM, standard error of mean. [a,b,c] Two different superscripts indicate a significant difference in the same row ($p < 0.05$).

2.2. Intestinal Permeability

Compared with the CON group, serum diamine oxidase (DAO) activity and D-lactate acid (D-LA) content were upregulated ($p < 0.05$) in the AS group (Figure 2). Compared with the AS group, COS downregulated ($p < 0.05$) serum DAO activity and D-LA content.
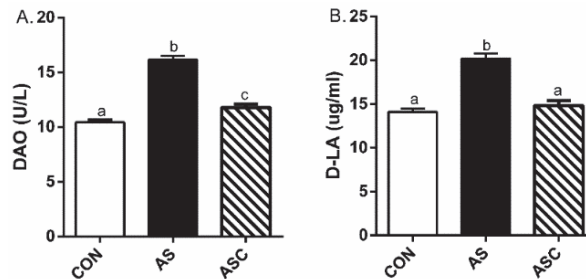
Figure 2. Effects of chitosan oligosaccharides on serum DAO and D-LA after hydrogen peroxide challenge. CON group, basal diet; AS group, basal diet + 0.1% H_2O_2 in drinking water; ASC, basal diet + 200 mg/kg COS + 0.1% H_2O_2 in drinking water. (**A**) DAO content; (**B**) D-LA activity. Values are means ± standard errors. Columns that have different numbers above them statistically differ ($p < 0.05$). [a,b,c] Columns that have different letter statistically differ ($p < 0.05$).

2.3. Antioxidant Capacity

Figure 3 presents the antioxidant indicators in the small intestinal mucosa. In duodenum, the malondialdehyde (MDA) content in the AS group was higher ($p < 0.05$) than the contents in the CON and ASC groups, but the glutathione peroxidase (GSH-Px) activity was lower ($p < 0.05$). In the jejunum, the MDA content in the AS group was higher ($p < 0.05$) than in the CON and ASC groups; the superoxide dismutase (SOD) activity in the CON group was higher ($p < 0.05$) than in the AS and ASC groups; the total antioxidant capacity (T-AOC) activity in the AS group was lower ($p < 0.05$) than in the CON and ASC groups. In the ileum, the MDA contents in the CON and ASC groups were lower ($p < 0.05$) than that in the AS group, but the GSH-Px and T-AOC activities were higher.
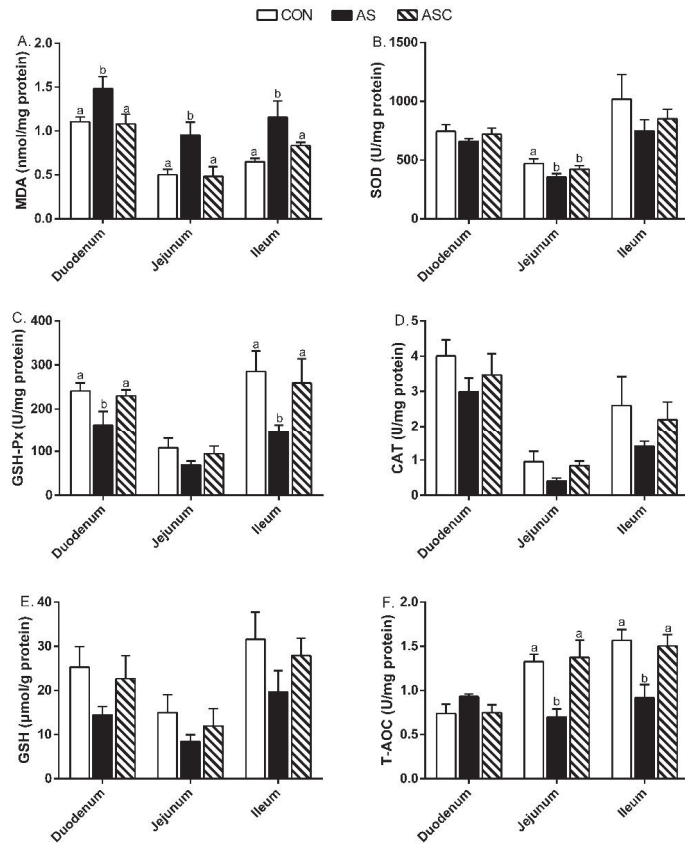
Figure 3. Effects of chitosan oligosaccharides on small intestine antioxidant indicators when challenged with hydrogen peroxide. CON group, basal diet; AS group, basal diet + 0.1% H_2O_2 in drinking water; ASC, basal diet + 200 mg/kg COS + 0.1% H_2O_2 in drinking water. (**A**) MDA content; (**B**) SOD activity; (**C**) GSH-Px activity; (**D**) CAT activity; (**E**) GSH content; (**F**) T-AOC activity. Values indicate means ± standard errors. [a,b] Columns that have different letter statistically differ ($p < 0.05$).

2.4. Free Radical Scavenging Activity

Figure 4 presents the free-radical scavenging capacities in jejunum mucosa. The 1,1-diphenyl-2-picrylhydrazyl (DPPH), 2,2′-azino-bis-3-ethylbenzothiazoline-6-sulfonic acid (ABTS), O_2^- (superoxide radical) and hydroxyl radical (OH^-) scavenging activities in the CON and ASC groups were higher ($p < 0.05$) than in the AS group.

2.5. Intestinal Mucosal Immunity

In the duodenum, the IL-6 and TNF-α contents in the AS group were enhanced ($p < 0.05$) compared to CON and ASC groups (Figure 5), but the IL-10 content was decreased ($p < 0.05$). In the ileum, the IL-6 content in the AS group was increased ($p < 0.05$) over CON and ASC groups, but the IL-10 content was decreased ($p < 0.05$).
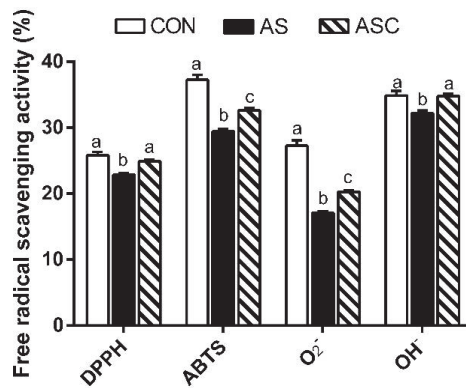
Figure 4. Effects of chitosan oligosaccharides on the free-radical scavenging activity of the jejunum when challenged with hydrogen peroxide. CON group, basal diet; AS group, basal diet + 0.1% H_2O_2 in drinking water; ASC group, basal diet + 200 mg/kg COS + 0.1% H_2O_2 in drinking water. The free-radical scavenging activity was calculated on the basis of the protein content (mg/mL) of the jejunum mucosa. Values indicate means ± standard errors. [a,b,c] Columns that have different letter statistically differ ($p < 0.05$).
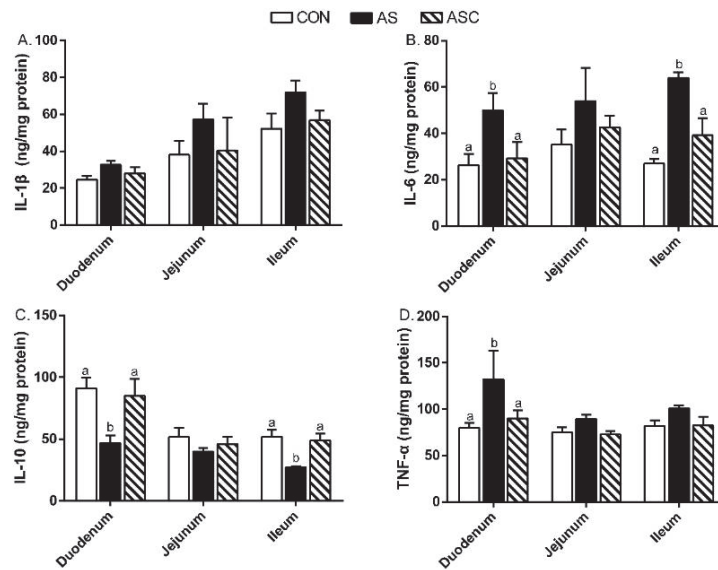
Figure 5. Effects of chitosan oligosaccharides on inflammatory cytokines in the small intestine when challenged with hydrogen peroxide. CON group, basal diet; AS group, basal diet + 0.1% H_2O_2 in drinking water; ASC group, basal diet + 200 mg/kg COS + 0.1% H_2O_2 in drinking water. (**A**) IL-1β content; (**B**) IL-6 content; (**C**) IL-10 content; (**D**) TNF-α content. Values are indicated as means ± standard errors. [a,b] Columns that have different letter statistically differ ($p < 0.05$).

Furthermore, we also examined the related cytokines' gene expression in the small intestine (Figure 6). In the duodenum, the relative gene expression levels of IL-1β and TNF-α in the AS group were higher ($p < 0.05$) than in the CON group; IL-6 in the AS group was enhanced ($p < 0.05$) over CON and ASC groups; IL-10 in the AS and ASC groups was less present ($p < 0.05$) compared to the CON group. In the jejunum, the relative gene

expression levels of IL-6 and TNF-α in the AS group were increased ($p < 0.05$) compared to CON and ASC groups; IL-10 in the AS and ASC groups was decreased ($p < 0.05$) compared to the CON group. In the ileum, the relative gene expression of IL-1β in the AS group was enhanced ($p < 0.05$) compared to the CON group; TNF-α in the AS group was higher ($p < 0.05$) than in CON and ASC groups.

Figure 6. Effects of chitosan oligosaccharides on inflammatory cytokine-related gene mRNA expression in the small intestine when challenged with hydrogen peroxide. CON group, basal diet; AS group, basal diet + 0.1% H_2O_2 in drinking water; ASC group, basal diet + 200 mg/kg COS + 0.1% H_2O_2 in drinking water. (**A**) relative IL-1β mRNA level; (**B**) relative IL-6 mRNA level; (**C**) relative IL-10 mRNA level; (**D**) relative TNF-α mRNA level. Values indicate means ± standard errors. [a,b] Columns that have different letter statistically differ ($p < 0.05$).

## 2.6. Intestinal Barrier Function-Related Gene Expression

In the duodenum, the relative gene expression of claudin in the AS group was decreased ($p < 0.05$) compared to CON and ASC groups (Figure 7). In the jejunum and ileum, the relative gene expression of zonula occludens (ZO)-1 in the AS group was decreased ($p < 0.05$) compared to CON and ASC groups. In addition, we found that the expression levels of ZO-1 and claudin protein in the AS group were decreased ($p < 0.05$) compared to CON and ASC groups (Figure 8); and the expression of occludin protein in the AS and ASC groups was decreased ($p < 0.05$) compared to the CON group in jejunum mucosa.

We also examined the critical gene expression in the antioxidant signaling pathway. As shown in Figure 9, in the duodenum, the relative gene expression of heme oxygenase (HO)-1 in the AS group was decreased ($p < 0.05$) compared to CON and ASC groups. In the jejunum, the relative gene expression of nuclear factor-erythroid 2-like 2 (Nrf2) in the AS group was lower ($p < 0.05$) than that in the CON group. In the ileum, the relative gene expression of Nrf2 in the AS group was decreased ($p < 0.05$) compared to the CON group; and the relative gene expression of HO-1 in the AS group was decreased ($p < 0.05$) compared to CON and ASC groups.

Figure 7. Effects of chitosan oligosaccharides on intestinal barrier-related gene mRNA expression of the small intestine when challenged with hydrogen peroxide. CON group, basal diet; AS group, basal diet + 0.1% H_2O_2 in drinking water; ASC group, basal diet + 200 mg/kg COS + 0.1% H_2O_2 in drinking water. (**A**) relative ZO-1 mRNA expression level; (**B**) relative occludin mRNA expression level; (**C**) relative claudin mRNA expression level. Values indicated as means ± standard errors. [a,b] Columns that have different letter statistically differ ($p < 0.05$).

Figure 8. Effects of chitosan oligosaccharides on tight junction protein expression in the jejunum when challenged with hydrogen peroxide. CON group, basal diet; AS group, basal diet + 0.1% H_2O_2 in drinking water; ASC group, basal diet + 200 mg/kg COS + 0.1% H_2O_2 in drinking water. [a,b,c] Columns that have different letter statistically differ ($p < 0.05$).
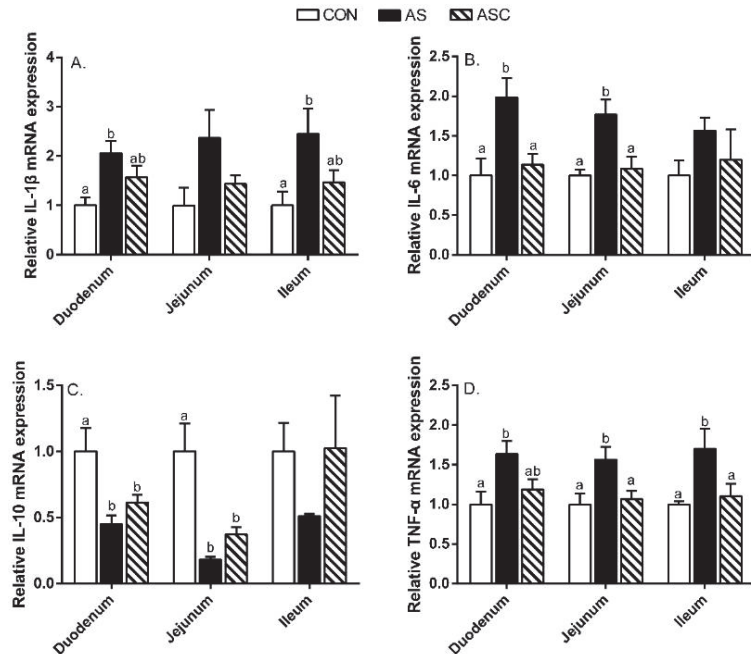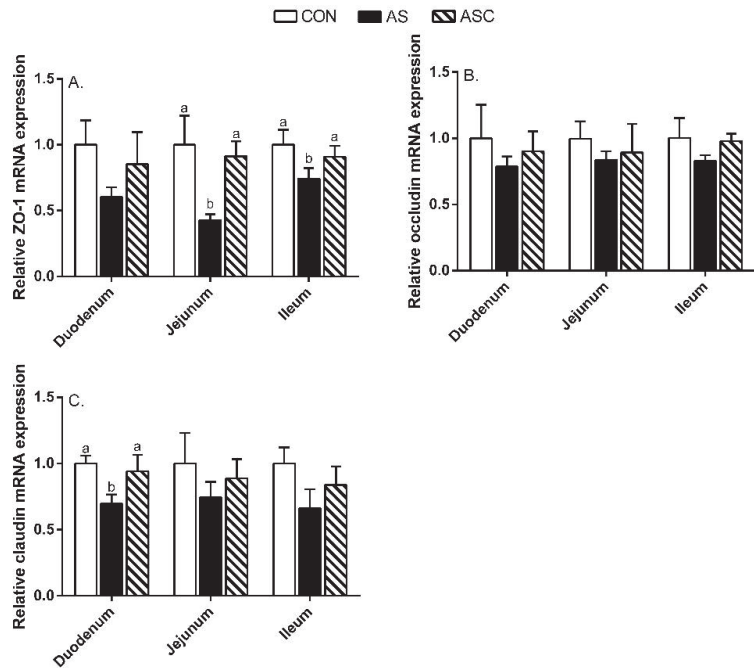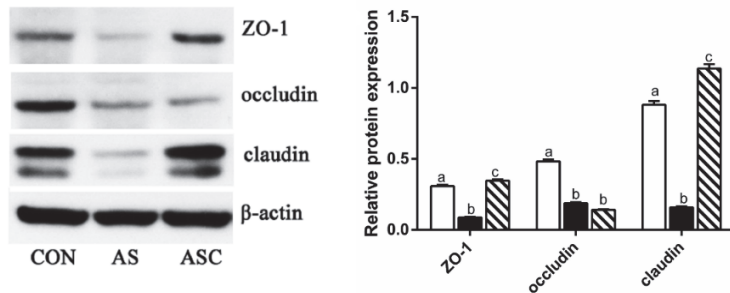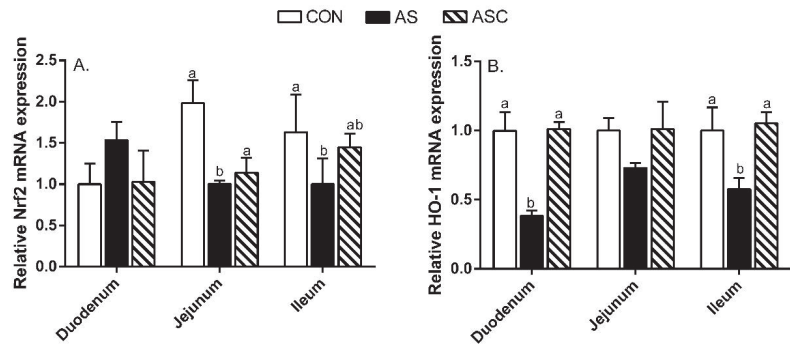
Figure 9. Effects of chitosan oligosaccharides on Nrf2 and HO-1 gene mRNA expression in the small intestine when challenged with hydrogen peroxide. CON group, basal diet; AS group, basal diet + 0.1% H_2O_2 in drinking water; ASC group, basal diet + 200 mg/kg COS + 0.1% H_2O_2 in drinking water. (**A**) relative Nrf2 mRNA expression level; (**B**) relative HO-1 mRNA expression level. Values indicated as means ± standard errors. [a,b] Columns that have different letter statistically differ ($p < 0.05$).

3. Discussion

Intestinal barrier integrity was commonly assessed by gut morphology, serum DAO activity, and D-LA activity. The gut morphology was a useful biomarker of the stress response of the intestinal tract [9,23,24]. The DAO activity and D-LA content were biomarkers of intestinal permeability [3,11,25]. In this study, oxidative stress decreased the VH of the small intestine, and enhanced DAO content and D-LA activity, demonstrating that oxidative stress resulted in intestinal injury by increasing intestinal permeability and decreasing VH [3,9]. As expected, COS decreased DAO content and D-LA activity, and increased the VH of the small intestine; hence, COS had positive effects on intestinal permeability. These results are also in line with former studies by Li et al. [21] and Zhao et al. [26], who indicated COS decreased serum DAO activity. The structure of the intestinal morphology reflected gut health status. Li et al. [21] illustrated COS increased the VH of the duodenum and ileum in broilers. Liu et al. [27] and Liu et al. [28] reported dietary COS supplementation increased the VH of the jejunum and ileum in weaning pigs. The positive effects of COS on intestinal permeability and morphology could explain the improving intestinal function with COS supplementation.

The tight junction proteins maintained and regulated the intestinal barrier function. The tight junction proteins mainly consisted of the transmembrane proteins claudin and occludin, and peripheral membrane protein ZO-1. Therefore, the decreased mRNA expression of ZO-1, claudin, and occludin reflected intestinal barrier dysfunction [4]. In this study, oxidative stress downregulated the protein expression of ZO-1, occludin, and claudin in the jejunum; and the mRNA expression of claudin in the duodenum and ZO-1 in the jejunum and ileum, which were all consistent with the results reported by Song et al. [29] and Cao et al. [1]. COS upregulated the protein expression of ZO-1 and claudin in the jejunum, and the mRNA expression of ZO-1 in the jejunum and ileum, and claudin in the duodenum—similarly to other studies on mice fed high-fat diets [30], dexamethasone-challenged broilers [31], and weaning pigs [32,33]. These results demonstrated that COS could alleviate oxidative-induced intestinal barrier function partly by maintaining the intestinal structure, intestinal permeability, and tight junction functionality.

Accumulating evidence indicates that oxidative status was an important factor in intestinal barrier function. An imbalance between oxidation and the antioxidant defense system leads to oxidative stress and inflammation, and finally, induces intestinal barrier dysfunction [12]. SOD, GSH-Px, and CAT were regarded as the main antioxidant enzymes for scavenging free radicals. GSH was regarded as the most important non-enzymatic

antioxidant which scavenges single oxygen molecules and hydroxyl radicals. The T-AOC can reflect the total antioxidant capacity. MDA is an indicator of oxidative stress [34]. H_2O_2 can stimulate ROS over-production, disrupt the activity of antioxidant enzymes, and induce lipid peroxidation [35,36]. Consistently, in this study, oxidative stress induced higher small intestine MDA content, along with lower duodenum and ileum mucosal GSH-Px activity, jejunum mucosal SOD activity, and jejunum and ileum mucosal T-AOC activity. COS reduced duodenum, jejunum, and ileum mucosal MDA content; and increased duodenum and ileum mucosal GSH-Px activity, and jejunum and ileum mucosal T-AOC activity, suggesting COS could alleviate intestinal mucosal oxidative stress by improving the antioxidative enzyme activity and decreasing MDA content. These results are consistent with Lan et al. [20], who indicated COS could increase SOD, CAT, GSH-Px, and T-AOC activity, and decrease the MDA level with an H_2O_2 challenge. Li et al. [21] also indicated COS increased SOD activity in the duodenum's mucosa and decrease the MDA level in the jejunum and ileum's mucosa in broilers. Similarly, Li et al. [22] indicated that dietary COS supplementation increased the inhibition of hydroxy radical capacity, and GSH, T-AOC, GSH-Px, and SOD activity, whereas decreased MDA content in the ileum mucosa of broilers. Nrf2 is a nuclear transcription factor and plays a vital role in antagonizing oxidative stress [37]. Our results show decreased mRNA expression of Nrf2 in the jejunum and ileum, and HO-1 in the duodenum and ileum by H_2O_2 challenge. Other studies illustrated the increased Nrf2 mRNA expression level could increase the mRNA expression of SOD and GSH-Px [3]; the decreased Nrf2 and HO-1 mRNA expression levels may be related to a response to oxidative stress. As expected, COS enhanced the mRNA expression of Nrf2 in the jejunum and HO-1 in the duodenum and ileum—similarly to other studies on doxorubicin-challenged rats [38] and mice fed a high-fat diet [39]. Collectively, the combined results illustrate that the increased antioxidant enzyme activity may be mediated by Nrf2/HO-1 signaling pathway. Additionally, the efficiency of the free-radical scavenging capacities reflected the neutralization of free radical capacities, or hydrogen donor capacity [40]. In this study, COS improved the radical scavenging capacity of the jejunum mucosa; that may relate to antioxidant capacity and hydrogen donation ability [17].

Inflammation cytokines play vital roles in the inflammatory and immune responses. The accumulating literature illustrates inflammation is an important marker in intestinal disfunction [3,12]. Chen et al. [12] indicated that over-production of cytokines could change the intestinal permeability and tight junction structure by modulating tight junction-related genes expression in weaning piglets. The over-production of IL-1β, IL-6, and TNF-α directly resulted in intestinal mucosal injury [41,42]. Therefore, suppressing the over-production of intestinal mucosal IL-1β, IL-6, and TNF-α was a useful way to maintain the intestinal function. Previous studies indicated that stressors could disturb the balance between anti- and pro-inflammatory responses by increasing pro-inflammatory cytokines' production [12,43,44]. In this study, the duodenum and ileum mucosal IL-6 content, and jejunum mucosal TNF-α level were higher, whereas the duodenum and ileum mucosal IL-10 levels were decreased, in the AS group compared to the CON group, indicating that oxidative stress resulted in inflammation in the intestine. Furthermore, the levels of mRNA expression of IL-1β in the duodenum and ileum, IL-6 in the duodenum and jejunum, and TNF-α in the small intestine in the AS group were increased compared to the CON group, but the expression levels of IL-10 in the duodenum and jejunum were decreased. Dietary COS supplementation decreased the duodenum and ileum mucosal IL-6 level and jejunum mucosal TNF-α level; inhibited the expression of IL-6 in the jejunum and ileum, and TNF-α in the jejunum and ileum; and increased the duodenum and ileum mucosal IL-10 levels, all of which was in consistent with the results of Hu et al. [33], who reported COS reduced IL-1β and TNF-α mRNA expression levels in jejunum mucosa in weaning pigs. Besides, COS decreased the IL-6 and TNF-α mRNA expression levels in the liver of mice fed a high-fat diet [39]. These results suggest that COS may alleviate intestinal inflammation by suppressing the levels of IL-1β, IL-6, and TNF-α [45,46]. However, in this study, we

ignored the immune cells in the mucosal immune system, especially the mast cells, which play a vital role in the regulation of intestinal mucosal immune function and intestinal barrier function. Further study would focus on this point.

In conclusion, COS had beneficial effects on intestinal integrity by improving the antioxidant capacity and suppressing the release of inflammatory cytokines. Dietary COS supplementation may be an effective nutritional strategy to alleviate the detrimental effects of oxidative stress.

4. Materials and Methods

4.1. Animals, Diets, and Experimental Design

In total, 30 male Sprague–Dawley rats (8–10 weeks old, 178.39 ± 5.12 g) were purchased from Beijing Administration Office of Laboratory Animals and acclimatized for 7 days before the experiment. The rats were provided with a pelleted diet, had free access to diet and water, and were housed at constant temperature (24 ± 2 °C) and relative humidity (60% ± 5%) on a 12-h light–dark cycle. The basal diet composition is shown in Table 2. The experimental protocol and use of rats were approved by the Animal Care and Use Committee of Guangdong Ocean University, Zhanjiang, China (SYXK-2018-0147, 2018).

Table 2. The composition of basal diet.

Ingredients (g/kg)	Basal Diet	Basal Diet with 200 mg/kg COS
Cornstarch	464.00	463.80
Chitosan oligosaccharides	0	0.20
Casein	140.00	140.00
Dextrinized cornstarch	155.00	155.00
Sucrose	100.00	100.00
Soybean oil	40.00	40.00
Cellulose acetate	50.00	50.00
Mineral premix [1]	35.00	35.00
Vitamin premix [2]	10.00	10.00
L-Methionine	1.80	1.80
L-Cystine	1.80	1.80
Choline bitartrate	2.30	2.30
Tert-butylhydroquinone	0.10	0.10
Gross energy (MJ/kg)	16.22	16.20

[1] Mineral premix (mg/kg of premix): $CaCO_3$, 3.70×10^5; KH_2PO_4, 1.96×10^5; $K_3C_6H_5O_7 \cdot H_2O$, 7.08×10^4; NaCl, 7.4×10^4; K_2SO_4, 4.66×10^4; MgO, 2.4×10^4; $FeC_6H_5O_7H_2O$, 6.06×10^3; $ZnCO_3$, 1.65×10^3; $MnCO_3$, 630; $CuCO_3$, 324; $NaSiO_3 \cdot 9H_2O$, 1.45×10^3; $CrK(SO_4) \cdot 12H_2O$, 275; LiCl, 17.4; H_3BO_3, 81.5; NaF, 63.5; $NiCO_3 \cdot 2Ni(OH)_2 \cdot 4H_2O$, 30.6; NH_4VO_3, 6.6; sucrose was added to make a total of 1 kg; [2] vitamin premix (mg/kg of premix): nicotinic, 3.0×10^3; calcium pantothenate, 1.6×10^3; pyridoxine hydrochloride, 700; thiamine hydrochloride, 600; riboflavin, 600; folic acid, 200; D-biotin, 20; cyanocobalamin, 2.5×10^3; a-tocopherol, 1.5×10^4; cholecalciferol, 250; phylloquinone, 75; sucrose was added to make a total of 1 kg.

H_2O_2 induced oxidative stress by generation of potent ROS [23–25]. ROS caused lipid peroxidation, membrane disintegration, and endothelial cell damage [26]. The 30 rats were randomly divided into three groups: CON, basal diet; AS group, basal diet + 0.1% H_2O_2 in drinking water; ASC, basal diet + 200 mg/kg COS + 0.1% H_2O_2 in drinking water.

4.2. Sample Collection

At the end of the experiment, all rats were anesthetized and sacrificed to collected blood samples through the eyeballs. The blood samples were centrifuged at 4 °C, $3200 \times g$, for 10 min to obtain serum for further analysis. The duodenum, jejunum, and ileum were divided into two parts, one part fixed in 10% buffered formalin for morphology analysis, the rest for collecting mucosa, and frozen in liquid nitrogen for further analysis.

4.3. Serum Diamine Oxidase (DAO) and D-Lactate Acid (D-LA)

Serum DAO activity and D-LA level were measured with commercial kits (Nanjing Jiancheng Institute of Bioengineering, Nanjing, China).

4.4. Intestinal Morphology

The intestinal morphology analysis was performed according our previously described methods [2].

4.5. Intestinal Antioxidant Parameters and Inflammatory Cytokines

About 1 g of each mucosal sample was homogenized at a ratio of 1:9 (weight/volume) with ice-cold PBS. Homogenate was centrifuged at $3200\times g$ for 10 min at 4 °C to obtain supernatant; Bradford method was used to determine the supernatant protein concentration. The antioxidant parameters and inflammatory cytokines were measured with corresponding assay kits (Nanjing Jiancheng Bioengineering Institute, Nanjing, China).

4.6. Free Radical Scavenging Activities

DPPH, ABTS, $O_2{}^-$, and OH^- scavenging activities were evaluated by following the methods described in another study [20].

4.7. Gene Expression Analysis

Total RNA extraction, cDNA reverse transcription, and real-time polymerase chain reaction analysis were done according to our previous described methods [47]. The primers are shown in Table 3. The relative mRNA expression was calculated by $2^{-\Delta\Delta Ct}$ method.

Table 3. Primers for real-time PCR.

Gene	Accession NO.	Primer Sequence (5′ to 3′)	Product Size (bp)
GAPDH	NM_017008.4	F: GGCAAGTTCAACGGCACAG R: GACGCCAGTAGACTCCACGAC	144
IL-1β	NC_005102.4	F: CCACCTCCAGGGACAGGATA R: TGGGATCTACACTCTCCAGC	132
IL-6	NM_012589.2	F: CAAGTCCGGAGAGGAGACT R: TTCTGACAGTGCATCATCGC	172
IL-10	NM_012854.2	F: TGCGACGCTGTCATCGATTT R: GTAGATGCCGGGTGGTTCAA	186
TNF-α	NM_012675.3	F: ACACACGAGACGCTGAAGT R: TCCAGTGAGTTCCGAAAGCC	93
ZO-1	NM_001106266.1	F: GCCAGCTTTAAGCCTCCAGA R: TGGCTTCGCTTGAGGTTTCT	144
Occludin	NM_031329.2	F: GATCTAGAGCCTGGAGCAACG R: ATTGGGTTTGAATTCATCCGGC	166
Claudin-1	NM_031699.2	F: GCTGTCATCGGGGGCATAAT R: CCTGGCCAAATTCATACCTGG	136
Nrf2	NM_031789.2	F: TTTGTAGATGACCATGAGTCG R: TGTCCTGCTGTATGCTGCTT	142
HO-1	NM_012580.2	F: TTAAGCTGGTGATGGCCTCC R: GTGGGGCATAGACTGGGTTC	90

4.8. Western Blot Analysis

The procedures of the Western blot assay were according to the description of Alhaithloul et al. [37].

4.9. Statistical Analysis

The individual rat was regarded as the experiment unit, SAS 2003 (version 9.1, SAS Institute Inc., Cary, NC, USA) was used to analyze the statistic. Duncan's multiple range test was used to check the variance among the groups, and the differences were considered significant at $p < 0.05$.

References

1. Cao, S.; Wang, C.; Yan, J.; Li, X.; Hu, C. Curcumin ameliorates oxidative stress-induced intestinal barrier injury and mitochondrial damage by promoting Parkin dependent mitophagy through AMPK-TFEB signal pathway. *Free Radic. Bio. Med.* **2020**, *147*, 8–22. [CrossRef] [PubMed]
2. Lan, R.; Li, Y.; Chang, Q.; Zhao, Z. Dietary chitosan oligosaccharides alleviate heat stress–induced intestinal oxidative stress and inflammatory response in yellow-feather broilers. *Poult. Sci.* **2020**, *99*, 6745–6752. [CrossRef] [PubMed]
3. Cheng, K.; Song, Z.; Li, S.; Yan, E.; Zhang, H.; Zhang, L.; Wang, C.; Wang, T. Effects of resveratrol on intestinal oxidative status and inflammation in heat-stressed rats. *J. Therm. Biol.* **2019**, *85*, 102415. [CrossRef] [PubMed]
4. Cheng, Y.; Chen, Y.; Chen, R.; Su, Y.; Zhang, R.; He, Q.; Wang, K.; Wen, C.; Zhou, Y. Dietary mannan oligosaccharide ameliorates cyclic heat stress-induced damages on intestinal oxidative status and barrier integrity of broilers. *Poult. Sci.* **2019**, *98*, 4767–4776. [CrossRef] [PubMed]
5. Lan, R.; Li, S.; Chang, Q.; Zhao, Z. Chitosan Oligosaccharides Protect Sprague Dawley Rats from Cyclic Heat Stress by Attenuation of Oxidative and Inflammation Stress. *Animals* **2019**, *9*, 1074. [CrossRef]
6. Wang, S.; Li, X.; Wang, W.; Zhang, H.; Xu, S. Application of transcriptome analysis: Oxidative stress, inflammation and microtubule activity disorder caused by ammonia exposure may be the primary factors of intestinal microvilli deficiency in chicken. *Sci. Total. Environ.* **2019**, *696*, 134035. [CrossRef]
7. Liu, Y.; Chen, F.; Odle, J.; Lin, X.; Jacobi, S.K.; Zhu, H.; Wu, Z.; Hou, Y. Fish oil enhances intestinal integrity and inhibits TLR4 and NOD2 signaling pathways in weaned pigs after LPS challenge. *J. Nutr.* **2012**, *142*, 2017–2024. [CrossRef]
8. Wu, S.; Pan, L.; Liao, H.; Yao, W.; Shen, N.; Chen, C.; Liu, D.; Ge, M. High-fat diet increased NADPH-oxidase-related oxidative stress and aggravated LPS-induced intestine injury. *Life Sci.* **2020**, *253*, 117539. [CrossRef]
9. Liu, G.; Zhu, H.; Ma, T.; Yan, Z.; Zhang, Y.; Geng, Y.; Zhu, Y.; Shi, Y. Effect of chronic cyclic heat stress on the intestinal morphology, oxidative status and cecal bacterial communities in broilers. *J. Therm. Biol.* **2020**, *91*, 102619. [CrossRef]
10. Wu, Q.; Liu, N.; Wu, X.; Wang, G.; Lin, L. Glutamine alleviates heat stress-induced impairment of intestinal morphology, intestinal inflammatory response, and barrier integrity in broilers. *Poult. Sci.* **2018**, *97*, 2675–2683. [CrossRef]
11. Song, Z.; Cheng, K.; Zhang, L.; Wang, T. Dietary supplementation of enzymatically treated Artemisia annua could alleviate the intestinal inflammatory response in heat-stressed broilers. *J. Therm. Biol.* **2017**, *69*, 184–190. [CrossRef] [PubMed]
12. Chen, J.; Yu, B.; Chen, D.; Huang, Z.; Mao, X.; Zheng, P.; Yu, J.; Luo, J.; He, J. Chlorogenic acid improves intestinal barrier functions by suppressing mucosa inflammation and improving antioxidant capacity in weaned pigs. *J. Nutr. Biochem.* **2018**, *59*, 84–92. [CrossRef] [PubMed]
13. Yun, S.H.; Moon, Y.S.; SoHn, S.H.; Jang, I.S. Effects of cyclic heat stress or vitamin C supplementation during cyclic heat stress on HSP70, inflammatory cytokines, and the antioxidant defense system in Sprague Dawley rats. *Exp. Anim.* **2012**, *61*, 543–553. [CrossRef] [PubMed]
14. Lee, S.I.; Kang, K.S. Function of capric acid in cyclophosphamide-induced intestinal inflammation, oxidative stress, and barrier function in pigs. *Sci. Rep.* **2017**, *7*, 1–12. [CrossRef] [PubMed]
15. Qiao, R.; Sheng, C.; Lu, Y.; Zhang, Y.; Ren, H.; Lemos, B. Microplastics induce intestinal inflammation, oxidative stress, and disorders of metabolome and microbiome in zebrafish. *Sci. Total Environ.* **2019**, *662*, 246–253. [CrossRef] [PubMed]
16. Zou, P.; Yang, X.; Wang, J.; Li, Y.; Yu, H.; Zhang, Y.; Liu, G. Advances in characterisation and biological activities of chitosan and chitosan oligosaccharides. *Food Chem.* **2016**, *190*, 1174–1181. [CrossRef] [PubMed]
17. Naveed, M.; Phil, L.; Sohail, M.; Hasnat, M.; Baig, M.M.F.A.; Ihsan, A.U.; Shumzaid, M.; Kakar, M.U.; Husain, T.; Akabar, M. Chitosan oligosaccharide (COS): An overview. *Int. J. Biol. Macromol.* **2019**, *129*, 827–843. [CrossRef]
18. Qiao, Y.; Bai, X.; Du, Y. Chitosan oligosaccharides protect mice from LPS challenge by attenuation of inflammation and oxidative stress. *Int. Immunopharmacol.* **2011**, *11*, 121–127. [CrossRef]
19. Liu, H.; Li, W.; Xu, G.; Li, X.; Bai, X.; Wei, P.; Yu, C.; Du, Y. Chitosan oligosaccharides attenuate hydrogen peroxide-induced stress injury in human umbilical vein endothelial cells. *Pharmacol. Res.* **2009**, *59*, 167–175. [CrossRef]
20. Lan, R.; Chang, Q.; An, L.; Zhao, Z. Dietary supplementation with chitosan oligosaccharides alleviates oxidative stress in rats challenged with hydrogen peroxide. *Animals* **2020**, *10*, 55. [CrossRef]
21. Li, J.; Cheng, Y.; Chen, Y.; Qu, H.; Zhao, Y.; Wen, C.; Zhou, Y. Dietary chitooligosaccharide inclusion as an alternative to antibiotics improves intestinal morphology, barrier function, antioxidant capacity, and immunity of broilers at early age. *Animals* **2019**, *9*, 493. [CrossRef] [PubMed]

22. Li, X.; Ding, X.; Peng, X.; Chi, X.; Cui, H.; Zuo, Z.; Fang, J. Effect of chitosan oligosaccharides on antioxidant function, lymphocyte cycle and apoptosis in ileum mucosa of broiler. *Kafkas Univ. Vet. Fak. Derg.* **2017**, *23*, 571–577.

23. Zou, Y.; Wei, H.; Xiang, Q.; Wang, J.; Zhou, Y.; Peng, J. Protective effect of quercetin on pig intestinal integrity after transport stress is associated with regulation oxidative status and inflammation. *J. Vet. Med. Sci.* **2016**, *78*, 1487–1494. [CrossRef] [PubMed]

24. Viveros, A.; Chamorro, S.; Pizarro, M.; Arija, I.; Centeno, C.; Brenes, A. Effects of dietary polyphenol-rich grape products on intestinal microflora and gut morphology in broiler chicks. *Poult. Sci.* **2011**, *90*, 566–578. [CrossRef] [PubMed]

25. Wei, L.; Li, Y.; Chang, Q.; Guo, G.; Lan, R. Effects of chitosan oligosaccharides on intestinal oxidative stress and inflammation response in heat stressed rats. *Exp. Anim.* **2021**, *70*. [CrossRef]

26. Zhao, P.; Piao, X.; Zeng, Z.; Li, P.; Xu, X.; Wang, H. Effect of Forsythia suspensa extract and chito-oligosaccharide alone or in combination on performance, intestinal barrier function, antioxidant capacity and immune characteristics of weaned piglets. *Anim. Sci. J.* **2017**, *88*, 854–862. [CrossRef]

27. Liu, P.; Piao, X.; Kim, S.; Wang, L.; Shen, Y.; Lee, H.; Li, S. Effects of chito-oligosaccharide supplementation on the growth performance, nutrient digestibility, intestinal morphology, and fecal shedding of *Escherichia coli* and *Lactobacillus* in weaning pigs. *J. Anim. Sci.* **2008**, *86*, 2609–2618. [CrossRef]

28. Liu, P.; Piao, X.; Thacker, P.; Zeng, Z.; Li, P.; Wang, D.; Kim, S. Chito-oligosaccharide reduces diarrhea incidence and attenuates the immune response of weaned pigs challenged with *Escherichia coli* K88. *J. Anim. Sci.* **2010**, *88*, 3871–3879. [CrossRef]

29. Song, D.; Cheng, Y.; Li, X.; Wang, F.; Lu, Z.; Xiao, X.; Wang, Y. Biogenic nanoselenium particles effectively attenuate oxidative stress-induced intestinal epithelial barrier injury by activating the Nrf2 antioxidant pathway. *ACS Appl. Mater. Interfaces* **2017**, *9*, 14724–14740. [CrossRef]

30. He, N.; Wang, S.; Lv, Z.; Zhao, W.; Li, S. Low molecular weight chitosan oligosaccharides (LMW-COSs) prevent obesity-related metabolic abnormalities in association with the modification of gut microbiota in high-fat diet (HFD)-fed mice. *Food Funct.* **2020**, *11*, 9947–9959. [CrossRef]

31. Osho, S.; Adeola, O. Chitosan oligosaccharide supplementation alleviates stress stimulated by in-feed dexamethasone in broiler chickens. *Poult. Sci.* **2020**, *99*, 2061–2067. [CrossRef] [PubMed]

32. Wan, J.; Jiang, F.; Xu, Q.; Chen, D.; Yu, B.; Huang, Z.; Mao, X.; Yu, J.; He, J. New insights into the role of chitosan oligosaccharide in enhancing growth performance, antioxidant capacity, immunity and intestinal development of weaned pigs. *Rsc. Adv.* **2017**, *7*, 9669–9679. [CrossRef]

33. Hu, S.; Wang, Y.; Wen, X.; Wang, L.; Jiang, Z.; Zheng, C. Effects of low-molecular-weight chitosan on the growth performance, intestinal morphology, barrier function, cytokine expression and antioxidant system of weaned piglets. *BMC Vet. Res.* **2018**, *14*, 215. [CrossRef] [PubMed]

34. Wu, X.; Cao, W.; Jia, G.; Zhao, H.; Chen, X.; Wu, C.; Tang, J.; Wang, J.; Liu, G. New insights into the role of spermine in enhancing the antioxidant capacity of rat spleen and liver under oxidative stress. *Anim. Nutr.* **2017**, *3*, 85–90. [CrossRef] [PubMed]

35. Ganie, S.; Haq, E.; Hamid, A.; Masood, A.; Zargar, M. Long dose exposure of hydrogen peroxide (H_2O_2) in albino rats and effect of Podophyllum hexandrum on oxidative stress. *Eur. Rev. Med. Pharmacol. Sci.* **2011**, *15*, 906–915. [CrossRef]

36. Duan, J.; Yin, J.; Ren, W.; Liu, T.; Cui, Z.; Huang, X.; Wu, L.; Kim, S.W.; Liu, G.; Wu, X. Dietary supplementation with L-glutamate and L-aspartate alleviates oxidative stress in weaned piglets challenged with hydrogen peroxide. *Amino Acids* **2016**, *48*, 53–64. [CrossRef]

37. Alhaithloul, H.A.; Alotaibi, M.F.; Bin-Jumah, M.; Elgebaly, H.; Mahmoud, A.M. Olea europaea leaf extract up-regulates Nrf2/ARE/HO-1 signaling and attenuates cyclophosphamide-induced oxidative stress, inflammation and apoptosis in rat kidney. *Biomed. Pharmacother.* **2019**, *111*, 676–685. [CrossRef]

38. Zhang, Y.; Ahmad, K.A.; Khan, F.U.; Yan, S.; Ihsan, A.U.; Ding, Q. Chitosan oligosaccharides prevent doxorubicin-induced oxidative stress and cardiac apoptosis through activating p38 and JNK MAPK mediated Nrf2/ARE pathway. *Chem. Biol. Interact.* **2019**, *305*, 54–65. [CrossRef]

39. Tao, W.; Sun, W.; Liu, L.; Wang, G.; Xiao, Z.; Pei, X.; Wang, M. Chitosan oligosaccharide attenuates nonalcoholic fatty liver disease induced by high fat diet through reducing lipid accumulation, inflammation and oxidative stress in C57BL/6 mice. *Mar. Drugs* **2019**, *17*, 645. [CrossRef]

40. Zhang, J.; Hu, Z.; Lu, C.; Bai, K.; Zhang, L.; Wang, T. Effect of various levels of dietary curcumin on meat quality and antioxidant profile of breast muscle in broilers. *J. Agr. Food Chem.* **2015**, *63*, 3880–3886. [CrossRef]

41. Al-Sadi, R.; Boivin, M.; Ma, T. Mechanism of cytokine modulation of epithelial tight junction barrier. *Front. Biosci.* **2009**, *14*, 2765. [CrossRef] [PubMed]

42. Hu, C.; Xiao, K.; Luan, Z.; Song, J. Early weaning increases intestinal permeability, alters expression of cytokine and tight junction proteins, and activates mitogen-activated protein kinases in pigs. *J. Anim. Sci.* **2013**, *91*, 1094–1101. [CrossRef] [PubMed]

43. Pié, S.; Lallès, J.P.; Blazy, F.; Laffitte, J.; Sève, B.; Oswald, I. Weaning is associated with an upregulation of expression of inflammatory cytokines in the intestine of piglets. *J. Nutr.* **2004**, *134*, 641–647. [CrossRef] [PubMed]

44. Ruan, Z.; Liu, S.; Zhou, Y.; Mi, S.; Liu, G.; Wu, X.; Yao, K.; Assaad, H.; Deng, Z.; Hou, Y. Chlorogenic acid decreases intestinal permeability and increases expression of intestinal tight junction proteins in weaned rats challenged with LPS. *PLoS ONE* **2014**, *9*, e97815. [CrossRef]

45. Hyung, J.H.; Ahn, C.B.; Kim, B.I.; Kim, K.; Je, J.Y. Involvement of Nrf2-mediated heme oxygenase-1 expression in anti-inflammatory action of chitosan oligosaccharides through MAPK activation in murine macrophages. *Eur. J. Pharmacol.* **2016**, *793*, 43–48. [CrossRef]
46. Liu, H.T.; Huang, P.; Ma, P.; Liu, Q.S.; Yu, C.; Du, Y.G. Chitosan oligosaccharides suppress LPS-induced IL-8 expression in human umbilical vein endothelial cells through blockade of p38 and Akt protein kinases. *Acta Pharmacol. Sin.* **2011**, *32*, 478–486. [CrossRef]
47. Lan, R.; Liu, F.; He, Z.; Chen, C.; Liu, S.; Shi, Y.; Liu, Y.; Yoshimura, Y.; Zhang, M. Immunolocalization of GnRHRI, gonadotropin receptors, PGR, and PGRMCI during follicular development in the rabbit ovary. *Theriogenology* **2014**, *81*, 1139–1147. [CrossRef]

Structure of the Polysaccharide Secreted by *Vibrio alginolyticus* CNCM I-5035 (Epidermist 4.0^TM)

Sophie Drouillard [1], Rémi Chambon [1], Isabelle Jeacomine [1], Laurine Buon [1], Claire Boisset [1], Anthony Courtois [2], Bertrand Thollas [2], Pierre-Yves Morvan [3], Romuald Vallée [3] and William Helbert [1,*]

[1] Centre de Recherches sur les Macromolécules Végétales (CERMAV), Université Grenoble Alpes, CNRS, 38000 Grenoble, France; sophie.drouillard@cermav.cnrs.fr (S.D.); remichambon@yahoo.fr (R.C.); isabelle.jeacomine@cermav.cnrs.fr (I.J.); laurine.buon.drouillard@cermav.cnrs.fr (L.B.); claire.boisset-helbert@cermav.cnrs.fr (C.B.)

[2] Polymaris Biotechnology, 160 Rue Pierre Rivoalon, 29200 Brest, France; Anthony.courtois@polymaris.com (A.C.); Bertrand.thollas@polymaris.com (B.T.)

[3] CODIF International, 35400 Roz-sur-Couesnon, France; py.morvan@codif.com (P.-Y.M.); r.vallee@codif.com (R.V.)

* Correspondence: william.helbert@cermav.cnrs.fr; Tel.: +33-(0)4-76-0376; Fax: +33-(0)4-7654-7203

Abstract: *Vibrio alginolyticus* (CNCM I-5035) secretes an exopolysaccharide used as ingredient in cosmetic industry under the trademark Epidermist 4.0^TM. It is appreciated for its ability to improve the physical and chemical barrier functions of the skin by notably increasing the keratinocyte differentiation and epidermal renewal. Composition analyses and in depth characterization of the polysaccharides as well as oligosaccharides obtained by mild acid hydrolyses revealed that it was composed of a repetition unit of three residues: D-galactose (D-Gal), D-*N*-acetylglucosamine (GlcNAc) and L-*N*-acetylguluronic acid, of which 30% (M/M) was acetylated in position 3. The complete structure of the polysaccharide was resolved giving the repetition unit: [→3)-α-D-Gal-(1→4)-α-L-GulNAcA/α-L-3OAc-GulNAcA-(1→4)-β-D-GlcNAc-(1→].

Keywords: exopolysaccharide; structure; NMR; *Vibrio alginolyticus*; Epidermist

1. Introduction

Polysaccharide are very complex and diverse macromolecules attested by the very high number of structures—19.773 entries to date—listed in the "Carbohydrate Structure Databank" (http://csdb.glycoscience.ru/database/index.html) [1–3]. The very wide structural diversity is explained by the stereochemistry of carbohydrate and the numerous possibilities of linkages between residues [4]. In addition to the complexity of the carbohydrate backbone, polysaccharides are often decorated by organic (e.g. lactate, acetate, amino acids) and inorganic (e.g. sulfate, phosphate) derivatives, therefore increasing the number of possible structures.

Many microorganisms, including marine bacteria, secrete extracellular polysaccharides, called exopolysaccharides (EPSs) [5,6]. Despite the numerous polysaccharide structures elucidated, the diversity of EPS seems largely underestimated and tools to predict their structures are still absent. The massive sequencing of DNA of isolated organisms (genomic) or extracted from the environment (metagenomics), did not allow the emergence of bioinformatic methods helping in the prediction of the structures of the biosynthesized polysaccharides. Therefore, solving the structure of the polysaccharides by chemical and spectroscopic methods follows a unique strategy. Because these approaches are fastidious, structural analyses are usually targeted on polysaccharides that present identified interest

in the understanding of their biological properties in vivo (e.g., antigenic properties), ex vivo (e.g., cosmeceutical properties), and their gelling or thickening properties.

In contrast to that of plant and algal polysaccharides, large-scale production of marine EPSs can be easily controlled independently of seasonal variation, for example. In addition, because of their very high molecular weight, EPSs can be easily separated from other molecules and be obtained at very high grade of purity. These technical advantages are not sufficient for the development of novel marine EPSs as gelling or thickening agents which are facing the already marketed terrestrial bacterial EPSs, such as xanthan (*Xanthomonas campestris*) or gellan (*Sphingomonas paucimobilis*) Recently, marine EPSs showing both interesting rheological properties and biological properties could be valorized in niche applications in the biomedical and cosmetic sectors. Among them, the elucidation of the structures of two EPSs secreted by two distinct *Vibrio alginolyticus* strains used as bioactive ingredients in cosmetic applications revealed original structures presenting decoration of the polysaccharide backbone by amino acids (strain CNCM I-4994) and the occurrence of the rare "nosturonic acid" residue (strain CNCM I-5034) [7,8].

In this line of investigations, the polysaccharide secreted by *Vibrio alginolyticus* CNCM I-5035 was recently developed as an ingredient in the cosmetics industry under the trademark Epidermist 4.0™ [9]. The polysaccharide has numerous beneficial effects on human skin validated in vitro and in vivo. Notably, it improves the physical and chemical barrier functions, by increasing the keratinocyte differentiation and epidermal renewal, and by increasing the immune defence against the infectious agents and pathogens involved in acne like *Cutibacterium acnes* (formerly *Propionibacterium acnes*). As for the previous *V. alginolyticus*, we have undertaken the complete structural analysis of the EPS, which revealed the occurrence of the rare 3O-acetyl-2-acetamido-2-deoxy-⟨-ʟ-guluronic acid and 2-acetamido-2-deoxy-⟨-ʟ-guluronic acid residues.

2. Results and Discussion

2.1. Composition of the Polysaccharide

Size-exclusion chromatography (SEC) coupled to multi-angle laser light scattering showed that the purified EPS was composed of one species of molecule having a molecular weight (MW) of 5.5×10^5 Da with a narrow polydispersity index of 1.025. Composition analysis using gas chromatography (GC), after complete hydrolysis of the polysaccharide and derivatization of the products, revealed galactose (Gal) and glucosamine (GlcN). Some signals of the chromatogram could not be attributed at this stage using standard residues available in the laboratory suggesting the occurrence of, at least, one additional residue (Supplementary Figure S1). Elemental analysis did not uncover any inorganic derivatives such as sulfate or phosphate ester groups. Absolute configuration analyses demonstrated that the two residues identified belonged to the ᴅ-series (Supplementary Figure S2).

The ^{1}H NMR spectrum of the polysaccharide (Figure 1A) showed four anomeric signals that we attributed to A, B, B′ and C residues (A-H1 = 5.13 ppm; B-H1 = 5.14, B′-H1:5.18 and C-H1 = 4.81 ppm). We noticed also three methyl groups attributed to three different acetyl groups (between 2.0 ppm and 2.3 ppm). The ring protons of the ⟨-linked residue A were assigned, starting from the anomeric proton A-H1, by successfully combining correlation spectroscopy (COSY, Supplementary Figure S3A) and total COSY (TOCSY) experiments. The chemical shifts of the corresponding carbons were determined using heteronuclear single-quantum correlation experiments (HSQC, Supplementary Figure S4A) and are reported in Table 1. The chemical shifts recorded were in agreement with the ⟨-ᴅ-galactose. The residue C corresponded to the ®-linked *N*-acetyl-glucosamine (C-H1 = 4.81 ppm; C-C1 = 103.19 ppm). The proton and carbon chemical shifts were also determined, highlighting the characteristic C-H2 = 3.81 ppm and C-C2 = 56.84 ppm chemical shift of the amine residue (Table 1).
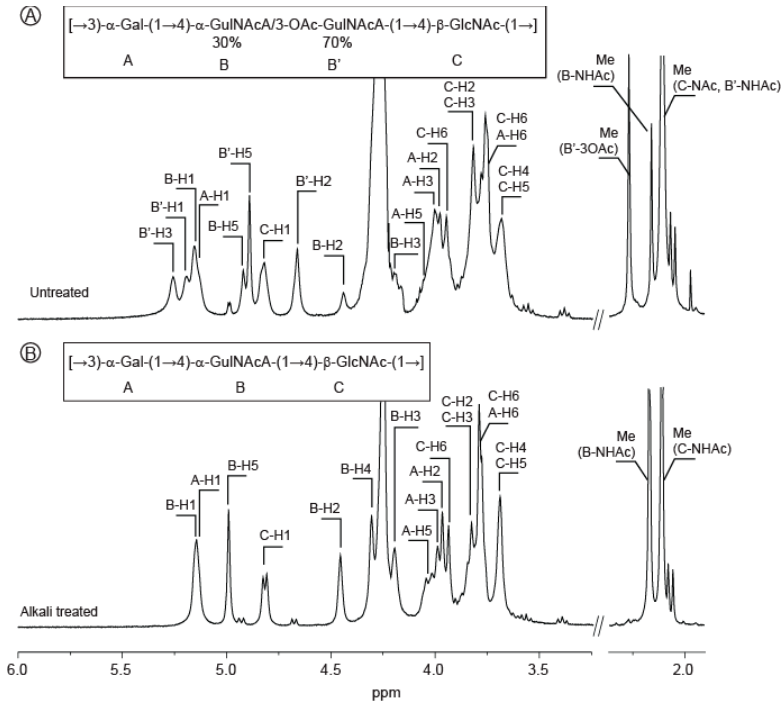
Figure 1. ^{1}H NMR spectra of the *Vibrio alginolyticus* exopolysaccharide. The spectra of the purified polysaccharides were recorded at 353 K prior to (**A**) or after alkaline treatment (**B**). Inset: chemical structure of the polysaccharide.

Table 1. ^{1}H and ^{13}C NMR chemical shifts (δ, ppm) of the *Vibrio alginolyticus* exopolysaccharide before and after alkaline treatment.

Sugar Residue		1	2	3	4	5	6(6a,6b)	NHAc (CH3,CO)	OAc (CH3,CO)
					EPS				
→3)-⟨-D-Gal-(1→	[1]H	5.13	3.95	3.99	4.26	4.05	3.77,3.93		
	[13]C	96.66	67.62	80.19	69.58	70.82	61.58		
→4)-⟨-L-GulNAcA-(1→	[1]H	5.14	4.44	4.18	4.30	4.92		2.16	
	[13]C	98.83	46.99	65.79	74.49	67.92	175.40	22.59, 174.47	
→4)-⟨-3OAc-L-GulNAcA-(1→	[1]H	5.18	4.66	5.26	4.31	4.89		2.11	2.27
	[13]C	97.1	45.62	67.84	71.68	68.1	175.75	22.59, 174.47	21.20, 174.00
→4)-®-D-GlcNAc-(1→	[1]H	4.81	3.81	3.79	3.68	3.68	3.77,3.94	2.11	
	[13]C	103.19	56.84	73.45	78.89	75.58	61.13	22.99, 175.50	
				Deacetylated EPS					
→3)-⟨-D-Gal-(1→	[1]H	5.14	3.95	3.95	4.25	4.00	3.77,3.93		
	[13]C	97.01	67.81	79.95	69.56	71.02	61.49		
→4)-⟨-L-GulNAcA-(1→	[1]H	5.14	4.45	4.19	4.30	4.99		2.17	
	[13]C	99.04	47.06	65.76	74.66	67.81	175.00	22.59, 174.47	
→4)-®-D-GlcNAc-(1→	[1]H	4.81	3.81	3.81	3.68	3.68	3.77,3.93	2.11	
	[13]C	103.1	56.92	73.33	78.71	75.59	61.08	22.99, 175.59	

After an alkaline treatment of the polysaccharide, the ^{1}H spectrum (Figure 1B) was simplified and three anomeric signals instead of four were then observed (A-H1 = 5.14 ppm; B-H1 = 5.14 ppm and C-H1 = 4.81 ppm). This alkaline treatment leads to the removal of one acetyl group (B'-3OAc = 2.27 ppm). Integration of the anomeric protons demonstrated an equimolar occurrence of the three residues A, B and C in the alkali-treated polysaccharide. Analyses of the 1D and 2D NMR spectra revealed that the ⟨-ᴅ-galactose (A) and the *N*-acetyl-®-ᴅ-glucosamine (C) were not modified by the alkaline treatment and that their respective ratio were also conserved. However, the amount of B residue found in the alkali-treated polysaccharide was equal to the sum of the B and B' residues, which disappeared after alkaline treatment.

The chemical shifts of the ring protons of the B residue were determined using COSY (Supplementary Figure S3B) and TOCSY analyses (Table 1). The chemical shifts of the carbon of the residue were deduced by studying the J^1 and J^3 carbon–proton correlations using HMBC and HSQC spectra (Supplementary Figure S2B, Table 1). In the HMBC spectra (Figure 2A), the strong correlation between the proton B-H5 = 4.99 ppm with a weak signal attributed to B-C6 at 175.0 ppm showed that the B residue carried a carboxyl group. The chemical shift of the carbon B-C2 = 47.06 ppm and the correlations of the carbonyl at 174.47 ppm with the proton B-H2 = 4.45 ppm and the methyl of the acetyl group at 2.17 ppm (correlated with the signal at 22.59 ppm in the HSQC spectrum, Figure S2B) showed that the B residue was a *N*-acetylated osamine (Figure 2A). The B-C2 chemical shift at 47.06 ppm was similar other published data of GulNAcA [10–15]. The C-2 NMR signal of the stereoisomers other than the *gulo* configuration showed a significantly lower-field position [16]. This hypothesis was also supported by comparison of calculated and observed chemical shifts. Calculations were conducted according to the method of Lipkind and co-workers [13]. Chemical shifts used for free ʟ-GulNAc used as reference were found in [17]. Altogether, the values recorded and calculated (Supplementary Table S1) showed that the B residue had all the characteristics of a 2-acetamido-2-deoxy-⟨-ʟ-guluronic acid (⟨-ʟ-GulNAcA).

The alkaline treatment of the polysaccharide led to the removal of the acetyl group (3-OAc-H = 2.27 ppm, 3-OAc-C = 21.20 ppm), which is accompanied by an increase in the amount of the B residue. Therefore, we hypothesized the B' residue was an acetylated form of the B residue. The proton and carbon chemical shifts of the B' residue determined by mono- and two-dimentional NMR experiments (Table 1) revealed that they were very similar to that of the B residue, except for the carbon B'-C3 = 67.84 (B-C3 = 65.79 ppm) and the proton B'-H3 = 5.26 ppm (B-H3 = 4.18 ppm) which differed substantially. In fact, the carbonyl of the acetyl group B'-3OAc at 174.00 ppm correlated with the proton B'-H3 = 5.26 ppm and the methyl group at 2.27 ppm (Figure 2B), showing that the B' residue was O-acetylated at the position 3. We concluded that the acetylation in the position 3 of the B residue gave the B' residue: 3O-acetyl-2-acetamido-2-deoxy-⟨-ʟ-guluronic acid (3OAc-GulNAcA). Integration of the anomeric signals suggested a B:B' ratio of 0.7:0.3 in the native polysaccharide. Finally, the native polysaccharide was made of four residues: ⟨-ᴅ-galactose, ⟨-ʟ-GulNAcA/⟨-ʟ-3OAc-GulNAcA and ®-ᴅ-GlcNAc.
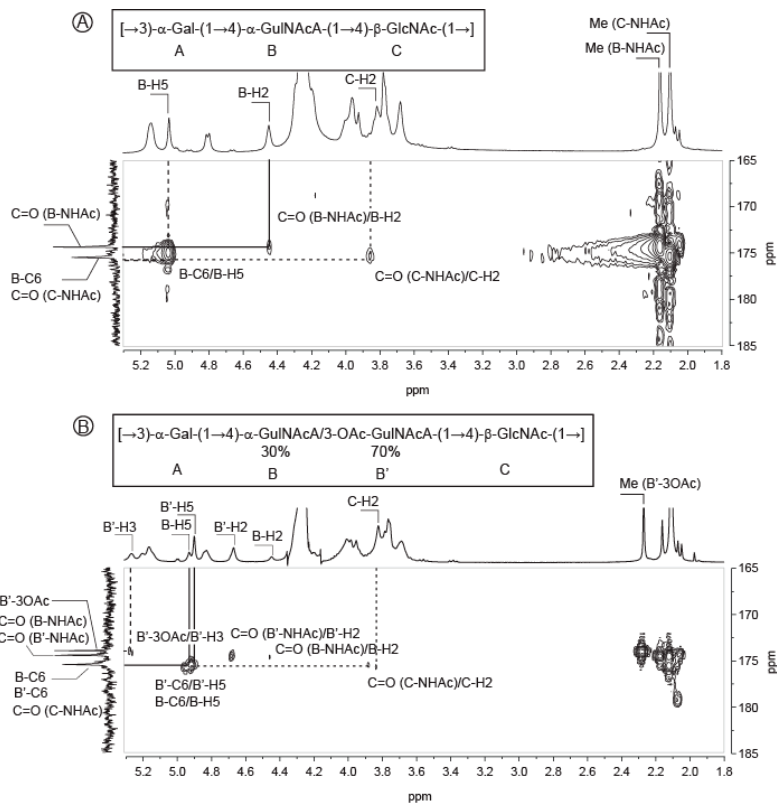
Figure 2. Detail of the HMBC spectra recorded at 353K on *Vibrio alginolyticus* exopolysaccharide highlighting the acetylation of the guluronic acid residue. (**A**) HMBC of the deacetylated exopolysaccharide at the position 3 of the GulNAcA; (**B**) HMBC of the untreated exopolysaccharide.

2.2. Structure of Oligosaccharides

The unmodified polysaccharide was subjected to mild acid hydrolysis with 0.1 M TFA. The resulting mixtures of oligosaccharides prepared were very complex and it was therefore very difficult to isolate pure oligosaccharides for in depth NMR analyses. We found that the mild acid degradation of the alkali treated polysaccharide—the deacetylated form—gave less complex mixtures which allowed the isolation of several pure oligosaccharides. The degradation products were fractionated, at first, by permeation gel chromatography (Figure 3A,B). At this step, in the case of a polysaccharide incubation of 90 min, one collected fraction contained a pure trisaccharide (Figure 3A). The other fractions contained oligosaccharides with the same degree of polymerization (e.g. di-, trisaccharides) but with various degrees of acetylation. Indeed, in order to obtain sufficiently large amounts of small oligosaccharides, the prolonged acid hydrolysis treatment required for the cleavage of the glycosidic bond has also lead to the removal of some *N*-linked acetyl groups. A second step of purification by semi-preparative anion exchange was necessary to isolate pure oligosaccharides. As illustrated in Figure 3, the fractions A and B collected from the degradation products of the 300 min hydrolysis (Figure 3B) contained several oligosaccharides that could be isolated (Figure 3C,D).
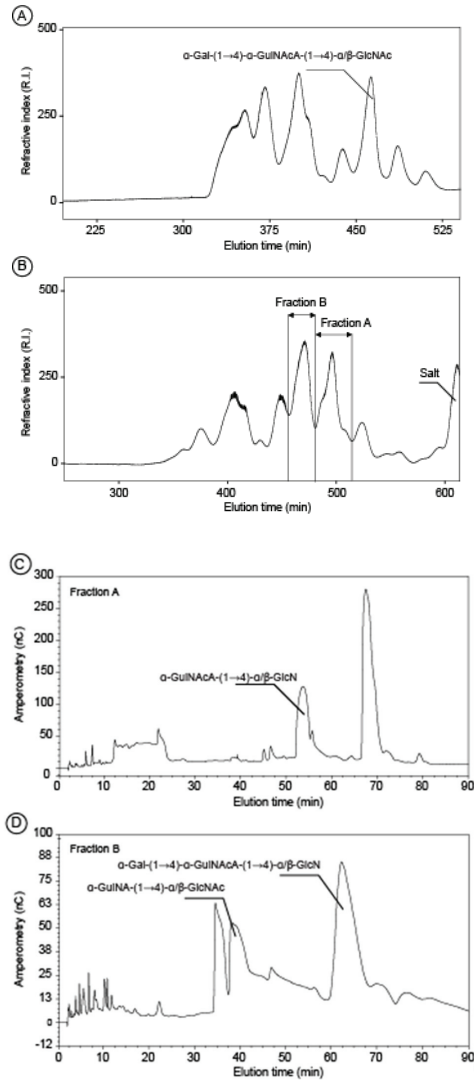
Figure 3. Chromatography experiments leading to the preparation of pure oligosaccharides (**A**) and (**B**) gel permeation chromatograms recorded on a mixture of oligosaccharides prepared by mild acid hydrolysis of *Vibrio alginolyticus* exopolysaccharide in 0.1M TFA at 100 °C for 90 min and 300 min, respectively. (**C**) and (**D**) Fractions A and B of the chromatogram (**B**) were further fractionated by anion exchange chromatography allowing purification of two disaccharides and one trisaccharide.

At the end, we collected two disaccharides and two trisaccharides in sufficient amounts for detailed analyses by NMR (^{1}H spectra in Figure 4). Proton and carbon signals were ascribed straightforwardly combining COSY (Supplementary Figure S5), HSQC (Supplementary Figure S6) and HMBC experiments and values reported in Table 2. The data recorded for the first disaccharide (Figure 4A) were in agreement with a disaccharide made of GulNAcA (residue B) linked to GlcN (deacetylated residue C, C^{da}) and allowed confirming the occurrence of 2-acetamido-2-deoxy-⟨-ʟ-guluronic acid (GulNAcA) in the polysaccharide. The HMBC spectrum recorded on this disaccharide (data not shown) was better

resolved than that of the native polymer and clearly revealed the linkage between B and C^{da} residues. The correlations between the carbon B-C1 (99.10 ppm) with the protons C^{da} -H4® (3.62 ppm) and C^{da} -C4⟨/® (78.86/78.95 ppm) with the proton B-H1 (5.08 ppm) demonstrated the GulNAcA residue was bound to the GlcN residue by a ⟨(1,4) linkage. The structure of the second disaccharide (Figure 4B) was also thoroughly examined. In contrast with the previous oligosaccharide, we observed a deacetylation on the B residue giving 2-amino-2-deoxy-⟨-L-guluronic acid (GulNA, B^{da}) but not deacetylation on the C residue (GlcNAc). Again, the ⟨(1,4) linkage was confirmed using HMBC experiments.

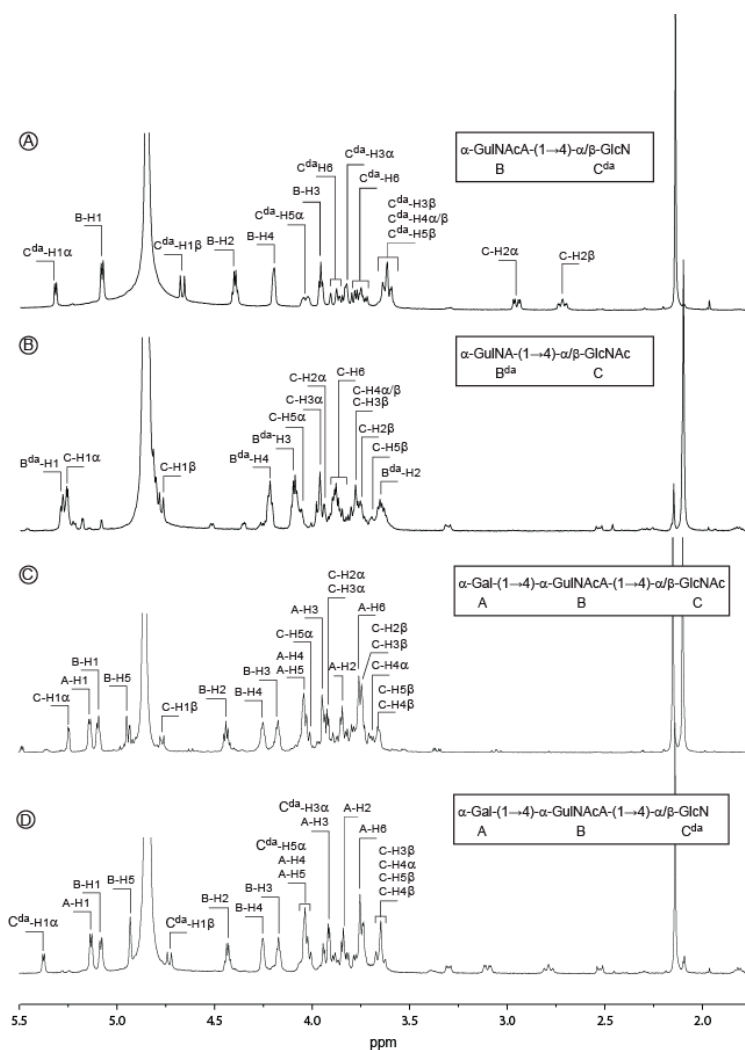**Figure 4.** ¹H NMR spectra recorded at 293K of the oligosaccharides purified by chromatography. The annotated spectra correspond to two disaccharides (**A,B**) and two trisaccharides (**C,D**). Inset: chemical structure of the oligosaccharides.

Table 2. ^{1}H and ^{13}C NMR chemical shifts (δ, ppm) of the *Vibrio alginolyticus* oligosaccharides purified after alkaline treatment and mild acid hydrolysis.

Sugar Residue		1	2	3	4	5	6(6a, 6b)	NHAc (CH$_3$,CO)
		Trisaccharide ABC						
〈-D-Gal-(1→	^{1}H	5.13	3.84	3.93	4.04	4.02	3.74, 3.74	
	^{13}C	96.84	69.42	70.31	70.07	71.61	61.83	
→4)-〈-L-GulNAcA-(1→	^{1}H	5.08	4.43	4.17	4.24	4.93		2.14
	^{13}C	99.06	47.28	65.89	74.82	68.25	175.89	22.93, 175.13
→4)-〈-D-GlcNAc	^{1}H	5.24	3.93	4.03	3.69	4.02	3.76, 3.85	2.09
	^{13}C	91.76	55.66	70.48	79.15	71.79	61.20	23.05, 175.66
→4)-®-D-GlcNAc	^{1}H	4.76	3.73	3.74	3.65	3.64	3.76, 3.85	2.09
	^{13}C	95.97	58.37	73.65	78.97	76.24	61.33	23.33, 175.89
		Trisaccharide ABC^{da}						
〈-D-Gal-(1→	^{1}H	5.13	3.84	3.93	4.04	4.03	3.75, 375	
	^{13}C	96.78	69.36	70.24	69.98	71.55	61.75	
→4)-〈-L-GulNAcA-(1→	^{1}H	5.08	4.43	4.17	4.25	4.93		2.14
	^{13}C	99.03	47.19	65.78	74.74	68.19	176.88	22.86, 175.08
→4)-〈-D-GlcN	^{1}H	5.37	3.10	3.91	3.65	4.04	3.76, 3.87	
	^{13}C	91.73	56.18	71.36	78.69	71.91	61.24	
→4)-®-D-GlcN	^{1}H	4.73	2.79	3.66	3.65	3.65	3.76, 3.87	
	^{13}C	96.46	58.76	74.47	78.69	76.29	61.05	
		Disaccharide B^{da}C						
〈-L-GulNA-(1→	^{1}H	5.27	3.64	4.10	4.21	4.82		
	^{13}C	97.85	48.17	69.56	70.97	68.93	177.22	
→4)-〈-D-GlcNAc	^{1}H	5.25	3.96	3.97	3.77	4.06	3.87, 3.92	2.09
	^{13}C	91.63	55.41	70.31	79.28	71.33	61.80	23.05, 175.70
→4)-®-D-GlcNAc	^{1}H	4.77	3.75	3.77	3.77	3.68	3.87, 3.92	2.09
	^{13}C	95.92	58.11	73.54	79.15	75.83	61.91	23.33, 175.96
		Disaccharide BC^{da}						
〈-L-GulNAcA-(1→	^{1}H	5.08	4.40	3.96	4.20	4.85		2.14
	^{13}C	99.10	47.10	70.34	71.29	68.75	177.48	22.84, 175.05
→4)-〈-D-GlcN	^{1}H	5.31	2.95	3.82	3.62	4.03	3.74, 3.87	
	^{13}C	92.47	56.29	72.41	78.86	71.73	61.25	
→4)-β-D-GlcN	^{1}H	4.66	2.72	3.62	3.62	3.64	3.74, 3.87	
	^{13}C	97.09	58.81	74.93	78.95	76.19	61.05	

da: deacetylated.

More interestingly, we purified a trisaccharide corresponding to the repetition unit of the polysaccharide eluting at 455 min in permeation gel chromatography (Figure 3A). As for the analyzed disaccharides, the C residue (GlcNAc) was located at the reducing end and the proton and carbon chemical shifts were very similar (Table 2). The ring proton of the B residue as well as the corresponding carbon were easily attributed after combining the COSY and HSQC experiments (Figure 5). The chemical shifts of the protons B-H3, B-H4 and B-H5 were higher than in the disaccharides, in agreement with its internal location in the trisaccharide instead of at the non-reducing end in the disaccharide. The 〈(1,4)

linkage between the B and C residues was validated by HMBC (Figure 6C): the correlations between the carbon B-C1 (99.06 ppm) with the protons C-H4⟨/® (3.69/3.65 ppm) and C-C4⟨/® (79.15/78.97 ppm) with the proton B-H1 (5.08 ppm) were well-identified. The expected chemical shifts of the residue A (⟨-D-Gal) were measured on the NMR spectra. The resolution of the HMBC spectra allowed clearly visualizing the linkage between the A and B residues. The anomeric carbon of the ⟨-Gal A-C1 (96.84 ppm) correlated with the proton B-H4 (4.24 ppm) and the carbon B-C4 (74.82 ppm) correlated with the proton A-H1 (5.13 ppm), demonstrating the ⟨(1,4) linkage between the two residues. Altogether, the data recorded were in agreement with a trisaccharide having the structure: ⟨-D-Gal-(1→4)-⟨-L-GulNAcA-(1→4)-⟨/®-D-GlcNAc.
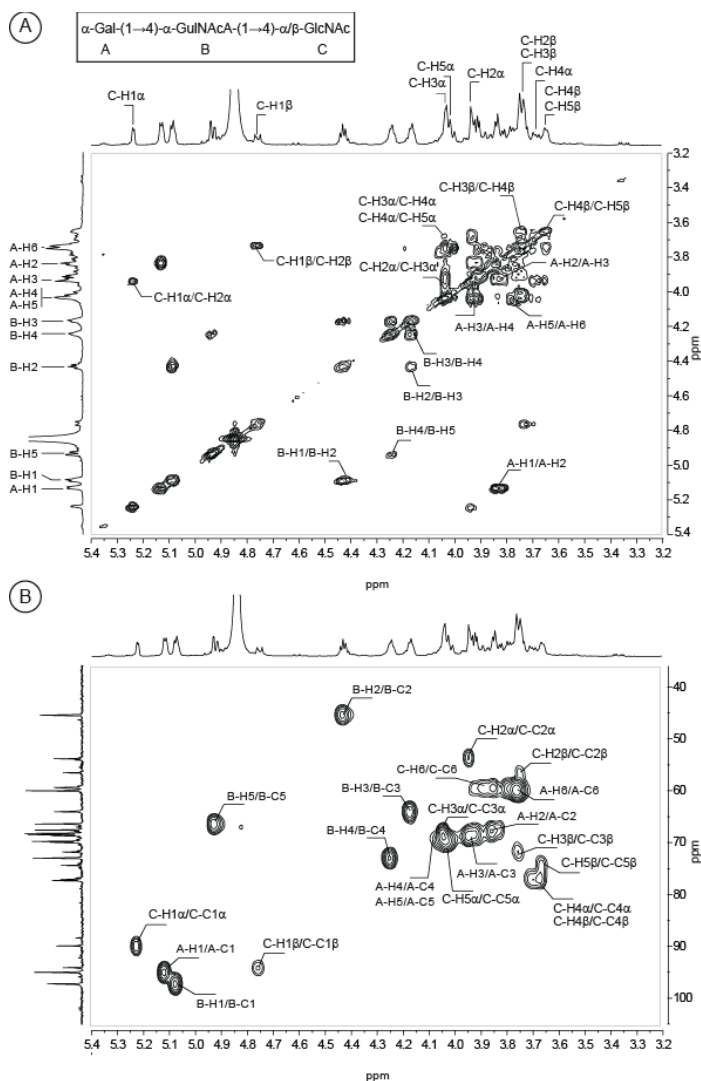
Figure 5. COSY (**A**) and HSQC (**B**) spectra recorded at 293K of the purified trisaccharide, whose structure corresponds to the repetition unit of the *Vibrio alginolyticus* exopolysaccharide.
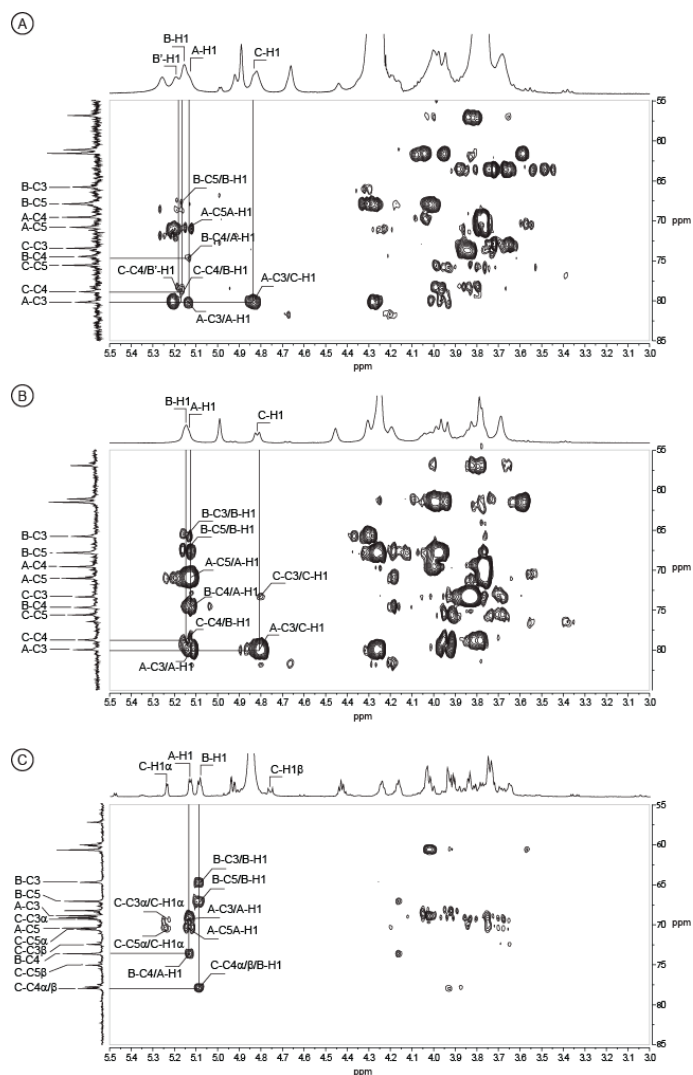
Figure 6. Detail of HMBC spectra. The spectra were recorded at 353K on the complete polysaccharide (**A**) and after alkali-treatment (**B**), and at 293K on the trisaccharide (**C**). ^{1}H/^{13}C heteronuclear correlations that helped to determine linkages between residues are indicated in the spectra.

MALDI-TOF Mass spectrometry experiments conducted in positive ionisation mode with the fraction enriched in the trisaccharide (Supplementary Figure S7) confirmed the expected molecular mass of the trisaccharide under the sodium form of the uronic acid function $[M + Na]^+$ ($m/z = 623$). The occurrence of the molecular species $[M - H + 2Na]^+$ is characteristic of an additional sodium ion interaction with the carboxylic function present in the oligosaccharide. Observation of such species confirmed the carboxylic function and excluded amide function, for example. A deacetylated form of the trisaccharide and two disaccharides were also observed in this fraction and their measured masses were also in agreement with the determined structure.

2.3. Structure of the Polysaccharide

Analyses of the native and alkali-treated polysaccharides, as well as the detailed characterization of purified di- and tri-saccharides, demonstrated that the polysaccharide is made of a trisaccharide repetition unit composed of ⟨-ᴅ-galactose, ⟨-ʟ-GulNAcA (or ⟨-ʟ-3OAc-GulNAcA) and ®-ᴅ-GlcNAc. Determination of the linkages between the residues were facilitated by the preparation of the pure oligosaccharides. However, we were not able to isolate oligosaccharides having the C residue (ᴅ-GlcNAc) linked to the A residue (⟨-ᴅ-Gal). Using the data accumulated by full analyses of the oligosaccharides, the NMR spectra of the polysaccharide and, more especially, the HBMC spectra were re-examined to highlight the connectivity between the C and A residues.

The correlations observed between the A and B residues, and B and C residues, in the oligosaccharides HMBC spectra were also observed in the HMBC spectra of the polysaccharides (Figure 6). The linkage between the C and A residues were also clearly identified: the A-C3 carbon (80.19 ppm) correlated with the C-H1 proton (4.81 ppm) (Figure 6) and reciprocally the C-C1 carbon of the native polysaccharide (103.19 ppm) correlated with the A-H3 proton (3.99 ppm) (not shown), demonstrating that the ®-ᴅ-GlcNAc (residue C) is linked to the ⟨-ᴅ-Gal (residue A) via a 1,3 linkage. The structure of the polysaccharide was therefore: [→3)-⟨-ᴅ-Gal-(1→4)-⟨-ʟ-GulNAcA/⟨-ʟ-3OAc-GulNAcA-(1→4)-®-ᴅ-GlcNAc-(1→]. This repetition unit was very similar to that found in the lipopolysaccharide extracted from *Pseudoalteromonas nigrifaciens* KMM161 [15]. The ^{13}C chemical shifts reported were in agreement with our analyses and supported our conclusions

In conclusion, the structure investigated in this study is the third exopolysaccharide structure secreted by a *V. alginolyticus* strain [7,8]. The composition of the repetition unit determined as well as the sequence of residues have no similarities, suggesting that the biosynthetic pathways of these polysaccharides probably have no common ancestor. The structural diversity found in *V. alginolyticus* strains is also true for all the strains of *Vibrio* genus. The Carbohydrate Structure Database [1,2] has 114 entries describing polysaccharides—including secreted polysaccharides or lipopolysaccharides—of the genus *Vibrio*. The structural diversity of the polysaccharides suggests a very high plasticity of the polysaccharide biosynthesis pathway of the strains belonging to the genus *Vibrio*.

3. Materials and Methods

3.1. Production, Isolation and Purification of the Vibrio alginolyticus Exopolysaccharide (VA-EPS)

VA-EPS was produced by *Vibrio alginolyticus* (CNCM I-5035) in a 30 L fermenter containing marine broth medium (30 g/L sea salts, 1 g/L yeast extracts, 4 g/L peptone) supplemented with glucose (30 g/L) at 25 °C. The culture medium was inoculated at 10% (*v/v*) with a bacterial suspension in the exponential growth phase. The pH was adjusted and maintained at 7.2 by automatic addition of 1 M NaOH. The medium was oxygenated at 15 L/min with an agitation rate of 350 rpm. After 72 h of fermentation, bacterial cells were removed from the culture medium by centrifugation (16,000× *g*, 30 min). The supernatant, containing the excreted VA-EPS, was then purified by filtration through a cellulose membrane (0.7 µm) and then by ultrafiltration (100 kDa). The filtration steps led to a loss of 20 to 30% biomass giving a purified 1 g/L VA-EPS in water. The sample was freeze-dried and stored at room temperature away from light and moisture.

3.2. Monosaccharide Analysis

The molar ratio of monosaccharides was determined according to [18], modified by [19]. The EPS was hydrolyzed with 3 M MeOH/ HCl at 110 °C for 4 h, followed by re-*N*-acetylation with Ac2O overnight at room temperature. The methyl glycosides were converted to their corresponding trimethylsilyl derivatives. Separation and quantification of the per-*O*-trimethylsilyl methyl glycosides were performed using gas–liquid chromatography (GLC) on an Agilent system equipped with a HP-5 ms capillary column (Agilent 0.25 mm × 30 m). The trimethylsilyl derivatives were analyzed using the

following temperature program: 120 °C for 1 min, 120 °C→180 °C at 3 °C/min, 180 °C to 200 °C at 3 °C/min, 200 °C for 5 min.

3.3. Methylation Analysis

Glycosyl-linkage positions were determined as described in [20]. The native EPS was carboxyl-reduced by treatment with N-cyclohexyl 1-N'[®(N-methyl-morpholino)-ethyl] carbodiimide p-toluene sulfonate and with NaBD$_4$ for 4 h at room temperature [21]. After dialysis against distilled water, hydroxyl groups were methylated using 2.5 N butyl lithium in hexanes and methyl iodide in DMSO [22]. The methylated compounds were extracted with CH$_2$Cl$_2$. The methylated products were then hydrolyzed in 2 M TFA for 2 h at 120 °C, then reduced with NaBD$_4$ in a NH$_4$OH solution for 30 min at 80 °C, and finally acetylated with 200 μL of 1-methyl imidazole and 2 mL of pyridine for 10 min at room temperature. GLC-mass spectrometry (MS) was performed on an Agilent instrument fitted with a high-performance 5 ms capillary column (Agilent, 0.25 mm × 30 m). The temperature program was 90 °C for 1 min, 90 °C to 300 °C at 5 °C/min, 300 °C for 1 min. Ionization was carried out in electron impact mode (EI, 70 eV).

3.4. Determination of Absolute Configuration

Assignment of absolute configuration of monosaccharide residues was adapted from the method of Gerwig [23,24]. A quantity of 2 mg of polysaccharide was dissoved in 500 μL of 4N TFA and maintained, in sealed glass tubes, for 4 h at 100 °C. After cooling, TFA was evaporated under a flux of nitrogen. Next, 500 μL of (S)-(+)-2-butanol and a drop of 13N TFA were added to the dried sample and the hermetically sealed glass tube was kept at 8 hours at 80 °C. Butanol and TFA were evaporated under nitrogen. Butylglycosides samples were then re-N-acetylated, converted to their corresponding trimethylsilyl derivatives and analyzed by GLC according to the protocol described in Section 3.2. for monosaccharide analysis.

3.5. Molecular Weight Determination

The molecular weight of VA-EPS was determined by high-performance size-exclusion chromatography (HPSEC) using an eighteen-angle light scattering detector, coupled with refractive index detection and specific refractive index increment dn/dc (DAWNTM HELEOS, Wyatt). Elution was performed on Shodex OHpak SB-805 HQ and OHpak SB-806 HQ placed in series (Phenomenex, exclusion limit <2 × 10^7 g/mol) with 0.1 M NaNO$_3$ as the eluent. To calculate the molecular mass, the dn/dc value used was 0.145 mL/g. The polydispersity index was calculated from the Mw/Mn ratio.

3.6. Acid Hydrolysis and Oligosaccharides Purification

VA-EPS underwent mild acid hydrolysis. A quantity of 300 mg of polysaccharide was solubilized in 75 mL of 0.1 M TFA and heated at 100 °C for 90 min or 300 min, respectively. After neutralization with 8N NH$_4$OH, the salts were eliminated by adding five volumes of acetone. The precipitate that contained the oligosaccharides was recovered by centrifugation. The pellet was resuspended in 2 mL of distilled water and the oligosaccharides were fractionated by size exclusion chromatography using a SEC Toyopearl HW-40 column (5 × 100 cm, Tosoh, exclusion limit <10^4 Da) with 0.1 M (NH$_4$)$_2$CO$_3$ as the eluent.

3.7. NMR

Carbon-13 and proton NMR spectra were recorded with a Bruker Avance 400 spectrometer operating at a frequency of 100.618 MHz for ^{13}C and 400.13 MHz for ^{1}H. Samples were solubilized in D$_2$O at a temperature of 293 K for the oligosaccharides and 353 K for the polysaccharide. Residual signal of the solvent was used as internal standard: HOD at 4.85 ppm at 293 K and 4.35 ppm at 343 K. ^{13}C spectra were recorded using 90° pulses, 20,000 Hz spectral width, 65,536 data points, 1.638 s

acquisition time, 1 s relaxation delay and between 8192 and 16,834 scans. Proton spectra were recorded with a 4006 Hz spectral width, 32,768 data points, 4.089 s acquisition time, 0.1 s relaxation delay and 16 scans. The ^{1}H and ^{13}C-NMR assignments were based on ^{1}H-^{1}H homonuclear and ^{1}H-^{13}C heteronuclear correlation experiments (correlation spectroscopy, COSY; heteronuclear multiple-bond correlation, HMBC; heteronuclear single quantum correlation, HSQC). They were performed with a 4006 Hz spectral width, 2048 data points, 0.255 s acquisition time, 1 s relaxation delay; 32 to 512 scans were accumulated.

Supplementary Materials: The following are available online at http://www.mdpi.com/1660-3397/18/10/509/s1, Figure S1: Composition analysis of the Vibrio alginolyticus exopolysaccharide, Figure S2: Determination of absolute configuration, Figure S3: COSY spectra of the Vibrio alginolyticus exopolysaccharide before (A) and after (B) alkaline treatment, Figure S4: HSQC spectra of the Vibrio alginolyticus exopolysaccharide before (A) and after (B) alkaline treatment, Figure S5: COSY spectra recorded at 293K of the two disccharides purified by chromatography, Figure S6: HSQC spectra recorded at 293K of the two disccharides purified by chromatography, Figure S7: Positive-ion reflectron MALDI-TOF mass spectrometry analysis of the enriched fraction of the trisaccharide obtained after hydrolysis of the Vibrio alginolyticus exopolysaccharide, Table S1: Comparison of the 13C NMR chemical shifts (δ, ppm) of the Vibrio alginolyticus exopolysaccharide and the calculated values [Lipkind, et al. (1988) Carbohydr. Res. 175, 59-75].

Author Contributions: B.T., A.C., P.-Y.M. and R.V. produced and purified the EPS. Preliminary sugar content and composition were also done by these authors. C.B. and L.B. determined the sugar content and the linkages by chemical methods. They also measured the molecular weight of the EPS. R.C., S.D. and I.J. performed chromatography, NMR experiments and analysis. W.H. lead the project and wrote the article. All authors have read and agreed to the published version of the manuscript.

Conflicts of Interest: The authors declare no conflict of interest.

References

1. Toukach, P.V.; Egorova, K.S. Carbohydrate structure database merged from bacterial, archaeal, plant and fungal parts. *Nucleic Acids Res.* **2016**, *44*, D1229–D1236. [CrossRef] [PubMed]

2. Toukach, P.; Egorova, K. Carbohydrate Structure Database (CSDB): Examples of Usage. In *A Practical Guide to Using Glycomics Databases*; Aoki-Kinoshita, K.F., Ed.; Springer: Tokyo, Japan, 2017; pp. 75–113.

3. Toukach, P.; Egorova, K. Bacterial, Plant, and Fungal Carbohydrate Structure Databases: Daily Usage. In *Glycoinformatics*; Lütteke, T., Frank, M., Eds.; Springer: New York, NY, USA, 2015; pp. 55–85.

4. Laine, R.A. A calculation of all possible oligosaccharide isomers both branched and linear yields $1.05 \times 10(12)$ structures for a reducing hexasaccharide—The isomer-barrier to development of single-method saccharide sequencing or synthesis systems. *Glycobiology* **1994**, *4*, 759–767. [CrossRef] [PubMed]

5. Sutherland, I.W. Microbial polysaccharides from Gram-negative bacteria. *Int. Dairy J.* **2001**, *11*, 663–674. [CrossRef]

6. Freitas, F.; Alves, V.D.; Reis, M.A.M. Advances in bacterial exopolysaccharides: From production to biotechnological applications. *Trends Biotechnol.* **2011**, *29*, 389–398. [CrossRef] [PubMed]

7. Drouillard, S.; Jeacomine, I.; Buon, L.; Boisset, C.; Courtois, A.; Thollas, B.; Morvan, P.-Y.; Vallée, R.; Helbert, W. Structure of the exopolysaccharide secreted by a marine strain *Vibrio alginolyticus*. *Mar. Drugs* **2018**, *16*, 164. [CrossRef] [PubMed]

8. Drouillard, S.; Jeacomine, I.; Buon, L.; Boisset, C.; Courtois, A.; Thollas, B.; Morvan, P.-Y.; Vallée, R.; Helbert, W. Structure of an amino acid-derived decorated exopolysaccharide secreted by a *Vibrio alginolyticus* strain. *Mar. Drugs* **2018**, *13*, 6723. [CrossRef] [PubMed]

9. Kanlayavattanakul, M.; Lourith, N. Cosmetics: Active Polymers. In *Encyclopedia of Polymer Applications*; Mishra, M., Ed.; CRC Press Taylor & Francis Group: London, UK, 2019; pp. 705–721.

10. Pantophlet, R.; Haseley, S.R.; Vinogradov, E.V.; Brade, L.; Holst, O.; Brade, H. Chemical and antigenic structure of the O-polysaccharide of the lipopolysaccharides from two *Acinetobacter haemolyticus* strains differing only in the anomeric configuration of one glycosyl residue in their O-antigens. *Eur. J. Biochem.* **1999**, *263*, 587–595. [CrossRef] [PubMed]

11. Leone, S.; Lanzetta, R.; Scognamiglio, R.; Alfieri, F.; Izzo, V.; Di Donato, A.; Parrilli, M.; Holst, O.; Molinaro, A. The structure of the O-specific polysaccharide from the lipopolysaccharide of *Pseudomonas* sp. OX1 cultivated in the presence of the azo dye Orange II. *Carbohydr. Res.* **2008**, *343*, 674–684. [CrossRef] [PubMed]

12. Yildiz, F.; Fong, J.; Sadovskaya, I.; Grard, T.; Vinogradov, E. Structural Characterization of the Extracellular Polysaccharide from *Vibrio cholerae* O1 El-Tor. *PLoS ONE* **2014**, *9*, e86751. [CrossRef] [PubMed]

13. Lipkind, G.M.; Shashkov, A.S.; Knirel, Y.A.; Vinogradov, E.V.; Kochetkov, N.K. A computer-assisted structural analysis of regular polysaccharides on the basis of 13C-n.m.r. data. *Carbohydr. Res.* **1988**, *175*, 59–75. [CrossRef]

14. Kondakova, A.N.; Novototskaya-Vlasova, K.A.; Drutskaya, M.S.; Senchenkova, S.N.; Shcherbakova, V.A.; Shashkov, A.S.; Gilichinsky, D.A.; Nedospasov, S.A.; Knirel, Y.A. Structure of the O-polysaccharide chain of the lipopolysaccharide of *Psychrobacter muricolla* 2pST isolated from overcooled water brines within permafrost. *Carbohydr. Res.* **2012**, *349*, 78–81. [CrossRef] [PubMed]

15. Gorshkova, R.P.; Nazarenko, E.L.; Zubkov, V.A.; Ivanova, E.P.; Gorshkova, N.M.; Isakov, V.V. Structure of O-specific polysaccharide from *Pseudoalteromonas nigrifaciens* strain KMM 161. *Biochemistry* **2002**, *67*, 672–675. [PubMed]

16. Knirel, Y.A.; Vinogradov, E.V.; Kocharova, N.A.; Shashkov, A.S.; Dmitriev, B.A.; Kochetkov, N.K. Synthesis and 13C-N.m.r. spectra of methyl 2,3-diacetamido-2,3-dideoxy-α-D-hexopyranosides and 2,3-diacetamido-2,3-dideoxy-D-hexoses. *Carbohydr. Res.* **1983**, *122*, 181–188. [CrossRef]

17. Michon, F.; Brisson, J.R.; Roy, R.; Ashton, F.E.; Jennings, H.J. Sructural determination of the capsular polysaccharide of *Neisseria-meningitidis* group-I: A two-dimensional NMR analysis. *Biochemistry* **1985**, *24*, 5592–5598. [CrossRef]

18. Kamerling, J.P.; Gerwig, G.J.; Vliegenthart, J.F.; Clamp, J.R. Characterization by gas-liquid chromatography-mass spectrometry and proton-magnetic-resonance spectroscopy of pertrimethylsilyl methyl glycosides obtained in the methanolysis of glycoproteins and glycopeptides. *Biochem. J.* **1975**, *151*, 491–495. [CrossRef]

19. Montreuil, J.; Bouquelet, S.; Debray, H.; Fournet, B.; Spik, G.; Strecker, G. Glycoproteines. In *Carbohydrates Analysis: A Practical Approach*; Chaplin, M.F., Kennedy, J.K., Eds.; IRL Press: Oxford, UK, 1986; pp. 143–204.

20. Hakomori, S.I. A rapid permethylation of glycolipid, and polysaccharide catalyzed by methylsulfinyl carbanion in dimethyl sulfoxide. *J. Biochem.* **1964**, *55*, 205–208. [PubMed]

21. Taylor, R.L.; Conrad, H.E. Stoichiometric depolymerization of polyuronides and glycosaminoglycans to monosaccharides following reduction of their carbodiimide activated carboxyl groups. *Biochemistry* **1972**, *11*, 1383. [CrossRef] [PubMed]

22. Kvernheim, A.L. Methylation analysis of polysaccharides with butyllithium in dimethyl sulfoxide. *Acta Chemica Scandinavia* **1987**, *B41*, 150–152. [CrossRef]

23. Gerwig, G.J.; Kamerling, J.P.; Vliegenthart, F.G. Determination of the D and L configuration of neutral polysaccharides by high resolution capillary G.L.C. *Carbohydr. Res.* **1978**, *62*, 349–357. [CrossRef]

24. Gerwig, G.J.; Kamerling, J.P.; Vliegenthart, F.G. Determination of the absolute configuration of monosaccharides in complex carbohydrate by capillary G.L.C. *Carbohydr. Res.* **1979**, *77*, 1–7. [CrossRef]

Characterization of Low Molecular Weight Sulfate Ulva Polysaccharide and its Protective Effect against IBD in Mice

Yuanyuan Li [1,2], Han Ye [1], Ting Wang [1], Peng Wang [1], Ruizhi Liu [2,*], Yinping Li [3,*], Yingying Tian [4] and Jingliang Zhang [4]

[1]   College of Food Science and Engineering, Ocean University of China, Qingdao 266003, China; yuanyuan032220@163.com (Y.L.); 17852720293@163.com (H.Y.); Wang_xx0419@163.com (T.W.); pengwang@ouc.edu.cn (P.W.)
[2]   State Environmental Protection Key Laboratory of Estuarine and Coastal Environment, Chinese Research Academy of Environmental Sciences, Beijing 100012, China
[3]   Shandong Provincial Key Laboratory of Biochemical Engineering, College of Marine Science and Biological Engineering, Qingdao University of Science and Technology, Qingdao 266042, China
[4]   Marine Biomedical Research Institute of Qingdao, Qingdao 266071, China; 15704317507@163.com (Y.T.); yupinghui7373262@126.com (J.Z.)
*   Correspondence: liu_ruizhi@163.com (R.L.); fmsboc@163.com (Y.L.)

Abstract: Inflammatory bowel disease (IBD) has been gradually considered a public health challenge worldwide. Sulfated polysaccharides, extracted from seaweed, have been shown to have an anti-inflammatory effect on the disease. In this study, LMW-ulvan, a unique sulfate Ulva polysaccharide with low molecular weight, was prepared using the enzymatic method. The structural characterization of LMW-ulvan and its protective effect on colitis induced by dextran sulfate sodium (DSS) were studied. The results showed that LMW-ulvan with molecular weight of 2.56 kDa consists of 57.23% rhamnose (Rha), 28.76% xylose (Xyl), 7.42% glucuronic acid (GlcA), and 1.77% glucose (Glc). Its backbone contains (1→3,4)-linked Rha, (1→4)-linked Xyl, and (1→4)-linked GlcA with small amounts of (1→4)-linked Rha residues; sulfate substitution was at C-3 of Rha. LMW-ulvan was found to reduce DSS-induced disease activity index, colon shortening, and colonic tissue damage, which were associated with decreased oxidative stresses and inflammation, thus improving the expression of tight junction proteins. These results indicate that LMW-ulvan is able to improve colitis and may be a promising application for IBD.

Keywords: *Ulva pertusa*; polysaccharides; colitis; anti-inflammatory; antioxidant

1. Introduction

Ulcerative colitis (UC), a significant form of inflammatory bowel disease (IBD), is a chronic inflammatory disorder of the colonic mucosa. It usually starts in the rectum and spreads to the colon proximally, in a continuous manner [1]. The global prevalence of IBD is increasing every year—more than 0.3% of the population suffers from the disease [2]. The pathogenesis of IBD is unclear; however, many researches claim that it is a result of genetic defects, unhealthy lifestyles, imbalance of intestinal microbiota, or immune dysbiosis [3–5]. Typical features of UC include structural and functional impairment of the intestinal mucosa, accompanied by diarrhea, rectal bleeding, and other symptoms [6]. Currently, surgery and drugs (including corticosteroids, aminosalicylic acid, and immunosuppressive agents) are the main strategies from a clinical aspect [7]. However, in addition to the high costs and incomplete treatment issues, these drug interventions have certain side-effects

and have been seen to lose efficacy in long-term use patients [8]. Consequently, more efforts should be made to enrich treatment and disease prevention methods.

Numerous reports have testified to inflammatory reactions being a crucial factor causing UC [9]. The cytokines secreted by intestinal epithelial cells are important markers of the intestinal immune system and regulate their inflammatory responses [10]. Pro-inflammatory cytokines such as tumor necrosis factor (TNF)-α, interferon (IFN)-γ, and interleukin (IL)-1β can promote an inflammatory response, eventually causing colon tissue injury, while anti-inflammatory cytokines such as IL-4 and IL-10 can reduce inflammation [11]. Excessive pro-inflammatory cytokines increase the production of reactive oxygen species (ROS), which ultimately cause intestinal epithelial cell injury and aggravate pathogenesis [12]. Hence, materials with the ability to recover abnormal levels of cytokines and oxidative stress may be promising therapeutics for IBD.

Ulvan is a kind of sulphated polysaccharide located in the cell walls of *Ulva*; it represents an abundant marine resource distributed worldwide. Ulvan extracted from different species of *Ulva* consists primarily of Rha (16.8–45.0%), GlcA (6.5–19.0%), Xyl (2.1–12.0%), iduronic acid (IdoA) (0.7–9.1%), Glc (0.5–6.8%), and sulphate (14.3–23.2%) and its backbone is mostly composed of α-1,4- and α-1,2,4- linked L-rhamnose, β-1,4- and terminally linked D-glucuronic acid and β-1,4-linked D-xylose [13]. Like other sulfated polysaccharides, ulvan exerts various therapeutic activities, such as antibacterial, immunostimulatory, antitumor, antioxidant, antihyperlipidemic, and anticoagulant properties [14,15]. Qi et al. (2005) reported that high sulfate content ulvan showed a stronger scavenging activity of superoxide and hydroxyl radicals, reducing power, and metal chelating ability [16]. In a research work by Li et al. (2018), the ulvan extracted from *Ulva pertusa* showed significant protection against liver damage by oxidative stress induced by a cholesterol-rich diet [17]. De Araújo et al. (2016) found that the enzymatic digestion of ulvan extracted from *Ulva lactuca* had a vascular anti-inflammatory effect by decreasing TNF-α and IL-1 levels [18]. Additionally, Berri et al. (2017) reported that ulvan extracted from *Ulva armoricana* was able to initiate and amplify the protective immune responses of the host, and regulate mucosal immunity against intestinal pathogens [19].

Reports on the antiinflammatory and antioxidant effects of ulvan are readily available, but few reports have been published on its protective effects in rats with DSS-induced colitis. In this study, LMW-ulvan produced by the enzymatic method was purified and characterized, and its potential to alleviate IBD symptoms in DSS-induced mice and protect the intestinal epithelial barrier were investigated.

2. Results and Discussion

2.1. Characterization of LMW-Ulvan

2.1.1. Determination of Molecular Weight of LMW-Ulvan

The average molecular weight of ulvan was 1068.2 kDa according to a previous research by Chi et al. (2020) [20]. Because of its high molecular weight, ulvan usually shows poor biological absorption compared to oligosaccharide [13]. Consequently, the ulvan was degraded by ulvan lyase and the purified LMW-ulvan was prepared using ion exchange chromatography (Figure 1A). The molecular weight distribution of LMW-ulvan was then measured (Figure 1B). According to the standard curve obtained from dextran standards with different molecular weights (logMw = −0.3643x + 10.049, R^2 = 0.991) and retention time of the polysaccharide peak, the weight-average molecular weight of LMW-ulvan was calculated to be 2.56 kDa.

2.1.2. Monosaccharide Composition Analysis of LMW-Ulvan

The LMW-ulvan generated in this study was mainly composed of 57.23% Rha, 28.76% Xyl, 7.42% GlcA, and 1.77% Glc (Figure 2). The monosaccharide composition of LMW-ulvan was slightly different from that of ulvan, whose molar percentage of Rha, Xyl, GlcA, IdoA, and Glc was 56.50%, 20.34%, 16.95%, 2.82%, and 3.39%, respectively [20]. The lyase used in this study belonged to the

PL25 family, which cleaves the (1→4) glycosidic bond between 3-*O*-sulfated Rha and GlcA [21]. After enzymatic hydrolysis, unsaturated uronic acid was formed in a β-elimination reaction [22]. Consequently, the characterization of ulvan lyase might be the reason for a significant decrease in percentage of GlcA.
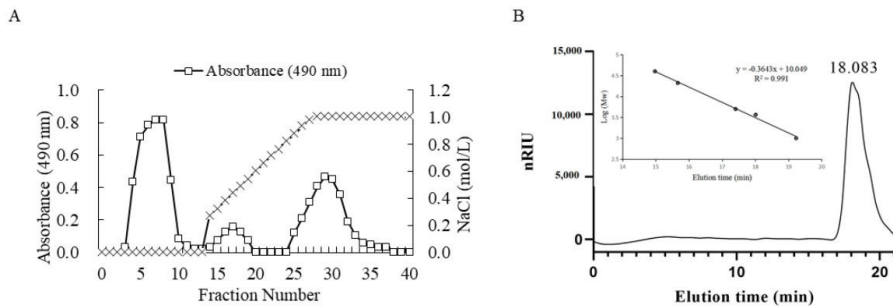

Figure 1. Purification of LMW-ulvan using a DEAE column (**A**) and its gel permeation chromatogram (**B**).
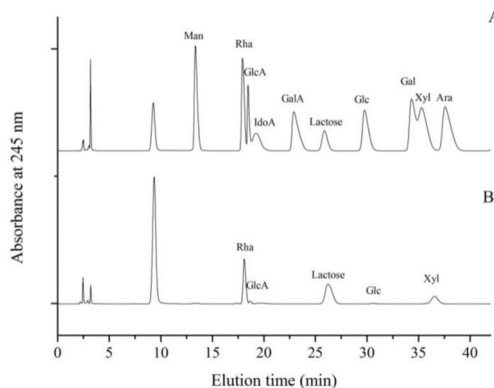
Figure 2. High performance liquid chromatography (HPLC) analyses of monosaccharide standards (**A**) and LMW-ulvan (**B**). Lactose is the internal standard.

2.1.3. Methylation and Gas Chromatography-Mass Spectrometer (GC-MS) Analysis of LMW-Ulvan

The integrated structure of LMW-ulvan, including linkages and sulfate substitution position, were further determined by methylation analysis and GC-MS. The completeness of methylation of LMW-ulvan and desulfated LMW-ulvan (dsLMW-ulvan) was confirmed by FT-IR spectroscopy with the disappearance of OH bands (data not shown). As shown in Table 1, LMW-ulvan mainly consisted of (1→3,4)-linked Rha, and (1→4)-linked Xyl with small amounts of (1→4)-linked Rha residues. Sulfate substitution was at C-3 of (1→4)-linked Rha because of the distinctive increase of amounts of (1→4)-linked Rha and significantly decrease of the amounts of (1→3,4)-linked Rha in dsLMW-ulvan. Besides, according to the characterization of ulvan lyase belonged to the PL25 family, which cleaves the (1→4) glycosidic bond between 3-*O*-sulfated Rha and GlcA [21]. Thus we deduced that there is 4-GlcAp-(1 in the LMW-ulvan. The linkages and sulfate substitution position of LMW-ulvan are similar to polysaccharide from *Ulva* species [23].

Table 1. Profile of partially *O*-methylated alditol acetates obtained by methylation analysis of LMW-ulvan.

O-Me-Alditol Acetate	Molar Percentage		Linkage Pattern
	LMW-Ulvan	**dsLMW-Ulvan**	
1,4,5-Tri-*O*-acetrl-2,3-di-*O*-metyl-L-Rha	6.65%	53.32%	→4)-Rha-(1→
1,3,4,5-Tetro-*O*-acetrl-2-*O*-metyl-L-Rha	50.12%	4.16%	→3,4)-Rha-(1→
1,4,5-Tri-*O*-acetrl-2,3-di-*O*-metyl-D-xyl	29.34%	28.45%	→4)-xyl-(1→

Desulfation of the LMW-ulvan: dsLMW-ulva, rhamnose: Rha, xylose: Xyl.

2.2. LMW-Ulvan Relieves the Manifestations of IBD Induced by DSS

To evaluate the anti-colitis effects of LMW-ulvan, the DSS was used to establish a model to mimic human UC and determine the therapeutic effect of LMW-ulvan [24]. Preliminary tests revealed that 30 mg/kg of LMW-ulvan showed no protective effects in IBD rats, while 50 mg/kg of LMW-ulvan began to show protective effects in IBD. Besides, 100 and 120 mg/kg of LMW-ulvan were more effective. Thus, 50 and 100 mg/kg were chosen for subsequent studies. The results of the acute toxicity experiment showed that an LMW-ulvan dose less than 1200 mg/kg showed no significant damage to ICR mice. Consequently, both doses used in this study were safe. The clinical symptoms of IBD in mice were comprehensively determined by changes in body weight (Figure 3A), colon length (Figure 3B), and DAI (disease activity index) score (Figure 3C). Body weight of the mice in the N group showed a gradual upward trend during the experiment period. In contrast, the body weight of the mice in the M group revealed a downward trend, especially after the fifth day. The loss in weight of the mice was significantly improved on treatment with LMW-ulvan of both dosages. There was no significant difference between the LP group and the PC group. Another indicator reflecting the severity of intestinal inflammation is colon length, which is restored with improvement in inflammation [25,26]. The colon length of mice in the M group was significantly shorter than that of the N group (Figure 3B). However, after treatment with LMW-ulvan, the colon was distinctly longer than that of the M group and similar to that of the PC group. In addition, the DAI score were also significantly reduced in the LMW-ulvan treatment group compared with that of the M group on the sixth day (Figure 3C). Spleen and thymus index was measured as an indirect marker of inflammation in all the experiment groups. As shown in Figure 3D,E, DSS decreased the thymus index and increased the spleen index significantly, reflecting on worse immune activity. LMW-ulvan was observed to improve the immune system because the spleen and thymus index of the HP group recovered to normal levels and showed no significant difference as compared to that of the N group. Besides, Figure 3E also showed that the LMW-ulvan of both dosages could significantly relieve splenomegaly induced by DSS.

2.3. LMW-Ulvan Reverses the Histological Injury of Colonic Epithelium Caused by DSS

Due to severe colitis, mice in the M group exhibited mucosal degeneration and necrosis, distortion of crypts, loss of goblet cells, and mucosal and submucosal infiltration of mononuclear inflammatory cells, as compared to that of the N group (Figure 4A,B). However, in all mice in the LP group, infiltration and aggregation of mononuclear inflammatory cells were observed in the submucosa of the colon, with improvement observed in epithelial degeneration and necrosis. In mice from the HP group, a nearly intact structure with few inflammatory cells as that of the N group was exhibited. This result indicates that LMW-ulvan could reduce the inflammatory infiltration and damage caused by DSS.
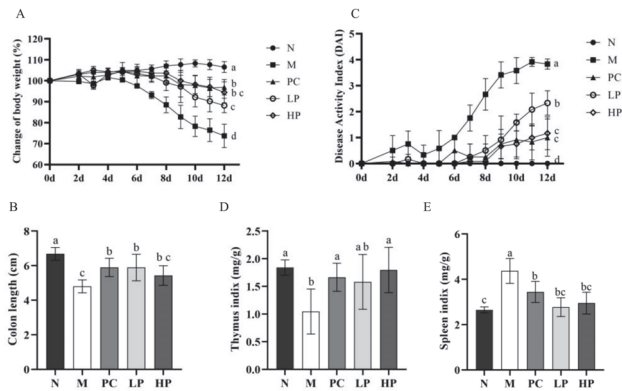
Figure 3. Assess the severity of IBD (Inflammatory bowel disease) in each group: (**A**) Change in body weight, (**B**) colon length of mice in each group, (**C**) DAI (disease activity index) score, (**D**) thymus index, and (**E**) spleen index. N: normal group, M: model, PC: positive control, LP: low dose LMW-ulvan (50 mg/kg), and HP: high dose LMW-ulvan (100 mg/kg).
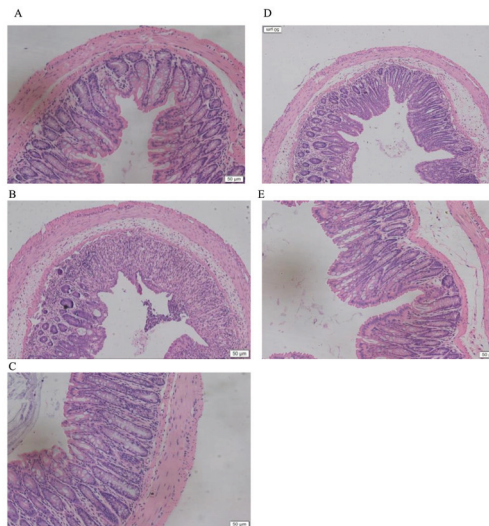
Figure 4. H&E staining of representative colons from different treatment groups (200×): (**A**) N group, (**B**) M group, (**C**) PC group, (**D**) LP group, and (**E**) HP group. N: normal group, M: model, PC: positive control, LP: low dose LMW-ulvan (50 mg/kg), and HP: high dose LMW-ulvan (100 mg/kg).

2.4. Effects of LMW-Ulvan on Cytokines in Colon Tissue and Serum

It is well known that an abnormal inflammatory response is one of the most striking features of IBD [27]. The result showed that DSS increased the levels of IL-1β and IFN-γ significantly and decreased the level of IL-4, when compared to the N group (Figure 5). After administration of LMW-ulvan, the levels of IL-1β, IFN-γ, and IL-4 in colon tissue and serum all recovered to normal levels. IL-1β is a kind of pro-inflammatory cytokine and its active form is regulated by caspase 1 secreted from the NLRP3 inflammasome [28]. In this study, LMW-ulvan reduced the level of IL-1β in the colon and serum, which indicated its possibility to suppress NLRP3 inflammasome activation. Activated Th cells are classified as type 1 of T helper cells (Th1) and type 2 of T helper cells (Th2) according to different

sorts and bioactivities of cytokines [29]. Usually, Th1 mediates a cell-mediated immune response, while Th2 mediates a humoral immune response [30]. IFN-γ and IL-4 are representative cytokines to coordinate immunity secreted by Th1 and Th2, respectively [31]. The IFN-γ/IL-4 ratio can also reflect the balance of Th1/Th2. The results showed that IFN-γ/IL-4 ratios in serum of the N, M, PC, LP, and HP groups were similar to that in the colon and were about 1.0, 2.5, 1.1, 1.2, and 1.1, respectively. Consequently, DSS disturbs the balance of Th1/Th2 toward to Th1 by increasing the value of IFN-γ and reducing the secretion of IL-4. The results indicated that LMW-ulvan could inhibit the Th1 cell response and improve the Th2 cell response, which is beneficial in alleviating the inflammatory damage caused by DSS.

Figure 5. Levels of inflammatory cytokines in serum and colon tissues. (**A**) interleukin (IL)-1β level in serum. (**B**) IL-4 level in serum. (**C**) interferon (IFN)-γ level in serum. (**D**) IL-1β level in colon. (**E**) IL-4 level in colon. (**F**) IFN-γ level in colon. N: normal group, M: model, PC: positive control, LP: low dose LMW-ulvan (50 mg/kg), and HP: high dose LMW-ulvan (100 mg/kg).
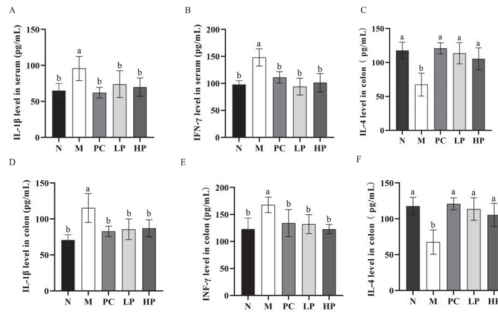
2.5. Effects of LMW-Ulvan on Malondialdehyde (MDA), GPx, and Catalase (CAT) in Colonic Tissue

Excessive inflammation augments oxidative stress, which has been associated with extensive infiltration of immune cells, and activation of NF-κB signaling and ER stress, thereby causing tissue damage and exacerbation of a patient's condition [12,32,33]. As shown in Figure 6, DSS significantly enhanced the MDA level, but downregulated the enzyme activity of GPx and CAT. LMW-ulvan at doses of 50 and 100 mg/kg significantly reduced ($p < 0.05$) the MDA level and increased the enzyme activity of GPx and CAT. Specifically, the activity of GPx and CAT of the HP group was restored to that of the normal group. MDA, an indicator reflecting the accumulation of ROS in response to oxidative damage, is one of the most important products of lipid peroxidation and could damage the mucosa [34], while GPx is an important component of the glutathione antioxidant system, which forms an antioxidant barrier in the gut mucosa [35]. Based on the above analysis, the protective effect of LMW-ulvan on IBD damage might be attributed to an enhanced antioxidant defense system.
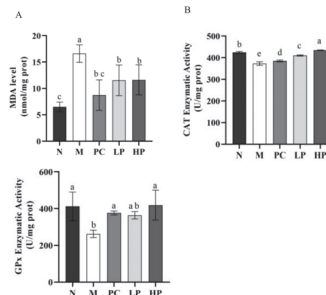

Figure 6. The level of MDA (**A**), activity of GPx (**B**), and activity of CAT(**C**). N: normal group, M: model, PC: positive control, LP: low dose LMW-ulvan (50 mg/kg), and HP: high dose LMW-ulvan (100 mg/kg).

2.6. Effect of LMW-Ulvan on mRNA Expression of Colonic Epithelial Tight Junction Protein

To ascertain whether LMW-ulvan treatment can protect the integrity of the intestinal barrier, the expression of claudin, occluding, and tight junction protein 1 (ZO-1) was detected at both protein and mRNA level (Figure 7). The expression of three tight junction components in the M group was reduced significantly ($p < 0.05$), while the expression in the LMW-ulvan treatment groups was increased to different degrees compared with that of the N group. For ZO-1 and claudin, the expression in both HP and LP groups was significantly increased and the low dose LMW-ulvan showed a similar effect as that of 5-aminosalicylic acid (5-ASA) (Figure 7C,D). For occludin, the expression level in both HP and LP groups showed no significant difference with that of the N group (Figure 7B). Claudin, occludin, and ZO-1 are the main components of tight junction, which is the most significant structure in the intestinal mucosal mechanical barrier [10]. The tight junction can effectively prevent enteric pathogens, antigens, and other substances from entering the intestinal mucosa, preventing the activation of immune cells and abnormal immune responses and maintaining stability of mucosal barrier function and intestinal permeability [36]. The improvement of LMW-ulvan on DSS-induced colitis might be closely related to its protective effect on the intestinal mucosal barrier by increasing the expression of tight junction proteins. Thus, LMW-ulvan could further inhibit the abnormal immune response in the intestinal mucosa, thus ameliorating mucosal barrier function and intestinal mucosal permeability.
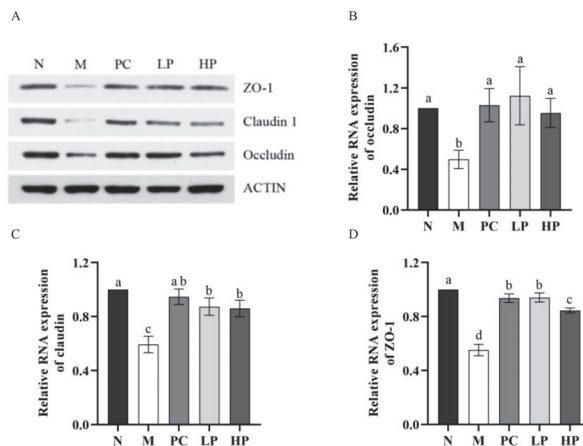
Figure 7. The expression of colonic epithelial tight junction protein. (**A**) Representative western blotting images for colonic epithelial tight junction protein. (**B**) The relative mRNA content of claudin. (**C**) The relative mRNA content of occludin. (**D**) The relative mRNA content of ZO-1. N: normal group, M: model, PC: positive control, LP: low dose LMW-ulvan (50 mg/kg), and HP: high dose LMW-ulvan (100 mg/kg).

3. Materials and Methods

3.1. Materials and Reagents

Ulva pertusa was collected from the coast near Weihai, China, in 2019. Ulvan lyase was provided by the Applied Microbiology Laboratory (Ocean University of China). DSS (36–50 kDa) and 5-aminosalicylic acid (5-ASA) were purchased from MP Biomedicals (Solon, CA, USA) and Sigma-Aldrich (St. Louis, MO, USA), respectively. ELISA detection kits for IL-1β, IL-4, IFN-γ, malonic dialdehyde (MDA), catalase (CAT), and glutathione peroxidase (GPx) were obtained from Dakewe Biotech Corporation (Beijing, China). Primary antibodies specific for β-actin, ZO-1, occluding, and claudin-1 were purchased from Protein Tech Group (Wuhan, China). The BCA Protein Assay Kit was purchased from Beijing Solarbio Science & Technology Co., Ltd. (Beijing, China). All other reagents were of analytical grade.

3.2. Enzymatic Preparation and Purification of LMW-Ulvan

The ulvan was extracted according to a method described by Qiao et al. (2020) [37]. It was then degraded though an enzymatic method described by Chi et al. (2020) [20] and crude enzymatic fractions with average molecular weight of 1–5 kDa were obtained by nanofiltration membrane system. The obtained fraction was purified using ÄKTAprime plus (GE Healthcare, Woburn, MA, USA) equipped with DEAE-Sepharose CL-6B column (1.6 × 10 cm). The fraction was pre-equilibrated with ultrapure water and then eluted with a linear gradient of 0–1 M NaCl at 1.0 mL/min. The purified fraction was then dialyzed, lyophilized, and nominated as LMW-ulvan.

3.3. Characterization of LMW-Ulvan

The total sugar content of LMW-ulvan was determined by phenol-sulfuric acid method [38]. Sulfate content was determined after hydrolysis of trifluoroacetic acid [39]. The molecular weights of LMW-ulvan were measured according to a method described by Ye et al. (2019) [40]. The Fourier transform infrared (FI-IR) spectra of LMW-ulvan were recorded using the Magna-IR560 spectrometer (Nicolet Instrument Corp., Madison, WI, USA) according to research by Cui et al. (2019) [41]. Its monosaccharide composition was measured by reversed-phase HPLC (Agilent Technologies, Santa Clara, CA, USA) after pre-column derivatization, according to a method described by Yu et al. (2017) [22].

3.4. Methylation Analysis of LMW-Ulvan

Desulfation of the LMW-ulvan was achieved according to Falshaw and Furneaux (1998) [42]. Briefly, the LMW-ulvan was converted to the pyridinium salt form by dialysis against pyridinium hydrochloride (0.1 M, adjusted to pH 6.8), then against distilled water, and finally lyophilised. The resulting materials was dissolved in 89:10:1 v/v Me_2SO-MeOH-pyridine, and heated for 4 h at 100 °C. After cooling, the desulfated product was recovered by dialysis, freeze-dried, and designated as dsLMW-ulvan.

Methylation analysis was performed as the reported method with some modification (Li et al., 2019) [23]. Briefly, 1 mg sample (LMW-ulvan or dsLMW-ulvan) dried by P_2O_5 was dissolved in 2.0 mL DMSO, and then 100 mg anhydrous NaH was added under nitrogen atmosphere. The mixture was stirred at 25 °C for 2 h under nitrogen atmosphere, and then 1 mL CH_3I was added dropwise in an ice-cold water bath. The mixture was incubated in the dark at 25 °C, stirring for 3 h. Finally, 1 mL distilled water was added to terminate the reaction, and then extracted with $CHCl_3$. The extract was washed with distilled water and evaporated to dryness. The methylated polysaccharide was converted into partially methylated alditol acetates, which were analysed by GC-MS (Thermo Fisher Scientific, MA, USA). The GC-MS analysis designed for methylation analysis was performed according to a report by Lin et al. (2016) [43].

3.5. Animals

Male C57BL/6 SPF mice (6 weeks, 18 ± 2 g) were purchased from Jinan Pengyue Experimental Animal Breeding Co., Ltd. (Shandong, China, License ID: SCXK2014-0007). The mice were adapted to a specific pathogen-free condition (12 h light/dark cycle, 22 ± 2 °C) for 7 days before the experiments, with free access to drinking water and a commercial diet. All procedures for this experiment were approved by the Animal Ethics Committee of Ocean University of China (certificate no. SYXK20120014).

3.6. The DSS-Induced Colitis Model

The colitis was induced by orally administering 2% (w/v) DSS drinking water for 5 days. The mice were randomly divided into five groups ($n = 10$)—the normal group (N group, drinking water), model group (M group, 2% DSS water), positive control group (PC group, 2% DSS water + 50 mg/kg 5-ASA), low dose LMW-ulvan group (LP group, 2% DSS water + 50 mg/kg LMW-ulvan), and high

dose LMW-ulvan group (HP group, 2% DSS water + 100 mg/kg LMW-ulvan). The mice's body weight, stool condition, and fecal bleeding were recorded daily. On the 13th day, the mice were sacrificed after fasting for eight hours.

3.7. Assessment of Severity of Colitis

The length of the colon was measured from the ileocecal junction to the anal verge [27]. The disease activity index (DAI) was calculated by average scores for changes in body weight loss, stool condition, and fecal bleeding, according to the DAI scoring system [44]. Briefly, loss in body weight was scored as follows: (i) weight loss: 0, no weight loss; 1, 1–5% loss; 2, 5–10% loss; 3, 10–15% loss; 4, more than 15% loss, (ii) stool consistency: 0, normal; 2, loose stools; 4, diarrhea, and (iii) fecal bleeding: 0, no blood; 2, positive hemoccult; 4, severe bleeding. The spleen and thymus were immediately weighted to calculate the spleen and thymus indices. Thymus or spleen index = thymus or spleen weight mg/body weight g.

3.8. Cytokines and Activities of Antioxidant Enzyme Assay

Blood was taken from the ocular orbit and centrifuged at 4000 rpm for 40 min at 4 °C to obtain serum. To the colon was added PBS to make 10% tissue homogenate. Then, the colonic homogenate was centrifuged at 4000 rpm for 15 min and the supernatant was taken for biochemical determination. The expression levels of the inflammatory cytokines, including IL-1β, IL-4, and IFN-γ, both in the serum and colon tissue, were determined by ELISA kits, according to the manufacture's protocol. The level of MDA and activity of CAT and GPx in the colon were measured according to the manufacturer's instructions.

3.9. Quantitative Real-Time Polymerase Chain Reaction (qRT-PCR) Analysis

Colon tissue was ground with liquid nitrogen and 10 μL β-mercaptoethanol and 500 μL Buffer GTC was added to it. Total RNA was then extracted according to the manufacturer's instructions. The extracted RNA was reverse-transcribed into cDNA (5X All-InOneMasterMix; abm, Vancouver, Canada) and qRT-PCR amplification was performed using the SYBR Green (TOYOBO, Osaka, Japan) reagent to examine the mRNA relative expressions of ZO-1, occludin, and claudin [40]. The mRNA expression from each sample was calculated by normalizing with β-actin as an endogenous control. The primer sequences are listed in Table 2.

Table 2. Primer sequences for qRT-PCR.

Gene.	Forward	Reverse
ZO-1	CGCGGAGAGAGACAAGATGT	AAACCCAGGAGCCCTGTGAA
claudin	CAACCACAATAGCGGCATCG	GCACAGACCTGCAAGGAGAT
occludin	GATCGTGTTTGCGGATGAGC	AGCCTCCTTAGCTCGTAGTCA
β-actin	CAAGGCATTGCTGACAGGATG	TGCTGATCCACATCTGCTGG

3.10. Western Blot (WB) Assay

According to the method described by Tian et al. (2020) [45], the WB procedure was as follows. Colon tissue was ground in the presence of liquid nitrogen and then lysed in RIPA lysis buffer for 30 min on ice. The lysates were centrifuged under the condition of 12,000 rpm at 4 °C for 10 min. The protein concentrations of the supernatants were detected by using a BCA protein assay kit. Then, the same amount of protein was separated by 12% SDS-PAGE and transferred to polyvinylidene difluoride (PVDF) membranes (Hybond, Sunnyvale, CA, USA) using a semidry transfer system (Bio-Rad, Hercules, CA, USA).The membranes were incubated with specific antibodies against β-actin, ZO-1,occluding, and claudin-1 overnight at 4 °C, and then HRP-conjugated secondary antibodies were incubated for 1 h at room temperature. All of the antibodies were diluted in tris buffered saline (TBS). The protein signals were analyzed using an ECL detection system (Tanon, Nanjing, China).

3.11. Statistics Analysis

All data were analyzed by using SPSS software 22 and expressed as the mean ± standard deviation of at least three separate experiments. Statistical significance was identified by one-way analysis of variance (ANOVA) and the Waller-Duncan test. The value of $p < 0.05$ was accepted as statistically different.

4. Conclusions

Our results revealed that LMW-ulvan enzymatic production of ulvan extracted from green algae U. pertusa consists of 57.23% rhamnose, 28.76% xylose, 7.42% glucuronic acid, and 1.77% glucose. Its backbone contained (1→3,4)-linked Rha, (1→4)-linked Xyl, and (1→4)-linked GlcA with small amounts of (1→4)-linked Rha residues; sulfate substitution was at C-3 of rhamnose. In addition, LMW-ulvan was able to relieve intestinal inflammation and oxidative damage caused by DSS. Meanwhile, LMW-ulvan was able to significantly increase mRNA levels of claudin, occluding, and ZO-1, which improve intestinal mucosal permeability. Consequently, the results of this study support the potential application of LMW-ulvan as a functional food ingredient for IBD.

Author Contributions: Conceptualization, Y.L. (Yuanyuan Li), R.L., and Y.L. (Yinping Li); Methodology, Y.L. (Yuanyuan Li), R.L., and Y.L. (Yinping Liu); Formal analysis, Y.L. (Yuanyuan Li), H.Y., T.W., P.W., and Y.T.; Investigation, Y.L. (Yuanyuan Li), H.Y., J.Z., and Y.L. (Yinping Li); Data curation, Y.L. (Yuanyuan Li); Writing, Y.L. (Yuanyuan Li), R.L., and Y.L. (Yinping Li); Visualization, Yuanyuan Li; Supervision, R.L. and Yinping Li; Project administration, R.L. and Y.L. (Yinping Li); Funding acquisition, R.L. and P.W. All authors have read and agreed to the published version of the manuscript.

Conflicts of Interest: The authors declare that they have no competing financial or non-financial conflict of interests.

References

1. Shao, S.; Wang, D.D.; Zheng, W.; Li, X.Y.; Zhang, H.; Zhao, D.Q.; Wang, M.X. A unique polysaccharide from Hericiumerinaceus mycelium ameliorates acetic acid-induced ulcerative colitis rats by modulating the composition of the gut microbiota, short chain fatty acids levels and GPR41/43 respectors. *Int. Immunopharmacol.* **2019**, *71*, 411–422. [CrossRef] [PubMed]
2. Jin, M.Y.; Wang, Y.X.; Yang, X.B.; Yin, H.; Nie, S.P.; Wu, X.Y. Structure characterization of a polysaccharide extracted from noni (Morindacitrifolia, L.) and its protective effect against DSS-induced bowel disease in mice. *Food Hydrocolloid.* **2019**, *90*, 189–197. [CrossRef]
3. Minerwilliams, W.; Moughan, P.J. Intestinal barrier dysfunction: Implications for chronic inflammatory conditions of the bowel. *Nutr. Res. Rev.* **2016**, *29*, 40–59. [CrossRef] [PubMed]
4. Hou, J.K.; Lee, D.; Lewis, J.D. Diet and inflammatory bowel disease: Review of patient-targeted recommendations. *Clin. Gastroenterol. H.* **2014**, *12*, 1592–1600. [CrossRef]
5. Rogler, G.; Vavricka, S.R. Exposome in IBD: Recent insights in environmental factors that influence the onset and course of IBD. *Inflamm. Bowel Dis.* **2015**, *21*, 400–408. [CrossRef]
6. Kanwal, S.; Joseph, T.P.; Aliya, S.; Song, S.Y.; Zubair, M.; Saleem, Z.; Nisar, M.A.; Wang, Y.; Meyiah, A.; Ma, Y.F.; et al. Attenuation of DSS induced colitis by Dictyophoraindusiata polysaccharide (DIP) via modulation of gut microbiota and inflammatory related signaling pathways. *J. Funct. Foods* **2020**, *64*, 103641. [CrossRef]
7. Hu, T.; Lin, Q.L.; Guo, T.; Yang, T.; Zhou, W.H.; Deng, X.F.; Yan, J.K.; Luo, Y.; Ju, M.M.; Luo, F.J. Polysaccharide isolated from Phellinus linteus mycelia exerts anti-inflammatory effects via MAPK and PPAR signaling pathways. *Carbohyd. Polym.* **2018**, *200*, 487–497. [CrossRef]
8. Wang, Y.L.; Ji, X.M.; Yan, M.L.; Chen, X.; Kang, M.Z.; Teng, L.P.; Wu, X.T.; Chen, J.H.; Deng, C. Protective effect and mechanism of polysaccharide from Dictyophoraindusiata on dextran sodium sulfate-induced colitis in C57BL/6 mice. *Int. J. Biol. Macromol.* **2019**, *140*, 973–984. [CrossRef]

9. Rodriguezcanales, M.; Jimenezrivas, R.; Canalesmartinez, M.M.; Garcialopez, A.J.; Riverayanez, N.; Nietoyanez, O.; Ledesmasoto, Y.; Sancheztorres, L.E.; Rodriguezsosa, M.; Terrazas, L.I.; et al. Protective effect of amphipterygiumadstringens extract on dextran sulphate sodium-induced ulcerative colitis in mice. *Mediat. Inflamm.* **2016**, *2016*, 8543561.

10. Shen, Y.M.; Zou, J.F.; Chen, M.J.; Zhang, Z.M.; Liu, C.; Jiang, S.; Qian, D.; Duan, J.A. Protective effects of Lizhong decoction on ulcerative colitis in mice by suppressing inflammation and ameliorating gut barrier. *J. Ethnopharmacol.* **2020**, *259*, 112919. [CrossRef]

11. Perrier, C.; Rutgeerts, P. Cytokine blockade in inflammatory bowel diseases. *Immunotherapy* **2011**, *3*, 1341–1352. [CrossRef] [PubMed]

12. Ji, Y.; Dai, Z.L.; Sun, S.Q.; Ma, X.S.; Yang, Y.; Tso, P.; Wu, G.Y.; Wu, Z.L. Hydroxyproline attenuates dextran sulfate sodium induced colitis in mice: Involvment of the NF-κB signaling and oxidative stress. *Mol. Nutr. Food Res.* **2018**, *62*, 1800494. [CrossRef]

13. Tziveleka, L.; Ioannou, E.; Roussis, V. Ulvan, a bioactive marine sulphated polysaccharide as a key constituent of hybrid biomaterials: A review. *Carbohyd. Polym.* **2019**, *218*, 355–370. [CrossRef] [PubMed]

14. Shi, Q.; Wang, A.; Lu, Z.; Qin, C.; Hu, J.; Yin, J. Overview on the antiviral activities and mechanisms of marine polysaccharides from seaweeds. *Carbohyd. Res.* **2017**, *453*, 1–9. [CrossRef] [PubMed]

15. Wijesekara, I.; Pangestuti, R.; Kim, S. Biological activities and potential health benefits of sulfated polysaccharides derived from marine algae. *Carbohyd. Polym.* **2011**, *84*, 14–21. [CrossRef]

16. Qi, H.; Zhao, T.; Zhang, Q.; Li, Z.; Zhao, Z.; Xing, R. Antioxidant activity of different molecular weight sulfated polysaccharides from Ulva pertusaKjellm (Chlorophyta). *J. Appl. Phycol.* **2005**, *17*, 527–534. [CrossRef]

17. Li, W.; Jiang, N.; Li, B.; Wang, M.; Chang, X.; Liu, H.; Zhang, L.; Yin, S.; Qi, H.; Liu, S. Antioxidant activity of purified ulvan in hyperlipidemic mice. *Int. J. Biol. Macromol.* **2018**, *113*, 971–975. [CrossRef]

18. De Araujo, I.W.; Rodrigues, J.A.; Quindere, A.L.; Silva, J.F.; Maciel, G.F.; Ribeiro, N.A.; de Sousa Oliveira Vanderlei, E.; Ribeiro, K.A.; Chaves, H.V.; Pereira, K.M.; et al. Analgesic and anti-inflammatory actions on bradykinin route of a polysulfated fraction from alga *Ulva lactuca*. *Int. J. Biol. Macromol.* **2016**, *92*, 820–830. [CrossRef]

19. Berri, M.; Oliver, M.; Holbert, S.; Dupont, J.; Demais, H.; Goff, M.L.; Collen, P.N. Ulvan from Ulva armoricana (Chlorophyta) activates the PI3K/Akt signaling pathway via TLR4 to induce intestinal cytokine production. *Algal Res.* **2017**, *28*, 39–47. [CrossRef]

20. Chi, Y.Z.; Zhang, M.F.; Wang, X.; Fu, X.J.; Guan, H.S.; Wang, P. Ulvan lyase assisted structural characterization of ulvan from Ulva pertusa and its antiviral activity against vesicular stomatitis virus. *Int. J. Biol. Macromol.* **2020**, *157*, 75–82. [CrossRef]

21. Ulaganathan, T.; Boniecki, M.T.; Foran, E.; Buravenkov, V.; Mizrachi, N.; Banin, E.; Helbert, W.; Cygler, M. New Ulvan-degrading polysaccharide lyase Family: Structure and catalytic mechanism suggests convergent evolution of active site architecture. *ACS Chem. Biol.* **2017**, *12*, 1269–1280. [CrossRef]

22. Yu, Y.; Li, Y.P.; Du, C.Y.; Mou, H.J.; Wang, P. Compositional and structural characteristics of sulfated polysaccharide from Enteromorpha prolifera. *Carbohyd. Polym.* **2017**, *165*, 221–228. [CrossRef] [PubMed]

23. Li, Y.P.; Wang, X.P.; Jiang, Y.C.; Wang, J.F.; Hwang, H.M.; Yang, X.H.; Wang, P. Structure characterization of low molecular weight sulfate Ulva polysaccharide and the effect of its derivative on iron deficiency anemia. *Int. J. Biol. Macromol.* **2019**, *126*, 747–754. [CrossRef] [PubMed]

24. Zhu, Y.; Li, X.; Chen, J.; Chen, T.J.; Shi, Z.M.; Lei, M.N.; Zhang, Y.J.; Bai, P.F.; Li, Y.F.; Fei, X. The pentacyclic triterpene Lupeol switches M1 macrophages to M2 and ameliorates experimental inflammatory bowel disease. *Int. Immunopharmacol.* **2016**, *30*, 74–84. [CrossRef] [PubMed]

25. Qiu, X.Y.; Li, X.; Wu, Z.; Zhang, F.; Wang, N.; Wu, N.; Yang, X.; Liu, Y.L. Fungal-bacterial interactions in mice with dextran sulfate sodium (DSS)-induced acute and chronic colitis. *RSC Adv.* **2016**, *6*, 65995–66006. [CrossRef]

26. Kim, D.; Lee, M.; Yoo, J.; Park, K.; Ma, J. Fermented herbal formula KIOM-MA-128 protects against acute colitis induced by dextran sodium sulfate in mice. *BMC Complem. Altern. M.* **2017**, *17*, 354. [CrossRef]

27. Zong, S.; Ye, Z.Y.; Zhang, X.M.; Chen, H.; Ye, M. Protective effect of Lachnum polysaccharide on dextran sulfate sodium-induced colitis in mice. *Food Funct.* **2020**, *11*, 846–859. [CrossRef]

28. Abderrazak, A.; Hadri, K.E.; Bosc, E.; Blondeau, B.; Slimane, M.N.; Büchele, B.; Simmet, T.; Couchie, D.; Rouis, M. Inhibition of the inflammasome NLRP3 by arglabin attenuates inflammation, protects pancreatic beta-cells from apoptosis, and prevents Type 2 diabetes mellitus development in ApoE2Ki mice on a chronic high-fat diet. *J. Pharmacol. Exp. Ther.* **2016**, *357*, 487–494. [CrossRef]

29. Zhao, Y.L.; Wang, J.B.; Shan, L.M.; Jin, C.; Xiao, X.H. Effect of Radix isatidis polysaccharides on immunological function and expression of immune related cytokines in mice. *Chin. J. Integr. Med.* **2008**, *14*, 207–211. [CrossRef]

30. Gao, X.; Qu, H.; Gao, Z.L.; Zeng, D.Y.; Wang, J.P.; Baranenko, D.; Li, Y.Z.; Lu, W.H. Protective effects of Ulva pertusa polysaccharide and polysaccharide iron (III) complex on cyclophosphamide induced immunosuppression in mice. *Int. J. Biol. Macromol.* **2019**, *133*, 911–919. [CrossRef]

31. Oestreich, K.J.; Weinmann, A.S. Transcriptional mechanisms that regulate T helper 1cell differentiation. *Curr. Opin. Immunol.* **2012**, *24*, 191–195. [CrossRef] [PubMed]

32. Zhang, Z.C.; Li, S.; Cao, H.Y.; Shen, P.; Liu, J.X.; Fu, Y.H.; Gao, Y.G.; Zhang, N.S. The protective role of phloretin against dextran sulfate sodium-induced ulcerative colitis in mice. *Food Funct.* **2019**, *10*, 422–431. [CrossRef] [PubMed]

33. Gong, J.; Wang, X.Z.; Wang, T.; Chen, J.J.; Xie, X.Y.; Hu, H.; Yu, F.; Liu, H.L.; Jiang, X.Y.; Fan, H.D. Molecular signal networks and regulating mechanisms of the unfolded protein response. *J. Zhejiang Univ. SC. B.* **2017**, *18*, 1–14.

34. Wang, Y.; Ouyang, Q.; Xia, B.; Liu, L.N.; Gu, F.; Zhou, K.F.; Mei, Q.; Shi, R.H.; Ran, Z.H.; Wang, X.D.; et al. Multicenter case-control study of the risk factors for ulcerative colitis in China. *World J. Gastroentero.* **2013**, *19*, 1827–1833. [CrossRef]

35. Li, R.Y.; Chen, Y.Y.; Shi, M.J.; Xu, X.X.; Zhao, Y.X.; Wu, X.J.; Zhang, Y.B. GegenQinlian decoction alleviates experimental colitis via suppressing TLR4/NF-κB signaling and enhancing antioxidant effect. *Phytomedicine* **2016**, *23*, 1012–1020. [CrossRef]

36. Kjellev, S. The trefoil factor family-small peptides with multiple functionalities. *Cell. Mol. Life Sci.* **2009**, *66*, 1350–1369. [CrossRef]

37. Qiao, L.K.; Yang, X.K.; Xie, R.Z.; Du, C.; Chi, Y.; Zhang, J.; Wang, P. Efficient production of ulvan lyase from Ulva prolifera by Catenovulum sp. LP based on stage-controlled fermentation strategy. *Algal Res.* **2020**, *46*, 101812.

38. DuBois, M.; Gilles, K.A.; Hamilton, J.K.; Rebers, P.A.; Smith, F. Colorimetric method for determination of sugars and related substances. *Anal. Chem.* **1956**, *28*, 350–356.

39. Tuulikki, T.T.; Hartiala, K. Method for determination of the sulfate content of glycosaminoglycans. *Anal. Chem.* **1971**, *41*, 471–476.

40. Ye, H.; Shen, Z.P.; Cui, J.F.; Zhu, Y.Z.; Li, Y.Y.; Chi, Y.Z.; Wang, J.F.; Wang, P. Hypoglycemic activity and mechanism of the sulfated rhamnose polysaccharides chromium(III) complex in type 2 diabetic mice. *Bioorg. Chem.* **2019**, *88*, 102942. [CrossRef]

41. Cui, L.; Wang, W.; Luo, L.; Ning, Q.; Xia, Z.; Chen, J.; Feng, L.; Wang, H.; Song, J.; Tan, X.B.; et al. Polysaccharide from Scutellariabaicalensis Georgi ameliorates colitis via suppressing NF-κB signaling and NLRP3 inflammasome activation. *Int. J. Biol. Macromol.* **2019**, *132*, 393–405. [CrossRef] [PubMed]

42. Falshaw, R.; Furneaux, R.H. Structural analysis of carrageenans from the tetrasporic stages of the red algae, Gigartina lanceata and Gigartina chapmanii (Gigartinaceae, Rhodophyta). *Carbohyd. Res.* **1998**, *307*, 325–331. [CrossRef]

43. Lin, L.Y.; Wang, P.P.; Du, Z.Y.; Wang, W.C.; Cong, Q.F.; Zheng, C.P.; Jin, C.; Ding, K.; Shao, C.H. Structural elucidation of a pectin from flowers of Lonicera japonica and its antipancreatic cancer activity. *Int. J. Biol. Macromol.* **2016**, *88*, 130–137. [CrossRef]

44. Jeon, Y.; Lee, J.; Lee, Y.; Kin, D. Puerarin inhibits inflammation and oxidative stress in dextran sulfate sodium-induced colitis mice model. *Biomed. Pharmacother.* **2020**, *124*, 109847. [CrossRef]

45. Tian, M.; Ma, P.; Zhang, Y.; Mi, Y.; Fan, D.D. Ginsenoside Rk3 alleviated DSS-induced ulcerative colitis by protectingcolon barrier and inhibiting NLRP3 inflammasome pathway. *Int. Immunopharmacol.* **2020**, *85*, 106645. [CrossRef] [PubMed]

Article

The Comparative Immunotropic Activity of Carrageenan, Chitosan and Their Complexes

Viktoriya N. Davydova [1,*,†], Irina V. Sorokina [2,†], Aleksandra V. Volod'ko [1],
Ekaterina V. Sokolova [1], Marina S. Borisova [2] and Irina M. Yermak [1]

[1]   G.B. Elyakov Pacific Institute of Bioorganic Chemistry, Far Eastern Branch, Russian Academy of Sciences, Prospect 100 let Vladivostoku 159, 690022 Vladivostok, Russia; morskaia@list.ru (A.V.V.); eka9739@yandex.ru (E.V.S.); imyer@mail.ru (I.M.Y.)
[2]   N.N. Vorozhtsov Novosibirsk Institute of Organic Chemistry, Siberian Branch of the Russian Academy of Sciences, Lavrentjev Ave. 9, 630090 Novosibirsk, Russia; sorokina.irina55@gmail.com (I.V.S.); mborisova@nioch.nsc.ru (M.S.B.)
*   Correspondence: vikdavidova@yandex.ru; Tel.: +7-423-231-40-50
†   These authors contributed equally to this work.

Abstract: The immunotropic activity of polyelectrolyte complexes (PEC) of κ-carrageenan (κ-CGN) and chitosan (CH) of various compositions was assessed in comparison with the initial polysaccharides in comparable doses. For this, two soluble forms of PEC, with an excess of CH (CH:CGN mass ratios of 10:1) and with an excess of CGN (CH: CGN mass ratios of 1:10) were prepared. The ability of PEC to scavenge NO depended on the content of the κ-CGN in the PEC. The ability of the PEC to induce the synthesis of pro-inflammatory (tumor necrosis factor-α (TNF-α)) and anti-inflammatory (interleukine-10 (IL-10)) cytokines in peripheral blood mononuclear cell was determined by the activity of the initial κ-CGN, regardless of their composition. The anti-inflammatory activity of PEC and the initial compounds was studied using test of histamine-, concanavalin A-, and sheep erythrocyte immunization-induced inflammation in mice. The highest activity of PEC, as well as the initial polysaccharides κ-CGN and CH, was observed in a histamine-induced exudative inflammation, directly related to the activation of phagocytic cells, i.e., macrophages and neutrophils.

Keywords: carrageenan; chitosan; polyelectrolyte complex; cytokine; nitric oxide; anti-inflammatory activity

1. Introduction

Natural polysaccharides are promising compounds for use in biomedicine and pharmaceuticals. The main prerequisites for this are the combination of their abundance and simplicity of preparation with biocompatibility and a broad spectrum of biological effects, such as immunostimulating, antioxidant, antitumor, antimicrobial, and antiviral.

One of the most well-known polysaccharides of red algae is carrageenan (CGN). CGN is a sulfated galactose copolymer composed of alternating units of D-galactose and 3,6-anhydro-galactose joined by α-1,3 and β-1,4-glycosidic linkages [1]. CGN is classified into various types such as λ, κ, ι, ε, μ, depending on the amount and location of sulfate groups as well as the presence or absence of 3,6-anhydro-galactose units [2]. CGNs have diverse activities including immunomodulatory [3], anticoagulant [4], antithrombotic [5], antiviral [6], and antitumor effects [7]. In recent years, CGNs have been increasingly used for pharmaceutical purposes. CGNs are one source of soluble dietary fibers [8]. Standard animal safety studies in which CGN was administered in diet showed no adverse effects [9]. Due to their biocompatibility, safety (USP35-NF30S1, BP2012, EP7.0), availability, wide range of biological activity, a simple thermo-reversible gelation mechanism, viscoelastic properties and the

ability to form complexes with polycations via electrostatic interactions, CGNs are ideal components to obtain new vehicles for the delivery therapeutic substances that can be retained at mucosal surfaces and release the drug slowly [10].

Chitosan (CH) is a natural polycation, β-1,4-linked glucosaminoglycan, which have some acetylated amino groups. CH is a non-toxic, biodegradable and non-immunogenic agent [11] used widely as a biomaterial with an established safety profile in humans, as pharmaceutical excipient, weight loss supplement [11], and as a major component of hemostatic dressings [12]. At relatively low pH (<6.5), chitosan is positively charged and soluble in dilute aqueous solutions [13] CGN.

Marine polysaccharides stimulate different types of immune system cells, both in vitro and in vivo, to produce and secrete molecules with immunostimulatory effects [14,15]. CGNs have been demonstrated to play an important role as free-radical scavengers and antioxidants for the prevention of oxidative damage in living organisms [16]. Our studies on the antioxidant capacity of CGN [17] have shown that the activity of carrageenans depends on the polysaccharide structure. Hence, they have therapeutic potential for the treatment of immunological disorders.

Inflammation is the first biological response of the immune system to infection or irritation. However, in some cases, it can become chronic, and lead to tissue damage [18]. Non-steroidal anti-inflammatories drugs are often used to treat of inflammation. However, their prolonged usage is followed by complications, including damage to the gastrointestinal tract and other side effects [19]. Therefore, the search for new bioactive compounds with anti-inflammatory activities with minimal adverse effects is of great importance. CGN. We have shown that chitosan with molecular weight of 110 kDa ex vivo inhibits the synthesis of anti-inflammatory cytokine, the tumor necrosis factor alpha (TNF-α) induced by endotoxin and stimulates synthesis of the anti-inflammatory cytokine interleukene (IL-10) by oral administration in the blood serum of mice [20]. We have also determined that κ-CGN [21] and chitosan [20] possess anti-inflammatory activity in a model of acetic acid induced colitis in mice. Recently, we have shown the inhibitory effect of CGNs on inflammation caused by endotoxin [22].

The mechanism of action of CGNs is not yet completely understood; however, dietary studies done in animals with food-grade CGN shown no intestinal inflammation [23]. There are some conflicting reports on the effects of CGN on the gastrointestinal tract what, may be in part due to the fact that a food-grade CGN is often confused with a degraded carrageenan, termed poligeenan [24]. In contrast to CGN, poligeenan is not produced biologically but only in the laboratory or commercially by subjecting CGN to very low pH at 0.9–1.3 and non-physiological temperatures of >80 °C for several hours [24]. High molecular weight or food-grade CGN is ingested at low dosages; is not absorbed across the intestinal epithelium, is wholly excreted in feces, does not enter the systemic circulation, and does not cause intestinal ulceration or inflammation. The safety of CGN is supported by a large number of animal oral safety studies in which no adverse effects were reported at high doses (up to 5% in diet) [9].

The obtaining of polyelectrolyte complexes (PEC) by binding two opposite charged polymers is the way to improve and expand the range of properties of polyionic polysaccharides. This allows the modification of their functional properties to improve stability and facilitate application. For example, stable forms of PEC CH-CGN can be obtained in soluble form, in the form of gels, films, sponges, and microparticles. PEC are promising materials for use in biomedicine and pharmaceuticals, since the combination of the favorable properties of each constituent polymer leads to new systems with improved properties, which quite often substantially differ from those of the individual polymers [25]. These properties can be modulated by adjusting the conditions of complex formation, i.e., varying pH, ionic strength, polysaccharide concentration, ratio of the biopolymers, and temperature [26]. In addition, PEC can easily adapt to the requirements dictated by specific applications, for example, by changing the composition of the monomer, the density of the formed bonds, particle size, surface charge density, or type of solvent [27]. We can expect synergies between the components of the complex, the predominance of the activity of one of the components, or the loss of one or another activity of the

starting polyions. Although the biological activity of polysaccharides has been actively studied, there is very little data on the physiological effects of complexes based on them.

We previously studied the conditions for the formation of a soluble form of PEC and found that the complexes have gastroprotective [28] and antibacterial [29] activity. The activity of the complexes in these tests exceeded the activity of the starting components [28].

The aim of this work was to study the anti-inflammatory activity of PEC, consisting of various compositions of κ-CGN and CH, in comparison with the initial polysaccharides taken in comparable doses. Tests of acute inflammation in mouse paw associated with the induction of a predominantly cellular immune response mediated by phagocytes (histamine test), B-lymphocytes (concanavalin A test) or T-lymphocytes (HRT reaction) were used. In ex vivo experiments, the effect of agents on the cytokine profile of donated blood was also evaluated.

2. Results

2.1. Characterisation of the Initial Polysaccharides

For the study of the anti-inflammatory activity of the polysaccharides, κ-CGN, CH and soluble forms of their PEC were prepared. κ-CGN from red algae *Chondrus armatus* was obtained as described earlier, it structure was determined according to [30]. The molecular weight (MW) of κ-CGN was determined by viscometry and was found to be 250 kDa.

CH was obtained by the alkaline deacetylation of crab chitin as described in [31]. The MW determined by viscometry was 110 kDa, and the deacetylation degree (DA), determined according [32] by FTIR-spectroscopy was 96%.

### 2.2. Characterization of PEC κ-CGN-CH

Activity of biopolymers is determined by numerous parameters, among which are the size of the molecule, its charge, density, solubility, the molecule conformation and flexibility of polysaccharide chain. The formation of the complex affects all these parameters; it is obvious that the activity of the complexes will differ from that of the original compounds.

The process of obtaining complexes of CH with CGN in soluble form was studied by us in detail earlier. It was shown that soluble complexes were obtained preferentially by mixing the starting components at given ratios with an excess of one of the components [33]. The complex formation of κ-CGN:CH 1:10 and 10:1 *w/w* was shown by centrifugation in a Percoll gradient [34].

In this study the soluble PEC with a κ-CGN:CH weight ratios of 10:1 and 1:10 were prepared by mixing solutions of the initial polysaccharides and characterized by dynamic light scattering (Figure 1).

The initial CH and κ-CGN presented as polydisperse particles, heterogeneous in size, with Z-average of about 1 μm (data not shown), which corresponds to their polysaccharide nature [35]. The nature of polysaccharides creates certain difficulties for their study by hydrodynamic methods. The mutual repulsion of charged groups along the polymer chain is the reason why the molecule becomes strongly extended, while its hydrophilic part is in the hydrate shell. This makes it difficult to study by the DLS (dynamic light scattering) and we could not obtain a size distribution for CGN and CH with an acceptable value of polydispersity index PdI. The surface potential of CH was +26.2 ± 2.3 mV, while that of κ-CGN was −50.7 ± 1.4 mV.

After complex formation, the polydispersity of the system was reduced significantly. The complex with an excess of CH (κ-CGN-CH 1:10 *w/w*) was fairly composed of homogeneous, positively charged particles with an average diameter of about 123 nm. Negatively charged particles of the complex with an excess of κ-CGN (κ-CGN-CH 10:1 *w/w*) was more polydisperse in size with an average diameter of about 325 nm.
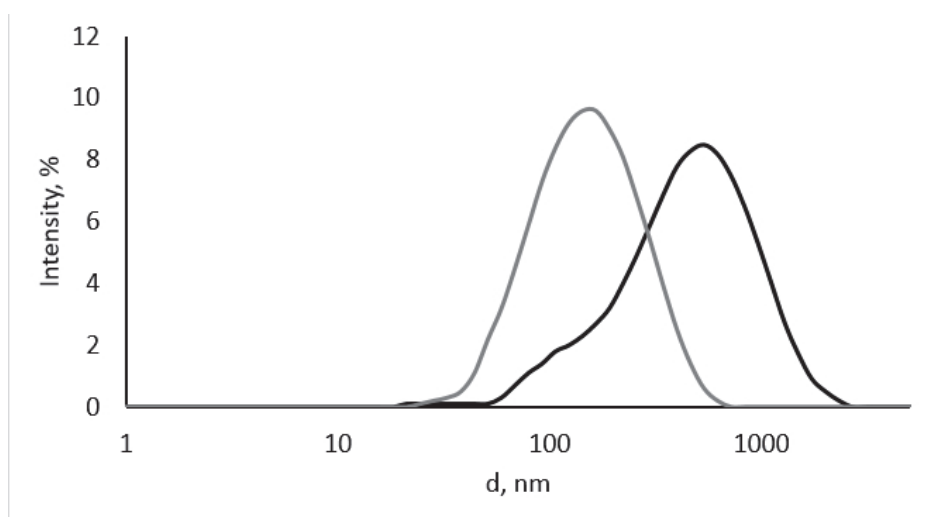
Complex	PdI	Z-Average, nm	ζ-potential, mV
k-CGN	1	> 1 µm	-50.7 ± 1.4
CH	0.770 ± 0.008	> 1 µm	+26.2 ± 2.3
k-CGN-CH 10:1 *w/w*	0.420 ± 0.062	324.8 ± 2.3	-36.6 ± 1.9
k-CGN-CH 1:10 *w/w*	0.275 ± 0.003	122.8 ± 0.9	+27.9 ± 0.9

Figure 1. Intensity particle size distribution of κ-CGN-CH 10:1 *w/w* (black line) and κ-CGN-CH 1:10 *w/w* (grey line) complexes measured on a Nano ZS (Malvern PANalytical, Malvern, UK) using scattering detection at 173°. The hydrodynamic diameters of the particles were automatically calculated with the instrument's software based on analysis of the autocorrelation function.

The charge of the PEC was determined by the polymer, that was in excess. The charge of CGN in the complex with its excess (κ-CGN-CH 10: 1 *w/w*) was partially neutralized, but the charge of the complex with an excess of CH (κ-CGN-CH 1:10 *w/w*) corresponded to the charge of the initial polycation, which may indicate surface localization of CH in the complex, shown by us earlier [29].

2.3. In Vitro Activity of the Initial Polysaccharides and Their Complexes

In biomedicine, much attention has been paid to natural antioxidants and their association with health benefits [36]. Taking into account the complexity of antioxidants action in vivo, different in vitro methodologies have been developed to estimate, in a simple experimental way, the capacity of antioxidants and their complex mixtures to neutralize the reactive oxygen and nitrogen species (ROS/RNS) [37].

We considered the potential antioxidant activity of κ-CGN, CH, and PEC determined by their ability to bind nitric oxide (NO) (Figure 2).
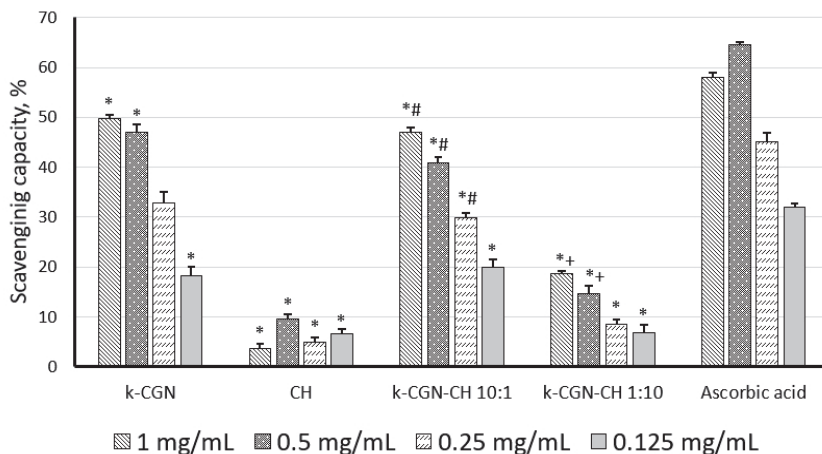
Figure 2. Nitric oxide scavenging effect of κ-carrageenan (κ-CGN), chitosan (CH) and their complexes. Statistical analysis was done by one-way ANOVA (analysis of variance). *—Differences between samples and the control were significant, $p < 0.05$; #—Differences between polyelectrolyte complexes (PEC) and κ-CGR were significant, $p < 0.05$; +—Differences between PEC and CH were significant, $p < 0.05$.

According to Figure 2, κ-CGN showed a pronounced ability to scavenge NO, and its activity (at 1 mg/mL, 0.5 mg/mL) was comparable to the action of the standard (ascorbic acid). CH did not show the ability to scavenge NO (Figure 2). The low activity of this polysaccharide in this test was noted earlier [38]. It was previously reported that with an increase in the MW of chitosan up to 100 kDa, its antioxidant activity have decreased [39]. Together with this, the CH used here had a MW of 110 kDa. The PEC with a high content of κ-CGN exhibited activity comparable to the activity of the initial κ-CGN. Unlike the initial polycation, the complex with a high CH content (κ-CGN-CH 1:10 *w/w*) exhibited antioxidant activity, although it was less pronounced than κ-CGN and the complex κ-CGN-CH 10:1 *w/w*.

2.4. Ex Vivo Activity of the Initial Polysaccharides and Their Complexes

The ability of polysaccharides and their complexes to induce the synthesis of pro-inflammatory cytokines, i.e., tumor necrosis factor-α (TNF-α), and anti-inflammatory cytokine, i.e., interleukine-10 (IL-10), in peripheral blood mononuclear cell (PBMCs) was studied. Both of these cytokines play important roles in the immune response, as they activate circulating cells and stimulate the production of chemokines and adhesion molecules [40]. Figure 3 shows that the ability of the polysaccharides and their PEC to activate cells and to induce cytokine synthesis has been correlated to the activity of LPS. At a high concentration (10 µg/mL) κ-CGN caused a strong increase in the level of cytokines, in comparison with the control, while at a low concentration (1–10 ng/mL) the activity was insignificant. CH was inert in this test.

The CGN and PEC did not show an anti-inflammatory activity in the presence of LPS (Figure 3c,d). Only chitosan at a concentration of 100 ng/mL had the ability to suppress of LPS-induced TNF-α and IL-10 production.

According to Figure 3, the ability of PEC to induce the synthesis of pro-inflammatory (TNF-α) and anti-inflammatory (IL-10) cytokines in the whole blood cell assay in both conditions (with and without LPS) is determined as the activity of the initial κ-CGN, regardless of their composition. The effect of the complex with an excess of CGN was similar to that the initial κ-GRG. The activity of the complex with an excess of CH was slightly lower than that of the initial κ-GRG, that possibly due to the presence of CH.
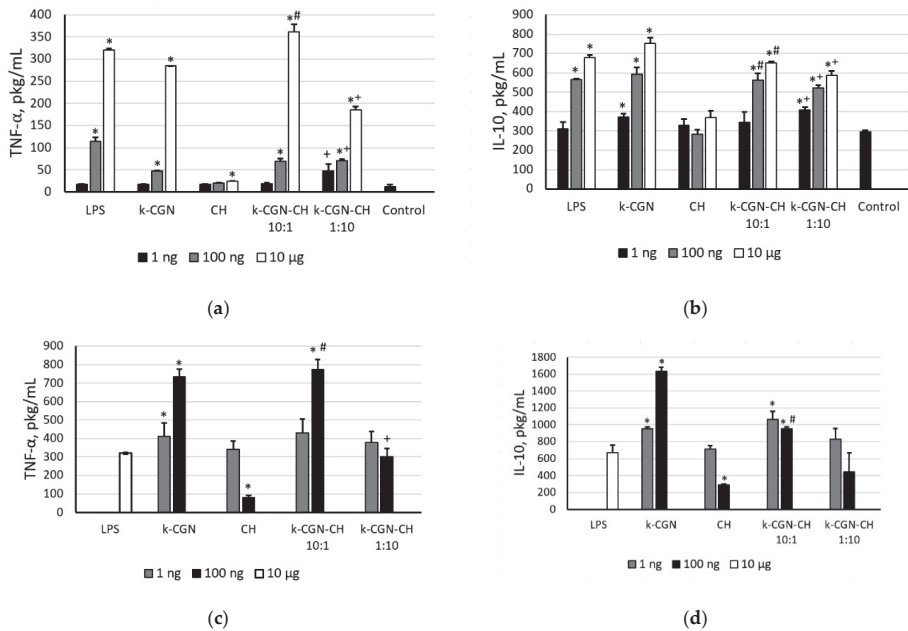
(a)

(b)

(c)

(d)

Figure 3. (**a**) Tumor necrosis factor-α (TNF-α) and (**b**) interleukine-10 (IL-10) level stimulated by κ-CGR, CH and complexes. TNF-α (**c**) and IL-10 (**d**) level stimulated by preliminary incubation of peripheral blood mononuclear cell (PBMCs) with *Escherichia coli* LPS (10 min), then by κ-CGN, CH, and complexes. Contents of a cytokine in serum are presented as a mean ± SD. Whole blood samples were obtained from 5 healthy subjects and incubated with the polysaccharides and PEC at different concentrations. The cytokine level in serum of normal donors (**a,b**) or the cytokine level in serum after preliminary incubation of PMBC with *E. coli* LPS (**c,d**) were considered as a negative control used for statistical calculation. Statistical analysis was done using one-way ANOVA. *—Differences between samples and the control were significant, $p < 0.05$; #—Differences between PEC and κ-CGR were significant, $p < 0.05$; +—Differences between PEC and CH were significant, $p < 0.05$.

2.5. In Vivo Anti-Inflammatory Activity of the Initial Polysaccharides and Their Complexes

The anti-inflammatory activity of PEC and the initial compounds was evaluated using histamine-, concanavalin A- and sheep erythrocyte immunization-induced paw edema in mice. The results are expressed as the inflammatory edema index (IEI) and percentage of anti-inflammatory activity (AIA) relative to the control group (Table 1).

In experiments in vivo, polysaccharides and complexes were administered intraperitoneally in the form of aqueous solutions to provide more efficient delivery of compounds. The doses of the complexes were selected taking into account their low toxicity and the ability to dissolve in the volume of the solvent (water) allowed for intraperitoneal administration to mice (0.2 mL/10 g of body weight). Doses of polysaccharides were taken in accordance with their maximum proportion in the composition of the complexes.

The data indicate that preventive i.p. injections of PEC and both polysaccharides significantly decreased local inflammation induced by histamine in mice. CH and PEC κ-CGN:CH 1:10 demonstrated the most potent decrease IEI values relative to the control group (1.8 and 1.7 times, correspondingly), which are insignificantly different from that of indomethacin (2.3 times) (Table 1). κ-CGN alone and PEC κ-CGN:CH 10:1 were less active in decreasing edema (1.4 and 1.3 times, correspondingly).

Table 1. Anti-inflammatory activity of κ-carrageenan (κ-CGN), chitosan (CH), and their polyelectrolyte complexes (PECs) in mouse paw edema tests.

Agent	Histamine-Induced Inflammation Test		Concanavalin A-Induced Inflammation Test		Delayed Type Hypersensitivity Reaction Test	
	IEI, %	AIA, %	IEI, %	AIA, %	IEI, %	AIA, %
Control	29.6 ± 2.0	0	18.6 ± 2.0	0	14.6 ± 0.6	0
κ-CGN:CH 10:1	22.44 ± 1.53 ** ##	37	20.0 ± 2.3 ##	0	14.6 ± 1.3	0
κ-CGN:CH 1:10	17.45 ± 3.04 **	51	20.9 ± 2.3 ##	0	14.0 ± 1.6	4
κ-CGN	20.77 ± 2.56 **#	37	9.8 ± 1.1 ** #	47	6.4 ± 1.0 ***	56
CH	16.70 ± 3.66 **	53	10.9 ± 1.6 * #	41	15.7 ± 1.7	0
Indomethacin	12.61 ± 1.11 ***	65	–	–	–	–
Diclofenac	–	–	7.2 ± 1.4 ***	61	–	–

* $p < 0.05$, ** $p < 0.01$, *** $p < 0.001$ differences with control group are significant; # $p < 0.05$, ## $p < 0.001$ differences with reference group are significant; IEI—inflammatory edema index, AIA—anti-inflammatory activity. Data represent as mean ± standard error (SEM); $n = 8$ mice in group. Statistical analyses were performed using "Statistica 6" software. The significant difference between groups was calculated by one-way ANOVA by Fisher test (at parametric distribution) or not—parametric Kruskal–Wallis test. A p-value of ≤0.05 was considered as statistically significant.

The results presented in Table 1 show a downward trend in activity of tested agents with higher level of the κ-CGN. It correlates with the data from the ex vivo experiments, indicating an increase in TNF-α production at a high dose of κ-CGN. TNF-α is a pro-inflammatory cytokine secreted by activated macrophages in an early stage of acute inflammation. The low level of TNF-α indicates attenuation of the inflammatory reaction in response to a low dose of κ-CGN.

In the concanavalin A inflammation test, κ-CGN and CH showed a moderate anti-inflammatory effect (lowering the edema index by 1.9 and 1.7 times, respectively, versus control) in comparison with diclofenac (2.6 times), while the complexes were not active (Table 1). In the DTH reaction, only κ-CGN alone inhibits inflammation. Both PECs and CH were inactive (Table 1).

3. Discussion

Polysaccharide PEC are well-tolerated macroorganism systems and can be used in various fields, such as drug delivery systems, cell cultivation and enzyme immobilization, or tissue reparation and regeneration [41]. However, despite the numerous studies devoted to the preparation and application of PEC, their biological activity and the modification of the activity of the initial polysaccharides after PEC formation have been studied insufficiently.

CH and CGN have pronounced immunostimulatory properties [1,20,34–36]. Therefore, this study was aimed at the comparative analysis of the effects of PEC and initial compounds on some components of the immune system associated with immunomodulating activity.

Immunity is the host physiological defense of an organism against pathogenic factors such as toxins, infectious microorganisms and viruses. The immune response passes on the collective and coordinated cooperation of specific cells and humoral mediators including vascular and cell adhesion molecules and proteins of the complement system. The most relevant cells involved in the immune response are lymphocytes, monocytes/macrophages, polymorphonuclear granulocytes, and mast cells. Macrophages and antigen-presenting cells (APC) are involved in all stages of non-specific immune responses and are responsible for phagocytosis, antigen processing and presentation, secretion of NO and cytokines such as and TNF-α, as well as antibody-dependent and cell-mediated cytotoxicity [42]. The effect of complexation on some cellular immunity reactions mediated by B- and T-lymphocytes in vitro, ex vivo and in vivo models have been considered.

In this study a comparative analysis of the immunotropic activity of polysaccharides and their complexes was carried out. The soluble complexes obtained by mixing the starting components at given ratios of κ-CGN-CH 1:10 *w/w* or κ-CGN-CH 10:1 *w/w*. The complexes formation was accompanied changes in the physicochemical parameters of the initial polysaccharides. After complex formation, the polydispersity of the initial polysaccharides was reduced significantly (Figure 1). According to our

earlier data [15] the macromolecular structure of PEC was different from the structures of the initial components in the appropriate concentrations. The mechanism of PEC complex particle formation is determined by the nature of the prevailing polymer. The particles in the soluble complexes κ-CGN-CH 1:10 *w/w* has surface localization of the polycation and stabilized by unreacted CH amine groups. The incorporation of CH into the network structure of CG for complexes κ-CGN-CH 10:1 *w/w* was assumed [15].

NO is a highly reactive free radical involved in a number of physiological and pathological processes [43]. NO acts immunologically as a cytotoxic agent on invading microorganisms in macrophages or on tumor cells [44]. Our studies on the antioxidant capacity of CGN [17] and studies on other polyionic polysaccharides have shown that antioxidant activity is determined by the location of ionic groups in the carbohydrate chain and by the molecular weight of this chain [38,45]. According to our results, the activity of PEC to scavenge of NO depends on the content of κ-CGN in the complex: PECs with a high content of κ-CGN exhibited activity comparable to the activity of the κ-CGN alone.

Sulfated polysaccharides are commonly reported as strong antioxidants, which is partly due to its ordered, extended structure. Sulfated polysaccharides usually trap free radicals in an electrostatic manner since the sulfate groups usually generate a highly acidic environment and the sulfur substitution may also weaken hydrogen bond interactions between polysaccharides [46]. This explains the high activity of the initial κ-CGN and the PEC κ-CGN:CH 10:1 *w/w*. It is noteworthy that the complex with a high content of CH, which, according to our early data [29], had surface localization of the polycation, also showed a low ability to scavenge NO, unlike the initial CH.

As already described in the literature, polysaccharides have an important immunostimulatory capacity through the production of cytokines [8,9,16]. The data presented in this study clearly demonstrate that κ-CGN and PEC at a low concentration (1 ng/mL) do not induce the pro-inflammatory TNF-α, which is an important mediator for the induction of many biological responses [47]. The initial CH did not have the ability to induce cytokine synthesis, but the PEC κ-CGN:CH 1:10 *w/w* was able to induce the synthesis of TNF-α and IL-10 in cells, although to a lesser extent than the original κ-CGN. Du et al. [48] suggested that the solubility and assembly of the components influence the immuno-pharmacological activities of glucans. Wang et al. [49] postulated that the relatively high bioactivity of polysaccharides can be attributed to good water solubility and expanded chain conformation. So, it can be assumed, that κ-CGN-CH 1:10 *w/w* PEC, with a small particle size and low polydispersity detected by dynamic light scattering (Figure 1) can facilitate contact with the cell compared to the initial more heterogeneous and tightly packed CH.

The results of this investigation indicate that PEC has anti-inflammatory activity against phagocytes, activated by histamine (Table 1). Histamine is the main mediator of the initial phase of acute inflammation. Intra-plantar injection of histamine induces the activation of resident macrophages and mast cells in the tissue of the mouse paw. The pro-inflammatory effects of histamine are also achieved through interactions with its receptors on the endothelium and blood leukocytes. Binding H1 receptors causes an increase in vascular permeability, as well as the formation of prostaglandin E2 (PGE2), leukotrienes and chemokines, which attract eosinophils and neutrophils to the site of inflammation [50]. Preventive i.p. administration of CH, κ-CGN and their water-soluble PEC of the 1:10 and 10:1 *w/w* compositions significantly delayed the development of acute local inflammation. Under these conditions, their activity was comparable to non-steroidal anti-inflammatory drugs, the effect of which is based on the inhibition of cyclooxygenase 1 and 2 on the membranes of endothelial and blood cells, followed by impaired synthesis of prostaglandins E2 and F2α, thromboxane A2, prostacyclin, leukotrienes, and the release of lysosomal enzymes. It can be assumed that polysaccharides use a similar mechanism as a result of direct contact with the membranes of effector cells. This is confirmed by our recent data on the ability of CGN to inhibit of PGE2 synthesis at low concentrations [51]. On the other hand, the scavenger abilities of κ-CGN and its water-soluble PEC could attenuate damage associated with highly active NO-species, which are produced by phagocytes, as shown in ex vivo experiments described here (Figure 2).

The inflammatory response induced by concanavalin A is an example of type I or immediate hypersensitivity, which is due to IgE antibody production and the development allergic sensitization. This type of inflammation is associated with the activation of Th2 cells and adaptive immunity. The polyvalent lectin concanavalin A stimulates the release of histamine and leukotrienes from mast cells and basophils, activates neutrophils, increases the activity of cyclooxygenase-2 (COG-2) and stimulates the proliferation and differentiation of Th2 lymphocytes. Lectin-activated cells secrete various inflammatory mediators, quickly causing severe edema and inflammation in the form of an allergic-like reaction, but without contact with a native allergen [52–54]. Intraperitoneal administration of CH and κ-CGN reduced mast cell degranulation and the subsequent development of inflammation. However, the PEC of the 1:10 and 10:1 *w/w* compositions had no anti-inflammatory activity. It is suggested that free CH and κ-CGN could occupy the membrane surface of mast cells and interrupt the binding of lectin molecules, or could block the transfer of pro-inflammatory signals from primary activated mast cells to the membrane receptors of effector cells (macrophages, neutrophils, or lymphocytes), thereby inhibiting downstream cytokine secretion and inflammation.

A similar effect was found with the DTH test which is based on T-cell immunity. In this case, T-lymphocytes, preliminary primed with antigen, stimulate the blast transformation and proliferation of cytotoxic T-lymphocytes. The secreted pro-inflammatory cytokines secreted by them stimulate the activity of macrophages and cytotoxic lymphocytes, which induce an inflammatory response and the development of a granuloma in the mouse paw [42]. Among the tested samples only κ-CGN alone decreased the DTH reaction, while the others did not (Table 1).

The particle surface charge could potentially control biopolymers binding to tissue both in vivo and in vitro. Cellular surfaces are dominated by negatively charged sulfated proteoglycans, molecules that play pivotal roles in cellular proliferation, migration, and motility [55], therefore, interactions between proteoglycans and positively charged particles are preferred [56]. At the same time negatively charged nanoparticles (NP) show highly increased bioadhesive properties and are absorbed by both M cells and absorptive enterocytes [57]. Jung et al. 57] has also shown that charges on the NP surface are not the only requirement, a combination of both NP surface charges and increased hydrophilicity of the matrix material seem to affect the gastrointestinal uptake in a positive sense. Unfortunately, to date, information on the correlation of activity depending on the charge of natural polysaccharides is very limited. We earlier have shown [29], that CH, CGN and their positively and negatively charged complexes had the different ability to suppress the biofilm formation by Gram-negative and Gram-positive microorganisms. CH and positively charged complexes inhibited only biofilm formation by Gram positive microorganisms (*B. subtilis*). CGN and negatively charged PEC prevented the formation of biofilm by Gram negative microorganisms (*E. coli*) and Gram positive microorganisms.

It could be expected that the activity of the studied PEC would be determined by the prevailing polysaccharide. However, only in the in vitro test, we observed some dependence of the ability to scavenge NO on the polysaccharide content in the PEC. In ex vivo test which is more complex systems, including not only cells but also different soluble serum components, the direct dependency of the activity of the PEC on the polysaccharide contents was not observed. It is much more difficult to carry out any correlations between the activity and surface characteristics of the objects in in vivo experiments. The overall protein concentrations in typical body fluids (e.g., blood, lung, gut) and intracellular environments can be as high as 0.35 gmL^{-1} [58]. These fluids may contain more than 3000 different proteins at widely differing concentrations. It was shown that nanomaterials adsorb biomolecules on contact with biological fluids [59]. Thus the components of the biological fluids can affect the manifestation of a biological activity of studied compounds and an activity determined in experiments in vitro and in vivo can manifest itself in different ways.

A comparison of in vivo test results suggests that the immunomodulatory effect of polysaccharides and the PEC was directly related to their ability to bind to the membrane receptors of immune cells and to influence signal transmission between components of the inflammatory process. The greatest activity of PEC, as well as the initial polysaccharides κ-CGN and CH, was observed in acute exudative

inflammation, directly related to the activation of phagocytic cells, i.e., macrophages and neutrophils. The macrophage surface bears pattern recognition receptors (PRRs), which can recognize and bind the molecules of bacterial polysaccharides [42]. Moreover several members of the TLR (toll-like receptor) family interact with exogenous peptidoglycans and polysaccharides to induce adaptive immunity and modulate immune response [60]. However, in tests mediated by B- and T-lymphocyte stimulation, PEC did not show activity, unlike the free polysaccharides. Thus, the complexation of the CH and κ-CGN led to a decrease in their immunological activity in terms of B- and T-cell immunity. It is assumed that this is due to specific physicochemical limitations that impede PEC interactions with membrane receptors on lymphocytes.

4. Materials and Methods

4.1. Polysacharides

A CH sample with molecular weight of 110 kDa and 6% degree of N-acetylation was obtained by alkaline treatment of crab chitin according to the published protocol [31]. It was deacetylated with the mixture of 40% aqueous solution of NaOH with isopropyl alcohol (1:16 *v:v*) under heating for 7 h at 100 °C. The pellet was filtered and dissolved in water acidified with hydrochloric acid (pH 3.5), dialyzed against water, and lyophilized [61].

The sample of κ-CGN was isolated by extraction with hot water from the red algae *Chondrus armatus* (Gigartinaceae). The algae were collected at Peter the Great Bay (Sea of Japan) washed with tap water in order to remove excess of salt. Dried and milled algae (50 g) were suspended in hot water (1.5 L) and the polysaccharides were extracted at 90 °C for 2 h in a water bath. The polysaccharides were fractionated into gelling KCl-insoluble and non-gelling KCl-soluble fractions and their structures were established according to a published protocol [62]. KCl-insoluble fraction, which according to the structural analysis was assigned to k-CGN have been used.

4.2. Complexes CGN:CH

The complexes of κ-CGN with CH were prepared by mixing solutions of the initial components at the given ratios as described in [33]. The concentration of the component in excess in the complex for all experiments was 0.1 mg/mL. The mixture was incubated for 15 min.

4.3. Dynamic Light Scattering (DLS) and Electrophoretic Properties of the CGN:CH Complexes

The sizes and ζ-potentials of the initial polysaccharides and their PECs in solution were determined using a ZetaSizer NanoZS system (Malvern PANalytical, Malvern, UK) operating at 633 nm. The measurements were performed at 25 °C. The hydrodynamic diameters of the particles were automatically calculated with the instrument's software based on analysis of the autocorrelation function. The ζ-potentials were calculated from the experimentally determined.

4.4. Determination of NO Scavenging Capacity (Microplate)

The reaction mixture containing sodium nitroprusside (10 mM, 75 μL) in phosphate buffered saline (PBS) and samples or reference compound were incubated at 25 °C for 150 min. Then, the Griess reagent (1% sulfanilamide, 0.1% naphthylethylene diamine dihydrochloride in 2% H_3PO_4) was added to the reaction mixture (1:1 = *v:v*). The absorbance of the chromophore formed during the diazotization of nitrite with sulfanilamide and subsequent coupling with napthylethylenediamine was measured at 546 nm. The percentage inhibition of NO generated was measured by comparing the absorbance values of the control and a sample in quadruplicate. Ascorbic acid was used as a positive control [63].

All data were expressed as mean ± standard deviation. Statistical analysis was done by one-way ANOVA. Differences were considered to be statistically significant if $p < 0.05$.

4.5. IL-10 and TNF-α Inducing Activity on the Human Blood Cells

Blood processing was performed using procedure of De Groote et al. [64]. Peripheral blood was collected by vena puncture into sterile siliconized tubes containing 30 IU of lithium heparinate per 5 mL tube diluted 1:5 in sterile Medium 199 (Sigma-Aldrich, Saint Louis, MO, USA) containing 300 mg/L of glutamine (Gibco, Life Technology, Darmstadt, Germany) and 50 μg/mL of gentamicin. Diluted blood (0.1 mL) was transferred into sterile polypropylene plates and then incubated with the samples or with LPS *E. coli* 10 μg (10 min), then with the samples (37 °C, 5% CO_2). After 24 h the supernatants were collected and frozen followed by cytokine determination using a specific ELISA kit ("Cytokine", Saint-Petersburg, Russia). The study protocol was approved by the medical ethics committee of the local hospital (Vladivostok, Russian Federation). Informed consent was obtained from all subjects who participated in the study. All donors were free of medicines administration for 14 days prior to blood sampling. Blood was drawn from the antecubital vein of normal healthy human volunteers and anticoagulated in plastic tubes (Greiner Bio-One International AG, Kremsmuenster, Austria) with 30 IU lithium heparinate used as an anticoagulant.

All data were expressed as mean ± standard deviation. Statistical analysis was done by one-way ANOVA. Differences were considered to be statistically significant if $p < 0.05$.

4.6. Biological Activity In Vivo

4.6.1. Animals

The biological experiments were carried out on outbred and C57BL/6 male mice housed in standard environmental conditions (room temperature, 12 h light/dark cycle). The animals had free access to standard pellet diet and water ad libitum. All experimental procedures were approved by the Local Bio-Ethical Committee of Medicine Chemistry Department of Novosibirsk Institute of Organic Chemistry SB RAS in accordance with European Communities Council Directive 86/609/EEC.

4.6.2. Anti-Inflammatory Activity

The anti-inflammatory activity of the polysaccharides and their PECs was evaluated on three mouse hind paw edema tests induced by histamine (exudative inflammation), concanavalin A (B-cells dependent inflammation) or delayed type hypersensitivity reaction (T-cells dependent inflammation) [65]. Control and experimental groups consisted of 8-10 animals each. In the histamine and concanavalin A tests of inflammation the substances were injected intraperitoneally (i.p.) in water solutions at doses 10.0 mg/kg (PECs) and 9.0 mg/kg (original κ-CGN or CH). In the test of delayed type hypersensitivity reaction (DTH) the substances were administered intraperitoneally at doses 5.0 mg/kg (PECs) and 4.5 mg/kg (κ-CGN or CH). The last dose values were equal to the highest quota of each polysaccharide in appropriate PEC. The dose of reference substances (indomethacin or diclofenac, "Fluka BioChemica" (Sigma-Aldrich, Saint Louis, MO, USA) was 50 mg/kg [66]. The control group of animals received water. At the end of experiment, the animals were sacrificed by cervical dislocation, the mouse hind paws were cut off at the ankle joint and weighed. The ratio of the difference in weight between the treated and untreated hind paws to the weight of the untreated hind paw was used as an inflammatory edema index (IEI). The anti-inflammatory activity (AIA) was presented as a difference between 100% and percentage of inflammation index versus to the control group.

4.6.3. Histamine-Induced Mouse Paw Edema Test

The outbred male albino mice were injected with 0.05 mL 0.01% histamine in saline solution into the plantar of the hind paw. The collateral paw was injected with saline solution. The tested compounds (κ-CGN, CH, and their PECs) were administered i.p. one hour before the histamine injection. The reference agent indomethacin was administered by the same way at the dose 50 mg/kg. The animals were sacrificed 5 h after the histamine injection.

4.6.4. Concavaline A-Induced Mouse Paw Edema Test

The male mice C57Bl/6 were injected with 0.02 mL 0.5% concanavaline A (Sigma-Aldrich, Saint Louis, MO, USA) in saline solution into the plantar of the hind paw. The collateral paw was injected with saline solution. The tested compounds were administered i.p. one hour before the concanavaline A injection. The reference agent diclofenac was administered by the same way at the 50 mg/kg dose. The animals were sacrificed one hour after the concanavaline A injection.

4.6.5. Delayed Type Hypersensitivity Reaction (DTH) Test

The tested compounds were administered intraperitoneally to the male mice C57Bl/6. One day later the sheep erythrocytes suspension (10^8 cells) was injected i.p. to control and experimental groups. At the fifth day after immunization the animals were subplantar injected with the sheep erythrocytes suspension (10^8 cells) into the hind paw. The collateral paw was injected with saline solution. The animals were sacrificed by cervical dislocation 24 h after the last antigen injection

4.6.6. Statistical Analysis

Statistical analyses were performed using "Statistica 6" software. The results of in vivo experiments are given as mean ± SD. The statistically significant difference between groups was calculated by one-way ANOVA by Fisher test (at parametric distribution) or not-parametric Kruskal–Wallis test. A p-value of ≤0.05 was considered as statistically significant.

References

1. Yermak, I.M.; Khotimchenko, Y.S. Chemical properties, biological activities and applications of carrageenans from red algae. *Recent Adv. Mar. Biotechnol.* **2003**, *9*, 207–255.
2. Van de Velde, F.; Knutsen, S. 1H and 13C high resolution NMR spectroscopy of carrageenans: Application in research and industry. *Trends Food Sci. Technol.* **2002**, *13*, 73–92. [CrossRef]
3. Yermak, I.M.; Barabanova, A.O.; Aminin, D.L.; Davydova, V.N.; Sokolova, E.V.; Solov'Eva, T.F.; Kim, Y.H.; Shin, K.S. Effects of structural peculiarities of carrageenans on their immunomodulatory and anticoagulant activities. *Carbohydr. Polym.* **2012**, *87*, 713–720. [CrossRef]
4. Sokolova, E.V.; Byankina, A.O.; Kalitnik, A.A.; Kim, Y.H.; Bogdanovich, L.N.; Solov'Eva, T.F.; Yermak, I.M. Influence of red algal sulfated polysaccharides on blood coagulation and platelets activation in vitro. *J. Biomed. Mater. Res. Part A* **2014**, *102*, 1431–1438. [CrossRef] [PubMed]
5. Ghosh, T.; Chattopadhyay, K.; Marschall, M.; Karmakar, P.; Mandal, P.; Ray, B. Focus on antivirally active sulfated polysaccharides: From structure-activity analysis to clinical evaluation. *Glycobiology* **2009**, *19*, 2–15. [CrossRef] [PubMed]
6. Gomaa, H.H.A.; Elshoubaky, G.A. Antiviral activity of sulfated polysaccharides carrageenan from some marine seaweeds. *Int. J. Curr. Pharm. Rev. Res.* **2016**, *7*, 34–42.
7. Yuan, H.; Song, J.; Li, X.; Li, N.; Liu, S. Enhanced immunostimulatory and antitumor activity of different derivatives of κ-carrageenan oligosaccharides from Kappaphycus striatum. *J. Appl. Phycol.* **2011**, *23*, 59–65. [CrossRef]
8. Lahaye, M.; Kaeffer, B. Seaweed dietary fibres: Structure, physico-chemical and biological properties relevant to intestinal physiology. *Sci. Aliment.* **1997**, *17*, 563–584.
9. Weiner, M.L. Food additive carrageenan: Part II: A critical review of carrageenan in vivo safety studies. *Crit. Rev. Toxicol.* **2014**, *44*, 244–269. [CrossRef]

10. Prajapati, V.D.; Maheriya, P.M.; Jani, G.K.; Solanki, H.K. Carrageenan: A natural seaweed polysaccharide and its applications. *Carbohydr. Polym.* **2014**, *105*, 97–112. [CrossRef]

11. Singla, A.K.; Chawla, M. Chitosan: Some pharmaceutical and biological aspects-an update. *J. Pharm. Pharmacol.* **2001**, *53*, 1047–1067. [CrossRef] [PubMed]

12. Kunio, N.R.; Riha, G.M.; Watson, K.M.; Differding, J.A.; Schreiber, M.A.; Watters, J.M. Chitosan based advanced hemostatic dressing is associated with decreased blood loss in a swine uncontrolled hemorrhage model. *Am. J. Surg.* **2013**, *205*, 505–510. [CrossRef] [PubMed]

13. Skjak-Braek, G.; Anthonsen, T.; Sandford, P.A. *Chitin and Chitosan: Sources, Chemistry, Biochemistry, Physical Properties and Applications*; Springer: Berlin/Heidelberg, Germany, 1989; ISBN 1851663959.

14. Pérez-Recalde, M.; Matulewicz, M.C.; Pujol, C.A.; Carlucci, M.J. In vitro and in vivo immunomodulatory activity of sulfated polysaccharides from red seaweed Nemalion helminthoides. *Int. J. Biol. Macromol.* **2014**, *63*, 38–42. [CrossRef] [PubMed]

15. Liu, Q.; Xu, S.; Li, L.; Pan, T.; Shi, C.L.; Liu, H.; Cao, M.; Su, W.; Liu, G. In vitro and in vivo immunomodulatory activity of sulfated polysaccharide from Porphyra haitanensis. *Carbohydr. Polym.* **2017**, *165*, 189–196. [CrossRef]

16. Suganya, A.M.; Sanjivkumar, M.; Chandran, M.N.; Palavesam, A.; Immanuel, G. Pharmacological importance of sulphated polysaccharide carrageenan from red seaweed Kappaphycus alvarezii in comparison with commercial carrageenan. *Biomed. Pharmacother.* **2016**, *84*, 1300–1312. [CrossRef]

17. Sokolova, E.V.; Barabanova, A.O.; Homenko, V.A.; Solov'eva, T.F.; Bogdanovich, R.N.; Yermak, I.M. In Vitro and Ex Vivo Studies of Antioxidant Activity of Carrageenans, Sulfated Polysaccharides from Red Algae. *Bull. Exp. Biol. Med.* **2011**, *150*, 426–428. [CrossRef]

18. Debnath, T.; Kim, D.; Lim, B. Natural Products as a Source of Anti-Inflammatory Agents Associated with Inflammatory Bowel Disease. *Molecules* **2013**, *18*, 7253–7270. [CrossRef]

19. Bruno, A.; Tacconelli, S.; Patrignani, P. Variability in the Response to Non-Steroidal Anti-Inflammatory Drugs: Mechanisms and Perspectives. *Basic Clin. Pharmacol. Toxicol.* **2014**, *114*, 56–63. [CrossRef]

20. Davydova, V.N.; Kalitnik, A.A.; Markov, P.A.; Volod'ko, A.V.; Popov, S.V.; Ermak, I.M. Cytokine-inducing and anti-inflammatory activity of chitosan and its low-molecular derivative. *Appl. Biochem. Microbiol.* **2016**, *52*, 476–482. [CrossRef]

21. Kalitnik, A.A.; Anastyuk, S.D.; Barabanova, A.O.B.; Glazunov, V.P.; Yermak, I.M.; Marcov, P.A.; Popov, S.V.; Ovodov, Y.S. Gelling polysaccharide from Chondrus armatus and its oligosaccharides: The structural peculiarities and anti-inflammatory activity. *Carbohydr. Polym.* **2015**, *115*, 768–775. [CrossRef]

22. Yermak, I.M.; Volod'ko, A.V.; Khasina, E.I.; Davydova, V.N.; Chusovitin, E.A.; Goroshko, D.L.; Kravchenko, A.O.; Solov'eva, T.F.; Maleev, V.V. Inhibitory effects of carrageenans on endotoxin-induced inflammation. *Mar. Drugs* **2020**, *18*, 248. [CrossRef] [PubMed]

23. McKim, J.M.; Wilga, P.C.; Pregenzer, J.F.; Blakemore, W.R. The common food additive carrageenan is not a ligand for Toll-Like- Receptor 4 (TLR4) in an HEK293-TLR4 reporter cell-line model. *Food Chem. Toxicol.* **2015**, *78*, 153–158. [CrossRef] [PubMed]

24. Weiner, M.L. Toxicological properties of carrageenan. *Agents Actions* **1991**, *32*, 46–51. [CrossRef] [PubMed]

25. Matricardi, P.; Di Meo, C.; Coviello, T.; Hennink, W.E.; Alhaique, F. Interpenetrating polymer networks polysaccharide hydrogels for drug delivery and tissue engineering. *Adv. Drug Deliv. Rev.* **2013**, *65*, 1172–1187. [CrossRef] [PubMed]

26. Schmitt, C.; Sanchez, C.; Desobry-Banon, S.; Hardy, J. Structure and technofunctional properties of protein-polysaccharide complexes: A review. *Crit. Rev. Food Sci. Nutr.* **1998**, *38*, 689–753. [CrossRef] [PubMed]

27. Murray, M.J.; Snowden, M.J. The preparation, characterisation and applications of colloidal microgels. *Adv. Colloid Interface Sci.* **1995**, *54*, 73–91. [CrossRef]

28. Volod'ko, A.V.; Davydova, V.N.; Chusovitin, E.; Sorokina, I.V.; Dolgikh, M.P.; Tolstikova, T.G.; Balagan, S.A.; Galkin, N.G.; Yermak, I.M. Soluble chitosan–carrageenan polyelectrolyte complexes and their gastroprotective activity. *Carbohydr. Polym.* **2014**, *101*, 1087–1093. [CrossRef]

29. Volod'ko, A.V.; Davydova, V.N.; Nedashkovskaya, O.I.; Terentieva, N.A.; Chusovitin, E.A.; Galkin, N.G.; Yermak, I.M. Morphology, electrokinetic characteristics and the effect on biofilm formation of carrageenan:chitosan polyelectrolyte complexes. *Int. J. Biol. Macromol.* **2018**, *117*, 1118–1124. [CrossRef]

30. Yermak, I.M.; Kim, Y.H.; Titlynov, E.A.; Isakov, V.V.; Solov'eva, T.F. Chemical structure and gel properties of carrageenans from algae belonging to the Gigartinaceae and Tichocarpaceae, collected from the Russian Pacific Coast. *J. Appl. Phycol.* **1999**, *11*, 41–48. [CrossRef]

31. Wolfrom, M.; Han, T. The Sulfonation of Chitosan. *J. Am. Chem. Soc.* **1959**, *870*, 1764–1766. [CrossRef]

32. Domszy, J.; Roberts, G. Evaluation of infrared spectroscopic techniques for analysing chitosan. *Die Makromol. Chem.* **1985**, *186*, 1671–1677. [CrossRef]

33. Volod'Ko, A.V.; Davydova, V.N.; Barabanova, A.O.; Soloveva, T.F.; Ermak, I.M. Formation of soluble chitosan-carrageenan polyelectrolyte complexes. *Chem. Nat. Compd.* **2012**, *48*. [CrossRef]

34. Davydova, V.N.; Volod'ko, A.V.; Sokolova, E.V.; Chusovitin, E.A.; Balagan, S.A.; Gorbach, V.I.; Galkin, N.G.; Yermak, I.M.; Solov'Eva, T.F. The supramolecular structure of LPS-chitosan complexes of varied composition in relation to their biological activity. *Carbohydr. Polym.* **2015**, *123*. [CrossRef] [PubMed]

35. Ratanathanawongs Williams, S.K.; Lee, D. Field-flow fractionation of proteins polysaccharides, synthetic polymers, and supramolecular assemblies. *J. Sep. Sci.* **2006**, *29*, 1720–1732. [CrossRef]

36. Kalim, M.D.; Bhattacharyya, D.; Banerjee, A.; Chattopadhyay, S. Oxidative DNA damage preventive activity and antioxidant potential of plants used in Unani system of medicine. *BMC Complement. Altern. Med.* **2010**, *10*. [CrossRef]

37. López-Alarcón, C.; Denicola, A. Evaluating the antioxidant capacity of natural products: A review on chemical and cellular-based assays. *Anal. Chim. Acta* **2013**, *763*, 1–10. [CrossRef]

38. Chen, S.K.; Tsai, M.L.; Huang, J.R.; Chen, R.H. In Vitro Antioxidant Activities of Low-Molecular-Weight Polysaccharides with Various Functional Groups. *J. Agric. Food Chem.* **2009**, *57*, 2699–2704. [CrossRef]

39. Kim, K.W.; Thomas, R.L. Antioxidative activity of chitosans with varying molecular weights. *Food Chem.* **2007**, *101*, 308–313. [CrossRef]

40. Duque, G.A.; Descoteaux, A. Macrophage cytokines: Involvement in immunity and infectious diseases. *Front. Immunol.* **2014**, *5*. [CrossRef]

41. Berger, J.; Reist, M.; Mayer, J.M.; Felt, O.; Gurny, R. Structure and interactions in chitosan hydrogels formed by complexation or aggregation for biomedical applications. *Eur. J. Pharm. Biopharm.* **2004**, *57*, 35–52. [CrossRef]

42. Rabson, A.; Roitt, I.M.; Delves, P.J. *Really Essential Medical Immunology*, 2nd ed.; Blackwell Publishing Ltd.: Oxford, UK, 2005.

43. Moncada, S.; Palmer, R.M.J.; Higgs, E.A. Nitric oxide: Physiology, pathophysiology, and pharmacology. *Pharmacol. Rev.* **1991**, *43*, 109–142. [PubMed]

44. Stuehr, D.J.; Nathan, C.F. Nitric oxide: A macrophage product responsible for cytostasis and respiratory inhibition in tumor target cells. *J. Exp. Med.* **1989**, *169*, 1543–1555. [CrossRef] [PubMed]

45. Ajisaka, K.; Agawa, S.; Nagumo, S.; Kurato, K.; Yokoyama, T.; Arai, K.; Miyazaki, T. Evaluation and comparison of the antioxidative potency of various carbohydrates using different methods. *J. Agric. Food Chem.* **2009**, *57*, 3102–3107. [CrossRef] [PubMed]

46. Wang, J.; Hu, S.; Nie, S.; Yu, Q.; Xie, M. Reviews on Mechanisms of In Vitro Antioxidant Activity of Polysaccharides. *Oxid. Med. Cell. Longev.* **2016**, *2016*, 1–13. [CrossRef]

47. Gouwy, M.; Struyf, S.; Proost, P.; Van Damme, J. Synergy in cytokine and chemokine networks amplifies the inflammatory response. *Cytokine Growth Factor Rev.* **2005**, *16*, 561–580. [CrossRef] [PubMed]

48. Du, B.; Lin, C.; Bian, Z.; Xu, B. An insight into anti-inflammatory effects of fungal beta-glucans. *Trends Food Sci. Technol.* **2015**, *41*, 49–59. [CrossRef]

49. Wang, Y.; Zhang, L.; Li, Y.; Hou, X.; Zeng, F. Correlation of structure to antitumor activities of five derivatives of a β-glucan from Poria cocos sclerotium. *Carbohydr. Res.* **2004**, *339*, 2567–2574. [CrossRef]

50. Amann, R.; Schuligoi, R.; Lanz, I.; Donnerer, J. Histamine-induced edema in the rat paw-effect of capsaicin denervation and a CGRP receptor antagonist. *Eur. J. Pharmacol.* **1995**, *279*, 227–231. [CrossRef]

51. Sokolova, E.V.; Kravchenko, A.O.; Sergeeva, N.V.; Davydova, V.N.; Bogdanovich, L.N.; Yermak, I.M. Effect of carrageenans on some lipid metabolism components in vitro. *Carbohydr. Polym.* **2020**, *230*. [CrossRef]

52. Dumonde, D.C.; Maini, R.N. The clinical significance of mediators of cellular immunity. *Clin. Exp. Allergy* **1971**, *1*, 123–139. [CrossRef]

53. Andreis, M.; Stastny, P.; Ziff, M. Experimental arthritis produced by injection of mediators of delayed hypersensitivity. *Rheum.Annu. Rev.* **1975**, *6*, 303–307. [CrossRef]

54. Bento, C.A.M.; Cavada, B.S.; Oliveira, J.T.A.; Moreira, R.A.; Barja-Fidalgo, C. Rat paw edema and leukocyte immigration induced by plant lectins. *Agents Actions* **1993**, *38*, 48–54. [CrossRef] [PubMed]

55. Bernfield, M.; Park, P.W.; Reizes, O.; Fitzgerald, M.L.; Lincecum, J.; Zako, M.; Gotte, M.; Park, P.W.; Reizes, O.; Fitzgerald, M.L.; et al. Functions of cell surface heparan sulfate proteoglycans. *Annu. Rev. Biochem.* **1999**, *68*, 729–777. [CrossRef]

56. Hartig, S.M.; Greene, R.R.; Dikov, M.M.; Prokop, A.; Davidson, J.M. Multifunctional nanoparticulate polyelectrolyte complexes. *Pharm. Res.* **2007**, *24*, 2353–2369. [CrossRef] [PubMed]

57. Jung, T.; Kamm, W.; Breitenbach, A.; Kaiserling, E.; Xiao, J.X.; Kissel, T. Biodegradable nanoparticles for oral delivery of peptides: Is there a role for polymers to affect mucosal uptake? *Eur. J. Pharm. Biopharm.* **2000**, *50*, 147–160. [CrossRef]

58. Klein, J. Probing the interactions of proteins and nanoparticles. *Proc. Natl. Acad. Sci. USA* **2007**, *104*, 2029–2030. [CrossRef]

59. Tenzer, S.; Docter, D.; Kuharev, J.; Musyanovych, A.; Fetz, V.; Hecht, R.; Schlenk, F.; Fischer, D.; Kiouptsi, K.; Reinhardt, C.; et al. Rapid formation of plasma protein corona critically affects nanoparticle pathophysiology. *Nat. Nanotechnol.* **2013**, *8*, 772–781. [CrossRef]

60. Liu, F.; Zhang, X.; Li, Y.; Chen, Q.; Liu, F.; Zhu, X.; Mei, L.; Song, X.; Liu, X.; Song, Z.; et al. Anti-inflammatory effects of a Mytilus coruscus α-D-glucan (MP-A) in activated macrophage cells via TLR4/NF-κB/MAPK pathway inhibition. *Mar. Drugs* **2017**, *15*, 294. [CrossRef]

61. Naberezhnykh, G.A.; Gorbach, V.I.; Likhatskaya, G.N.; Davidova, V.N.; Solov'eva, T.F. Interaction of chitosans and their N-acylated derivatives with lipopolysaccharide of gram-negative bacteria. *Biochemistry* **2008**, *73*, 432–441. [CrossRef]

62. Barabanova, A.O.; Shashkov, A.S.; Glazunov, V.P.; Isakov, V.V.; Nebylovskaya, T.B.; Helbert, W.; Solov'eva, T.F.; Yermak, I.M. Structure and properties of carrageenan-like polysaccharide from the red alga Tichocarpus crinitus (Gmel.) Rupr. (Rhodophyta, Tichocarpaceae). *J. Appl. Phycol.* **2008**, *20*, 1013–1020. [CrossRef]

63. Sokolova, E.V.; Barabanova, A.O.; Bogdanovich, R.N.; Khomenko, V.A.; Solov'eva, T.F.; Yermak, I.M. In vitro antioxidant properties of red algal polysaccharides. *Biomed. Prev. Nutr.* **2011**, *1*, 161–167. [CrossRef]

64. De Groote, D.; Zangerle, P.F.; Gevaert, Y.; Fassotte, M.F.; Beguin, Y.; Noizat-Pirenne, F.; Pirenne, J.; Gathy, R.; Lopez, M.; Dehart, I.; et al. Direct stimulation of cytokines (IL-1β, TNF-α, IL-6, IL-2, IFN-γ and GM-CSF) in whole blood. I. Comparison with isolated PBMC stimulation. *Cytokine* **1992**, *4*, 239–248. [CrossRef]

65. Khlebnicova, T.S.; Piven, Y.A.; Baranovsky, A.V.; Lakhvich, F.A.; Sorokina, I.V.; Tolstikova, T.G. Fluorine-containing lupane triterpenoid acid derivatives: Design, synthesis and biological evaluation as potential anti-inflammatory agents. *Steroids* **2019**, *147*, 62–69. [CrossRef] [PubMed]

66. Bednarczyk-Cwynar, B.; Zaprutko, L.; Marciniak, J.; Lewandowski, G.; Szulc, M.; Kaminska, E.; Wachowiak, N.; Mikolajczak, P.L. The analgesic and anti-inflammatory effect of new oleanolic acid acyloxyimino derivative. *Eur. J. Pharm. Sci.* **2012**, *47*, 549–555. [CrossRef]

marine drugs

MDPI

Glyceroglycolipid Metabolism Regulations under Phosphate Starvation Revealed by Transcriptome Analysis in *Synechococcus elongatus* PCC 7942

Xinrui Xu [1,2,3] and Xiaoling Miao [1,2,3,*]

[1]   State Key Laboratory of Microbial Metabolism, School of Life Sciences and Biotechnology,
      Shanghai Jiao Tong University, 800 Dongchuan Road, Shanghai 200240, China; xuxinrui0603@163.com
[2]   Joint International Research Laboratory of Metabolic & Developmental Sciences,
      Shanghai Jiao Tong University, Shanghai 200240, China
[3]   Biomass Energy Research Center, Shanghai Jiao Tong University, Shanghai 200240, China
*   Correspondence: miaoxiaoling@sjtu.edu.cn; Tel.: +86-21-3420-7028

Abstract: Glyceroglycolipids, abundant in cyanobacteria's photosynthetic membranes, present bioactivities and pharmacological activities, and can be widely used in the pharmaceutical industry. Environmental factors could alter the contents and compositions of cyanobacteria glyceroglycolipids, but the regulation mechanism remains unclear. Therefore, the glyceroglycolipids contents and the transcriptome in *Synechococcus elongatus* PCC 7942 were analyzed under phosphate starvation. Under phosphate starvation, the decrease of monogalactosyl diacylglycerol (MGDG) and increases of digalactosyl diacylglycerol (DGDG) and sulfoquinovosyl diacylglycerol (SQDG) led to a decrease in the MGDG/DGDG ratio, from 4:1 to 5:3, after 12 days of cultivation. However, UDP–sulfoquinovose synthase gene *sqdB*, and the SQDG synthase gene *sqdX*, were down-regulated, and the decreased MGDG/DGDG ratio was later increased back to 2:1 after 15 days of cultivation, suggesting the regulation of glyceroglycolipids on day 12 was based on the MGDG/DGDG ratio maintaining glyceroglycolipid homeostasis. There are 12 differentially expressed transcriptional regulators that could be potential candidates related to glyceroglycolipid regulation, according to the transcriptome analysis. The transcriptome analysis also suggested post-transcriptional or post-translational regulations in glyceroglycolipid synthesis. This study provides further insights into glyceroglycolipid metabolism, as well as the scientific basis for glyceroglycolipid synthesis optimization and cyanobacteria glyceroglycolipids utilization via metabolic engineering.

Keywords: glyceroglycolipid metabolism; phosphate starvation; transcriptome; glyceroglycolipid homeostasis

1. Introduction

Glyceroglycolipids are widely distributed in plants, microalgae and cyanobacteria. Monogalactosyl diacylglycerol (MGDG), digalactosyl diacylglycerol (DGDG) and sulfoquinovosyl diacylglycerol (SQDG) are the three main glyceroglycolipids in the photosynthetic membrane, which are essential for photosynthesis [1]. In cyanobacteria, about 50% of the photosynthetic membrane lipids are MGDG, 20% are DGDG and 16% are SQDG [2]. Glyceroglycolipids present both bioactivities and pharmacological activities, and can be widely used in the pharmaceutical industry [3]. Microalgae and cyanobacteria are competitive sources of glyceroglycolipids because of their abundant glyceroglycolipids, their simple cell structure and their eco-friendly characteristic. Many glyceroglycolipids with pharmaceutical value have been isolated from microalgae and cyanobacteria. MGDG with pro-apoptotic activity is extracted from *Phaeodactylum tricornutum* [4]. MGDG from *Tetraselmis chuii* and *Nannochloropsis granulate*

have anti-inflammatory activities [5]. MGDG and DGDG from *Chlorella Vulgaris* [6] and *Phormidium tenue* [7] also present anti-tumor activities. In addition, SQDG, with eukaryotic DNA polymerase inhibitory activity, has been extracted from *Gigartina tenella* [8]. The SQDG isolated from the cyanobacteria *Lyngbya lagerheimii* [9] and *Phormidium tenue* [10] have AIDS-antiviral activities. Recent studies have also identified the immuno-stimulatory activity and the potential against Alzheimer's disease of SQDG derived from microalgae [5].

Environmental factors directly influence the accumulation of many metabolites. Phosphate—the main ingredient of nucleic acid, protein and phospholipids—is an essential element in organism growth. However, phosphate is often limited in natural environments [11]. To cope with phosphate limitation, organisms have acquired different strategies, including ultrastructural rearrangements, C reallocation, transcriptome reprograming, and metabolome and lipid remodeling [11]. Glyceroglycolipid accumulation could be strongly regulated by phosphate concentration. In plants, the synthesis of some kinds of glyceroglycolipids (like DGDG and SQDG) will be induced when phosphate is lacking during cultivation, in order to supplement the shortage of phospholipids so as to maintain both the structures and functions of membranes [12,13]. A similar phenomenon was also reported in the cyanobacteria *Synechococcus elongatus* PCC 7942, wherein phosphate starvation resulted in a decrease in phospholipid and an increase in SQDG [14]. In *Chlamydomonas nivalis*, DGDG increased while MGDG decreased under phosphate deprivation [15]. In addition, an increase in total glyceroglycolipids is common in microalgae and cyanobacteria when exposed to a phosphate deficiency condition [16–18].

Glyceroglycolipid-related synthases have been well researched for decades. SQDG synthases present a high homology between plants and microalgae. UDP-sulfoquinovose synthase (EC: 3.13.1.1) (SQD1) and SQDG synthase (EC: 2.4.1.-) (SQD2) are involved in the SQDG synthesis in both plants and eukaryotic microalgae [19,20]. In cyanobacteria, sqdB (EC: 3.13.1.1) and sqdX (EC: 2.4.1.-), responsible for SQDG synthesis [21,22], show high sequence similarity with SQD1 and SQD2, respectively [23]. However, genetic differences exist between MGDG and DGDG synthases in plants and microalgae. In plants, three MGDG synthases (EC: 2.4.1.46) (MGD1, MGD2 and MGD3) [24–26] and two DGDG synthases (EC: 2.4.1.241) (DGD1 and DGD2) [27,28] have been identified. MGD1 and DGD1 participate in the synthesis of the bulk of MGDG and DGDG, respectively, while DGD2 is involved in DGDG synthesis under specific growth conditions [28], with MGD2 and MGD3 providing MGDG as a precursor [29]. In *Chlamydomonas reinhardtii*, only orthologues of MGD1 and DGD1 were identified [20,30], but a second isoform of the DGDG synthase, resembling the plant DGD2, was additionally found in *Ostreococcus tauri* [20]. In cyanobacteria, no homolog for the plant-type DGDG synthase has been detected [31], and dgdA (EC: 2.4.1.241) (the DGDG synthase in cyanobacteria) is only distantly related to DGD1 [23,32]. MGDG synthesis in cyanobacteria is more complicated. All cyanobacteria are likely to synthesize MGDG through the epimerization of monoglucosyl diacylglycerol (MGlcDG) [33] by the MGlcDG synthase (EC: 2.4.1.336) (mgdA) [34,35] and the MGlcDG epimerase (EC 5.1.3.34) (mgdE) [36]. Some studies have reported that phosphate deficiency would stimulate the expression of glyceroglycolipid-related synthases [17,37–39], but the underlying regulation mechanism is still poorly understood.

Metabolic engineering could modify the metabolisms of an organism so as to produce specific metabolites. According to recent reports, overexpressing a bHLH transcription factor [40] and a bZIP transcription factor [41] could enhance biomass and lipid productivity in *Nannochloropsis salina*. Overexpressing a soybean transcription factor, GmDof4, significantly enhanced the lipid production in *Chlorella ellipsoidea*, without sacrificing biomass [42]. The available information regarding the key regulators involved in cyanobacteria glyceroglycolipid metabolism is currently still deficient, which limits the development of cyanobacteria glyceroglycolipids utilization.

Previous studies in our lab indicated a decrease in MGDG and increases in DGDG and SQDG in *Synechococcus* sp. under phosphate starvation [2]. To investigate the relationship between phosphate starvation and glyceroglycolipid metabolism, the transcriptome of the cyanobacteria model organism *Synechococcus elongatus* PCC 7942 under phosphate starvation was analyzed in this

study, which provided further insights into glyceroglycolipid metabolism under phosphate starvation, and a scientific basis for cyanobacteria glyceroglycolipids utilization in metabolic engineering.

2. Results and Discussion

2.1. Changes in Glyceroglycolipid Composition in Synechococcus elongatus PCC 7942 under Phosphate Starvation

Our previous research demonstrated that the content of total glyceroglycolipids increased over all growth stages, and glyceroglycolipid composition changed in *S. elongatus* PCC 7942, under phosphate starvation, which helps cyanobacteria adapt to unfavorable conditions [43]. In order to gain more insight into glyceroglycolipid changes triggered by phosphate starvation, the growth, and dynamic variations in the composition, of three different glyceroglycolipids in *S. elongatus* PCC 7942 were investigated under the initial phosphate concentrations of 0.04 g/L and 0 g/L (Figure 1).
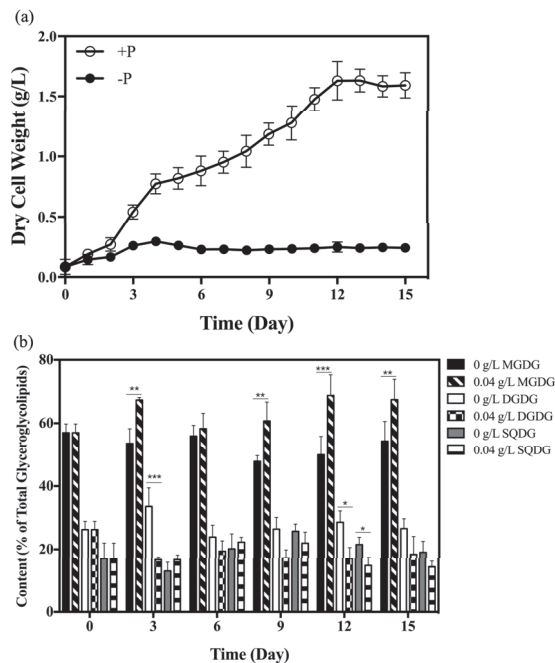

Figure 1. Growth (**a**) and dynamic changes in glyceroglycolipid composition (**b**) in *S. elongatus* PCC 7942 under phosphate concentrations of 0.04 g/L (+P) and 0 g/L (−P). Values are the means ± standard deviations from the three separately grown cultures. 2-way ANOVA test (* $p < 0.05$, ** $p < 0.01$, *** $p < 0.001$).

The growth of *S. elongatus* PCC 7942 under phosphate concentrations of 0.04 g/L reached a stationary phase after 12 days of cultivation (Figure 1a). The maximum biomass concentrations, with 0.04 g/L and 0 g/L phosphate, were 1.63 g/L and 0.25 g/L, respectively.

Under phosphate starvation, the difference in MGDG content was significant on day 3 ($p = 0.0044$), day 9 ($p = 0.0067$), day 12 ($p = 0.0004$) and day 15 ($p = 0.006$). The difference in DGDG content was significant on day 3 ($p = 0.0009$) and day 12 ($p = 0.0145$) under phosphate starvation. The difference in SQDG content was significant on day 12 ($p = 0.0327$). The largest difference in the composition of glyceroglycolipids in *S. elongatus* PCC 7942, caused by phosphate starvation, was observed on day 12 (Figure 1b). The MGDG content was 50% of the total glyceroglycolipids under phosphate starvation on day 12, which was 0.72 times lower than that in the phosphate-rich culture (69% of total glyceroglycolipids) (Figure 1b). DGDG and SQDG contents were 29% and 21% of total

glyceroglycolipids, respectively, under phosphate starvation on day 12, which were respectively 1.70 and 1.50 times higher than that in the phosphate-rich culture (17% and 14% of total glyceroglycolipids) (Figure 1b), respectively. Many studies have already illustrated that phosphate starvation or limitation would cause lipid remodeling in many species, and found that the increased glyceroglycolipids could functionally substitute the degrading phospholipids [13,17,44]. This result demonstrated that the increase of total glyceroglycolipids content in *S. elongatus* PCC 7942 (Supplementary Figure S1) mainly resulted from the accumulation of DGDG and SQDG under phosphate starvation (Figure 1b), the same as *Synechocystis* sp. PCC 6803 [31], indicating their importance in adapting to phosphate stress [43].

2.2. Expressions of Glyceroglycolipid Synthase Genes in Synechococcus elongatus PCC 7942 under Different Phosphate Concentrations

To explore the changes in glyceroglycolipid composition at the transcriptional level, the expressions of glyceroglycolipid synthase genes in *S. elongatus* PCC 7942, cultivated under the initial phosphate concentrations of 0.04 g/L and 0 g/L for 12 days, were determined by qRT-PCR. In *S. elongatus* PCC 7942, *mgdA* (Synpcc7942_1083), *mgdE* (Synpcc7942_0861), *dgdA* (Synpcc7942_0986), *sqdB* (Synpcc7942_0578) and *sqdX* (Synpcc7942_0579) are the five glyceroglycolipid synthase genes.

The expression levels of *mgdA* and *mgdE* showed no significant differences under phosphate starvation (Figure 2a,b). The expression of *mdgA* is not regulated by the SphS–SphR two component system in response to inorganic phosphate [45]. The mgdA–mgdE system in cyanobacteria was replaced by MGD1 in eukaryotic microalgae and plants [33]. In *Arabidopsis*, the expression of *MGD1* is not induced by phosphate deficiency [29]. Moreover, the expression of *mdgA* also showed no differences under heat stress [46]. Thus, the mgdA–mgdE system may not be regulated at the transcriptional level.
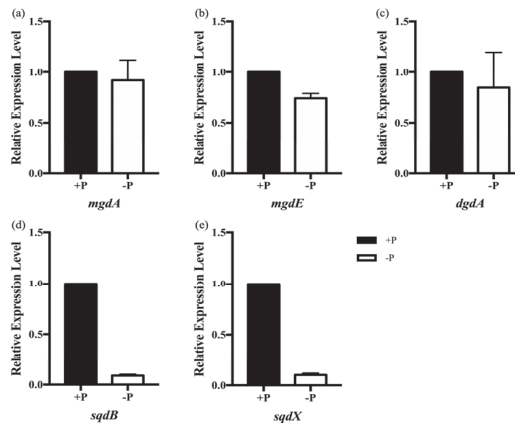

Figure 2. Relative gene expressions of *mgdA* (**a**), *mgdE* (**b**), *dgdA* (**c**), *sqdB* (**d**) and *sqdX* (**e**) in *S. elongatus* PCC 7942 cultivated under phosphate concentrations of 0.04 g/L (+P) and 0 g/L (−P) for 12 days. Values are the means ± standard deviations from the three separately grown cultures. The expression level of each glyceroglycolipid synthase gene under phosphate concentration of 0.04 g/L (+P) was set to 1.

As mentioned above, the increased DGDG accounted for the majority of the increased total glyceroglycolipids, and DGDG levels were increased throughout the whole culture period (Figure 1b and Supplementary Figure S2). However, the expression level of *dgdA* showed no significant differences under phosphate starvation (Figure 2c). In plants, both *DGD1* and *DGD2* can be up-regulated under conditions of phosphate deficiency [47]. This result suggested that the regulation of DGDG synthases in cyanobacteria might be different from that in plants, since an evolutionary gap exists between DGDG synthases in plants and cyanobacteria [31].

SQDG has been regarded as a surrogate for phosphatidylglycerol (PG), and SQDG synthases will be specifically induced upon phosphate starvation [1,17]. Interestingly, the expression levels of *sqdB* and *sqdX* were down-regulated by 90% (Figure 2d,e). The degrees of down-regulation in *sqdB* and *sqdX* are comparable, since *sqdB* and *sqdX* are likely to form an operon called *sqdBX* [48]. In this study, SQDG content was increased under phosphate starvation on day 12. It showed a slightly decreased trend after 12 days of cultivation, although this was not statistically significant (Supplementary Figure S2).

2.3. Global Transcriptomic Analysis under Different Phosphate Concentrations

To further investigate the regulatory mechanism of changes in glyceroglycolipid composition, the transcriptome of *S. elongatus* PCC 7942, cultivated under the initial phosphate concentrations of 0.04 g/L and 0 g/L, for 12 days, was analyzed. As shown in Figure 3a and Supplementary Table S1, 2660 genes in total were analyzed, among which 165 genes (6.2%) were significantly up-regulated and 172 genes (6.5%) were significantly down-regulated under phosphate starvation conditions, compared with the levels under 0.04 g/L phosphate concentration.
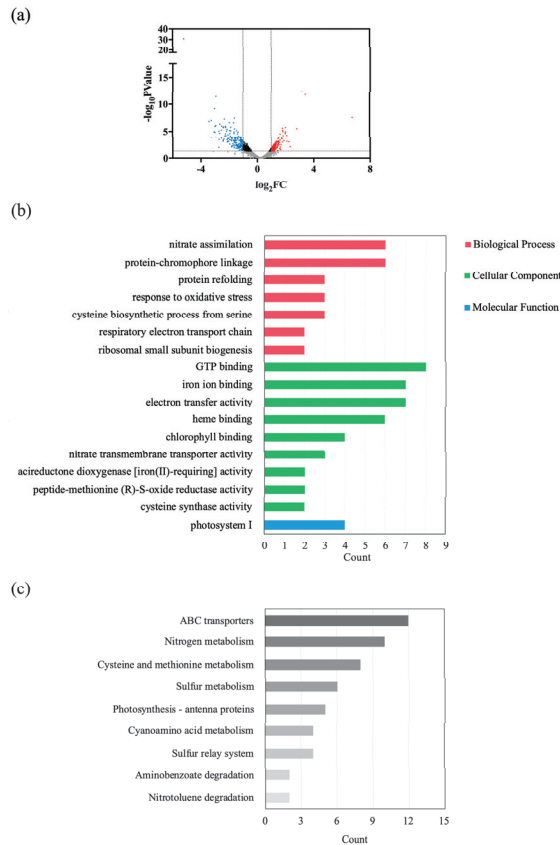

Figure 3. DEGs, and GO and KEGG enrichment of DEGs under phosphate starvation in *S. elongatus* PCC 7942. All DEGs were defined under *p*-value < 0.05 and fold change values (FC) ≥ 2 or ≤ 0.5. (**a**) Volcano plot of DEGs. Red and blue represent up-regulated and down-regulated DEGs, respectively. (**b**) Representative enriched GO terms of DEGs. Bars represent number of DEGs. (**c**) Representative enriched pathways of DEGs. Bars represent number of DEGs.

The Gene Ontology (GO) enrichment of differentially expressed genes (DEGs), illustrated in Figure 3b and Supplementary Table S2, significantly enriched 17 GO terms. The most enriched GO term was GTP binding (Figure 3b), in which three DEGs were significantly down-regulated and five DEGs were significantly up-regulated (Supplementary Table S3), indicating the active signals transmitting under phosphate starvation. Notably, a gene coding the *Escherichia coli* Ras-like protein (*era*, Synpcc7942_0160) was significantly up-regulated, with a fold change value of 2.42 under phosphate starvation (Supplementary Table S3). In *S. elongatus* PCC 7942, an *era* overexpression strain exhibited significantly higher amounts of fatty acids compared to wild type [49]. Protein Era is highly conserved [50], and *ERA-related GTPase* (*ERG*) in plants is always related to chloroplast biogenesis [51–53], revealing its homologous function with cyanobacteria. Depletion of an Era-type GTP-binding protein resulted in abnormal chloroplasts lacking thylakoid membranes in rice, which indicated its importance in chloroplast development [54]. It could be speculated from this evidence in the literature that the accumulation of total glyceroglycolipids under phosphate starvation may be associated with the up-regulation of *era*.

The other two highly enriched GO terms were iron ion binding and electron transfer activity, suggesting electron transport was severely affected after 12 days of cultivation under phosphate starvation. The Kyoto Encyclopedia of Genes and Genomes (KEGG) enrichment of DEGs (Figure 3c and Supplementary Table S4) showed that nine metabolic pathways were significantly affected by phosphate starvation, of which the three most enriched were ABC transporters, nitrogen metabolism, and cysteine and methionine metabolism. Similar responses were commonly implicated when organisms were exposed to adverse conditions [55,56].

Besides, GTP-binding proteins play important roles in the cell cycle, cell division and ribosome maturation [57]. We analyzed the DEGs involved in the cell cycle, cell division and ribosome maturation. According to GO enrichment (Supplementary Table S2) and KEGG enrichment (Supplementary Table S4), these metabolisms were not significantly enriched (p-value > 0.05) under conditions of phosphate starvation on day 12, though one gene involved in the cell cycle, two genes involved in cell division and nine genes involved in ribosome maturation were differentially expressed under phosphate starvation.

2.4. Differential Expressions of Genes Involved in Glyceroglycolipid Synthesis

The glyceroglycolipid synthesis pathway, based on KEGG annotation, is shown in Figure 4a. In total, 12 genes were involved in this pathway. However, the UDP-glucose pyrophosphorylase (EC: 2.7.7.9) (*ugp*) responsible for transforming glucose-1-phosphate to UDP-glucose remained unidentified. In *S. elongatus* PCC 7942, a conserved hypothetical protein coded by Synpcc7942_0148 showed a percent identity of 49% with the *ugp* in *Synechocystis* sp. PCC 6803, coded by *slr0207* [58], indicating Synpcc7942_0148 is possibly responsible for UDP-glucose synthesis. Moreover, the unique cyanobacteria UDP-glucose pyrophosphorylase (*cugP*), coded by *sll1558*, which is annotated as mannose-1-phosphate guanyltransferase (EC:2.7.7.13) (GMPP) but displays *ugp* activity, was identified in *Synechocystis* sp. PCC 6803 [59]. In *S. elongatus* PCC 7942, GMPP coded by Synpcc7942_1973 showed a percent identity of 79% with the product of *sll1558*, suggesting it is involved in UDP-glucose synthesis as a *cugP*.

According to transcriptome analysis, *mgdA, mgdE* and *dgdA* showed no significant differences in expression under conditions of phosphate starvation, while *sqdB* and *sqdX* were down-regulated, with fold changes of 0.63 and 0.43, respectively (Figure 4a and Supplementary Table S5), the same as the results of qRT-PCR. Moreover, the expressions of other genes related to glyceroglycolipid synthesis, and the two possible candidates responsible for UDP-glucose synthesis (Synpcc7942_0148 and Synpcc7942_1973), showed no significant differences under phosphate starvation as well (Figure 4a), except for *pgm* (Synpcc7942_0156), which is responsible for transforming glucose-6-phosphate into glucose-1-phosphate, and which was up-regulated with a fold change of 1.93 (Figure 4a and Supplementary Table S5). The up-regulation of *pgm* will lead to an accumulation of glucose-1-phosphate,

the precursor of UDP-glucose, which provides glycosyl for glyceroglycolipid synthesis, thus accounting for the increase of glyceroglycolipids.
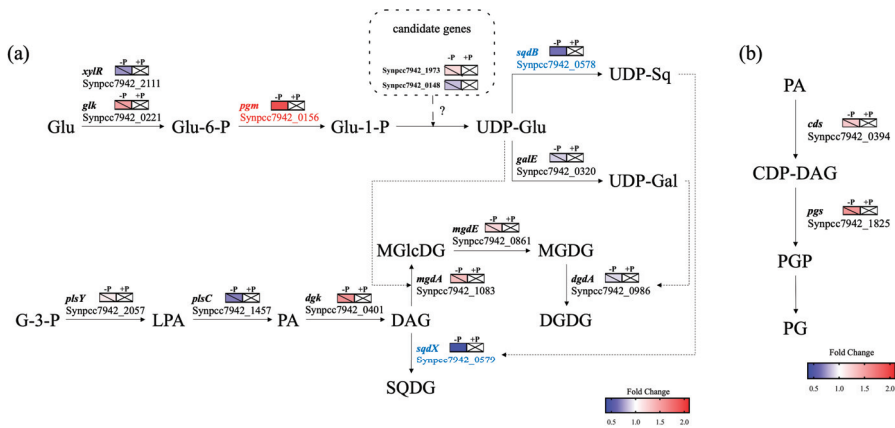

Figure 4. Metabolic pathway of glyceroglycolipid synthesis (**a**) and phospholipid synthesis (**b**) in *Synechococcus elongatus* PCC 7942. Pathways were reconstructed based on the KEGG annotation and the gene expression (colored rectangles) derived from transcriptome data of *S. elongatus* PCC 7942 (*p*-value < 0.05). Control groups (+P) are represented by rectangles with crosses. Genes up-regulated under phosphate starvation are indicated in red. Genes down-regulated are indicated in blue. Genes with no significant changes are indicated in black with diagonal lines in rectangles. *xylR*: xylose repressor (EC: 2.7.1.2); *glk*: glucokinase (EC: 2.7.1.2); *pgm*: phosphoglucomutase (EC: 5.4.2.2); *galE*: UDP-galactose epimerase (EC: 5.1.3.2); *sqdB*: UDP-sulfoquinovose synthase (EC: 3.13.1.1); *sqdX*: SQDG synthase (EC: 2.4.1.-); *plsY*: acyl-phosphate glycerol-3-phosphate acyltransferase (EC: 2.3.1.275); *plsC*: 1-acyl-sn-glycerol-3-phosphate acyltransferase (EC: 2.3.1.51); *dgk*: diacylglycerol kinase (EC: 2.7.1.107); *mgdA*: MGlcDG synthase (EC: 2.4.1.336); *mgdE*: MGlcDG epimerase (EC: 5.1.3.34); *dgdA*: DGDG synthase (EC: 2.4.1.241); *cds*: phosphatidate cytidylyltransferase (EC: 2.7.7.41); *pgs*: CDP-diacylglycerol-glycerol-3-phosphate 3-phosphatidyltransferase (EC: 2.7.8.5). Glu: glucose; Glu-6-P: glucose-6-phosphate; Glu-1-P: glucose-6-phosphate; UDP-Glu: UDP-glucose; UDP-Gal: UDP-galactose; UDP-Sq: UDP-sulfoquinovose; G-3-P: glycerol-3-phosphate; LPA: Lysophosphatidic acid; PA: phosphatidic acid; DAG: diacylglycerol; CDP-DAG: CDP-diacylglycerol; PGP: phosphatidylglycerophosphate; PG: phosphatidylglycerol; MGlcDG: monoglucosyl diacylglycerol; MGDG: monogalactosyl diacylglycerol; DGDG: digalactosyl diacylglycerol; SQDG: sulfoquinovosyl diacylglycerol.

Besides the de novo synthesis of glyceroglycolipids, phosphate starvation could directly influence phospholipid degradation through phospholipases [17,44,60] to provide precursors of glyceroglycolipids. The phosphatidic acid (PA) produced by type D phospholipases (PLDs) would also be a candidate in the activation of MGDG synthesis, acting as a signal molecule [61]. Unlike various phospholipids existing in plants, eukaryotic microalgae and other photosynthetic organisms, PG is the only phospholipid in the thylakoid and cytoplasmic membranes of cyanobacteria [62], but the phosphatidylglycerophosphatase (EC: 3.1.3.27) (pgp) responsible for PG synthesis remains unidentified in most cyanobacteria. Whereas PG was degraded by phosphate starvation in our previous study [43], no significant differences were shown in the expressions of the two annotated genes related to the PG synthesis (Figure 4b) and Synpcc7942_0302 coding of the only identified PLD (Supplementary Table S5). In *Nannochloropsis oceanica*, phospholipid degradation mainly resulted from the up-regulation of type A phospholipases (PLAs) under conditions of phosphate limitation, since PLD genes were suppressed [17], although phosphatidylcholine (PC) hydrolyzation by PLDs is a main strategy for phospholipid degradation under cold stress [63]. In *Synechocystis* PCC6803, the remolding of PG

involves reactions catalyzed by phospholipases A1 and A2, although the phospholipases have not yet been identified [64]. As yet, no homologs of PLA have been identified in *S. elongatus* PCC 7942.

The high catalytic rates of related enzymes may be a possible cause of this phenomenon. Besides, not all glyceroglycolipid-related genes respond to phosphate deficiency at the transcriptional level [29]. Meanwhile, the evidence in the literatures suggests that galactolipid synthesis in plants is not only modified at the transcriptional level, but also at the post-transcriptional [65] or post-translational level [61,66]. Selão et al. also demonstrated that lipid-synthesizing enzymes in both *Synechococcus* and *Synechocystis* must be regulated at the post-translational level, by temperature, rather than at the transcriptional level [45]. These results suggest that a more complicated regulatory mechanism exists in glyceroglycolipid synthesis.

2.5. Glyceroglycolipid Homeostasis in Glyceroglycolipid Synthesis under Phosphate Starvation

Microalgae, cyanobacteria and plants all possess mechanisms for establishing lipid homeostasis in thylakoid membranes [1]. The overexpressions of *sqdB* and *sqdX* would lead to up-regulations of *mgdA*, *mgdE* and *dgdA*, so as to maintain lipid homeostasis [67]. In this study, because DGDG increased and MGDG decreased under phosphate starvation, the MGDG/DGDG ratio fell to 5:3 on day 12 (4:1 in the phosphate-rich culture) (Figure 1b). This result was similar to the result for *M. subterraneus*, in which the MGDG/DGDG ratio was 2:1 in the control culture, which then decreased to about 1:1 under P-deprivation [68]. The MGDG/DGDG ratio appears stable under favorable controlled conditions [1], and it is crucial for the physical state of chloroplast membranes [68]. The control of the MGDG/DGDG ratio is a main feature of thylakoid lipid homeostasis [1]. Because of the decrease in the MGDG/DGDG ratio under phosphate starvation, more MGDG had to be synthesized in order to maintain the original MGDG/DGDG ratio. Besides, MGDG itself plays an important role in the proper development of thylakoid membranes in plants [65,69], and the synthesis of MGDG can be activated by lipid molecules (like PA, SQDG and PG) [45,66,70], indicating the importance of MGDG regulation in maintaining lipid homeostasis.

The expressions of *sqdB* and *sqdX* were down-regulated after 12 days of cultivation (Figure 2d,e and Figure 4a). It could be inferred that this phenomenon was associated with lipid homeostasis regulation. Because MGDG and SQDG are synthesized with the same precursors (diacylglycerol and UDP-glucose), the down-regulation of *sqdB* and *sqdX* could result in more precursors participating in MGDG synthesis. Besides, the down-regulation of *sqdB* and *sqdX* could also result in more precursors being available for DGDG synthesis. However, unlike DGDG synthesis, which is more strongly regulated at the transcriptional level, post-transcriptional and post-translational regulations are more important for MGDG synthesis in plants [65]. The increased level of SQDG under conditions of phosphate starvation could activate the activity of mgdA [45]. Thus, the available precursors provided by the down-regulation of *sqdB* and *sqdX* are likely to contribute more to MGDG synthesis. Moreover, the up-regulation of *pgm* (Figure 4a) could also provide an adequate precursor for MGDG synthesis. Under phosphate starvation, the MGDG/DGDG ratio increased back to 2:1 after 15 days of cultivation (Figure 1b). Thus, the down-regulation of *sqdB* and *sqdX*, together with the increased level of SQDG, contributed to the activating of MGDG synthesis under phosphate starvation.

Moreover, MGDG, DGDG and SQDG are essential for maintaining the stability of the photosystem [71,72]. Our previous study showed that the functions of the photosystem were nearly damaged when exposed to phosphate stress [43]. In this study, genes related to photosynthesis were repressed (Supplementary Table S6) by phosphate starvation. In plants, galactolipid biosyntheses are coordinated with photosynthetic protein synthesis [66]. Thus, the photosynthetic apparatus was likely to be disrupted, in part, by changes in the MGDG/DGDG ratio resulting from phosphate starvation, and a proper ratio of thylakoid membrane lipids was needed to help the photosynthetic apparatus recover.

In summary, in order to maintain the integrity of photosynthetic membranes and the photosynthetic apparatus, the regulation of glyceroglycolipid composition is based on the MGDG/DGDG ratio, which helps *S. elongatus* PCC 7942 maintain resiliency when exposed to favorable conditions in culture.

2.6. Regulatory Networks Involved in Glyceroglycolipid Synthesis

In plants and eukaryotic microalgae, some lipid-related transcription factors, like Dofs [73], are glyceroglycolipid-related. Nevertheless, transcriptional regulation is quite different between eukaryotes and prokaryotes. To determine the transcriptional regulators related to glyceroglycolipid metabolism under conditions of phosphate starvation in *S. elongatus* PCC 7942, 12 differentially expressed transcription regulators were selected, of which six were up-regulated and six were down-regulated (Table 1). These 12 transcription regulators can be divided into eight types: MarR family (1), MerR family (1), two component system (4), ArsR family (1), BadM/Rrf2 family (1), XRE family (2), GntR family (1) and DevT-like transcriptional factor (1). Most of these differentially expressed transcription regulators are involved in responses to various environmental stress conditions.

Table 1. Differentially expressed transcription regulators under phosphate starvation. Up-regulated genes (FC > 1) and down-regulated genes (FC < 1) were ordered by FC values.

Gene ID	Annotation	FC	*p*-Value
Synpcc7942_0938	transcriptional regulator, ArsR family	8.79281803	5.0074E-13
Synpcc7942_2585	transcriptional regulator, BadM/Rrf2 family	2.43751415	0.00232243
Synpcc7942_2416	two component transcriptional regulator, winged helix family	2.15739652	0.04603509
Synpcc7942_0110	transcriptional regulator, XRE family	2.13386852	0.02139503
Synpcc7942_1897	putative transcription factor DevT-like	2.12534589	0.00718275
Synpcc7942_1725	transcriptional regulator, GntR family	1.94907168	0.04567919
Synpcc7942_2305	two component transcriptional regulator, winged helix family, nblR	0.72020702	0.04515754
Synpcc7942_1739	transcriptional regulator, MerR family	0.61129814	0.02357565
Synpcc7942_0556	two component transcriptional regulator, winged helix family	0.61086684	0.01166383
Synpcc7942_2466	two component transcriptional regulator, winged helix family	0.58625772	0.03952819
Synpcc7942_1159	transcriptional regulator, MarR family	0.57296615	0.0038297
Synpcc7942_0764	transcriptional regulator, XRE family	0.47965835	0.00047173

However, the genes coding the SphS–SphR phosphate sensing system and genes regulated by the system [74] showed no significant differences on day 12 of phosphate starvation, suggesting that these genes may respond to phosphate starvation at an early stage. Interestingly, an OmpR family response regulator gene *nblR* (Synpcc7942_2305), which regulates the degradation of phycobilisome (PBS) through the *nbl* pathway, as an activator of the PBS degradation protein gene's (*nblA*) transcription under stresses [75], was down-regulated under phosphate starvation. However, *nblA* (Synpcc7942_2127) was significantly up-regulated (Supplementary Table S1), indicating that the down-regulation of *nblR* on day 12 was not to regulate PBS degradation. Sato et al. inferred that the *sqdB* might be involved in S-starvation-induced PBS degradation, particularly in *Synechococcus* [48]. It could be supposed that *sqdB* somehow belongs to the *nbl* pathway, and *nblR* is a probable signaling component in *sqdBX* regulation. In addition, some photosynthesis-associated transcription factors, like HY5 (a basic Leu zipper transcription factor) and GOLDEN2-LIKE (GLK), play pivotal roles in plant glyceroglycolipid regulation [66]. Therefore, glyceroglycolipid metabolism and the formation of photosynthetic machineries may be affected mutually. Besides, the up-regulated XRE family transcription regulator gene Synpcc7942_0110 was probably a hub gene under phosphate starvation, according to the protein–protein interaction analysis of DEGs (Supplementary Figure S3), which indicated that Synpcc7942_0110 played an important role in the global regulation of *S. elongatus* PCC 7942 under phosphate starvation.

The post-transcriptional and post-translational regulations are of great significance to glyceroglycolipid metabolism in plants. In the detached cotyledons of cucumber with impaired *csMGD1* expression, light may activate MGDG biosynthesis in a post-transcriptional manner [76]. According to transcriptome analysis, three genes involved in sulfur relay system were significantly up-regulated (Supplementary Tables S1 and S4), suggesting that active tRNA modification under phosphate starvation contributed to metabolic regulation [77,78]. The activities of MGDG synthases can be modified by thioredoxins at the post-translational level [66]. In this study, a thioredoxin

reductase gene (Synpcc7942_0623), a thioredoxin gene (Synpcc7942_1793) and a thioredoxin peroxidase gene (Synpcc7942_2309) were significantly up-regulated (Supplementary Table S1), all of which may contribute to activating MGDG synthesis. Like SQDG, PA and PG also play important roles in activating MGD1 [66,70]. Moreover, PG contributes to inducing MGDG synthesis by anchoring MGD1 and bringing substrates closer to the active site [66]. The information concerning the post-transcriptional and post-translational regulations involved in the glyceroglycolipid metabolism of cyanobacteria is still deficient, and thus more future studies are needed. In plants, auxin and cytokinin act as mediums between environmental conditions and the glyceroglycolipid metabolism [47,76]. Kobayashi et al. demonstrated that changes in plant membrane lipids during phosphate starvation are regulated by Pi signaling and auxin/cytokinin cross-talk [47]. In *S. elongatus* PCC 7942, increased SQDG, induced by overexpressions of *sqdB* and *sqdX*, would result in the abnormal expression of cell division-related genes and abnormal cell division [67]. The cell division protein gene *FtsQ* (Synpcc7942_2377) and the GroES protein gene (Synpcc7942_2314) involved in cell division were also important in global regulation under conditions of phosphate starvation (Supplementary Figure S3). Glyceroglycolipid synthesis and cell division could interact with each other. Taken together, it could be inferred that the glyceroglycolipid metabolism in cyanobacteria, under phosphate starvation, is regulated not only by Pi signaling, but also by other types of signaling and other metabolic pathways as well.

2.7. qRT-PCR Confirmations of Differentially Expressed Transcripts

qRT-PCR was used to confirm the accuracy of the transcriptomic analysis and measure the relative expression of selected transcripts. The results in Table 2 show that 82.4% of the measured transcripts (14 out of 17) followed the same trend as the RNA-Seq data, except for Synpcc7942_2416, Synpcc7942_1897 and Synpcc7942_1725. According to Celine, E. et al. [79], because of technical differences, over 80% of the measured genes having concordant expression represents a high concordance between RT-qPCR and RNA-seq. The expression of DEGs in transcriptomic analysis was reliable.

Table 2. qRT-PCR analysis of different genes under phosphate starvation in *Synechococcus elongatus* PCC 7942.

Gene ID	Annotation	FC	qRT-PCR
Synpcc7942_0938	transcriptional regulator, ArsR family	8.792818	$2^{3.18}$
Synpcc7942_2585	transcriptional regulator, BadM/Rrf2 family	2.437514	$2^{3.82}$
Synpcc7942_2416	two component transcriptional regulator, winged helix family	2.157397	$2^{-0.84}$
Synpcc7942_0110	transcriptional regulator, XRE family	2.133869	$2^{2.78}$
Synpcc7942_1897	putative transcription factor DevT-like	2.125346	$2^{-1.01}$
Synpcc7942_1725	transcriptional regulator, GntR family	1.949072	$2^{-1.58}$
Synpcc7942_1083	a probable glycosyltransferase, mgdA	1.33778	$2^{-0.14}$
Synpcc7942_0861	a conserved hypothetical protein, mgdE	1.205566	$2^{-0.43}$
Synpcc7942_0986	a probable glycosyltransferase, dgdA	0.90492	$2^{-0.32}$
Synpcc7942_2305	two component transcriptional regulator, winged helix family	0.720207	$2^{-2.79}$
Synpcc7942_0578	UDP-sulfoquinovose synthase, sqdB	0.634708	$2^{-3.54}$
Synpcc7942_1739	transcriptional regulator, MerR family	0.611298	$2^{-3.70}$
Synpcc7942_0556	two component transcriptional regulator, winged helix family	0.610867	$2^{-3.49}$
Synpcc7942_2466	two component transcriptional regulator, winged helix family	0.586258	$2^{-4.39}$
Synpcc7942_1159	transcriptional regulator, MarR family	0.572966	$2^{-4.38}$
Synpcc7942_0764	transcriptional regulator, XRE family	0.479658	$2^{-1.02}$
Synpcc7942_0579	sulfolipid sulfoquinovosyl diacylglycerol biosynthesis protein, sqdX	0.425591	$2^{-3.34}$

2.8. Reconstruction of Putative Glyceroglycolipid Regulatory Networks Based on Transcriptomic Evidence

Based on the transcriptomic evidence, a putative model for the glyceroglycolipids metabolism in *S. elongatus* PCC 7942, under phosphate starvation, was reconstructed (Figure 5).
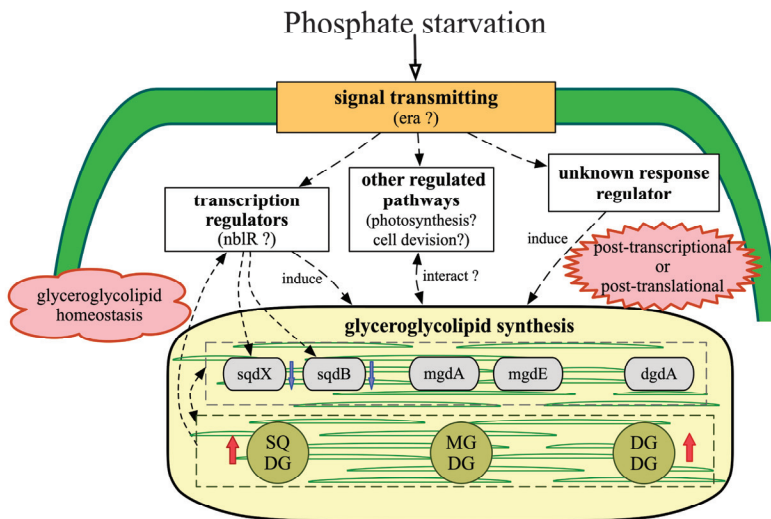
Figure 5. Putative model for glyceroglycolipid metabolism in *S. elongatus* PCC 7942 under phosphate starvation, reconstructed from transcriptomic evidence in this study. Dotted arrows indicate the regulation between each part.

Under phosphate starvation, the signals transmitting through GTP-binding proteins are active. The increase in total glyceroglycolipids mainly results from the accumulation of DGDG and SQDG as functional substitutes for phospholipids under phosphate starvation [43]. However, the changes in the composition of total glyceroglycolipids result in a sharp decrease of the MGDG/DGDG ratio, which disrupts the normal function of the plastid membrane [1]. To maintain glyceroglycolipid homeostasis, the down-regulations of *sqdB* and *sqdX* result in more precursors participating in MGDG synthesis, and the increased SQDG could act as an activator to enhance the activity of mgdA [45]. Transcriptional regulation, together with post-transcriptional and post-translational regulations, comprise an efficient strategy for glyceroglycolipid synthesis. Besides, glyceroglycolipids synthesis could interact with other metabolic pathways [66,67].

Hence, it could be proposed that the changes in glyceroglycolipid composition are emergency strategies of *S. elongatus* PCC 7942 adapting to phosphate starvation, and after 12 days of cultivation, glyceroglycolipid homeostasis plays a more important role in the recovery from phosphate starvation.

3. Materials and Methods

3.1. Cyanobacteria Species and Treatments

The cyanobacteria species in this study is *Synechococcus elongatus* PCC 7942 provided by Prof. Dingji Shi (Shanghai Ocean University, Shanghai, China).

S. elongatus PCC 7942 was cultivated in a 1-L Erlenmeyer flask with 500 mL working volume of modified BG-11 medium, under a temperature of 25 ± 2 °C and aeration rate of 140 μmol/m^2/s. Standard BG-11 contains 0.04 g/L K_2HPO_4 concentration, while phosphate-starved BG-11 lacks K_2HPO_4. The light intensity was 8000 lx. The initial pH was 8.0.

The culture's optical densities were measured at 730 nm by a UV-Vis spectrophotometer (Tianmei, Shanghai, China). Cell density was calculated with the equation: cell density (g/L) = $0.3349 \times OD_{730} - 0.0129$ ($R^2 = 0.9926$). Standard curves are shown in Supplementary Material, Figure S4.

3.2. Glyceroglycolipid Analysis

Three different glyceroglycolipids were separated with a modified method of thin-layer chromatography (TLC) (Huanghai, Yantai, China) [43,80]. First, total lipids were extracted from cyanobacteria with a modified method [2,81]. Freeze-dried cyanobacteria powder (0.2 g) was broken by a cell crusher (Tissuelyser-24, Jingxin, Shanghai) at 50 Hz for 10 min. Then the broken cells were suspended in a 5-mL solvent mixture of chloroform/methanol (v/v 2:1). After being stirred for 20 min, the samples were centrifuged at 8000 rpm for 10 min. The procedure was repeated three times until the total lipids were fully extracted. The solvent phase was transferred and evaporated in a water bath (Shanghai YIHENG Technical Co. Ltd., Shanghai, China) at 65 °C and then dried in a drying oven (Jinghong, Shanghai, China) at 50 °C until the weight was stable. Then the total lipids were weighed with analytical balance (BS 124S, Sartorius, Göttingen, Germany) and redissolved in chloroform/methanol (v/v 2:1) at a concentration of 10 μg/μL. The developing solvent was acetone/toluene/water (v/v/v 91:30:8). Different glyceroglycolipids were visualized in iodine vapor.

For quantitative analysis, fatty acid methyl esters of each glyceroglycolipid were prepared with 2 mL anhydrous 1 N methanolic HCl, and then incubated at 80 °C for 30 min [82]. The fatty acid profiles of different glyceroglycolipids were analyzed by AutoSystem XL GC/TurboMass MS (Perkin Elmer, Rodgau, Germany) [81]. The internal control was nonadecanoic acid.

The methods of calculating the content of each glyceroglycolipid were based on the method of Benning [80]. A total of six samples (two for each of the three cultures) per strain were analyzed, and means and standard deviations were calculated.

3.3. RNA Extraction, Library Preparation and Sequencing

Cyanobacteria cells were harvested in triplicate by centrifugation on day 12 under the phosphate concentrations of 0 and 0.04 g/L, respectively. Cells were immediately transferred to liquid nitrogen for later processing. Total RNA of each harvested sample was extracted with TRIzol reagent (Invitrogen Life Technologies) according to the manufacturer's protocol. The sequencing library of each harvested sample was generated using a TruSeq RNA Sample Preparation Kit (Illumina, San Diego, CA, USA). The library was then sequenced on a HiSeq platform (Illumina) by Shanghai GeneFund Biotechnology Co. Ltd.

3.4. Transcript Quantification and Differential Expression Analysis

The clean reads were obtained by trimming raw reads from the sequencing with a Cutadapt tool [83] and a Trimmomatic tool [84]. The quality of clean reads was also assessed via FastQC tool [85]. Then, the high-quality trimmed reads were mapped to the reference genome by Bowtie2 [86]. Gene expression data were obtained and quantified with the fragments per kilobase of exon per million reads mapped method (FPKM) by HTSeq [87]. Empirical analysis of Digital Gene Expression in R (EdgeR) was applied for differential expression analysis [88]. Genes with p-value < 0.05 and fold change values (FC) ≥ 2 or ≤ 0.5 were regarded as DEGs.

GO enrichment analysis and KEGG enrichment analysis of DEGs were performed based on the hypergeometric distribution [89]. All DEGs were mapped to each GO term [90] and KEGG pathway [91]. The GO terms and the KEGG pathways of DEGs with a p-value < 0.05 were considered significantly enriched.

3.5. Experimental Validation of Gene Expression with qRT-PCR

The synthesis of cDNA was performed using FastKing RT Kit (With gDNase) (TIANGEN, Beijing, China). The gene-specific quantitative real-time PCR primers used in this study were documented in Supplementary Table S7. Real-time PCR was performed using a SuperReal PreMix Plus (SYBR Green) (TIANGEN, Beijing, China), and was carried out using an Eppendorf Mcep Realplex 4s System (Eppendorf, Hamburg, Germany). Reactions started at 95 °C for 15 min, followed by 40 cycles of 95 °C for 10 s and 60 °C for 25 s, and a melting curve step at 60–95 °C. Each qRT-PCR reaction

was performed on three biological replicates. The relative expression levels were normalized to the glyceraldehyde-3-phosphate dehydrogenase (GAPDH) gene (*gap3*, Synpcc7942_1939), RNA polymerase sigma factor gene (*rpoD*, Synpcc7942_0649) [92] and phosphoenolpyruvate carboxylase gene (*ppc*, Synpcc7942_2252) [93], and were calculated using the $2^{-\Delta\Delta CT}$ method [94].

4. Conclusions

The glyceroglycolipid composition of *S. elongatus* PCC 7942 changes to adapt to phosphate starvation. Glyceroglycolipid composition is regulated post-transcriptionally or post-translationally, allowing for more efficient adaptation to phosphate stress conditions. However, after 12 days of cultivation, the glyceroglycolipid composition is mainly regulated based on the MGDG/DGDG ratio in order to maintain the glyceroglycolipid homeostasis, which is beneficial in maintaining resilience when exposed to the preferred culture conditions again.

Supplementary Materials: The following are available online at http://www.mdpi.com/1660-3397/18/7/360/s1, Figure S1: Total glyceroglycolipids content under phosphate starvation. Values are the means ± standard deviations from the three separately grown cultures. Figure S2: Glyceroglycolipids relative content under phosphate starvation given by TLC-scanner. (a) MGDG. (b) DGDG. (c) SQDG. Values are the means ± standard deviations from the three separately grown cultures. Figure S3: PPI analysis of differentially expressed genes in *Synechococcus elongatus* PCC 7942 under different phosphate concentrations (0, 0.04g/L) after being cultivated for 12 days (Genes with annotation in String database are represented by abbreviation. Genes without annotation in String database are represented by gene number. Names of genes with degree less than 5 are not shown). Figure S4: Standard curve of OD_{730} and Dry Cell Weight of *Synechococcus elongatus* PCC 7942. Table S1: Differentially expressed genes under phosphate starvation in *Synechococcus elongatus* PCC 7942. Table S2: Enriched GO terms under phosphate starvation in *Synechococcus elongatus* PCC 7942. Table S3: Expression of genes in GO term GTP binding in *Synechococcus elongatus* PCC 7942 under phosphate starvation. Table S4: Enriched KEGG pathways under phosphate starvation in *Synechococcus elongatus* PCC 7942. Table S5: Expression of genes participating in glyceroglycolipid synthesis in *Synechococcus elongatus* PCC 7942 under phosphate starvation. Table S6: Expression of genes related to photosynthesis in *Synechococcus elongatus* PCC 7942 under phosphate starvation. Table S7: Primers used in qRT-PCR.

Author Contributions: Conceptualization, X.X. and X.M.; methodology, X.X. and X.M.; software, X.X.; validation, X.X. and X.M.; formal analysis, X.X.; investigation, X.X.; resources, X.X. and X.M.; data curation, X.X.; writing—original draft preparation, X.X.; writing—review and editing, X.X. and X.M.; visualization, X.X.; supervision, X.M.; project administration, X.M.; funding acquisition, X.M. All authors have read and agreed to the published version of the manuscript.

Conflicts of Interest: The authors declare no conflict of interest.

References

1. Boudiere, L.; Michaud, M.; Petroutsos, D.; Rebeille, F.; Falconet, D.; Bastien, O.; Roy, S.; Finazzi, G.; Rolland, N.; Jouhet, J.; et al. Glycerolipids in photosynthesis: Composition, synthesis and trafficking. *Biochim. Biophys. Acta* **2014**, *1837*, 470–480. [CrossRef]

2. Wang, X.; Shen, Z.; Miao, X. Nitrogen and hydrophosphate affects glycolipids composition in microalgae. *Sci. Rep.* **2016**, *6*, 30145. [CrossRef] [PubMed]

3. Zhang, J.; Li, C.; Yu, G.; Guan, H. Total synthesis and structure-activity relationship of glycoglycerolipids from marine organisms. *Mar. Drugs* **2014**, *12*, 3634–3659. [CrossRef] [PubMed]

4. Andrianasolo, E.H.; Haramaty, L.; Vardi, A.; White, E.; Lutz, R.; Falkowski, P. Apoptosis-Inducing Galactolipids from a Cultured Marine Diatom, Phaeodactylum tricornutum. *J. Nat. Prod.* **2008**, *71*, 1197–1201. [CrossRef]

5. Riccio, G.; De Luca, D.; Lauritano, C. Monogalactosyldiacylglycerol and Sulfolipid Synthesis in Microalgae. *Mar. Drugs* **2020**, *18*, 237. [CrossRef] [PubMed]

6. Morimoto, T.; Nagatsu, A.; Murakami, N.; Sakakibara, J.; Tokuda, H.; Nishino, H.; Iwashima, A. Anti-tumour-promoting glyceroglycolipids from the green alga, chlorella vulgaris. *Phytochemistry* **1995**, *40*, 1433–1437. [CrossRef]

7. Shirahashi, H.; Murakami, N.; Watanabe, M.; Nagatsu, A.; Sakakibara, J.; Tokuda, H.; Nishino, H.; Iwashima, A. Isolation and identification of anti-tumor-promoting principles from the fresh-water cyanobacterium Phormidium tenue. *Chem. Pharm. Bull.* **1993**, *41*, 1664–1666. [CrossRef] [PubMed]

8. Mizushina, Y.; Watanabe, I.; Ohtaa, K.; Takemura, M.; Sahara, H.; Takahashi, N.; Gasa, S.; Sugawara, F.; Matsukage, A.; Yoshida, S.; et al. Studies on inhibitors of mammalian DNA polymerase α and β: Sulfolipids from a pteridophyte, *Athyrium niponicum*. *Biochem. Pharmacol.* **1998**, *55*, 537–541. [CrossRef]

9. Gustafson, K.R.; Cardellina, J.H.; Fuller, R.W.; Weislow, O.S.; Kiser, R.F.; Snader, K.M.; Patterson, G.M.L.; Boyd, M.R. AIDS-Antiviral Sulfolipids From Cyanobacteria (Blue-Green Algae). *J. Natl. Cancer Inst.* **1989**, *81*, 1254–1258. [CrossRef]

10. Loya, S.; Reshef, V.; Mizrachi, E.; Silberstein, C.; Rachamim, Y.; Carmeli, S.; Hizi, A. The Inhibition of the Reverse Transcriptase of HIV-1 by the Natural Sulfoglycolipids from Cyanobacteria: Contribution of Different Moieties to Their High Potency. *J. Nat. Prod.* **1998**, *61*, 891–895. [CrossRef]

11. Alipanah, L.; Winge, P.; Rohloff, J.; Najafi, J.; Brembu, T.; Bones, A.M. Molecular adaptations to phosphorus deprivation and comparison with nitrogen deprivation responses in the diatom Phaeodactylum tricornutum. *PLoS ONE* **2018**, *13*, e0193335. [CrossRef] [PubMed]

12. Murakami, H.; Nobusawa, T.; Hori, K.; Shimojima, M.; Ohta, H. Betaine Lipid Is Crucial for Adapting to Low Temperature and Phosphate Deficiency in Nannochloropsis. *Plant Physiol.* **2018**, *177*, 181–193. [CrossRef] [PubMed]

13. Nakamura, Y. Phosphate starvation and membrane lipid remodeling in seed plants. *Prog. Lipid Res.* **2013**, *52*, 43–50. [CrossRef] [PubMed]

14. Shimojima, M. Biosynthesis and functions of the plant sulfolipid. *Prog. Lipid Res.* **2011**, *50*, 234–239. [CrossRef] [PubMed]

15. Lu, N.; Wei, D.; Chen, F.; Yang, S.T. Lipidomic profiling reveals lipid regulation in the snow alga Chlamydomonas nivalis in response to nitrate or phosphate deprivation. *Process. Biochem.* **2013**, *48*, 605–613. [CrossRef]

16. Liang, K.; Zhang, Q.; Gu, M.; Cong, W. Effect of phosphorus on lipid accumulation in freshwater microalga *Chlorella* sp. *J. Appl. Phycol.* **2012**, *25*, 311–318. [CrossRef]

17. Muhlroth, A.; Winge, P.; El Assimi, A.; Jouhet, J.; Marechal, E.; Hohmann-Marriott, M.F.; Vadstein, O.; Bones, A.M. Mechanisms of Phosphorus Acquisition and Lipid Class Remodeling under P Limitation in a Marine Microalga. *Plant Physiol.* **2017**, *175*, 1543–1559. [CrossRef]

18. Gasparovic, B.; Godrijan, J.; Frka, S.; Tomazic, I.; Penezic, A.; Maric, D.; Djakovac, T.; Ivancic, I.; Paliaga, P.; Lyons, D.; et al. Adaptation of marine plankton to environmental stress by glycolipid accumulation. *Mar. Environ. Res.* **2013**, *92*, 120–132. [CrossRef]

19. Yu, B.; Xu, C.; Benning, C. *Arabidopsis* disrupted in SQD2 encoding sulfolipid synthase is impaired in phosphate-limited growth. *Proc. Natl. Acad. Sci. USA* **2002**, *99*, 5732–5737. [CrossRef]

20. Li-Beisson, Y.; Thelen, J.J.; Fedosejevs, E.; Harwood, J.L. The lipid biochemistry of eukaryotic algae. *Prog. Lipid Res.* **2019**, *74*, 31–68. [CrossRef]

21. Frentzen, M. Phosphatidylglycerol and sulfoquinovosyldiacylglycerol: Anionic membrane lipids and phosphate regulation. *Curr. Opin. Plant Biol.* **2004**, *7*, 270–276. [CrossRef] [PubMed]

22. Villanueva, L.; Bale, N.; Hopmans, E.C.; Schouten, S.; Damste, J.S. Diversity and distribution of a key sulpholipid biosynthetic gene in marine microbial assemblages. *Environ. Microbiol.* **2014**, *16*, 774–787. [CrossRef] [PubMed]

23. Hölzl, G.; Dörmann, P. Chloroplast Lipids and Their Biosynthesis. *Annu. Rev. Plant Biol.* **2019**, *70*, 51–81. [CrossRef] [PubMed]

24. Aronsson, H.; Schottler, M.A.; Kelly, A.A.; Sundqvist, C.; Dormann, P.; Karim, S.; Jarvis, P. Monogalactosyldiacylglycerol deficiency in *Arabidopsis* affects pigment composition in the prolamellar body and impairs thylakoid membrane energization and photoprotection in leaves. *Plant Physiol.* **2008**, *148*, 580–592. [CrossRef]

25. Murakawa, M.; Shimojima, M.; Shimomura, Y.; Kobayashi, K.; Awai, K.; Ohta, H. Monogalactosyldiacylglycerol synthesis in the outer envelope membrane of chloroplasts is required for enhanced growth under sucrose supplementation. *Front. Plant Sci.* **2014**, *5*, 280. [CrossRef]

26. Miège, C.; Maréchal, E.; Shimojima, M.; Awai, K.; Block, M.A.; Ohta, H.; Takamiya, K.; Douce, R.; Joyard, J. Biochemical and topological properties of type A MGDG synthase, a spinach chloroplast envelope enzyme

catalyzing the synthesis of both prokaryotic and eukaryotic MGDG. *Eur. J. Biochem.* **1999**, *265*, 990–1001. [CrossRef]

27. Froehlich, J.E.; Benning, C.; Dormann, P. The digalactosyldiacylglycerol (DGDG) synthase DGD1 is inserted into the outer envelope membrane of chloroplasts in a manner independent of the general import pathway and does not depend on direct interaction with monogalactosyldiacylglycerol synthase for DGDG biosynthesis. *J. Biol. Chem.* **2001**, *276*, 31806–31812. [CrossRef]

28. Kelly, A.A.; Dormann, P. DGD2, an *Arabidopsis* gene encoding a UDP-galactose-dependent digalactosyldiacylglycerol synthase is expressed during growth under phosphate-limiting conditions. *J. Biol. Chem.* **2002**, *277*, 1166–1173. [CrossRef]

29. Awai, K.; Marechal, E.; Block, M.A.; Brun, D.; Masuda, T.; Shimada, H.; Takamiya, K.; Ohta, H.; Joyard, J. Two types of MGDG synthase genes, found widely in both 16:3 and 18:3 plants, differentially mediate galactolipid syntheses in photosynthetic and nonphotosynthetic tissues in *Arabidopsis thaliana*. *Proc. Natl. Acad. Sci. USA* **2001**, *98*, 10960–10965. [CrossRef]

30. Riekhof, W.R.; Sears, B.B.; Benning, C. Annotation of genes involved in glycerolipid biosynthesis in Chlamydomonas reinhardtii: Discovery of the betaine lipid synthase BTA1Cr. *Eukaryot. Cell* **2005**, *4*, 242–252. [CrossRef]

31. Awai, K.; Watanabe, H.; Benning, C.; Nishida, I. Digalactosyldiacylglycerol is required for better photosynthetic growth of *Synechocystis* sp. PCC6803 under phosphate limitation. *Plant Cell Physiol.* **2007**, *48*, 1517–1523. [CrossRef] [PubMed]

32. Maida, E.; Awai, K. Digalactosyldiacylglycerol is essential in *Synechococcus elongatus* PCC 7942, but its function does not depend on its biosynthetic pathway. *Biochim. Biophys. Acta* **2016**, *1861*, 1309–1314. [CrossRef] [PubMed]

33. Sato, N.; Awai, K. Diversity in Biosynthetic Pathways of Galactolipids in the Light of Endosymbiotic Origin of Chloroplasts. *Front. Plant Sci.* **2016**, *7*, 117. [CrossRef] [PubMed]

34. Yuzawa, Y.; Shimojima, M.; Sato, R.; Mizusawa, N.; Ikeda, K.; Suzuki, M.; Iwai, M.; Hori, K.; Wada, H.; Masuda, S.; et al. Cyanobacterial monogalactosyldiacylglycerol-synthesis pathway is involved in normal unsaturation of galactolipids and low-temperature adaptation of *Synechocystis* sp. PCC 6803. *Biochim. Biophys. Acta* **2014**, *1841*, 475–483. [CrossRef] [PubMed]

35. Awai, K.; Kakimoto, T.; Awai, C.; Kaneko, T.; Nakamura, Y.; Takamiya, K.; Wada, H.; Ohta, H. Comparative genomic analysis revealed a gene for monoglucosyldiacylglycerol synthase, an enzyme for photosynthetic membrane lipid synthesis in cyanobacteria. *Plant Physiol.* **2006**, *141*, 1120–1127. [CrossRef]

36. Awai, K.; Ohta, H.; Sato, N. Oxygenic photosynthesis without galactolipids. *Proc. Natl. Acad. Sci. USA* **2014**, *111*, 13571–13575. [CrossRef]

37. Kobayashi, K.; Awai, K.; Nakamura, M.; Nagatani, A.; Masuda, T.; Ohta, H. Type-B monogalactosyldiacylglycerol synthases are involved in phosphate starvation-induced lipid remodeling, and are crucial for low-phosphate adaptation. *Plant J.* **2009**, *57*, 322–331. [CrossRef]

38. Kelly, A.A.; Froehlich, J.E.; Dormann, P. Disruption of the two digalactosyldiacylglycerol synthase genes DGD1 and DGD2 in *Arabidopsis* reveals the existence of an additional enzyme of galactolipid synthesis. *Plant Cell* **2003**, *15*, 2694–2706. [CrossRef]

39. Okazaki, Y.; Shimojima, M.; Sawada, Y.; Toyooka, K.; Narisawa, T.; Mochida, K.; Tanaka, H.; Matsuda, F.; Hirai, A.; Hirai, M.Y.; et al. A Chloroplastic UDP-Glucose Pyrophosphorylase from *Arabidopsis* Is the Committed Enzyme for the First Step of Sulfolipid Biosynthesis. *Plant Cell* **2009**, *21*, 892–909. [CrossRef]

40. Kang, N.K.; Kim, E.K.; Sung, M.G.; Kim, Y.U.; Jeong, B.R.; Chang, Y.K. Increased biomass and lipid production by continuous cultivation of Nannochloropsis salina transformant overexpressing a bHLH transcription factor. *Biotechnol. Bioeng.* **2019**, *116*, 555–568. [CrossRef]

41. Kwon, S.; Kang, N.K.; Koh, H.G.; Shin, S.E.; Lee, B.; Jeong, B.R.; Chang, Y.K. Enhancement of biomass and lipid productivity by overexpression of a bZIP transcription factor in *Nannochloropsis salina*. *Biotechnol. Bioeng.* **2018**, *115*, 331–340. [CrossRef] [PubMed]

42. Zhang, J.; Hao, Q.; Bai, L.; Xu, J.; Yin, W.; Song, L.; Xu, L.; Guo, X.; Fan, C.; Chen, Y.; et al. Overexpression of the soybean transcription factor GmDof4 significantly enhances the lipid content of *Chlorella ellipsoidea*. *Biotechnol. Biofuels* **2014**, *7*, 128. [CrossRef]

43. Peng, Z.; Feng, L.; Wang, X.; Miao, X. Adaptation of *Synechococcus* sp. PCC 7942 to phosphate starvation by glycolipid accumulation and membrane lipid remodeling. *Biochim. Biophys. Acta* **2019**, *1864*, 158522. [CrossRef]

44. Abida, H.; Dolch, L.J.; Mei, C.; Villanova, V.; Conte, M.; Block, M.A.; Finazzi, G.; Bastien, O.; Tirichine, L.; Bowler, C.; et al. Membrane glycerolipid remodeling triggered by nitrogen and phosphorus starvation in Phaeodactylum tricornutum. *Plant Physiol.* **2015**, *167*, 118–136. [CrossRef] [PubMed]

45. Selao, T.T.; Zhang, L.; Arioz, C.; Wieslander, A.; Norling, B. Subcellular localization of monoglucosyldiacylglycerol synthase in *Synechocystis* sp. PCC6803 and its unique regulation by lipid environment. *PLoS ONE* **2014**, *9*, e88153. [CrossRef] [PubMed]

46. Shimojima, M.; Tsuchiya, M.; Ohta, H. Temperature-dependent hyper-activation of monoglucosyldiacylglycerol synthase is post-translationally regulated in *Synechocystis* sp. PCC 6803. *FEBS Lett.* **2009**, *583*, 2372–2376. [CrossRef] [PubMed]

47. Kobayashi, K.; Masuda, T.; Takamiya, K.; Ohta, H. Membrane lipid alteration during phosphate starvation is regulated by phosphate signaling and auxin/cytokinin cross-talk. *Plant J.* **2006**, *47*, 238–248. [CrossRef]

48. Sato, N.; Kamimura, R.; Kaneta, K.; Yoshikawa, M.; Tsuzuki, M. Species-specific roles of sulfolipid metabolism in acclimation of photosynthetic microbes to sulfur-starvation stress. *PLoS ONE* **2017**, *12*, e0186154. [CrossRef] [PubMed]

49. Voshol, G.P.; Meyer, V.; van den Hondel, C.A. GTP-binding protein Era: A novel gene target for biofuel production. *BMC Biotechnol.* **2015**, *15*, 21. [CrossRef]

50. Johnstone, B.H.; Handler, A.A.; Chao, D.K.; Nguyen, V.; Smith, M.; Ryu, S.Y.; Simons, E.L.; Anderson, P.E.; Simons, R.W. The widely conserved Era G-protein contains an RNA-binding domain required for Era function in vivo. *Mol. Microbiol.* **1999**, *33*, 1118–1131. [CrossRef]

51. Cheng, P.; Li, H.; Yuan, L.; Li, H.; Xi, L.; Zhang, J.; Liu, J.; Wang, Y.; Zhao, H.; Zhao, H.; et al. The ERA-Related GTPase AtERG2 Associated with Mitochondria 18S RNA Is Essential for Early Embryo Development in *Arabidopsis*. *Front. Plant Sci.* **2018**, *9*, 182. [CrossRef]

52. Suwastika, I.N.; Denawa, M.; Yomogihara, S.; Im, C.H.; Bang, W.Y.; Ohniwa, R.L.; Bahk, J.D.; Takeyasu, K.; Shiina, T. Evidence for lateral gene transfer (LGT) in the evolution of eubacteria-derived small GTPases in plant organelles. *Front. Plant Sci.* **2014**, *5*, 678. [CrossRef] [PubMed]

53. Jeon, Y.; Ahn, C.S.; Jung, H.J.; Kang, H.; Park, G.T.; Choi, Y.; Hwang, J.; Pai, H.S. DER containing two consecutive GTP-binding domains plays an essential role in chloroplast ribosomal RNA processing and ribosome biogenesis in higher plants. *J. Exp. Bot.* **2014**, *65*, 117–130. [CrossRef] [PubMed]

54. Sun, Y.; Tian, Y.; Cheng, S.; Wang, Y.; Hao, Y.; Zhu, J.; Zhu, X.; Zhang, Y.; Yu, M.; Lei, J.; et al. WSL6 encoding an Era-type GTP-binding protein is essential for chloroplast development in rice. *Plant Mol. Biol.* **2019**. [CrossRef] [PubMed]

55. Yan, Y.; Zheng, X.; Apaliya, M.T.; Yang, H.; Zhang, H. Transcriptome characterization and expression profile of defense-related genes in pear induced by Meyerozyma guilliermondii. *Postharvest Biol. Technol.* **2018**, *141*, 63–70. [CrossRef]

56. Choi, S.Y.; Park, B.; Choi, I.G.; Sim, S.J.; Lee, S.M.; Um, Y.; Woo, H.M. Transcriptome landscape of Synechococcus elongatus PCC 7942 for nitrogen starvation responses using RNA-seq. *Sci. Rep.* **2016**, *6*, 30584. [CrossRef] [PubMed]

57. Verstraeten, N.; Fauvart, M.; Versees, W.; Michiels, J. The universally conserved prokaryotic GTPases. *Microbiol. Mol. Biol. Rev.* **2011**, *75*, 507–542. [CrossRef] [PubMed]

58. Du, W.; Liang, F.; Duan, Y.; Tan, X.; Lu, X. Exploring the photosynthetic production capacity of sucrose by cyanobacteria. *Metab. Eng.* **2013**, *19*, 17–25. [CrossRef]

59. Maeda, K.; Narikawa, R.; Ikeuchi, M. CugP is a novel ubiquitous non-GalU-type bacterial UDP-glucose pyrophosphorylase found in cyanobacteria. *J. Bacteriol.* **2014**, *196*, 2348–2354. [CrossRef]

60. Zavaleta-Pastor, M.; Sohlenkamp, C.; Gao, J.L.; Guan, Z.; Zaheer, R.; Finan, T.M.; Raetz, C.R.; Lopez-Lara, I.M.; Geiger, O. Sinorhizobium meliloti phospholipase C required for lipid remodeling during phosphorus limitation. *Proc. Natl. Acad. Sci. USA* **2010**, *107*, 302–307. [CrossRef]

61. Boudiere, L.; Botte, C.Y.; Saidani, N.; Lajoie, M.; Marion, J.; Brehelin, L.; Yamaryo-Botte, Y.; Satiat-Jeunemaitre, B.; Breton, C.; Girard-Egrot, A.; et al. Galvestine-1, a novel chemical probe for the study of the glycerolipid homeostasis system in plant cells. *Mol. Biosyst.* **2012**, *8*, 2023–2035. [CrossRef]

62. Wada, H.; Murata, N. Membrane Lipids in Cyanobacteria. In *Lipids in Photosynthesis: Structure, Function and Genetics*; Springer: Dordrecht, The Netherlands, 1998.

63. Gu, Y.; He, L.; Zhao, C.; Wang, F.; Yan, B.; Gao, Y.; Li, Z.; Yang, K.; Xu, J. Biochemical and Transcriptional Regulation of Membrane Lipid Metabolism in Maize Leaves under Low Temperature. *Front. Plant Sci.* **2017**, *8*, 2053. [CrossRef] [PubMed]

64. Laczko-Dobos, H.; Frycak, P.; Ughy, B.; Domonkos, I.; Wada, H.; Prokai, L.; Gombos, Z. Remodeling of phosphatidylglycerol in *Synechocystis* PCC6803. *Biochim. Biophys. Acta* **2010**, *1801*, 163–170. [CrossRef] [PubMed]

65. Kobayashi, K.; Fujii, S.; Sasaki, D.; Baba, S.; Ohta, H.; Masuda, T.; Wada, H. Transcriptional regulation of thylakoid galactolipid biosynthesis coordinated with chlorophyll biosynthesis during the development of chloroplasts in *Arabidopsis*. *Front. Plant Sci.* **2014**, *5*, 272. [CrossRef] [PubMed]

66. Kobayashi, K. Role of membrane glycerolipids in photosynthesis, thylakoid biogenesis and chloroplast development. *J. Plant Res.* **2016**, *129*, 565–580. [CrossRef] [PubMed]

67. Sato, N.; Ebiya, Y.; Kobayashi, R.; Nishiyama, Y.; Tsuzuki, M. Disturbance of cell-size determination by forced overproduction of sulfoquinovosyl diacylglycerol in the cyanobacterium *Synechococcus elongatus* PCC 7942. *Biochem. Biophys. Res. Commun.* **2017**, *487*, 734–739. [CrossRef]

68. Khozin-Goldberg, I.; Cohen, Z. The effect of phosphate starvation on the lipid and fatty acid composition of the fresh water eustigmatophyte Monodus subterraneus. *Phytochemistry* **2006**, *67*, 696–701. [CrossRef]

69. Masuda, S.; Harada, J.; Yokono, M.; Yuzawa, Y.; Shimojima, M.; Murofushi, K.; Tanaka, H.; Masuda, H.; Murakawa, M.; Haraguchi, T.; et al. A Monogalactosyldiacylglycerol Synthase Found in the Green Sulfur Bacterium Chlorobaculum tepidum Reveals Important Roles for Galactolipids in Photosynthesis. *Plant Cell* **2011**, *23*, 2644–2658. [CrossRef]

70. Dubots, E.; Botte, C.; Boudiere, L.; Yamaryo-Botte, Y.; Jouhet, J.; Marechal, E.; Block, M.A. Role of phosphatidic acid in plant galactolipid synthesis. *Biochimie* **2012**, *94*, 86–93. [CrossRef]

71. Sakurai, I.; Mizusawa, N.; Wada, H.; Sato, N. Digalactosyldiacylglycerol is required for stabilization of the oxygen-evolving complex in photosystem II. *Plant Physiol.* **2007**, *145*, 1361–1370. [CrossRef]

72. Kobayashi, K.; Narise, T.; Sonoike, K.; Hashimoto, H.; Sato, N.; Kondo, M.; Nishimura, M.; Sato, M.; Toyooka, K.; Sugimoto, K.; et al. Role of galactolipid biosynthesis in coordinated development of photosynthetic complexes and thylakoid membranes during chloroplast biogenesis in *Arabidopsis*. *Plant J.* **2013**, *73*, 250–261. [CrossRef] [PubMed]

73. Manan, S.; Chen, B.; She, G.; Wan, X.; Zhao, J. Transport and transcriptional regulation of oil production in plants. *Crit. Rev. Biotechnol.* **2016**, *37*, 641–655. [CrossRef] [PubMed]

74. Tiwari, B.; Singh, S.; Kaushik, M.S.; Mishra, A.K. Regulation of organophosphate metabolism in cyanobacteria. A review. *Microbiology* **2015**, *84*, 291–302. [CrossRef]

75. Salinas, P.; Ruiz, D.; Cantos, R.; Lopez-Redondo, M.L.; Marina, A.; Contreras, A. The regulatory factor SipA provides a link between NblS and NblR signal transduction pathways in the cyanobacterium *Synechococcus* sp. PCC 7942. *Mol. Microbiol.* **2007**, *66*, 1607–1619. [CrossRef]

76. Yamaryo, Y.; Kanai, D.; Awai, K.; Shimojima, M.; Masuda, T.; Shimada, H.; Takamiya, K.-I.; Ohta, H. Light and Cytokinin Play a Co-operative Role in MGDG Synthesis in Greening Cucumber Cotyledons. *Plant Cell Physiol.* **2003**, *44*, 844–855. [CrossRef]

77. El Yacoubi, B.; Bailly, M.; de Crecy-Lagard, V. Biosynthesis and function of posttranscriptional modifications of transfer RNAs. *Annu. Rev. Genet.* **2012**, *46*, 69–95. [CrossRef]

78. Wang, Y.; Pang, C.; Li, X.; Hu, Z.; Lv, Z.; Zheng, B.; Chen, P. Identification of tRNA nucleoside modification genes critical for stress response and development in rice and *Arabidopsis*. *BMC Plant Biol.* **2017**, *17*, 261. [CrossRef] [PubMed]

79. Everaert, C.; Luypaert, M.; Maag, J.L.V.; Cheng, Q.X.; Dinger, M.E.; Hellemans, J.; Mestdagh, P. Benchmarking of RNA-sequencing analysis workflows using whole-transcriptome RT-qPCR expression data. *Sci. Rep.* **2017**, *7*, 1–11. [CrossRef]

80. Hartel, H.; Dormann, P.; Benning, C. DGD1-independent biosynthesis of extraplastidic galactolipids after phosphate deprivation in *Arabidopsis*. *Proc. Natl. Acad. Sci. USA* **2000**, *97*, 10649–10654. [CrossRef]

81. Wu, H.; Miao, X. Biodiesel quality and biochemical changes of microalgae *Chlorella pyrenoidosa* and *Scenedesmus obliquus* in response to nitrate levels. *Bioresour. Technol.* **2014**, *170*, 421–427. [CrossRef] [PubMed]

82. Peng, Z.; Miao, X. Monoglucosyldiacylglycerol participates in phosphate stress adaptation in *Synechococcus* sp. PCC 7942. *Biochem. Biophys. Res. Commun.* **2020**, *522*, 662–668. [CrossRef] [PubMed]

83. Martin, M. Cutadapt removes adapter sequences from high-throughput sequencing reads. *EMBnet. J.* **2011**, *17*, 10–12. [CrossRef]

84. Bolger, A.M.; Lohse, M.; Usadel, B. Trimmomatic: A flexible trimmer for Illumina sequence data. *Bioinformatics* **2014**, *30*, 2114–2120. [CrossRef]

85. Hwang, S.G.; Kim, K.H.; Lee, B.M.; Moon, J.C. Transcriptome analysis for identifying possible gene regulations during maize root emergence and formation at the initial growth stage. *Genes Genom.* **2018**, *40*, 755–766. [CrossRef] [PubMed]

86. Langmead, B.; Salzberg, S.L. Fast gapped-read alignment with Bowtie 2. *Nat. Methods* **2012**, *9*, 357–359. [CrossRef] [PubMed]

87. Anders, S.; Pyl, P.T.; Huber, W. HTSeq—A Python framework to work with high-throughput sequencing data. *Bioinformatics* **2015**, *31*, 166–169. [CrossRef]

88. Zhou, L.; Cheng, D.; Wang, L.; Gao, J.; Zhao, Q.; Wei, W.; Sun, Y. Comparative transcriptomic analysis reveals phenol tolerance mechanism of evolved *Chlorella strain*. *Bioresour. Technol.* **2017**, *227*, 266–272. [CrossRef] [PubMed]

89. Sun, X.; Shen, J.; Bai, F.; Xu, N. Transcriptome profiling of the microalga *Chlorella pyrenoidosa* in response to different carbon dioxide concentrations. *Mar. Genom.* **2016**, *29*, 81–87. [CrossRef]

90. Ashburner, M.; Ball, C.; Blake, J.; Botstein, D.; Butler, H.; Cherry, J.M.; Davis, A.; Dolinski, K.; Dwight, S.; Eppig, J.; et al. Gene Ontology: Tool for the unification of biology. *Nat. Genet.* **2000**, *25*, 25–29. [CrossRef]

91. Kanehisa, M.; Goto, S. KEGG: Kyoto encyclopedia of genes and genomes. *Nucleic Acids Res.* **2000**, *28*, 27–30. [CrossRef]

92. Scherer, P.I.; Raeder, U.; Geist, J.; Zwirglmaier, K. Influence of temperature, mixing, and addition of microcystin-LR on microcystin gene expression in Microcystis aeruginosa. *Microbiologyopen* **2017**, *6*. [CrossRef] [PubMed]

93. Woodger, F.J.; Badger, M.R.; Price, G.D. Inorganic carbon limitation induces transcripts encoding components of the CO_2-concentrating mechanism in *Synechococcus* sp. PCC7942 through a redox-independent pathway. *Plant Physiol.* **2003**, *133*, 2069–2080. [CrossRef] [PubMed]

94. Livak, K.J.; Schmittgen, T.D. Analysis of relative gene expression data using real-time quantitative PCR and the 2(-Delta Delta C(T)) Method. *Methods* **2001**, *25*, 402–408. [CrossRef] [PubMed]

Inhibitory Effects of Carrageenans on Endotoxin-Induced Inflammation

Irina M. Yermak [1,*], **Aleksandra V. Volod'ko** [1], **Eleonora I. Khasina** [2], **Viktoriya N. Davydova** [1], **Evgeniy A. Chusovitin** [3], **Dmitry L. Goroshko** [3,4], **Anna O. Kravchenko** [1], **Tamara F. Solov'eva** [1] and **Victor V. Maleev** [5]

[1] G.B. Elyakov Pacific Institute of Bioorganic Chemistry, Far Eastern Branch, Russian Academy of Sciences, Prospect 100 let Vladivostoku 159, Vladivostok 690022, Russia; morskaia@list.ru (A.V.V.); viktoria@piboc.dvo.ru (V.N.D.); kravchenko_25.89@mail.ru (A.O.K.); soltaf@mail.ru (T.F.S.)

[2] Federal Scientific Center of the East Asia Terrestrial Biodiversity, Far Eastern Branch, Russian Academy of Sciences, Prospect 100 let Vladivostoku 159, Vladivostok 690022, Russia; eleonorakhas@mail.ru

[3] Institute for Automation and Control Processes, Far Eastern Branch, Russian Academy of Sciences, 5 Radio St., Vladivostok 690041, Russia; eliot@list.ru (E.A.C.); goroshko@iacp.dvo.ru (D.L.G.)

[4] Far Eastern Federal University, 8 Sukhanova St., Vladivostok 690950, Russia

[5] Central Research Institute of Epidemiology, Russian Federal Service for Supervision of Consumer Rights Protection and Human Welfare, 3a, Novogireyevskaya St., Moscow 111123, Russia; maleyev@pcr.ru

* Correspondence: imyer@mail.ru; Tel.: +8-423-231–14–30

Abstract: The inhibitory effects of carrageenans (CRGs) on lipopolysaccharide (LPS) induced inflammation in a mouse model of endotoxemia and in complex therapy of patients with enteric infections of Salmonella etiology were studied. The atomic force microscopy (AFM) examination of LPS and its mixture with CRGs showed that the LPS morphology is significantly changed under the action of κ- and κ/β-CRGs. CRGs were able to increase the synthesis of anti-inflammatory interleukin 10 (IL-10) in vitro, and, at low concentrations, their activity in the mixture with LPS was higher. The protective effect of CRGs against *Escherichia coli* LPS was studied in vivo by monitoring the biochemical and pathomorphological parameters. The κ- and κ/β-CRGs and food supplement "Carrageenan-FE" increased the nonspecific resistance of mice to *E. coli* LPS at the expense of the inhibition of processes of thymus involution, adrenals hypertrophy, thyroid atrophy, hypercorticoidism, glycogenolysis, and lactate acidosis. The estimation of the therapeutic action of food supplement Carrageenan-FE in complex therapy of patients with enteric infections of Salmonella etiology is given. Carrageenan-FE restores the system of hemostasis and corrects some biochemical indicators and parameters in the immune systems of patients. These results allow us to hope for the practical application of CRGs for lowering the endotoxemia level in patients under the development of the infectious process caused by Gram-negative bacteria.

Keywords: carrageenan; lipopolysaccharide; macromolecular structure; nonspecific resistance to lipopolysaccharide; cytokines; enteric infections; salmonellosis

---

1. Introduction

The phenomenon of subclinically elevated levels of endotoxin in the bloodstream has recently been termed "metabolic endotoxemia" [1,2]. This elevation is not evident in the clinical setting, but is currently being studied as a significant potential etiology of chronic diseases such as atherosclerosis, type II diabetes mellitus, Parkinson's disease, pancreatitis, amyotrophic lateral sclerosis, Alzheimer's disease, and cancer metastasis that arise in the context of chronic low-severity inflammation [1–3]. Endotoxins are known to consist of amphiphilic lipopolysaccharide (LPS) macromolecules located on

the surface of Gram-negative bacteria. Released from bacteria in vivo or administered in an isolated form, endotoxins exert both physiological and powerful pathophysiological effects in higher organisms and, thus, represent important virulence factors of Gram-negative bacteria [4]. Circulating LPS is bioactive in vivo and correlates with measures of innate and adaptive immune activation [5]. LPS is the primary target for interaction with components of the host immune system, which can be activated by LPS to produce synthesis of tumor necrosis factor-alpha (TNF-α), interleukin (IL)-6, IL-8, and free radicals, such as reactive oxygen species (ROS) [6]. The overexpression of these pro-inflammatory mediators may result in fever, severe damage of tissues, coagulopathy, endothelial dysfunction, vascular instability, apoptosis, multiorgan failure, and septic shock. The gastrointestinal tract is involved in the initial response to the systemic inflammatory reaction [7]. Impaired intestinal barrier function and/or increased epithelial permeability may promote the translocation of bacteria and endotoxin from the gut into the body, increasing the susceptibility to infections [8].

The gut microbiota seems able to promote systemic low-grade inflammation, insulin resistance, and enhanced cardiovascular risk through a mechanism that involves the increased exposure to bacterial products coming from the gut, particularly to the LPS [9,10]. Rich sources of LPS live in the upper respiratory and gastrointestinal tracts, especially in the mouth and colon. LPS may also be found in foodstuffs [11].

Emerging human clinical studies have demonstrated that diet and nutritional supplements have demonstrated the ability to provide clinically important reductions in circulating endotoxins and improve related effects, such as inflammation and other negative health markers [12]. Food fibers are in close contact with the large intestine's immune system, which composes a significant part of the common immune system. The deficiency of food fibers in the diet promotes the appearance of many gastrointestinal and metabolic diseases [13].

Seaweed polysaccharides, such as carrageenans (CRGs), are one source of soluble dietary fibers [14]. CRGs are sulfated linear galactans, whose basic structural units are disaccharide-carrabiose, consisting of alternating β-1,3-linked and α-1,4-linked galactose residues. Variation in this basic structure results from the 3,6-anhydrogalactose content, location, and number of sulfate groups [15]. The three most industrially exploited types, namely κ-, ι-, and λ-CRG, are distinguished by the presence of one, two, and three ester-sulfate groups per repeating disaccharide unit, respectively. Native carrageenans always represent complex hybrid structures or are generally a mixture of galactans composed of different carrabiose types. The hybrid nature of CRGs at the molecular level is responsible for changes in the biological and physico-chemical properties of CRGs compared with those of their homopolymeric ideal types [16].

Although CRGs have been used as safe food ingredients for a long time, they are also used as a classical model for inducing inflammation. Inflammation induced by carrageenan was originally described by Winter [17]. The CRG-induced edema, as an inflammation model, is usually used to assess the contribution of natural products to resist the biochemical changes associated with acute inflammation. When CRG is injected, acute inflammation with edema appears, along with a production of free radicals as well as a release of the inflammatory mediators [18]. At the same time, intensive studies have shown that CRGs can be regarded not only as foodstuff ingredients, due to a wide spectrum of biological and physiological activities, such as antiviral [19], anticoagulant [20], antitumor [21], and immunomodulatory activities [22]. At present, CRG has been included in the United States Pharmacopeia 35-National Formulary 30S1 (USP35-NF30S1), the British Pharmacopoeia 2012 (BP2012), and the European Pharmacopoeia 7.0 (EP7.0), implying that CRG may have a promising future as a pharmaceutical excipient. According to the JECFA, only degraded carrageenans were associated to adverse effects and should not be used as food additives. It known that degraded low-molecular-weight carrageenan exhibits toxicological properties at high doses, stimulates ulceration of the fecal mucosa, histopathological changes, epithelial thinning, slight erosion, cellular infiltration, and other negative changes in animal organisms [23]. Native high-molecular-weight carrageenan is safe and non-toxic product. The safety of CRGs is supported by a large number of animal oral safety studies in which no

adverse effects were reported at high doses (up to 5% in the diet) [24]. The wide range of potential pharmacological applications of different types of CRGs is the main reason for the increased interest in these polysaccharides. The effect of sulfated polysaccharides on metabolic endotoxemia has only been studied in animals. It has been shown that the administration of sulfated polysaccharides to high fat-diet-fed mice increased the amount of short-chain fatty acids in the intestinal tract, decreased the blood LPS or LPS binding protein concentration, and attenuated weight gain [25,26]. The influence of CRG on LPS and on the antibacterial host defense systems, such as the chemotactic responses to heat-killed bacteria or LPS in the pleural cavity and interleukin-1 production by pleural macrophages, was studied by Tatede et al. [27]. Their results demonstrate the potential activity of iota-CRG to enhance antibacterial host defense systems in mice. The administration of κ-CRG has been reported to increase the phagocytic activity of carp, *Cyprinus carpio*, and its resistance against *Edwardsiella tarda* and *Aeromonas hydrophila* administered via intraperitoneal injection [28]. The administration of iota-CRG has been reported to increase the innate immune response of the orange-spotted grouper, *Epinephelus coioides*, and its resistance against *Vibrio alginolyticus* administered via injection [29]. It has been shown that white shrimp, *Litopenaeus vannamei*, that received lambda-CRG exhibited higher immune ability as well as resistance against Gram-negative bacterium *V. alginolyticus* [30].

In a previous study, we showed that the administration of CRGs significantly prolonged the survival of mice against LPS challenge [31]. The degree of protection depended on the structure of the CRGs, their dose, route, and time of administration. We previously demonstrated a potential application of CRGs as protectors against S and R forms of *Proteus mirabilis* LPS. We concluded that CRGs might be considered as anti-endotoxin agents, neutralizing LPS and abolishing their proapoptotic activity [32]. The results obtained in this study by three serological methods indicate the role of *P. mirabilis* lipid A in the binding to different CRGs. The lipid A component is responsible for much LPS toxicity. At the same time, it is known that in the macromolecular mechanism of endotoxin induction many of the observed biological effects of LPS can be related to their physical state, mainly to the three-dimensional supramolecular structure of the LPS assembly [33]. We previously demonstrated that LPS interact with polysaccharide chitosan, which is accompanied by the essential modification of some immunological properties of LPS [34,35]. Later we discovered a transformation of the supramolecular structure of LPS after binding to chitosan [36]. It was necessary to establish whether a change in the macromolecular structure of LPS occurs in the presence of CRG.

In the present study, we examined the effect of CRGs on LPS-induced endotoxemia in mice as well as the influence of the biologically active food supplement "Carrageenan-FE" on the immune system and hemostasis parameters of patients with food borne infections caused by Gram-negative bacteria. To explain the mechanism of the protective effect of CRGs on LPS, the effect of these polysaccharides on the supramolecular structure of LPS was studied.
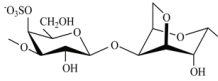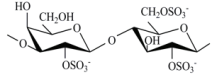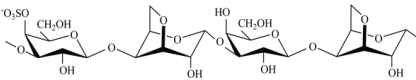
2. Results

2.1. Carrageenans

Polysaccharides were extracted from red seaweed, namely *Chondrus armatus* and *Tichocarpus crinitus*, with water at 90 °C. The obtained extracts were purified of low-molecular-weight impurities by column filtration, and polysaccharides were precipitated from solutions by precipitation in alcohol. The yield of polysaccharides from *C. armatus* was 50% (designated as unfractionated or total polysaccharide (Σ)), and the yield from *T. crinitus* was 30%. The polysaccharides were separated using 4% KCl into KCl-insoluble and KCl-soluble fractions. The structures of the polysaccharides were studied by ^{13}C-NMR and FTIR spectroscopy. The obtained spectra were compared with the spectra of polysaccharides isolated by us earlier from these species of algae [37,38]. The identity of the spectra indicated that the KCl-insoluble fraction from *C. armatus* was κ-CRG (G4S-DA-carrabiose) with traces of ι-CRG (G4S-DA2S-carrabiose), which were randomly distributed along the polysaccharide chain as a single insertion [37]. The KCl-soluble fraction from *C. armatus* was represented mainly by λ-CRG.

According to data obtained by ^{13}C-NMR and FTIR spectroscopy, the KCl-insoluble polysaccharides from *T. crinitus* had hybrid structures. On the basis of the analysis of spectra compared with data obtained previously, these polysaccharides were identified as κ/β-CRG [38]. Therefore, CRGs are differentiated by the presence of 3,6-anhydro-D-galactose in κ- and κ/β-CRG as well as by the different numbers and positions of ester sulfate groups. λ-CRG has a higher degree of sulfatation.

The chemical structures of the disaccharide repeating units of the CRGs and viscometric molecular weights of CRGs [39], calculated by the Mark–Kuhn–Houwink equation, are listed in Table 1.

Table 1. Chemical structures of the repeating units of CRG from algae belonging to families Gigartinaceae and Tichocarpaceae.

Source of Carrageenans	Type of CRG	Structure of Disaccharide Repeating Unit	Mw, kDa
C. armatus Gigartinaceae	Kappa (κ)		560
	Lambda (λ)		185
T. crinitus Tichocarpaceae	Kappa/beta (κ/β) (60:40)		172

2.2. Atomic Force Microscopy of LPS and LPS–GRG Mixtures

The influence of CRGs on the morphology of LPS was investigated by atomic force microscopy (AFM). According to the AFM data, κ-CRG at 0.1 mg/mL (Figure 1a) is a densely branched network structure formed by fibers with a height of about 1.0–1.5 nm and a lateral size of 51 ± 15 nm (root mean square (σRMS) = 0.726 nm). The network structure was also observed for κ/β-CRG at 0.1 mg/mL (Figure 1b). The network is also formed by fibers but they are grouped into bundles and as a result the network looks less dense than the network of κ-CRG. These fibers have a height of about 0.9–1.5 nm, with a thickness of 36 ± 11 nm (σRMS = 0.705 nm). λ-CRG differs from the other investigated carrageenan types with a high sulfation degree and the absence of 3,6- anhydrogalactose. λ-CRG is presented in the form of a random coil (Figure 1c). According to the AFM data, λ-CRG at 0.1 mg/mL forms an unordered structure consisting of particles with an irregular spherical segment (σRMS = 0.951 nm). The density of the particles is about 1.1×1010 cm^{-1}, they are distributed almost uniformly over the surface, but there are a number of particle agglomerations. The height and lateral size of the particles are about 1.8–2.0 nm and 38 ± 9 nm, respectively.

The AFM image of *E. coli* LPS shows micelle-like particles typical for amphiphilic polymers (σRMS = 25.859 nm). The large particles easily seen in Figure 1d have a density of 2.6×108 cm^{-2} and they are nonuniformly distributed over the sample surface. The average large particle height is about 50.9 nm. Most particles have an elongated irregular shape with a large lateral size of 651 ± 452 nm and a small lateral size of 334 ± 115 nm; the aspect ratio is about 2. A detailed analysis of the large particles revealed that they consist of small particles, of which the lateral size can only be roughly estimated to be about 40 nm because of a lack of resolution.
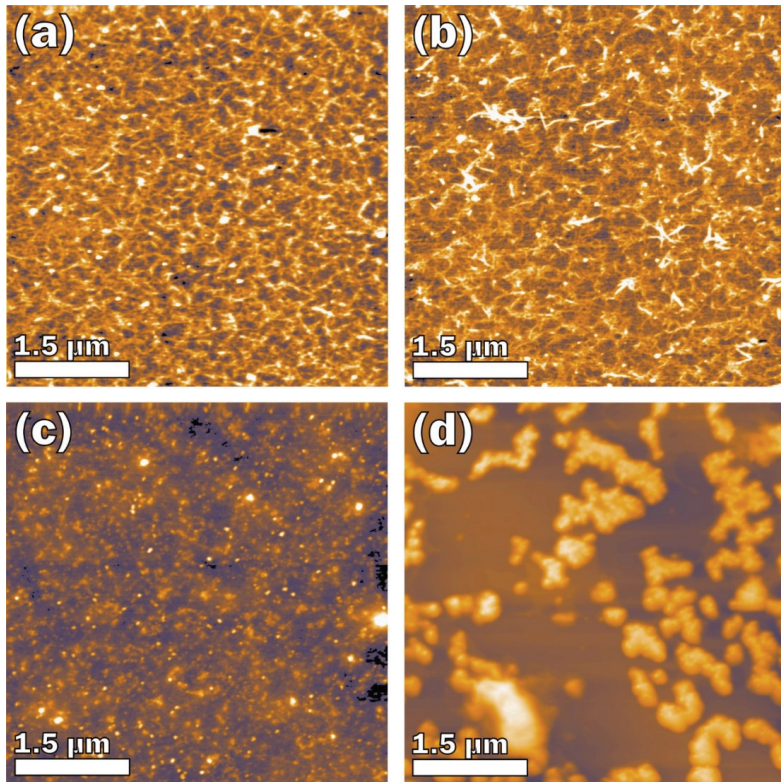
Figure 1. AFM topography images: (**a**) κ-CRG, 0.1 mg/mL; (**b**) κ/β-CRG, 0.1 mg/mL; (**c**) lambda-CRG, 0.1 mg/mL; and (**d**) LPS, 0.05 mg/mL.

The image of the *E. coli* LPS with CRG mixtures at the 2:1 *w/w* ratio between components (Figure 2) showed that the macromolecular structures of the mixtures are quite different from the structures of the initial components at the same concentrations. In the case of κ-CRG and κ/β-CRG, the number of separate fibers is significantly decreased. In the complex κ-CRG + LPS, one can see fragments of the network with many spherical particles as can be seen in clean *E. coli* LPS (Figure 2a), and some worm-like structures (Figure 2a, inset). The lateral size and height of the spherical particles are 35 ± 3 and 1.65 ± 0.60 nm, respectively, while the width and height of the fibers in the worm-like structures are 60 ± 18 and 7.0 ± 1.1 nm, respectively. The fibers in the κ/β-CRG + LPS mixture are organized in a continuous network with round-shaped holes (Figure 2b), while the worm-like structures are either incorporated into the network or just lie over it. The width and height of the fibers in the worm-like structures are 49 ± 11 and 6.6 ± 1.4 nm, respectively, which are slightly smaller than the corresponding values in the κ-CRG + LPS mixture. The value of σRMS for both mixtures (Figure 2a,b) increased to more than twice that for the initial CRGs: 2.594 nm for κ-CRG + LPS and 1.989 nm for κ/β-CRG + LPS.

The morphology of λ-CRG in the complex with *E. coli* LPS also changed (Figure 2c). Instead of separated particles, one can see short fibers that are uniformly distributed over the surface rather than arranged in a network. The width and height of the fibers are 27 ± 3 and 0.74 ± 0.15 nm, respectively. *E. coli* LPS in this mixture also forms the worm-like structures that are incorporated into a layer of uniformly distributed fibers of λ-CRG. The width and height of the fibers in the worm-like structures are 62 ± 13 and 8.6 ± 2.0 nm, respectively.
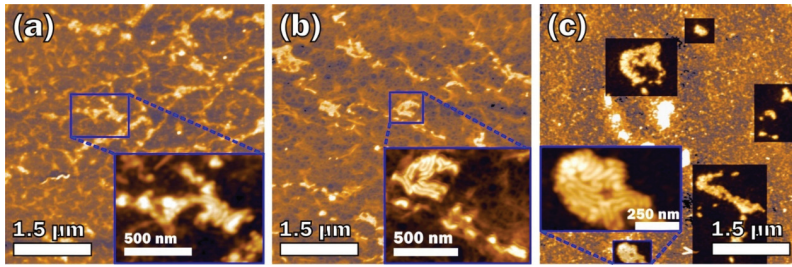
Figure 2. AFM topography images of mixtures in ratio 2:1 *w/w*: (**a**) κ-CRG + LPS; (**b**) κ/β-CRG + LPS; and (**c**) λ-CRG + LPS.

2.3. Effect of LPS and CRGs on the Production of Cytokines by Human Cells

Experiments were performed to determine the effect of CRGs on the activation of the synthesis of LPS-induced IL-10 and TNF-α in human blood cells.

As shown in Figure 3a, CRGs induced the synthesis of TNF in cells only at high polysaccharide concentrations. Σ-CRG at C = 1 μg/mL showed a high activity with respect to the synthesis of the pro-inflammatory cytokine, similar to the effect of LPS at C = 10 μg/mL. At the same time, CRGs induced the synthesis of IL-10 in a dose-dependent manner similar to LPS. κ/β-CRG can induce IL-10 synthesis and is weakly dependent on the polysaccharide concentration.
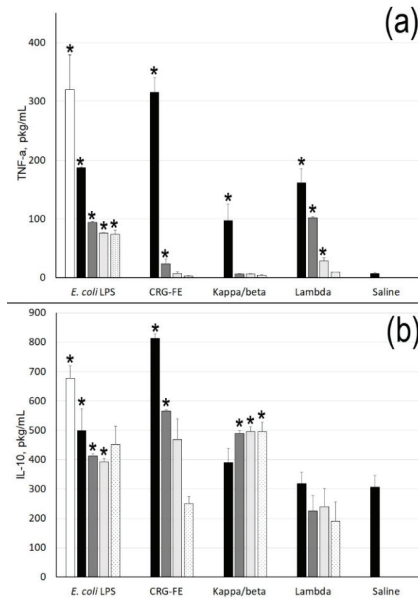
Figure 3. TNF-α (**a**) and IL-10 (**b**) levels stimulated by *E. coli* LPS and carrageenans. Concentrations of samples: 10 μg/mL (white column), 1 μg/mL (black), 100 ng/mL (gray), 10 ng/mL (light gray), and 1 ng/mL (black-dot). Mean (±SD) contents of cytokine in serum are presented. Whole blood was obtained from five healthy subjects and incubated with the samples at different concentrations. The level of cytokines in serum of normal donors was considered as a negative control used for statistical significance calculation. * Differences between the samples and the control were significant, $p < 0.05$.

The preliminary incubation of cells with LPS (C = 10 µg/mL) followed by treatment with λ-CRG did not have an influence on IL-10 production, whereas treatment with κ- and κ/β-CRG (Figure 4) increased the production of IL-10 and slightly reduced the synthesis of TNF in cells.
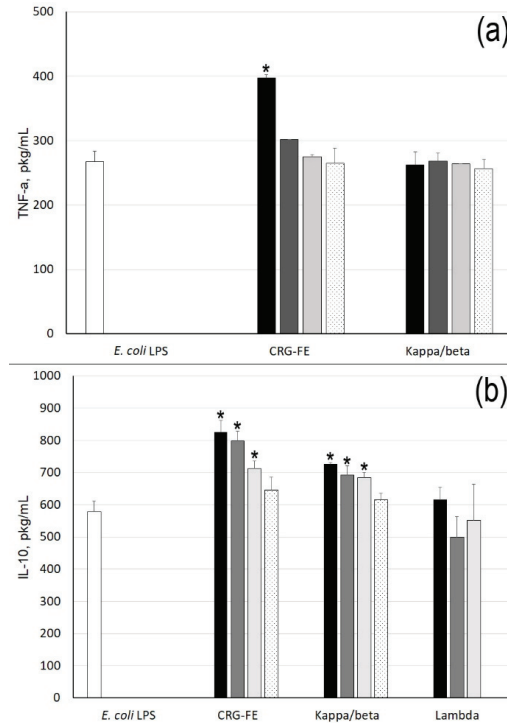

Figure 4. TNF-α (**a**) and IL-10 (**b**) levels stimulated by preliminary incubation cells with *E. coli* LPS (10 min), and then CRGs. Concentrations of samples: 10 µg/mL (white column), 1 µg/mL (black); 100 ng/mL (gray); 10 ng/mL (light gray), and 1 ng/mL (black-dot). Mean (±SD) contents of cytokine in serum are presented. The level of cytokines in serum stimulated by *E. coli* LPS (10 µg/mL) was considered as a control used for statistical significance calculation. * Differences between samples and the control were significant, $p < 0.05$.

2.4. Effect of CRGs on Stress Reaction of Mice Induced with E. coli LPS

When considering the effect of *E. coli* LPS injection for five days, it was found that the physiological status of animals exhibits considerable changes. The stress response to LPS- intoxication in mice is manifested by thymus involution, thyroid atrophy, and adrenal gland hypertrophy, at the same time as an increase of the serum corticosterone level, a decrease of the concentrations of adenosine triphosphate (ATP) and glycogen in liver, and lactate acidosis (Table 2).

The results of this study show that administration of κ-CRG, κ/β–CRG, and ∑-CRG led to the minimization of physiological disorders and metabolic homeostasis in mice exposed to LPS- intoxication. The relative masses of the thymus, thyroid, and adrenal glands of animals in the LPS + ∑-CRG group differed from the norm only by 22%, 10%, and 12%, respectively, whereas, in the mice of LPS group, the deviations were 36%, 21%, and 30%, respectively. In the LPS + κ/β-CRG group, the relative masses of the thymus, thyroid and adrenals were less than in the control group by 16%, 7% and 5%, respectively (Table 2). After the administration of the κ- and κ/β-CRGs, the serum corticosterone level in mice intoxicated with *E. coli* LPS were reduced by 32% relative to the LPS group. The administration of

∑-CRG and κ/β-CRG led to 22% and 17% lowered lactate storage in mice liver relative to the LPS group. The use of κ-CRG, κ/β-CRG, and ∑-CRG contributed to more effective conservation of the energetic substrate ATP and glycogen in liver. The concentration of ATP and glycogen in mice liver were on average 18% higher than in the LPS group.

In this study, κ-CRG significantly minimized adrenal gland hypertrophy, and the depletion of ATP and glycogen in mice liver, whereas λ-CRG did not have an effect on the stress response of mice exposed to *E. coli* LPS.

Table 2. The effect of different types of CRG on some physiological parameters in mice intoxicated with *E. coli* LPS.

Groups	Relative Organ Masses, mg/g BM			
	Liver	**Thymus**	**Thyroid**	**Adrenals**
control	54.16 ± 6.60	1.98 ± 0.22	0.175 ± 0.016	0.217 ± 0.018
LPS	62.79 ± 7.83 [a]	1.27 ± 0.16 [a]	0.138 ± 0.018 [a]	0.282 ± 0.032 [a]
LPS + ∑-CRG.	60.06 ± 4.77	1.55 ± 0.12 [b]	0.157 ± 0.013 [b]	0.243 ± 0.033 [b]
LPS + κ/β-CRG	61.48 ± 5.74	1.67 ± 0.16 [b]	0.162 ± 0.017 [b]	0.228 ± 0.031 [b]
LPS + κ-CRG	55.25 ± 5.85 [b]	1.43 ± 0.22	0.148 ± 0.039	0.254 ± 0.014 [b]
LPS + λ-CRG	60.14 ± 4.96	1.29 ± 0.17	0.153 ± 0.032	0.265 ± 0.029
Biochemical parameters				
Groups	**Serum corticosterone, μmol/L**	**Liver ATP, μmol/g**	**Liver lactate, μmol/g**	**Liver glycogen, μmol/g**
control	0.28 ± 0.043	2.72 ± 0.222	1.88 ± 0.443	232.6 ± 43.89
LPS	0.39 ± 0.047 [a]	2.00 ± 0.377 [a]	2.53 ± 0.350 [a]	176.6 ± 17.33 [a]
LPS + ∑-CRG	0.30 ± 0.047 [b]	2.45 ± 0.337 [b]	2.10 ± 0.395 [b]	220.4 ± 41.04 [b]
LPS + κ/β-CRG	0.30 ± 0.071 [b]	2.31 ± 0.140 [b]	2.21 ± 0.217 [b]	210.6 ± 20.46 [b]
LPS + κ-CRG	0.33 ± 0.080	2.52 ± 0.338 [b]	2.44 ± 0.308	230.8 ± 30.22 [b]
LPS + λ-CRG	0.38 ± 0.047	2.06 ± 0.076	2.60 ± 0.359	185.6 ± 35.82

BM, body mass; ATP, adenosine triphosphate; mean ± SD (n = 8 observations); [a] $p < 0.05$ compared with the control group; [b] $p < 0.05$ compared with the LPS group used Student's *t*-test.

2.5. The Effects of Food Supplement Carrageenan-FE on the Immune System and Hemostasis Parameters in Patients with Food Borne Toxicoinfection

The medico-biological study was carried out in accordance with The Code of Ethics of the World Medical Association (Declaration of Helsinki) and the biologically active food supplement Carrageenan-FE based on the ∑- CRG, was used.

Investigation of the parameters of the hemostasis system showed that 18 patients with food borne toxicoinfection, caused by *Salmonella enterica*, showed signs of a hypercoagulation (first phase of disseminated intravascular coagulation) and 24 patients showed symptoms of a hypocoagulation (second phase syndrome). For patients with hypercoagulation, there was a reduction of platelet aggregation by an average of 65%, and, in patients with hypocoagulation, the degree of aggregation increased on average by 22%. In patients on the third day of treatment with CRG, there was a decrease of leukocytosis, decreasing to normal amounts of activated immune cells, and an increase in relation to the total population of T-lymphocytes and the absolute number of lymphocytes in peripheral blood and their immunoregulatory subpopulations (Table 3).

Table 3. The average values of immunological parameters in patients with acute enteric infections in the course of the disease with treatment Carrageenan-FE.

Indicator		On Admission to the Hospital N = 42	3- Days of Therapy		Control N = 20
			With CRG-FE N = 22	Without CRG-FE N = 20	
Leukocytes * 109/L, abs		8.3 ± 3.3	6.6 ± 2.9 †‡	5.7 ± 1.8	6.45 ± 1.5
neutrophils,	%	81.4 ± 8.5 *	60.8 ± 8.9 ‡	67.8 ± 5.7	62.5 ± 11.4
	abs × 109/L	6.8 ± 3.2 *	4.2 ± 2.7 ‡	3.9 ± 1.3	4.12 ± 1.6
lymphocytes	%	13.7 ± 6.9 *	31.5 ± 7.5 †‡	26 ± 5.4 *	34.0 ± 10.6
	abs × 109/L	1.0 ± 0.4 *	2.0 ± 0.7 †‡	1.4 ± 0.3 *	2.1 ± 0.6
CD3+	%	66.4 ± 8.4	73.5 ± 7.4 ‡	74.2 ± 5.2	68.7 ± 7.3
	abs × 109/L	0.7 ± 0.3 *	1.4 ± 0.5 †‡	1.0 ± 0.2 *	1.42 ± 0.3
CD4+	%	43.0 ± 20.0	45.7 ± 7.4	49.8 ± 4.1 *	40.0 ± 17.0
	abs × 109/L	0. 5 ± 0.2 *	0.9 ± 0.3 ‡	0.76 ± 0.2	0.81 ± 0.1
CD8+	%	22.3 ± 14.5	24.5 ± 6.4	22.8 ± 5.2	25.6 ± 6.0
	abs × 109/L	0.3 ± 0.1 *	0.5 ± 0.2	0.4 ± 0.2	0.6 ± 0.2
CD4+/CD8+		2.2 (0.4–4.8)	2.0 (0.9–3.6)	2.4 (1.5–3.4)	1.6 (1.1–2.5)
CD 19 %	%	15.4 ± 5.1	11.7 ± 3.4 ‡	10.9 ± 4.0	12.4 ± 3.5
	abs × 109/L	0.2 ± 0.1 *	0.2 ± 0.1 †‡	0.2 ± 0.1 *	0.3 ± 0.1

mean ± SD (n, see Table 3); * $p < 0.05$ compared with the control group; † $p < 0.05$ compared with the without CRG-FE group; ‡ $p < 0.05$ compared with the on admission to hospital group used Student's *t*-test.

3. Discussion

The emergence of multi-drug resistant Gram-negative bacteria "super bugs" are becoming a serious therapeutic problem. Animal and human studies indicate LPS as an antigen that activates the immune system, playing an important role in the pathogenesis of metabolic chronic diseases [11]. The application of bactericidal antibiotics, apart from killing the bacteria, may lead to the massive release of endotoxin. The search for non-toxic effective endotoxin binding and neutralizing compounds is an ongoing process.

One of the promising ways to inhibit the harmful inflammatory responses of endotoxins is to bind LPS with certain polycations, which can interact with lipid A as a result, blocking this toxic center of the endotoxin. In recent years, it has been demonstrated that antimicrobial peptides from the Pep 19-2.5 family, which were designed to bind to LPS, act as anti-inflammatory agents against sepsis and endotoxic shock caused by severe bacterial infections. The peptide-mediated neutralization of LPS and LP involves changes in various physical parameters, including both the gel to liquid crystalline phase transition of the acyl chains and the three-dimensional aggregate structures of the LPS [40]. It is known that LPS as amphiphilic molecules tend to form supramolecular aggregates in aqueous solutions at concentrations above the critical micellar concentration. LPS molecules may aggregate into different physical structures, including micelles, inverted micelles, or bilayers and undergo lamellar to inverted hexagonal or cubic phase transitions depending on the physiochemical environment [41]. The complex hydrodynamic geometry exhibited by LPS in dilute suspensions may have consequences for the interpretation of LPS biological activity in the host immune response [42].

As shown by our previously obtained data using dynamic light scattering, CRGs changed the surface charge and the particle size of LPS. This process depended on the structural type of carrageenan, the initial concentration of the components, and their proportion in the solution [43]. In the current work, AFM was used to study the probable modification of LPS morphology due to the effect of CRGs. Compared with other microscopic methods, AFM is characterized by minimal artifacts related to the fixation and staining of samples. Furthermore, the height and width of objects on AFM images may provide additional information about the degree of association and polymer heterogeneity. The macromolecular structures of LPS with κ-, κ/β-, and λ-CRGs were investigated. Comparative

AFM examination of LPS and its mixture with CRGs showed that LPS morphology is significantly changed under the action of the polysaccharide. The macromolecular structure of LPS, determined using AFM, shows a change in LPS aggregates of the micellar structure into worm-shaped formations in the presence of CRGs. In the case of κ- and κ/β-CRGs, the number of separate fibers of CRG is significantly decreased. The AFM images show that the LPS vermicular structure is integrated into a three-dimensional network of κ- and κ/β-CRGs (incorporated into the network or just lying over it). In a mixture with λ-CRG, a change in the LPS macromolecular structure is also observed (Figure 2c). However, in this case, the absence of the three-dimensional structure of λ-CRG does not limit the assembly of these vermiform LPS particles into larger associates. It is worth nothing that the worm-like structures form the densest agglomerates in λ-CRG. We suppose that the worm-like structures consist of LPS, which has changed its morphology under the influence of the CRG network consistent with the electron microscopy data we obtained earlier [43].

It is known that, when entering the bloodstream during local or systemic Gram-negative infections, endotoxin has an impact on almost all the systems of an organism, causing a number of pathophysiological changes [44]. Recently, in a LPS-induced endotoxemia mouse model, it has been shown that hirsutanol A (isolated from the red-algae-derived marine fungus *Chondrostereum* sp.) pretreatment improved endotoxemia-induced acute sickness behavior, including acute motor deficits and anxiety-like behavior [45].

A nonspecific resistance of the organism to *E. coli* LPS induced by CRG was studied in the present work. We investigated the effect of different structural types of CRGs on the LPS-induced intoxication of animals by the degree of variability of biochemical and pathological parameters to those most adequately responding to any valid stressor, including bacterial endotoxin. In our experiments, LPS parenterally injected into mice (in a nonlethal dose) caused significant changes of these parameters. Preventive oral administration of CRGs significantly reduced the morphological, endocrine, and metabolic disorders caused by endotoxin in the liver, thymus, spleen, adrenal glands, and blood of animals (Table 2). The results of these studies have shown that biochemical and pathomorphological manifestations of endotoxemia induced by intraperitoneal injection of bacterial LPS were less pronounced in the mice that received CRGs. ∑-, κ-, and κ/β-CRGs increase the resistance of the host organism to bacterial LPS. As seen in these experiments, these CRGs are more active than λ-CRG, which has a high degree of sulfation and does not form a three-dimensional structure. As shown by the AFM data (Figure 2), LPS is embedded in the three-dimensional structure of κ- and κ/β-CRGs, which probably contributes to a greater screening of its toxicity. Moreover, as we recently showed, κ- and κ/β-CRGs have the most powerful mucoadhesive properties, which may prevent LPS from landing on the epithelial layer [46].

Our data are consistent with results that demonstrate how fucoidan prevented endotoxin-induced damage in a mouse model of endotoxemia and increased the mice's resistance to LPS. The parenteral or per os administration of fucoidan resulted in decreasing the degree of microcirculatory disorders and secondary dystrophic-destructive changes in parenchymal organs of mice with endotoxemia [47].

Although the mechanisms responsible for the CRG effects require further study, the data obtained provide strong evidence for a normalizing effect of CRGs on the state of organs of mice with endotoxemia. The CRG-induced host resistance to endotoxin may result from a variety of reasons, one of which may be associated with a change in the macromolecular structure of LPS. The resistance to endotoxin induced by CRGs can be attributed to the immunomodulating effect of polysaccharide. As is known, CRGs and endotoxins also stimulate the biosynthesis of different mediators of the immune system, such as IL-10, IL-8, IL-6, and TNF-α [6,44]. Since cytokines play a critical role in regulating inflammatory and immunological processes of the host, in vivo administration of CRGs may influence antibacterial host-defense systems. It is known that IL-10 has great potential for use in the treatment of inflammatory and immune illnesses. It has been shown that IL-10 protects mice against lethal doses of endotoxin [48]. In addition, IL-10 treatment inhibits the activation of cytokine synthesis during experimental endotoxemia in primates [49] and humans [50] and in microglia cell cultures [51].

Previously we have shown [22] that CRGs of different structural types induced the synthesis of the anti-inflammatory cytokine IL-10 in human blood cells, which rose with an increase in polysaccharide concentration. κ/β-CRG showed fairly high activity independent of the concentration. κ/β-CRG under oral administration into mice possesses a protective effect and reduces an intensity of inflammatory response induced by LPS probably due to some modulating effect on the cellular activity of peritoneal leukocytes and to a greater degree on cytokine production [52].

In the present work, κ/β-CRG caused an increase in the level of the cytokine IL-10 in blood compared with the control (Figure 3). The effect of ∑-CRG on the induction of IL-10 synthesis exceeded the LPS effect at the same concentration by almost more than 1.5 times. Along with this, ∑-CRGs and κ/β-CRG at concentrations of 1–100 ng/mL showed weak activity to stimulate the synthesis of pro-inflammatory cytokine TNF-α. These polysaccharides also enhanced the effect of LPS, increasing the synthesis of the anti-inflammatory cytokine IL-10 in a test with the pre-treatment of blood cells with *E. coli* LPS. λ-CRG showed a different effect on the stimulation of cytokine synthesis in cells. This polysaccharide did not have the ability to stimulate the synthesis of anti-inflammatory cytokine IL-10, but it possessed an adequate ability to induce pro-inflammatory cytokine synthesis increasing the level of TNF-α in serum at 1 µg/mL and 100 ng/mL, which was comparable to the effect of LPS at the same concentrations.

Known disorders of coagulation or disseminated intravascular coagulation (DIC) induced by endotoxin lead to multiple-organ dysfunction [53]. An important role in the development of DIC has been shown to belong to platelets and LPS-induced platelet aggregation [54]. Earlier in the in vitro experiment, we showed that CRGs significantly inhibited LPS-induced upregulation of reactive oxygen species reduced or completely inhibited collagen-induced platelet aggregation and decreased their aggregation activity caused by the cooperative effect of LPS and collagen [43]. In the clinical study, we showed the effects of food supplement Carrageenan-FE on the immune system and lipid profile in patients with cardiovascular disease. Carrageenan-FE moderately modulated all of the immunity system markers and caused statistically significant decreases in the biomarkers of chronic inflammation [55].

It is known that the overreaction of the immune system into fragments of bacterial cells, such as LPS, underlies many inflammatory bowel diseases. In this regard, in the complex treatment of intestinal infections, the use of agents that restore normal microflora is indicated [56]. In the current study, we investigated the therapeutic effect of CRG in complex therapy of patients with enteric infections of Salmonella etiology. Our results show that the application of food supplement Carrageenan-FE in the standard therapy of toxicoinfections contributes to the correction of hemostasis. In this case, the action of CRG had a modulating regulatory pattern: in patients with hypercoagulation, a decrease in platelet aggregation activity was observed, and, in patients with hypocoagulation, the degree of aggregation increased. The application of Carrageenan-FE in the standard therapy scheme corrected some biochemical indicators and parameters of the immune system of the patient organism more actively in comparison with a control. A quick recovery of the immune system of patients taking CRG is likely due to its immunoregulatory properties.

These results allow us to hope for the practical application of CRGs for lowering the endotoxemia level in patients under the development of the infectious process caused by Gram-negative bacteria.

4. Materials and Methods

4.1. Polysaccharides

Algae: The following species of red algae were collected at The Peter the Great Bay, Japan Sea, which is near the border between the boreal and tropical zones: *Chondrus armatus* (Gigartinales, Gigartinaceae) and *Tichocarpus crinitus* (S.G. Gmelin) (Gigartinales, Tichocarpoaceae). All algae were harvested at the end of August and identified by Prof. E. Titlynov and T. Titlynova (National Scientific Center of Marine Biology, Far-Eastern Branch of the Russian Academy of Sciences). The selected

seaweeds were in the vegetative form lacking any reproductive organs. The algae were washed with tap water to remove excess of salt. Bleaching of the seaweed was by maintaining the specimen in pure acetone for 3 days prior being dried in the air.

Extraction of CRGs: Dried and milled algae (50 g) were suspended in hot water (1.5 h) and the polysaccharides were extracted at 90 °C for 2 h in a water bath. The residue was removed by centrifugation and supernatant poured into ethanol (3 volumes), yielding the crude extract (unfractionated) of polysaccharides. The crude extracts were purified by redissolving in water, concentrated, dialyzed, and freeze-dried, yielding Σ-CRG. Then, the polysaccharides were separated into gelling KCl-insoluble and non-gelling KC1-soluble fractions as described previously [34] and their structures were established according to the published protocol. λ- and k-CRGs from *C. armatus* and κ/β-CRG from *T. crinitus* were obtained. The biologically active food supplement Carrageenan-FE (Pacific Institute of Bioorganic Chemistry Far East Branch of the Russian Academy of Sciences) is composed of κ- and λ-CRGs from *C. armatus* at a ratio 3:1 (*v/v*) and is labeled as Σ-CRG. The endotoxin admixture in samples of CRGs was determined by the fluorogenic endotoxin detection assay PyroGene rFC purchased from Lonza (USA) in accordance with test instruction. The level of environmental endotoxin was low: 0.60 EU mL^{-1} in doses of 100 mg/mL.

Commercial LPS from *Escherichia coli* 055:B5 (Cat No: L2880, Lot No: 102M4017V, Sigma, St. Louis, MO, USA) was used in the study.

Molecular Weight Estimation: Viscosimetric molecular weight of the polysaccharide sample was calculated using the Mark–Kuhn–Houwink equation: $|\eta| = KmM\alpha$, where $|\eta|$ is the intrinsic viscosity and Km and α are empirical constants for carrageenan constituting 3×10^{-3} and 0.95 at 25 °C in 0.1 M NaCl, respectively, according to the literature data for this polymer–solvent system [36]. The viscosity of polysaccharide solution (1–2 mg/mL in 0.1 M NaCl) was measured with a modified Ubbellohde viscometer (Design Bureau Puschino, Russia) with a capillary diameter of 0.3 mm at 25 °C, the time of accuracy being within ±0.1 s. The intrinsic viscosity of the CRGs sample was calculated by the extrapolation of the dependence ln (η)rel/C to infinite dilution using the least squares method.

4.2. Atomic Force Microscopy (AFM)

LPS was dissolved in distilled de-ionized water at concentration of 0.05 mg/mL; CRG samples were at concentrations of 0.1 mg/mL. The LPS–CRG mixture were prepared at the same concentrations. The CRG solution was mixed with LPS solution (2:1 *w/w*). Aliquots (12 μL) of the aqueous solutions of complex and their initial component were deposited onto freshly cleaved mica and dried at 37 °C for 24 h or at 70 °C for 30 s (for LPS). The morphology of CRG, LPS, and their mixtures was studied in air by AFM (Solver P47) in the tapping contact mode using a tip with the radius of 10 nm.

4.3. IL-10 and TNF-α Inducing Activity on the Human Blood Cells

The blood processing was performed using procedure of De Groote et al. Peripheral blood was collected by vena puncture into sterile siliconized tubes containing 30 IU of lithium heparinate per 5 mL tube diluted 1:5 in sterile Medium 199 (Sigma-Aldrich, Saint Louis, MO, USA) containing 300 mg/L of glutamine (Gibco, Life Technology, Darmstadt, Germany) and 50 μg/mL of gentamicin. Diluted blood (0.1 mL) was transferred into sterile polypropylene plates and then incubated with the LPS, carrageenans, or with LPS and carrageenan (370 °C, 5% CO$_2$). After 24 h, the supernatants were collected and frozen followed by cytokine determination using a specific ELISA kit ("Cytokine", Saint-Petersburg, Russia). The study protocol was approved by the medical ethics committee of the local hospital (Vladivostok, Russia). Informed consent was obtained from all subjects who participated in the study. All donors were free of medicine administration for 14 days prior to blood sampling. Blood was drawn from the antecubital vein of normal healthy human volunteers and anticoagulated in plastic tubes (Greiner Bio-One International AG, Kremsmuenster, Austria) with 30 IU lithium heparinate used as an anticoagulant.

4.4. Animals and Diets

The work was carried out in accordance with "Directives 2010/63/EU of the European Parliament and the Council of the European Union for the Protection of Animals used for Scientific Goals" and approved by the Federal Scientific Center of biodiversity FEB RAS Animal Care and Use Committee.

Mature male CD-1 mice were obtained from G.B. Elyakov Pacific Institute of Bioorganic Chemistry, FAR RAS (Vladivostok, Russia). The mice with body mass of 22–24 g kept in standard conditions of the vivarium at a controlled temperature 20–22 °C and ambient humidity 60–65%. Light were maintained on an artificial 12 h light–dark cycle. Each experimental group consisted of eight animals, each mouse in the cage had a floor area of 70 cm^2, which corresponds to international standards. The mice were provided with water standard feed compliant GOST R 50258-92 (CJSC ProKorm, Russia) ad libitum.

4.5. Experimental Design

This part of the study consisted of estimating the influence of different types of carrageenans on the physiological state of mice intoxicated *E. coli* LPS.

The mice were randomly allocated into six groups. All animals except the control group were given intraperitoneally LPS solution in dose 1 mg/kg body mass (0.1 mg/mL, pH 7.0) for five days. The control group received intraperitoneally 0.2 mL saline. The mice of the control and LPS groups were given only standard feed, whereas mice of other groups daily administrated CRGs suspensions in dose 100 mg/kg body mass (4 mg/mL, pH 7.0) 1 h before LPS injection through gastric gavage. At the end of experiment, mice were killed by decapitation, and their inner organs were removed and weighed. The blood samples were centrifuged at $1.200 \times g$ for 15 min. Relative organ masses of liver, thymus, thyroid, and adrenals were calculated as organ mass (mg)/body mass (g). Serum corticosterone concentrations were determined by the fluorometric method [57]. The glycogen content in liver was estimated with the anthrone reagent [58]. The adenosine triphosphate (ATP) and lactate levels in liver were measured enzymatic spectrophotometric methods used test-system with nicotinamide coenzymes NADF and NAD•H, respectively [59,60]. Statistical analysis was performed using Student's t-criterion for unpaired data, and p-values of less than 0.05 were considered significant. All data presented as mean ± standard deviation.

4.6. Medico-Biological Study of Food Supplement Carrageenan-FE

Ethical approval: The medico-biological study was carried out in accordance with The Code of Ethics of the World Medical Association (Declaration of Helsinki). Informed consent was obtained from all subjects who participated in the study.

The medical-clinical study of food supplementation Carrageenan-FE was carried out on the basis of the permission of the State Committee for Standardization of the Russian Federation (No.035/002158) and the consent of the ethics committee of the Central Research Institute of Epidemiology of the Federal Service on Customers Rights protection and human Well-being Surveillance (Moscow, Russia).

The food supplement Carrageenan-FE (Pacific Institute of Bioorganic chemistry, Far East Branch of the Russian Academy of Sciences, Vladivostok, Russia) is composed of two structural types of CRG. The supplement meets the requirements for food supplements and is recommended as an additional source of food fiber.

Patients diagnosed with enteric infection diseases and healthy volunteers were selected for current clinical trial based on an analysis out-patient medical records obtained from Ethical Committee in the framework of the Central Research Institute of Epidemiology of the Federal Service on Customers Rights Protection and Human Well-being Surveillance. After the patients were selected, they were enrolled in the current clinical trial to test the effects of the CRG-food supplement. The study of the therapeutic effect of CRG-FE in patients with enteric infection diseases with *Salmonella* etiology was carried out at a clinical infectious hospital (Moscow, Russia).

Dynamic examination of 42 patients (men and women, average age 31 years) with severe intoxication syndrome was conducted. Patients came to the hospital for 1–3 days with signs of intoxication: body temperature of up to 38–39 °C, chills, headache, frequent (10–15 times per day) loose stools, nausea, and repeated vomiting. Patients (22) received per os 150 mg of Carrageenan-FE administered together with 150 mL of Ringer solution to three times per day. In the second group, patients received 150 mL of the same solution (standard therapy). In the control group were healthy patients. The results were evaluated by clinical data and research parameters of hemostasis and immunological status. Hemostasis was characterized by the following parameters: prothrombin time, thrombin time, activated partial thromboplastin time, fibrinogen level, and platelet aggregation activity. To assess the state of immune system, relative and absolute number of lymphocytes, T lymphocytes (CD3+), and B-lymphocytes (CD19+), as well as immunoregulatory subpopulation of T-cells helpers (CD4+) and T cytotoxic lymphocytes (CD8+) were calculated. Investigations were carried out by flower cytometer EPICS XL (Beckman Coulter) using monoclonal antibodies IO-Test (double label). Functional activity of venous blood neutrophils was determined via spontaneous and stimulated with the test NBT (NBT-test) and expressed as conventional units.

4.7. Statistical Analysis

All measurements were done in three replicates. All results are expressed as mean ± the standard deviation compared by ANOVA. All differences were considered to be statistically significant if $p < 0.05$. Data were analyzed using the software Statistic 6.0. (StastSoft, Tulsa, OK, USA). To confirm the normal distribution of variables, Shapiro–Wilks test was performed.

5. Conclusions

In the present investigation, we revisited the effect of different types of CRGs on the LPS-induced intoxication of animals by the degree of variability of biochemical and pathological parameters to those most adequately responding to any valid stressor, including bacterial endotoxin. The data demonstrate that endotoxemia induced by intraperitoneal injection of bacterial LPS was less pronounced in the mice that received CRGs. ∑-, κ- and κ/β-CRGs increasing the resistance of the host organism to bacterial LPS are more active than λ-CRG, which has a high degree of sulfation and does not form a three-dimensional structure. LPS morphology is significantly changed under the action of the polysaccharide. According to AFM data, LPS is embedded in the three-dimensional structure of κ- and κ/β-CRGs, which probably contributes to a greater screening of its toxicity. The host resistance to endotoxin, induced by CRGs, can be caused by its effect on the macromolecular structure of LPS as well as the modulation of cytokine production of the organism by polysaccharide action.

We investigated the therapeutic effect of CRG in complex therapy of patients with enteric infections of Salmonella etiology. Our results show that the application of food supplement Carrageenan-FE in the standard therapy of toxicoinfections contributes to the correction of hemostasis and corrected some biochemical indicators and parameters of the immune system of the patient organism more actively in comparison with a control.

The results of our study reveal the potential application of CRG for treatment of Gram-negative infections associated with the accumulation of endotoxin in an organism.

References

1. Fuke, N.; Nagata, N.; Suganuma, H.; Ota, T. Regulation of gut microbiota and metabolic endotoxemia with dietary factors. *Nutrients* **2019**, *11*, 2277. [CrossRef]
2. Chang, S.; Li-Wu, L. Training Effects of Different Approaching Steps on Overarm Throwing Performance for Boys Aged 7–12 Years. *Sport. Exerc. Res.* **2010**, *12*, 191–209.
3. Kiechl, S.; Egger, G.; Mayr, M.; Wiedermann, C.J.; Bonora, E.; Oberhollenzer, F.; Muggeo, M.; Xu, Q.; Wick, G.; Poewe, W.; et al. Chronic Infections and the Risk of Carotid Atherosclerosis. *Circulation* **2001**, *103*, 1064–1070. [CrossRef]
4. Lugtenberg, B.; Van Alphen, L. Molecular architecture and functioning of the outer membrane of Escherichia coli and other gram-negative bacteria. *Biochim. Biophys. Acta—Rev. Biomembr.* **1983**, *737*, 51–115. [CrossRef]
5. Stoll, L.L.; Denning, G.M.; Weintraub, N.L. Potential Role of Endotoxin as a Proinflammatory Mediator of Atherosclerosis. *Arterioscler. Thromb. Vasc. Biol.* **2004**, *24*, 2227–2236. [CrossRef] [PubMed]
6. Rietschel, E.T.; Brade, H.; Holst, O.; Brade, L.; Müller-Loennies, S.; Mamat, U.; Zähringer, U.; Beckmann, F.; Seydel, U.; Brandenburg, K.; et al. Bacterial Endotoxin: Chemical Constitution, Biological Recognition, Host Response, and Immunological Detoxification. In *Pathology of Septic Shock*; Springer: Berlin/Heidelberg, Germany, 1996; pp. 39–81, ISBN 978-3-642-80186-0.
7. Hassoun, H.T.; Kone, B.C.; Mercer, D.W.; Moody, F.G.; Weisbrodt, N.W.; Moore, F.A. Post-injury multiple organ failure: The role of the gut. *Shock* **2001**, *15*, 1–10. [CrossRef] [PubMed]
8. Lee, S.H. Intestinal Permeability Regulation by Tight Junction: Implication on Inflammatory Bowel Diseases. *Intest. Res.* **2015**, *13*, 11. [CrossRef] [PubMed]
9. Cani, P.D.; Amar, J.; Iglesias, M.A.; Poggi, M.; Knauf, C.; Bastelica, D.; Neyrinck, A.M.; Fava, F.; Tuohy, K.M.; Chabo, C.; et al. Metabolic Endotoxemia Initiates Obesity and Insulin Resistance. *Diabetes* **2007**, *56*, 1761–1772. [CrossRef]
10. Cani, P.D.; Bibiloni, R.; Knauf, C.; Waget, A.; Neyrinck, A.M.; Delzenne, N.M.; Burcelin, R. Changes in Gut Microbiota Control Metabolic Endotoxemia-Induced Inflammation in High-Fat Diet-Induced Obesity and Diabetes in Mice. *Diabetes* **2008**, *57*, 1470–1481. [CrossRef]
11. Gomes, J.M.G.; de Assis Costa, J.; de Alfenas, R.C.G. Metabolic endotoxemia and diabetes mellitus: A systematic review. *Metabolism* **2017**, *68*, 133–144. [CrossRef]
12. Brown, B.I. Nutritional Management of Metabolic Endotoxemia: A Clinical Review. *Altern. Ther. Health Med.* **2017**, *23*, 42–54. [PubMed]
13. Estruch, R.; Martinez-Gonzalez, M.A.; Corella, D.; Basora-Gallisa, J.; Ruiz-Gutierrez, V.; Covas, M.I.; Fiol, M.; Gomez-Gracia, E.; Lopez-Sabater, M.C.; Escoda, R.; et al. Effects of dietary fibre intake on risk factors for cardiovascular disease in subjects at high risk. *J. Epidemiol. Commun. Heal.* **2009**, *63*, 582–588. [CrossRef] [PubMed]
14. Lahaye, M.; Kaeffer, B. Seaweed dietary fibres: Structure, physico-chemical and biological properties relevant to intestinal physiology. *Sci. Aliments* **1997**, *17*, 563–5834.
15. Knutsen, S.H.; Myslabodski, D.E.; Larsen, B.; Usov, A.I. A Modified System of Nomenclature for Red Algal Galactans. *Bot. Mar.* **1994**, *37*, 163–169. [CrossRef]
16. Yermak, I.M.; Khotimchenko, Y.S. Chemical properties, biological activities and applications of carrageenan from red algae. *Recent Adv. Mar. Biotechnol.* **2003**, *9*, 207–255.
17. Winter, C.A.; Risley, E.A.; Nuss, G.W. Carrageenin-Induced Edema in Hind Paw of the Rat as an Assay for Antiinflammatory Drugs. *Exp. Biol. Med.* **1962**, *111*, 544–547. [CrossRef]
18. Huang, M.-H.; Wang, B.-S.; Chiu, C.-S.; Amagaya, S.; Hsieh, W.-T.; Huang, S.-S.; Shie, P.-H.; Huang, G.-J. Antioxidant, antinociceptive, and anti-inflammatory activities of Xanthii Fructus extract. *J. Ethnopharmacol.* **2011**, *135*, 545–552. [CrossRef]
19. Ghosh, T.; Chattopadhyay, K.; Marschall, M.; Karmakar, P.; Mandal, P.; Ray, B. Focus on antivirally active sulfated polysaccharides: From structure–activity analysis to clinical evaluation. *Glycobiology* **2009**, *19*, 2–15. [CrossRef]
20. Pereira, M.G.; Benevides, N.M.B.; Melo, M.R.S.; Valente, A.P.; Melo, F.R.; Mourão, P.A.S. Structure and anticoagulant activity of a sulfated galactan from the red alga, Gelidium crinale. Is there a specific structural requirement for the anticoagulant action? *Carbohydr. Res.* **2005**, *340*, 2015–2023. [CrossRef]

21. Zúñiga, E.A.; Matsuhiro, B.; Mejías, E. Preparation of a low-molecular weight fraction by free radical depolymerization of the sulfated galactan from Schizymenia binderi (Gigartinales, Rhodophyta) and its anticoagulant activity. *Carbohydr. Polym.* **2006**, *66*, 208–215. [CrossRef]

22. Yermak, I.M.; Barabanova, A.O.; Aminin, D.L.; Davydova, V.N.; Sokolova, E.V.; Solov'eva, T.F.; Kim, Y.H.; Shin, K.S. Effects of structural peculiarities of carrageenans on their immunomodulatory and anticoagulant activities. *Carbohydr. Polym.* **2012**, *87*, 713–720. [CrossRef]

23. Cohen, S.M.; Ito, N. A Critical Review of the Toxicological Effects of Carrageenan and Processed Eucheuma Seaweed on the Gastrointestinal Tract. *Crit. Rev. Toxicol.* **2002**, *32*, 413–444. [CrossRef] [PubMed]

24. Weiner, M.L. Food additive carrageenan: Part II: A critical review of carrageenan in vivo safety studies. *Crit. Rev. Toxicol.* **2014**, *44*, 244–269. [CrossRef] [PubMed]

25. Zhu, Z.; Zhu, B.; Sun, Y.; Ai, C.; Wang, L.; Wen, C.; Yang, J.; Song, S.; Liu, X. Sulfated Polysaccharide from Sea Cucumber and its Depolymerized Derivative Prevent Obesity in Association with Modification of Gut Microbiota in High-Fat Diet-Fed Mice. *Mol. Nutr. Food Res.* **2018**, *62*, 1800446. [CrossRef] [PubMed]

26. Hu, S.; Wang, J.; Xu, Y.; Yang, H.; Wang, J.; Xue, C.; Yan, X.; Su, L. Anti-inflammation effects of fucosylated chondroitin sulphate from Acaudina molpadioides by altering gut microbiota in obese mice. *Food Funct.* **2019**, *10*, 1736–1746. [CrossRef]

27. Tateda, K.; Irifune, K.; Shimoguchi, K.; Tomono, K.; Matsumoto, T.; Kaku, M.; Yamaguchi, K.; Hirakata, Y. Potential Activity of Carrageenan to Enhance Antibacterial Host-Defense Systems in Mice. *J. Infect. Chemother.* **1995**, *1*, 59–63. [CrossRef]

28. Fujiki, K.; Shin, D.H.; Nakao, M.; Yano, T. Protective effect of κ-carrageenan against bacterial infections in carp Cyprinus carpio. *J. Fac. Agric. Kyushu Univ.* **1997**, *42*, 113–119.

29. Cheng, A.-C.; Chen, Y.-Y.; Chen, J.-C. Dietary administration of sodium alginate and κ-carrageenan enhances the innate immune response of brown-marbled grouper Epinephelus fuscoguttatus and its resistance against Vibrio alginolyticus. *Vet. Immunol. Immunopathol.* **2008**, *121*, 206–215. [CrossRef]

30. Yeh, S.-T.; Chen, J.-C. Immunomodulation by carrageenans in the white shrimp Litopenaeus vannamei and its resistance against Vibrio alginolyticus. *Aquaculture* **2008**, *276*, 22–28. [CrossRef]

31. Ermak, I.M.; Barabanova, A.O.; Kukarskikh, T.A.; Solovyova, T.F.; Bogdanovich, R.N.; Polyakova, A.M.; Astrina, O.P.; Maleyev, V.V. Natural polysaccharide carrageenan inhibits toxic effect of gram-negative bacterial endotoxins. *Bull. Exp. Biol. Med.* **2006**, *141*, 230–232. [CrossRef]

32. Arabski, M.; Barabanova, A.; Gałczyńska, K.; Węgierek-Ciuk, A.; Dzidowska, K.; Augustyniak, D.; Drulis-Kawa, Z.; Lankoff, A.; Yermak, I.; Molinaro, A.; et al. Modification biological activity of S and R forms of Proteus mirabilis and Burkholderia cepacia lipopolysaccharides by carrageenans. *Carbohydr. Polym.* **2016**, *149*, 408–414. [CrossRef]

33. Shnyra, A.; Hultenby, K.; Lindberg, A.A. Role of the physical state of Salmonella lipopolysaccharide in expression of biological and endotoxic properties. *Infect. Immun.* **1993**, *61*, 5351–5360. [CrossRef] [PubMed]

34. Yermak, I.M.; Davidova, V.N.; Gorbach, V.I.; Luk'yanov, P.A.; Solov'eva, T.F.; Ulmer, A.J.; Buwitt-Beckmann, U.; Rietschel, E.T.; Ovodov, Y.S. Forming and immunological properties of some lipopolysaccharide–chitosan complexes. *Biochimie* **2006**, *88*, 23–30. [CrossRef] [PubMed]

35. Solov'eva, T.; Davydova, V.; Krasikova, I.; Yermak, I. Marine Compounds with Therapeutic Potential in Gram-Negative Sepsis. *Mar. Drugs* **2013**, *11*, 2216–2229. [CrossRef] [PubMed]

36. Davydova, V.N.; Volod'ko, A.V.; Sokolova, E.V.; Chusovitin, E.A.; Balagan, S.A.; Gorbach, V.I.; Galkin, N.G.; Yermak, I.M.; Solov'eva, T.F. The supramolecular structure of LPS–chitosan complexes of varied composition in relation to their biological activity. *Carbohydr. Polym.* **2015**, *123*, 115–121. [CrossRef] [PubMed]

37. Yermak, I.M.; Kim, Y.H.; Titlynov, E.A.; Isakov, V.V.; Solov'eva, T.F. Chemical structure and gel properties of carrageenans from algae belonging to the Gigartinaceae and Tichocarpaceae, collected from the Russian Pacific coast. In *Sixteenth International Seaweed Symposium*; Springer: Dordrecht, The Netherlands, 1999; pp. 555–562.

38. Barabanova, A.O.; Yermak, I.M.; Glazunov, V.P.; Isakov, V.V.; Titlyanov, E.A.; Solov'eva, T.F. Comparative study of carrageenans from reproductive and sterile forms of Tichocarpus crinitus (Gmel.) Rupr (Rhodophyta, Tichocarpaceae). *Biochemistry* **2005**, *70*, 350–356. [CrossRef] [PubMed]

39. Rochas, C.; Rinaudo, M.; Landry, S. Role of the molecular weight on the mechanical properties of kappa carrageenan gels. *Carbohydr. Polym.* **1990**, *12*, 255–266. [CrossRef]

40. Heinbockel, L.; Weindl, G.; Martinez-de-Tejada, G.; Correa, W.; Sanchez-Gomez, S.; Bárcena-Varela, S.; Goldmann, T.; Garidel, P.; Gutsmann, T.; Brandenburg, K. Inhibition of Lipopolysaccharide- and Lipoprotein-Induced Inflammation by Antitoxin Peptide Pep19-2.5. *Front. Immunol.* **2018**, *9*, 1704. [CrossRef]

41. Brandenburg, K. Fourier transform infrared spectroscopy characterization of the lamellar and nonlamellar structures of free lipid A and Re lipopolysaccharides from Salmonella minnesota and Escherichia coli. *Biophys. J.* **1993**, *64*, 1215–1231. [CrossRef]

42. Aurell, C.A.; Hawley, M.E.; Wiström, A.O. Direct Visualization of Gram-Negative Bacterial Lipopolysaccharide Self-Assembly. *Mol. Cell Biol. Res. Commun.* **1999**, *2*, 42–46. [CrossRef]

43. Yermak, I.M.; Sokolova, E.V.; Davydova, V.N.; Solov'eva, T.F.; Aminin, D.L.; Reunov, A.V.; Lapshina, L.A. Influence of red algal polysaccharides on biological activities and supramolecular structure of bacterial lipopolysaccharide. *J. Appl. Phycol.* **2016**, *28*, 619–627. [CrossRef]

44. Luche, E.; Cousin, B.; Garidou, L.; Serino, M.; Waget, A.; Barreau, C.; André, M.; Valet, P.; Courtney, M.; Casteilla, L.; et al. Metabolic endotoxemia directly increases the proliferation of adipocyte precursors at the onset of metabolic diseases through a CD14-dependent mechanism. *Mol. Metab.* **2013**, *2*, 281–291. [CrossRef] [PubMed]

45. Jan, J.-S.; Yang, C.-H.; Wang, M.-H.; Lin, F.-L.; Yen, J.-L.; Hsieh, I.; Khotimchenko, M.; Lee, T.-H.; Hsiao, G. Hirsutanol A Attenuates Lipopolysaccharide-Mediated Matrix Metalloproteinase 9 Expression and Cytokines Production and Improves Endotoxemia-Induced Acute Sickness Behavior and Acute Lung Injury. *Mar. Drugs* **2019**, *17*, 360. [CrossRef] [PubMed]

46. Yermak, I.M.; Davydova, V.N.; Kravchenko, A.O.; Chistyulin, D.A.; Pimenova, E.A.; Glazunov, V.P. Mucoadhesive properties of sulphated polysaccharides carrageenans from red seaweed families Gigartinaceae and Tichocarpaceae. *Int. J. Biol. Macromol.* **2020**, *142*, 634–642. [CrossRef]

47. Kuznetsova, T.; Besednova, N.; Somova, L.; Plekhova, N. Fucoidan Extracted from Fucus evanescens Prevents Endotoxin-Induced Damage in a Mouse Model of Endotoxemia. *Mar. Drugs* **2014**, *12*, 886–898. [CrossRef]

48. Howard, M.; Muchamuel, T.; Andrade, S.; Menon, S. Interleukin 10 protects mice from lethal endotoxemia. *J. Exp. Med.* **1993**, *177*, 1205–1208. [CrossRef]

49. van der Poll, T.; Jansen, P.M.; Montegut, W.J.; Braxton, C.C.; Calvano, S.E.; Stackpole, S.A.; Smith, S.R.; Swanson, S.W.; Hack, C.E.; Lowry, S.F.; et al. Effects of IL-10 on systemic inflammatory responses during sublethal primate endotoxemia. *J. Immunol.* **1997**, *158*, 1971–1975.

50. Pajkrt, D.; Camoglio, L.; Tiel-van Buul, M.C.; de Bruin, K.; Cutler, D.L.; Affrime, M.B.; Rikken, G.; van der Poll, T.; ten Cate, J.W.; van Deventer, S.J. Attenuation of proinflammatory response by recombinant human IL-10 in human endotoxemia: Effect of timing of recombinant human IL-10 administration. *J. Immunol.* **1997**, *158*, 3971–3977.

51. Kremlev, S.G.; Palmer, C. Interleukin-10 inhibits endotoxin-induced pro-inflammatory cytokines in microglial cell cultures. *J. Neuroimmunol.* **2005**, *162*, 71–80. [CrossRef]

52. Kalitnik, A.A.; Karetin, Y.A.; Kravchenko, A.O.; Khasina, E.I.; Yermak, I.M. Influence of carrageenan on cytokine production and cellular activity of mouse peritoneal macrophages and its effect on experimental endotoxemia. *J. Biomed. Mater. Res. Part A* **2017**, *105*, 1549–1557. [CrossRef]

53. Cohen, J. The immunopathogenesis of sepsis. *Nature* **2002**, *420*, 885–891. [CrossRef] [PubMed]

54. Salat, A.; Murabito, M.; Boehm, D.; Bodingbauer, G.; Pulaki, S.; Sautner, T.; Mueller, M.R.; Fuegger, R. Endotoxin Enhances In Vitro Platelet Aggregability in Whole Blood. *Thromb. Res.* **1999**, *93*, 145–148. [CrossRef]

55. Sokolova, E.V.; Bogdanovich, L.N.; Ivanova, T.B.; Byankina, A.O.; Kryzhanovskiy, S.P.; Yermak, I.M. Effect of carrageenan food supplement on patients with cardiovascular disease results in normalization of lipid profile and moderate modulation of immunity system markers. *PharmaNutrition* **2014**, *2*, 33–37. [CrossRef]

56. Kilpatrick, D.C. Immunological aspects of the potential role of dietary carbohydrates and lectins in human health. *Eur. J. Nutr.* **1999**, *38*, 107–117. [CrossRef] [PubMed]

57. Glick, D.; Von Redlich, D.; Levine, S. Fluorometric Determination of Corticosterone and Cortisol in 0.02–0.05 Milliliters of Plasma or Submilligram Samples of Adrenal Tissue1. *Endocrinology* **1964**, *74*, 653–655. [CrossRef]

58. Seifter, S.; Dayton, S.; Novic, B.; Muntwyler, E. The estimation of glycogen with the anthrone reagent. *Arch. Biochem.* **1950**, *25*, 191–200.

59.   Hohorst, H.J. Bestimmung mit Lactate-Dehydrogenase und NAD. In *Methoden der Enzymatischen Analyse*; Bergmeyer, H.U., Ed.; Akademie-Verlag: Berlin, Germany, 1970; pp. 1425–1429.

60.   Lamprecht, W.; Trautschold, I. Adenosin-5′-triphosphat. Bestimmung mit Hexokinase und Glucose-6-phosphat Dehydrogenase. In *Methoden der Enzymatischen Analyse*; Bergmeyer, H., Ed.; Akademie-Verlag: Berlin, Germany, 1970; pp. 2024–2033.

Immunostimulatory Effect of Sulfated Galactans from the Green Seaweed *Caulerpa cupressoides* var. *flabellata*

Jefferson da Silva Barbosa [1,2,3], **Diego Araújo Sabry** [1], **Cynthia Haynara Ferreira Silva** [1],
Dayanne Lopes Gomes [4], **Arquimedes Paixão Santana-Filho** [5], **Guilherme Lanzi Sassaki** [5] and
Hugo Alexandre Oliveira Rocha [1,2,*]

[1] Laboratório de Biotecnologia de Polímeros Naturais—BIOPOL, Departamento de Bioquímica,
    Universidade Federal do Rio Grande do Norte, Natal 59.078-970, Rio Grande do Norte, Brazil;
    jefferson.barbosa@ifrn.edu.br (J.d.S.B.); popoh.diego@gmail.com (D.A.S.);
    cynthiahaynara@gmail.com (C.H.F.S.)

[2] Programa de Pós-Graduação em Ciências da Saúde, Universidade Federal do Rio Grande do Norte (UFRN),
    Natal 59012-570, Rio Grande do Norte, Brazil

[3] Instituto Federal de Educação, Ciência e Tecnologia do Rio Grande do Norte (IFRN)—Campus,
    São Gonçalo do Amarante 59291-727, Rio Grande do Norte, Brazil

[4] Instituto Federal de Educação, Ciência e Tecnologia do Piauí (IFPI)—Campus, BR 020, s/n,
    São Raimundo Nonato 64770-000, Bairro Primavera, Brazil; dayanne.oliveira@ifpi.edu.br

[5] Departamento de Bioquímica e Biologia Molecular, Universidade Federal do Paraná (UFPR),
    Curitiba 81.531-980, Paraná, Brazil; arquimetal@gmail.com (A.P.S.-F.); sassaki@ufpr.br (G.L.S.)

*   Correspondence: hugo@cb.ufrn.br; Tel.: +55-84-99999-9561

Abstract: Sulfated polysaccharides (SPs) obtained from green seaweeds are structurally heterogeneous molecules with multifunctional bioactivities. In this work, two sulfated and pyruvated galactans were purified from *Caulerpa cupressoides* var. *flabellata* (named SP1 and SP2), and their immunostimulatory effect was evaluated using cultured murine macrophage cells. Both SPs equally increased the production of nitric oxide, reactive oxygen species, and the proinflammatory cytokines TNF-α and IL-6. NMR spectroscopy revealed that both galactans were composed primarily of 3)-β-D-Galp-(1$\rightarrow$3) units. Pyruvate groups were also found, forming five-membered cyclic ketals as 4,6-*O*-(1′carboxy)-ethylidene-β-D-Galp residues. Some galactoses are sulfated at C-2. In addition, only SP2 showed some galactose units sulfated at C-4, indicating that sulfation at this position is not essential for the immunomodulatory activity of these galactans. Overall, the data showed that the galactans of *C. cupressoides* exhibited immunostimulating activity with potential therapeutic applications, which can be used in the development of new biomedical products.

Keywords: sulfated polysaccharides; galactans; green seaweed; NMR; immunostimulation; inflammatory mediators

1. Introduction

Current epidemiological data indicate an increase in immunological diseases. This has stimulated the search for a class of molecules, generally called immunomodulatory molecules, capable of increasing or suppressing the immune response in immune-mediated diseases [1].

Research on natural compounds that can modulate the immune response has become a focus in the experimental field, since such compounds have potential applications in the areas of immunopharmacology and oncotherapy. Different authors have reported that polysaccharides obtained from plants, fungi, and seaweed are able to modify various cellular processes and consequently possess a

variety of bioactivities, particularly potent effects on immune function [2–4]. Thus, immunostimulatory compounds, such as sulfated polysaccharides (SPs), have potential applications in the treatment of infections, immunodeficiencies, and cancer [5].

In this context, macrophages have been used as a study model in the identification of compounds with immunomodulatory properties [6,7]. Together with neutrophils, these cells constitute the body's first line of defense [8]. Through their antigen-presenting ability, they also play an important role in adaptive immunity [9]. Activation of macrophages is a key event in innate and adaptive immunity and is essential for defense mechanisms. Once activated by foreign agents, these cells can phagocytose and kill microorganisms and tumor cells, as well as produce molecules that recruit and activate other cells to the site of infection. In response to this stimulus, macrophages increase the production of reactive nitrogen intermediates such as nitric oxide (NO), reactive oxygen species (ROS), and proinflammatory cytokines such as TNF-α and IL-6 [10]. Therefore, macrophages are often used to evaluate the immunomodulatory effects of bioactive compounds from natural sources [11,12].

Although an increasing number of studies on the immunomodulatory activity of SPs from green seaweeds are being conducted, the extent of their activities varies greatly among different species of seaweed, and the structure correlations remain undefined [13].

The SPs of green seaweeds consist mainly of galactose, xylose, arabinose, mannose, rhamnose, glucuronic acid, and/or glucose [14]. The proportion of these monosaccharides seems to differ with the genus of the seaweed; for example, in seaweeds of the genera *Monostroma* and *Ulva*, it is more common to find rhamnose [15], whereas homo- and heterogalactans are common in the seaweeds of the genus *Caulerpa* [16], which are known to synthesize polysaccharides with immunomodulatory activities. Xylogalactans from *Caulerpa lentillifera* were found to exhibit a potent immunomodulatory effect by stimulating phagocytosis and increasing NO and cytokine secretion in RAW 264.7 macrophages [17]. In another work, Sun et al. [18] found that xylogalactomannans increased cell proliferation, phagocytosis, NO secretion, and alkaline phosphatase activity in macrophages. Galactans of *C. cupressoides* var. *lycopodium* showed antinociceptive and anti-inflammatory effects in vivo by reducing leukocyte migration in the peritoneal cavity of rats [19], while galactans of *Caulerpa mexicana* showed antinociceptive effect and decreased paw edema and myeloperoxidase activity in mice [20]. Ribeiro et al. [21] observed that *Caulerpa racemosa* SPs also exhibited antinociceptive and anti-inflammatory activities in an in vivo mouse model.

Less information is available on the SPs of the macroalga *C. cupressoides* var. *flabellata* and their immunomodulatory effects. This species synthesizes SPs that have antioxidant, anticoagulant, and antiproliferative activities in vitro [22]. Costa et al. [23] obtained four SPs populations with different characteristics regarding molecular weight and sulfate content. Monosaccharide composition analysis showed that galactose was the main constituent for all fractions; although glucose, mannose, xylose, rhamnose, and fucose were found, their proportions were different in each fraction. Subsequently, Barbosa et al. [24] investigated the immunostimulatory potential of these four polysaccharide fractions to determine their capacity to stimulate the production of different inflammatory mediators in the RAW 264.7 cell line. Of these, the so-called CCB-F1.0 fraction had a potent effect on the production of NO, ROS, and the cytokines TNF-α and IL-6. Although the SPs of the CCB-F1.0 fraction were determined to be composed of 76.47% total sugars and 17.95% sulfate, have a molecular weight of 155 kDa, and consist of galactose, mannose, and xylose in the ratio of 1.0:0.1:0.6 [23], further structural details of the polysaccharides of this fraction were not determined. Therefore, the present work aimed to purify the SPs of the CCB-F1.0 fraction of *C. cupressoides* var. *flabellata* and to characterize them structurally using nuclear magnetic resonance spectroscopy. In addition, to confirm that CCB-F1.0 immunomodulatory activity came from these molecules, the effects of SPs on some immunostimulating mediators (NO, ROS, and cytokines) using RAW 264.7 murine macrophages cells were investigated.

2. Results and Discussion

2.1. Purification of SPs

Initially, to obtain the SPs-rich extracts, proteolysis and methanol precipitation steps were performed. After these procedures, the SPs were fractioned with increasing volumes of propanone until the fraction CCB-F1.0 was obtained as described by Costa et al. [23]. Then, the SPs of this fraction were purified by ion exchange chromatography and eluted in a stepwise NaCl gradient (0.25–1.0 M). As shown in Figure 1, the elution of CCB-F1.0 (50 mg) generated three peaks in the chromatogram, corresponding to the molarities of 0.525 M (15.5 mg), 0.675 M (4.2 mg), and 0.9 M (1.8 mg), respectively. Based on this elution profile, the SPs obtained were labeled SP1, SP2, and SP3. Furthermore, SP1, SP2, and SP3 yielded 72%; 19.5%, and 8.5% (w/w) of the eluted SPs present in CCB-F1.0, respectively. Because of the lower yield obtained in the SP3 purification, the following analyses were not performed with this material.
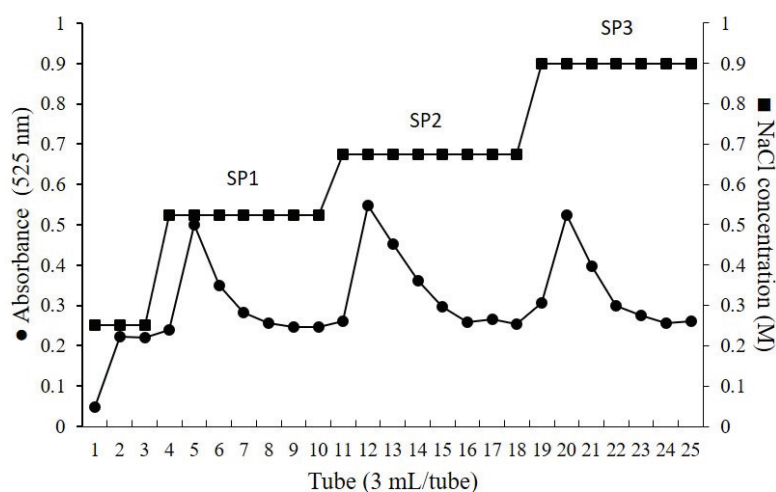
Figure 1. Stepwise elution profile of SPs from *C. cupressoides* on a HiTrap DEAE FF column.

Physicochemical analysis showed that SP1 and SP2 were composed mainly of polysaccharides and low quantity of protein, ~0.25% and 0.20%, respectively. In addition, both SPs were composed mainly of galactose, sulfate, and traces of mannose, as seen in Table 1.

Table 1. Chemical composition of CCB-F1.0 and purified sulfated polysaccharides from *Caulerpa cupressoides*.

Samples	Sulfate (%)	Protein (%)	Molar Ratio			
			Gal	Man	Xyl	SO$_4$
CCB-F1.0	17.8 ± 0.2	0.19 ± 0.03	1	0.1	0.6	0.56
SP1	9.35 ± 0.17	0.25 ± 0.04	1	0.08	n.d.	0.27
SP2	12.4 ± 0.1	0.20 ± 0.03	1	0.09	n.d.	0.98

Gal = galactose; Man = mannose; Xyl = xylose, SO$_4$ = sulfate, n.d. = not detected.

SP1 and SP2 were further analyzed by gel permeation chromatography (GPC) in a Sephadex® G-100 column to determine their homogeneity, as seen in Figure S1. The chromatograms of the *Caulerpa* SPs showed a single peak. Furthermore, the chromatogram obtained from GPC was used to calculate the apparent molecular weight using a regression equation determined using different molecular

weight standards. Thus, the molecular weight of SP1 and SP2 was found to be 125 and 135 kDa, respectively. These values were similar to those demonstrated by Costa el al. [23] in the studies of SPs in the CCB-F1.0 fraction.

2.2. NMR Analysis

NMR spectroscopy analysis is the most frequently used analytical technique for the structural characterization of sulfated glycans [25]. The analysis of 1H-NMR, as seen in Figures S2 and S3, COSY, as seen in Figures S4 and S5, and HSQCed, as seen in Figure 2 and Figure S6, spectra resulted in the identification of four main structural units of SP1 and SP2, labeled A to D, as seen in Figure 2A,C. The signals of the anomeric hydrogens of units A, B, C, and D were 4.69, 4.52, 4.82, and 4.69 ppm, respectively. These anomeric values indicated that all identified units are in the β configuration [26,27]. With the chemical shifts of the anomeric hydrogens, it was possible to determine the $^1H/^{13}C$ correlation in an HSQCed experiment, as seen in Figure 2A.
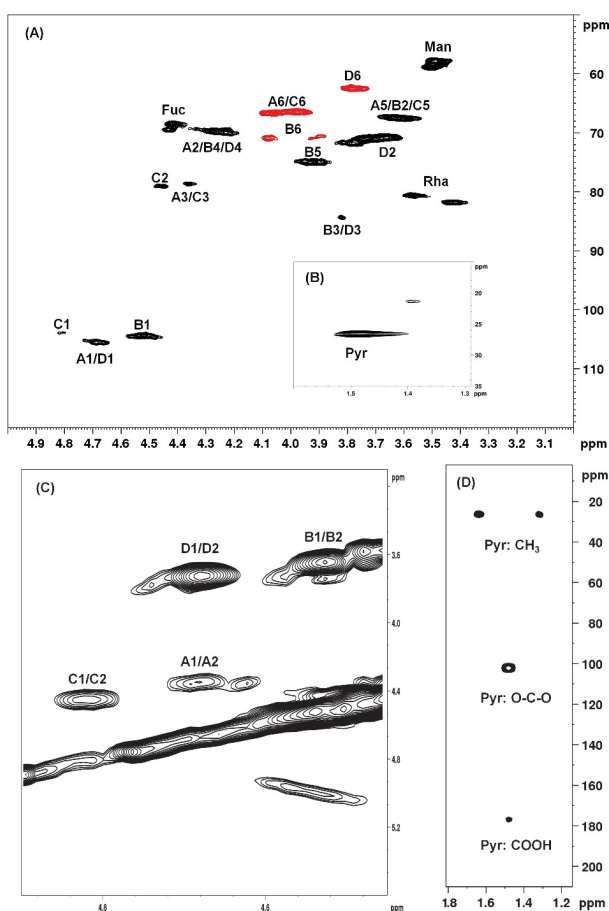
Figure 2. 2D-NMR spectra of SP1. (**A**) $^1H/^{13}C$ correlation 2D-NMR spectrum (HSQCed). (**B**) $^1H/^{13}C$ correlation 2D-NMR spectrum (HSQCed) of pyruvate. (**C**) $^1H/^1H$ correlation 2D-NMR spectrum (COSY). (**D**) $^1H/^{13}C$ correlation 2D-NMR spectrum (HMBC) of pyruvate.

Table 2 presents the results of the HSQCed analysis. As can be observed, SP1 and SP2 are very similar because these polysaccharides have many common structural characteristics, which can be confirmed by analyzing the spectra present in Supplementary Figures S2–S6. Therefore, only the spectra of SP1 are presented in Figure 2. The main difference between the two SPs was the signal of position 4 of unit B: in SP1, it was at 4.27/69.8 ppm, whereas in SP2, it was at 5.00/78.3 ppm. This result indicated the presence of a sulfate group at position 4 of a galactose in SP2 [28]. Furthermore, anomeric signals of 4.90/103.6 and 4.87/104.5 ppm were identified in SP2, but it was not possible to identify the other positions of the unit. These values have been described as characteristic of pyruvate galactan structural units in positions 4 and 6 [29] and in positions 3 and 4 [30], respectively.

Table 2. Signal assignments (ppm) of NMR spectra of SP1 and SP2 from *C. cupressoides*.

Structural Unit	Chemical Shifts (ppm)					
	H-1/C-1	H-2/C-2	H-3/C-3	H-4/C-4	H-5/C-5	H-6/C-6
SP1						
A	4.69/105.5	4.27/69.8	4.36/78.7	3.79/71.8	3.65/67.6	3.97/66.5
B	4.52/104.4	3.65/70.8	3.81/84.4	4.27/69.8	3.92/74.9	4.00/71.0
C	4.82/103.9	4.45/79.1	4.36/78.7	n.d.	3.60/67.6	3.97/66.5
D	4.69/105.5	3.73/71.0	3.81/84.4	4.27/69.8	n.d.	3.78/62.5
SP2						
A	4.69/105.5	4.27/69.8	4.36/78.7	3.79/71.8	3.65/67.6	3.97/66.5
B	4.52/104.4	3.65/70.8	3.96/83.7	5.00/78.3	3.92/74.9	4.00/71.0
C	4.82/103.9	4.56/76.8	4.50/77.3	4.12/69.8	3.60/67.6	3.97/66.5
D	4.69/105.5	3.73/71.0	3.81/84.4	4.27/69.8	n.d.	3.78/62.5
→3)4,6Pyr-β-D-Gal*p*-(1→ [a]	4.60/105.0	4.20/69.6	4.20/79.5	n.d./71.6	3.60/67.0	3.90/65.9
→3,6)-β-D-Gal*p*-(1→ [b]	4.53/104.5	3.72/71.3	3.85/83.7	4.23/69.8	3.92/74.9	3.92;4.02/70.8
→3)4,6Pyr-β-D-Gal*p*2S-(1→ [c]	4.85/103.5	4.48/76.2	4.39/77.2	4.11/71.8	3.54/66.9	3.85;3.97/65.9
→3)-β-D-Gal*p*-(1→ [b]	4.68/105.5	3.78/71.7	3.85/83.5	4.19/69.8	3.71/76.2	3.79/62.3
→3,6)-β-D-Gal*p*4S-(1→ [b]	4.58/104.4	3.73/72.2	4.05/80.0	4.91/79.5	4.05/74.5	n.d.

n.d. = not detected. Signals reported in literature: [a] Fernández et al. [30]; [b] Bilan et al. [28]; [c] Arata et al. [29].

Through the analysis of HSQCed spectra, it was also possible to determine each of the 4 structural unit constituents of the SPs. Unit A presents anomeric correlation between hydrogen and carbon at 4.69/105.5 ppm. In addition, it was possible to observe the presence of a signal at 1.48/26.4 ppm corresponding to pyruvate, as seen in Figure 2B, as one of the substituents of units A and C, as seen in Table 2, linked at O-4 and O-6. The presence of pyruvate was also confirmed in the HMBC spectrum, as seen in Figure 2D. Thus, both the A and C units are in the form of 4,6-*O*-(1-carboxyethylidene)-β-D-galactose or →3)4,6Pyr-β-D-Gal*p*-(1→. Unit B has 4.52/104.4 ppm as H1/C1 correlation. In addition, there are chemical shifts at 3.81/84.4 and 4.00/71.0 ppm at positions 3 and 6, respectively, which are characteristics of β(1→3,6)-linked units [28]. Unit C presents an anomeric signal at 4.82/103.9 ppm, but also shows signals of pyruvylation at positions 4 and 6. However, when compared to unit A, it is possible to observe that positions C1 and C2 are deshielded, probably due the presence of a sulfate group at C2 [29]; this unit was identified as →3)4,6Pyr-β-D-Gal*p*2S-(1→. Unit D has 4.69/105.5 ppm as H1/C1 correlation and a chemical shift of position 3 (3.81/84.4 ppm) corresponding to →3)-β-D-Gal*p*-(1→ [28].

We detected some signals that are not part of any of the four systems we have marked, as seen in Table 2. Costa et al. [23] showed CBB-F1.0 made of galactose:xylose:mannose (1.0:0.6:0.1) and traces of fucose and rhamnose. Thus, these signals may be indicative of the presence of these monosaccharides in SP1 and SP2. The signal at 4.41/68.5–69.5 ppm corresponds to H5/C5 correlation of fucose units [31]. The presence of *O*-methyl-mannose was confirmed by the signal at 3.49/57.8–58.8 ppm [32]. We also found two signals that correspond to *O*-methyl-rhamnose (3.57/80.6 ppm) and (3.42/81.8 ppm) [33,34]. However, we were not able to identify spin systems that confirm the presence of these monosaccharides. Most likely, these sugars can be randomly distributed throughout the galactan structures.

Overall, the studies of NMR spectra ensure that the →3,6)-β-D-Gal*p*-(1→ is the predominant unit of these polysaccharides, as seen in Figure 3B. However, galactopyranosyl units linked by β1→3

linkages are also found, as seen in Figure 3D, as there are units containing 3,4-*O*-(1′ carboxy)-ethylidene, as seen in Figure 3A, and 2-*O*-sulfate, as seen in Figure 3C.
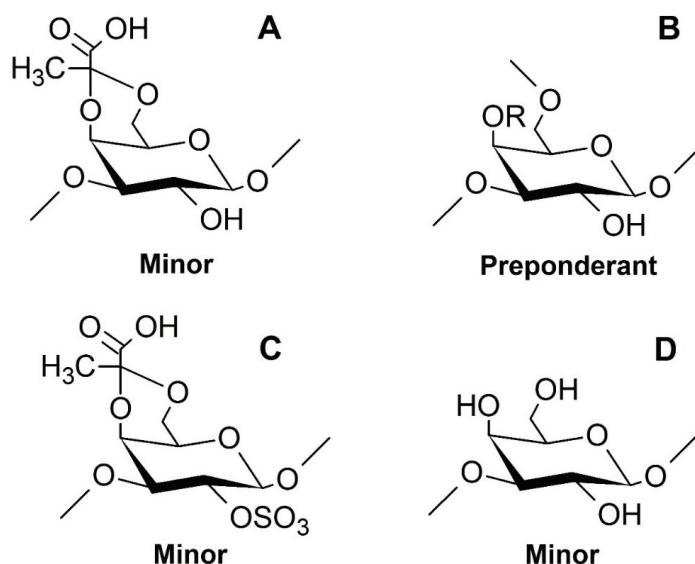

Figure 3. Proposed structures of the components found in the SP1 and SP2. The radical R corresponds to hydrogen atoms (H) or sulfate groups (SO$_4$); however, for SP1, R = H. (**A**): →3)4,6Pyr-β-ᴅ-Gal*p*-(1→; (**B**): →3,6)-β-ᴅ-Gal*p*-(1→, for SP1 and →3,6)-β-ᴅ-Gal*p*4S-(1→, for SP2; (**C**): →3)4,6Pyr-β-ᴅ-Gal*p*2S-(1→; (**D**): →3)-β-ᴅ-Gal*p*-(1→.

The presence of β-ᴅ-galactans in green algae has also been reported in other works. Ciancia et al. [35] identified a 3-linked β-ᴅ-galactan, partially sulfated at C6 and pyruvylated at positions 4 and 6, from *Bryopsis plumosa*. Species of the genus *Codium* synthesize galactans consisting of partially sulfated C4 and/or C6 β-ᴅ-galactopyranose residues with significant pyruvate content [26–28,30]. Sulfated and pyruvylated galactans were also isolated from the tropical green algae species *Penicillus capitatus*, *Udotea flabellum*, and *Halimeda opuntia* [29]. However, studies on sulfated and pyruvylated galactans obtained from green algae with immunostimulating properties are scarce. Because of that, a question arose. Would these galactans be responsible for the immunomodulatory activity that was observed in CCB-1.0 and was it shown by Barbosa et al. [24]? Therefore, the effect of these galactans on the levels of some immunomodulation mediators (NO, ROS, and cytokines) was evaluated.

2.3. Cell Viability

Macrophages play several roles in the biology of organisms, including development, homeostasis, and repair, as well as the immune response against pathogens [36]. The evaluation of the viability of RAW 264.7 murine macrophages has previously been used as an indicator of the activation of macrophages and, subsequently, for the characterization of the immunomodulatory potential of new compounds with biomedical applications [37]. Among these analyses, the capacity to reduce MTT to formazan crystals by mitochondrial dehydrogenases is an important measure for evaluating cell viability. Therefore, the effect of SP1 and SP2 on the ability of RAW 264.7 macrophages to reduce MTT after an exposure period of 24 h at concentrations ranging from 12.5 to 100 µg/mL was initially evaluated. As shown in Figure 4, a statistically significant ($p < 0.05$) increase in MTT reduction capacity was promoted by SP1 at concentrations of 12.5 and 25 µg/mL, whereas for the other concentrations, the values did not differ from that of the negative control. For SP2, the cell viability did not differ

from that of the negative control, except at the highest concentration (100 µg/mL), which caused a statistically significant decrease ($p < 0.05$) in MTT reduction capacity of around 30%. In this case, the higher SP2 concentration may have interfered with mitochondrial metabolism and consequently led to a reduction of cell viability. These results suggest that at concentrations less than 100 µg/mL, SP1 and SP2 do not cause considerable cytotoxic effects on RAW 264.7 macrophages. For the following analyses, the concentration of 100 µg/mL of SP2 was excluded because it promoted a reduction in cell viability and potentially had a cytotoxic effect.
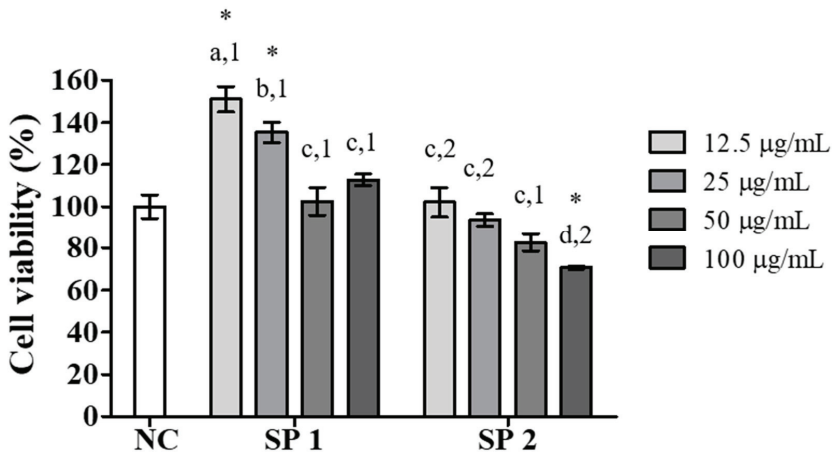
Figure 4. Effects of SP1 and SP2 of *C. cupressoides* on the cell viability of RAW 264.7 macrophages. NC—negative control. The data are presented as the mean ± standard deviation ($n = 3$). Different letters represent statistically significant differences between the different SPs ($p < 0.05$). Different numbers represent statistically significant differences between the same concentrations of the two SPs ($p < 0.05$). * represents samples that presented statistically significant differences in relation to the negative control ($p < 0.05$).

2.4. NO Production

Stimulatory effects of algae polysaccharides on macrophages result in the production of NO through the induction of the enzyme inducible nitric oxide synthase [38,39]. NO is a highly reactive molecule that is important for the functioning of the immune system, and it has cytotoxic effects on pathogenic microorganisms and cancer cells [40]. Therefore, NO production in the supernatant of RAW 264.7 murine macrophages stimulated with *C. cupressoides* SPs was evaluated. The NO production induced by SP1 and SP2 at concentrations between 12.5 and 100 µg/mL, expressed in relation to the amount of NO produced in the positive control (2 µg/mL LPS), is shown in Figure 5. SP1 promoted a statistically significant increase ($p < 0.05$) in the production of NO at concentrations of 50 and 100 µg/mL, whereas for SP2, the concentrations of 25 and 50 µg/mL showed the greatest stimulatory effect on the production of NO. These results were similar to those reported in other works that evaluated the effects of SPs obtained from different species of seaweed on the ability of induce NO production in macrophages [41–43].
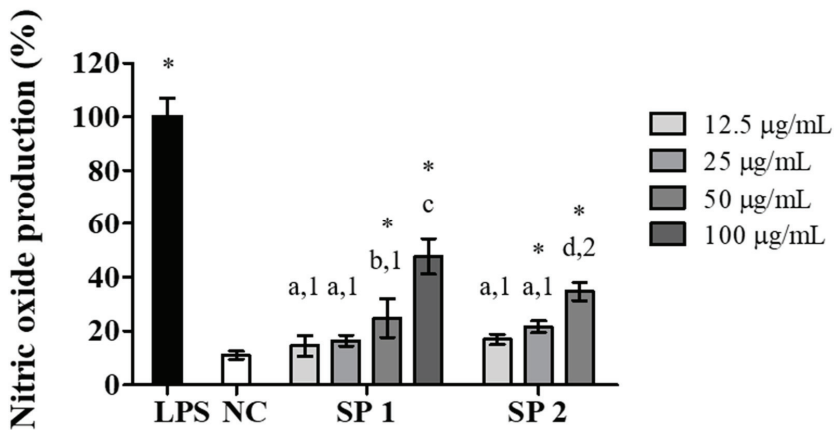
Figure 5. Effects of SP1 and SP2 of *C. cupressoides* on NO production. NC—negative control; LPS—bacterial lipopolysaccharide (2 µg/mL). The data demonstrate the mean ± standard deviation ($n = 3$). Different letters represent statistically significant differences between SPs concentrations ($p < 0.05$). Different numbers represent statistically significant differences between the same concentrations of different SPs ($p < 0.05$). * represents samples that had a statistically significant difference in relation to the negative control ($p < 0.05$).

Studies on the immunostimulatory effect of polysaccharides have revealed that these molecules are capable of binding to several receptors on the surface of macrophages, which can activate several intracellular signaling pathways. As a result of this activation, the expression of genes that encode different inflammatory mediators, such as NO and cytokines, is initiated [44–46]. Some structural requirements, necessary for the immunostimulatory activity of algae polysaccharides, have been identified by Leiro et al. [47]. They found that the desulfation of polysaccharides from *Ulva rigida* was a determining factor for its immunostimulatory activity. The presence of the sulfate group was also shown to be an important characteristic for the effect of *Sargassum angustifolium* polysaccharides on NO production [48]. For SPs from *Ulva intestinales*, the lower molecular weight of one of the fractions was found to be a fundamental characteristic for immunostimulatory activity [13]. In another study, Bahramzadeh et al. [49] proposed that the compaction of the SPs obtained from *Cystoseira indica* seemed to be a more determinant characteristic for its immunostimulatory capacity than the size of the molecule and its degree of sulfation. However, the monosaccharide composition, sulfate content, and ultrastructure of *C. lentifera* polysaccharides appeared to have been crucial for their effect on NO production in RAW 264.7 macrophages [18]. Therefore, a systematic and in-depth study that aimed to relate the individual and/or combined structural characteristics of *C. cupressoides* SPs and their immunostimulatory effect was needed.

2.5. Production of Intracellular ROS

During the processes of the recognition and response to harmful cell agents, phagocytic cells produce NO and ROS [50]. Thus, ROS production is an important indicator of macrophage function [51]. Because the treatment of RAW 264.7 macrophages with the purified SPs of *C. cupressoides* promoted a stimulatory effect on NO production, it was determined whether there would be a similar effect on the production of intracellular ROS. Figure 6 shows the effect of treatment with SP1 and SP2 on the production of ROS after a 24 h exposure period at concentrations ranging from 12.5 to 100 µg/mL. The displacements of the histograms shown in A and B indicated that the two SPs promoted an increase in ROS production. Analysis of the fluorescence intensity emitted by cells treated with the SPs in relation to that of the positive control (2 µg/mL LPS) revealed a statistically significant

increase ($p < 0.01$) in all evaluated conditions, as seen in Figure 6C. These results are consistent with the effects of immunostimulating polysaccharides on ROS production reported in other studies. Wang et al. [52] reported that SPs from *Ascophyllum nodosum* significantly increased intracellular ROS levels in macrophages. In another study, sulfated galactans from the algae *Gracilaria lemaneiformis* also promoted stimulatory effects on ROS production [53], whereas the treatment of peritoneal macrophages with arabinogalactan and fucoidan increased the production of reactive oxygen and nitrogen species [54]. Although the increase in ROS production, induced by SP1 and SP2, was lower than that observed in the positive control, their stimulatory effects can be considered to be relevant and safe for macrophage activation because the excess production of ROS can lead to severe oxidative damage in cells.
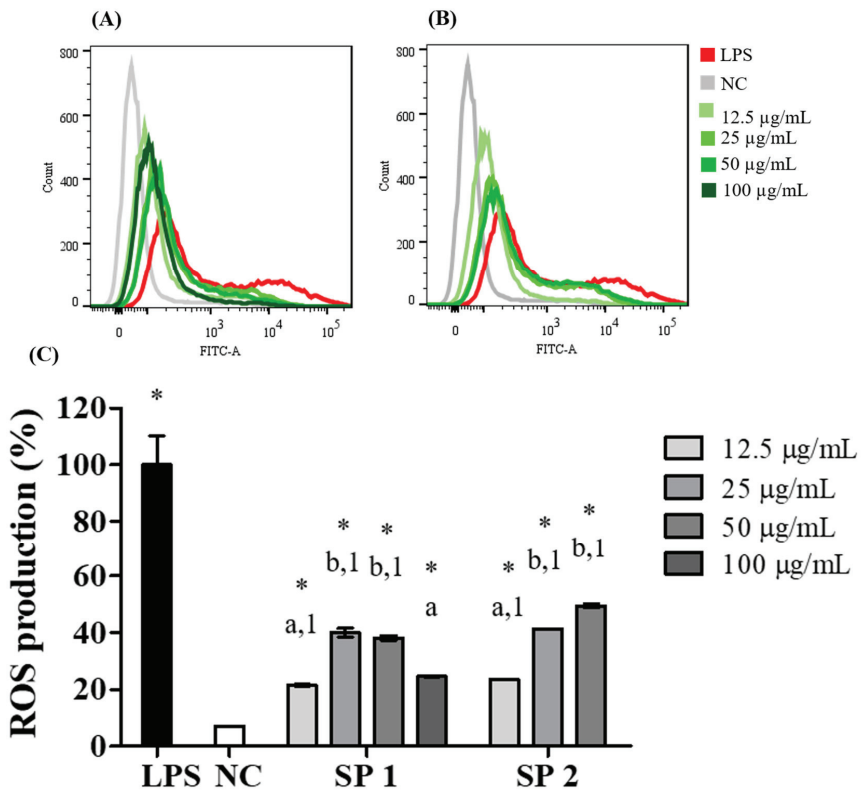
Figure 6. Production of ROS. Histograms representative of the effects of different concentrations of SP1 (**A**) and SP2 (**B**) on intracellular ROS production quantified by flow cytometry. NC—negative control; LPS—bacterial lipopolysaccharide (2 μg/mL). (**C**) Percentage of intracellular ROS production in relation to that of LPS-stimulated cells. The data are presented as the mean ± standard deviation ($n = 3$). Different letters represent statistically significant differences between SPs concentrations ($p < 0.01$). Different numbers represent statistically significant differences between the same concentrations of different SPs ($p < 0.01$). * represents samples that had a statistically significant differences in relation to the negative control ($p < 0.01$).

2.6. Proinflammatory Cytokine Production

Secretion of proinflammatory cytokines by activated macrophages is directly involved in the defense against pathogen invasion. These molecules play an important regulatory role in cell growth,

proliferation, and immunity [55]. When exposed to immunostimulatory agents, macrophages secrete inflammatory mediators, including NO, ROS, and cytokines such as TNF-α and IL-6 [56,57]. Here, both cytokines were quantified in the supernatant of RAW 264.7 macrophages exposed to SP1 and SP2 at concentrations of 100 and 50 μg/mL, respectively. As shown in Figure 7A, a statistically significant increase ($p < 0.01$) of TNF-α production was observed in cells treated with SP1 and SP2, compared to that in the negative control. It should be noted that the effect of these SPs on the production of TNF-α was higher than that in the cells stimulated with LPS (positive control). SP1 and SP2 also promoted a statistically significant increase ($p < 0.01$) in the levels of IL-6, compared to that in the negative control, as seen in Figure 7B.
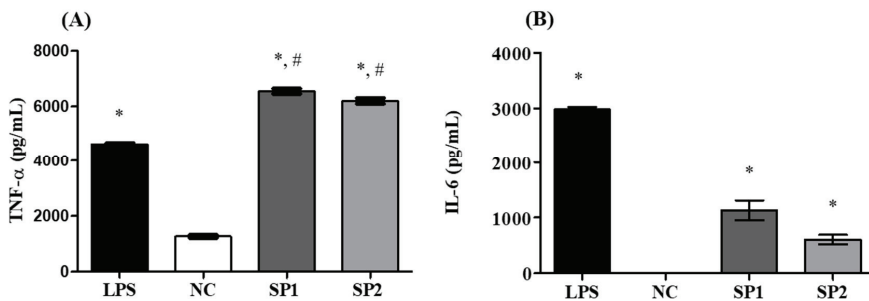
Figure 7. Production of the proinflammatory cytokines TNF-α (**A**) and IL-6 (**B**). NC—negative control; LPS—bacterial lipopolysaccharide (2 μg/mL). The data are presented as the mean ± standard deviation. * represents samples that had a statistically significant differences in relation to the negative control ($p < 0.01$). # represents statistically significant increases ($p < 0.01$) in relation to LPS. SP1 and SP2 were evaluated at concentrations of 100 μg/mL and 50 μg/mL, respectively. IL-6 was not detected in the NC group.

The quantification of the proinflammatory cytokines TNF-α and IL-6 in macrophage cultures is an important assessment in studies on the immunomodulatory effects of polysaccharides obtained from algae. SPs from *Cyclocarya paliurus* increased the immunostimulatory activity of RAW macrophages through the production and secretion of various inflammatory mediators, including TNF-α and IL-6 [58]. In another study, the fucoidan from *Undaria pinnatifida* had a potent stimulatory effect on the production of TNF-α and IL-6 [59]. Similar effects on TNF-α and IL-6 secretion in RAW 264.7 macrophages were also observed in the study by Liu et al. [43] that evaluated the effects of *Porphyra haitanensis* SPs as well as in the work by Ren et al. [53] that evaluated the immunostimulatory effect of the polysaccharides from *Gracilaria lemaneiformis*. In a previous study, we showed that CCB-F1.0 promoted a significant increase in the production of IL-6 and TNF-α [24]. However, to investigate this effect, CCB-F1.0 was tested in concentrations 8 and 16 times higher than SP1 and SP2, respectively. These findings indicate that the purification process enabled isolation of the compounds with more proinflammatory effect. Therefore, *C. cupressoides* SPs may play an important role in stimulating the immune response mediated by macrophages.

3. Materials and Methods

3.1. Materials

1,9-Dimethyl-methylene blue zinc chloride double salt (DMMB), 2',7'-dichlorofluorescin diacetate (DCFH-DA), 3-(4,5-dimethylthiazolyl-2)-2,5-diphenyltetrazolium bromide (MTT), deuterium oxide (D_2O), and Griess reagent were purchased from Sigma Chemical Company (St. Louis, MO, USA). Dulbecco's modified Eagle's medium (DMEM) and fetal bovine serum (FBS) were obtained from Cultilab (Campinas, SP, Brazil). Penicillin and streptomycin were purchased from Gibco (Fort Worth,

TX, USA). The kit for cytokine analysis was purchased from BD Biosciences (San Jose, CA, USA). Lipopolysaccharide (LPS), *Escherichia coli* 055: B5 was obtained from Santa Cruz Biotechnology (Dallas, TX, USA). All the other solvents and chemical products were of analytical grade.

3.2. Seaweed Collection

The green macroalgae *C. cupressoides* var. *flabellata* was collected in the city of Nísia Floresta, on the southern coast of the state of Rio Grande do Norte, Brazil. After the collection, the seaweed was transported to the Laboratório de Biotecnologia de Polímeros Naturais of the Biochemistry Department, Universidade Federal do Rio Grande do Norte, for the removal of epiphytic species, sediment, and encrusted organisms and subsequent extraction of their SPs. The material collection occurred under authorization of Brazilian National Management System Genetic Heritage and Associated Traditional Knowledge (loose translation) SisGen n° A0D4240.2.1.1.

3.3. Extraction of SPs

To obtain the SPs-rich extract, the seaweeds were dried, crushed, delipidated with ethanol, and submitted to proteolysis. The proteolytic digestion was conducted with 100 g of this powdered seaweed, 0.25 M NaCl (500 mL) pH = 8.0, and a mixture of alkaline proteases (Prolav 750, Prozyn Biosolutions, São Paulo, SP, Brazil) at 15 mg/g powdered seaweed; for 18 h at 60 °C. The SPs-rich extract was obtained after filtration and centrifugation (10,000× *g* for 20 min, 4 °C), and it was submitted to fractionation step as described by Costa et al. [23]. Briefly, 0.3 volumes of propanone (4 °C) was dropped to the SPs-rich extract under gentle agitation and maintained for 24 h. The material was centrifuged (10,000× *g* for 20 min, 4 °C), dried, and kept in the dark until further use. The fractionation was repeated by adding 0.5, 1.0, and 2.0 volumes of propanone to the supernatant. Based on the propanone volumes used, the fractions were named CCB-F0.3, CCB-F0.5, CCB-F1.0, and CCB-F2.0, respectively.

3.4. Purification of SPs by Liquid Ion Exchange Chromatography

The SPs of the CCB-F1.0 fraction were purified with a fast protein liquid chromatography (FPLC) system at ÄKTA-GE (Healthcare Life Sciences, Little Chalfont, Bucks, UK) using a 5 mL HiTrap DEAE FF column (GE Healthcare, Westborough, MA, USA). To prepare the sample, the CCB-F1.0 fraction was solubilized in 0.25 M NaCl at concentration of 5 mg/mL, filtered using 0.22 μm filters, and injected into the column (1 mL). The SPs bound to the column were eluted by applying a stepwise NaCl gradient (0.525, 0.675, and 0.9 M), based on a first elution with continuous gradient ranging from NaCl 0.25 to 3.0 M. All peaks were monitored by DMMB metachromasia and absorbance at 525 nm [60]. This procedure was repeated ten times. Then, the material (each peak) obtained was pooled and dialyzed (MW cut-off of 6 kDa) against distilled water and lyophilized.

3.5. Physicochemical Analysis

Total sugar content determination was performed by the phenol-sulphuric acid method using galactose as the reference sugar [61]. Sulfate content was determined by the barium chloride-gelatin method [62]. Protein content was measured as described by Bradford [63]. Monosaccharide composition was determined by nuclear magnetic resonance spectroscopy as described by Sassaki and coworkers (2014) [64]. Briefly, samples (5 mg) were hydrolyzed with 2 M HCl for 4 h at 100 °C. Then, the solution was neutralized, evaporated, and the residue dissolved in D_2O for NMR analysis (~600 μL). A diluted D_2O–H_2SO_4 solution was used for adjusting pH value to 3.5. Finally, quantitative-HSQC (Q-HSQC) spectra were obtained at 27 °C using a hsqcetgpsisp2.2 pulse sequence on Bruker spectrometers (Bruker, Billerica, MA, USA).

3.6. Molecular Weight and Homogeneity Determination

Molecular weight and homogeneity SPs from *C. cupressoides* were determined by gel permeation chromatography (GPC). Each fraction was dissolved to a final concentration of 10 mg/mL and applied to a column containing Sephadex® G-100 (135 × 1 cm i.d.; Sigma Chemical Company, St. Louis, MO, USA). GPC was performed using an isocratic elution mode. The molecular weight was estimated by reference to a calibration curve made by dextran standards (10, 40, 70, 147, and 500 kDa). Homogeneity of SPs was evaluated by chromatographic profile. The SPs elution was monitored by sugar determination according to Dubois et al. [61].

3.7. NMR Spectroscopy

NMR spectra were obtained using a Bruker Avance III Ascend 600 MHz (14.1 T) spectrometer (Billerica, MA, USA) equipped with a 5 mm inverse probe. Each sample had its ^{1}H 90° pulse calibrated and transmitter frequency offset calculated = 1881.69 Hz (SP1) and 2822.59 Hz (SP2), and the value was used to all following experiments, which were conducted at 70 °C with samples (20 mg/mL) previous solubilized with deuterium oxide (D_2O) without spinning. 1D-NMR spectra were obtained using a presat sequence pulse (zgpr) to suppress solvent peak. Presat experiments were performed with a spectral width (SWH) of 4795.396 Hz, size of fid (TD) = 64k, and number of scans (NS) = 8. 2D-NMR homonuclear (^{1}H–^{1}H) COSY (Correlation Spectroscopy) analysis were performed using Bruker's cosygpprqf pulse sequence with SWH = 4795.396 Hz, TD = 2048 (F2) × 256 (F1), number of dummy scans (DS) = 16, NS = 16, and relaxation delay = 1.5 s. 2D-NMR heteronuclear (^{1}H–^{13}C) HSQCed (Edited Heteronuclear Single Quantum Coherence) analysis were performed using Bruker's hsqcedetgpsisp2.2 pulse sequence with SWH = 4795.396 Hz (F2) × 16667.754 Hz (F1), TD = 2048 (F2) × 256 (F1), DS = 16, NS = 32, and relaxation delay = 1.0 s. HMBC (Heteronuclear Multiple Bond Correlation) analysis were performed using Bruker's hmbcgpndqf pulse sequence with SWH = 4789.272 Hz (F2) × 20124.867 Hz (F1), TD = 2048 (F2) × 256 (F1), DS = 16, NS = 46, and relaxation delay = 1.0 s. The chemical shift of ^{1}H and ^{13}C were expressed in δ (ppm) relative to TMSP (trimethylilsilylpropionate) as an internal standard (δ = 0 ppm). NMR spectra analysis was conducted using Bruker's TopSpin v 4.0.6 software (Bruker, Billerica, MA, USA). The proposed structures were designed using ChemSketch v.12.0 software (ACD/Labs, Toronto, ON, Canada).

3.8. Cell Culture

The RAW 264.7 macrophage cell line (ATCC number TIB-71) was cultured in DMEM supplemented with FBS (10% v/v) and antibiotics (100 U/mL penicillin and 100 µg/mL streptomycin). The cells were incubated at 37 °C in a humidified atmosphere with 5% CO_2. For maintenance of the cells, the culture medium was changed every three days, and the cells were further subcultured at the 80% confluency using a cell scraper.

3.9. MTT Reduction Test

The ability of RAW 264.7 macrophages to reduce MTT was evaluated according to the previously described method of Mosmann [65] to analyze the effect of SPs on cell viability. Initially, the cells were seeded in 96-well plates at a density of 1×10^4 /well. After treatment with the SPs at the different concentrations tested (12.5–100 µg/mL) for 24 h, the culture medium was replaced with 100 µL of MTT (1 mg/mL dissolved in DMEM). Then, the cells were incubated for 4 h at 37 °C. Subsequently, the culture supernatant was discarded, and the crystals of formazan were solubilized in ethanol, 100 µL/well. Absorbance was measured with an Epoch microplate spectrophotometer (Biotek Instruments Inc., Winooski, VT, USA) at 570 nm. Cell viability was calculated in relation to the negative control using the formula: % viability = (Atest/AControl) × 100, in which Atest corresponds to the absorbance of the experimental group and Acontrol corresponds to the absorbance of the negative control.

3.10. NO Production

The nitrite levels released in the supernatant of the cultured RAW 264.7 cells were quantified to evaluate the immunostimulatory effect of the SPs of *C. cupressoides*, as described previously [66]. Initially, the cells were cultured (3×10^5/well) in 24-well plates and exposed to different concentrations of the purified SPs (12.5–100 μg/mL) for 24 h. LPS (2 μg/mL) was used as a positive control. After the treatment time, 100 μL of the supernatant was collected and mixed with 100 μL of Griess reagent and incubated for 10 min at room temperature in the dark. Absorbance was measured at 540 nm with a microplate spectrophotometer. Sodium nitrite was used as a standard, and the results were expressed as the percentage of nitrite production in relation to that of the positive control (LPS) according to the formula: % of nitrite production = (Atest/ALPS) × 100, in which Atest corresponds to absorbance of the experimental group and ALPS corresponds to the absorbance of LPS (positive control).

3.11. Intracellular ROS Production

The levels of intracellular oxygen reactive species were evaluated by quantifying the fluorescence emitted by 2′,7′-dichlorofluorescein, the oxidized form of 2′,7′-dichlorofluorescein diacetate (DCFH-DA). For this, RAW 264.7 macrophages were cultured (3×10^5/well) in 24-well plates and exposed to SPs for 24 h. LPS (2 μg/mL) was used as a positive control. After treatment, the supernatant was discarded, cells were washed with phosphate buffered saline (PBS), and 100 μM DCFH-DA in DMEM containing 1% FBS was added, followed by incubation at 37 °C for 2 h. Then, the DCFH was removed, the cells were washed twice with PBS, and the emitted fluorescence was measured on a flow cytometer (FACSCanto II, BD Biosciences, Eugene, OR, USA) with FACSDiva software, version 6.1.2 (Becton Dickson, Franklin Lakes, NJ, USA). The results were analyzed in FlowJo software (FlowJo, Ashland, OR, USA) and expressed as % of fluorescence emitted relative to that of LPS-treated cells.

3.12. Cytokine Production

For quantification of the cytokines IL-6 and TNF-α, the supernatant of the cells that were exposed to SPs in the experiment to evaluate ROS levels was used. The cytokines were quantified using the BD Cytometric Bead Array (CBA) Mouse Th1/Th2/Th17 Cytokine Kit according to the manufacturer's instructions using a flow cytometer (FACSCanto II, BD Biosciences, OR, USA). The results were recorded with FACSDiva software and analyzed using FCAP Array software, version 3.0 (BD, Franklin Lakes, NJ, USA).

3.13. Statistical Analysis

Statistical analysis was performed using Prism 5 (GraphPad Prism, version 5.00, San Diego, CA, USA). Results were expressed as the mean ± standard deviation. Statistical differences between the groups were assessed using analysis of variance and the Student Newman–Keuls post-test. Differences were considered significant at $p < 0.05$.

4. Conclusions

In this study, two sulfated and pyruvated galactans were obtained from an SP-rich fraction from *C. cupressoides* seaweed. Structurally, both galactans are similar, differing only by the presence of a sulfation at position 4 in one of the SP2 units. In addition, the galactans had an immunostimulatory effect, as evidenced by the increased production of NO, ERO, and the cytokines IL-6 and TNF-α. These findings indicate that sulfation at C-4 is not essential for the immunomodulatory action of these galactans. Overall, these results suggest that *C. cupressoides* SPs represent potential candidates for the development of new products with immunomodulatory properties of biomedical interest, with applications including the treatment of hypoimmunity or immunodeficiency conditions.

References

1. Catanzaro, M.; Corsini, E.; Rosini, M.; Racchi, M.; Lanni, C. Immunomodulators inspired by nature: A review on on curcumin and echinacea. *Molecules* **2018**, *23*, 2778. [CrossRef] [PubMed]

2. Shi, L. Bioactivities, isolation and purification methods of polysaccharides from natural products: A review. *Int. J. Biol. Macromol.* **2016**, *92*, 37–48. [CrossRef] [PubMed]

3. Wasser, S.P. Medicinal mushrooms in human clinical studies. Part I. Anticancer, oncoimmunological, and immunomodulatory activities: A Review. *Int. J. Med. Mushrooms* **2017**, *19*, 279–317. [CrossRef]

4. Yu, Y.; Shen, M.; Song, Q.; Xie, J. Biological activities and pharmaceutical applications of polysaccharide from natural resources: A review. *Carbohydr. Polym.* **2018**, *183*, 91–101. [CrossRef]

5. Zhang, W.; Du, J.Y.; Jiang, Z.; Okimura, T.; Oda, T.; Yu, Q.; Jin, J.O. Ascophyllan purified from *Ascophyllum nodosum* induces Th1 and Tc1 immune responses by promoting dendritic cell maturation. *Mar. Drugs* **2014**, *12*, 4148–4164. [CrossRef] [PubMed]

6. Sun, H.; Zhang, J.; Chen, F.; Chen, X.; Zhou, Z.; Wang, H. Activation of RAW264.7 macrophages by the polysaccharide from the roots of *Actinidia eriantha* and its molecular mechanisms. *Carbohydr. Polym.* **2015**, *121*, 388–402. [CrossRef] [PubMed]

7. Xie, S.Z.; Hao, R.; Zha, X.Q.; Pan, L.H.; Liu, J.; Luo, J.P. Polysaccharide of *Dendrobium huoshanense* activates macrophages via toll-like receptor 4-mediated signaling pathways. *Carbohydr. Polym.* **2016**, *146*, 292–300. [CrossRef] [PubMed]

8. Jackaman, C.; Tomay, F.; Duong, L.; Abdol Razak, N.B.; Pixley, F.J.; Metharom, P.; Nelson, D.J. Aging and cancer: The role of macrophages and neutrophils. *Ageing Res. Rev.* **2017**, *36*, 105–116. [CrossRef]

9. Beutler, B. Innate immunity: An overview. *Mol. Immunol.* **2004**, *40*, 845–859. [CrossRef]

10. Lee, J.S.; Kwon, D.S.; Lee, K.R.; Park, J.M.; Ha, S.J.; Hong, E.K. Mechanism of macrophage activation induced by polysaccharide from *Cordyceps militaris* culture broth. *Carbohydr. Polym.* **2015**, *120*, 29–37. [CrossRef]

11. Wei, Z.; Chen, G.; Zhang, P.; Zhu, L.; Zhang, L.; Chen, K. *Rhizopus nigricans* polysaccharide activated macrophages and suppressed tumor growth in CT26 tumor-bearing mice. *Carbohydr. Polym.* **2018**, *198*, 302–312. [CrossRef] [PubMed]

12. Yang, Y.; Zhao, X.; Li, J.; Jiang, H.; Shan, X.; Wang, Y.; Ma, W.; Hao, J.; Yu, G. A β-glucan from *Durvillaea Antarctica* has immunomodulatory effects on RAW264.7 macrophages via toll-like receptor 4. *Carbohydr. Polym.* **2018**, *191*, 255–265. [CrossRef] [PubMed]

13. Tabarsa, M.; You, S.G.; Dabaghian, E.H.; Surayot, U. Water-soluble polysaccharides from *Ulva intestinalis*: Molecular properties, structural elucidation and immunomodulatory activities. *J. Food Drug Anal.* **2018**, *26*, 599–608. [CrossRef] [PubMed]

14. Ngo, D.; Kim, S. Sulfated polysaccharides as bioactive agents from marine algae. *Int. J. Biol. Macromol.* **2013**, *62*, 70–75. [CrossRef]

15. Tsubaki, S.; Oono, K.; Hiraoka, M.; Onda, A.; Mitani, T. Microwave-assisted hydrothermal extraction of sulfated polysaccharides from *Ulva* spp. and *Monostroma latissimum*. *Food Chem.* **2016**, *210*, 311–316. [CrossRef]

16. Wang, L.; Wang, X.; Wu, H.; Liu, R. Overview on biological activities and molecular characteristics of sulfated polysaccharides from marine green algae in recent years. *Mar. Drugs* **2014**, *12*, 4984–5020. [CrossRef]

17. Maeda, R.; Ida, T.; Ihara, H.; Sakamoto, T. Immunostimulatory activity of polysaccharides isolated from *Caulerpa lentillifera* on macrophage Cells. *Biosci. Biotechnol. Biochem.* **2012**, *76*, 501–505. [CrossRef]

18. Sun, Y.; Gong, G.; Guo, Y.; Wang, Z.; Song, S.; Zhu, B.; Zhao, L.; Jiang, J. Purification, structural features and immunostimulatory activity of novel polysaccharides from *Caulerpa lentillifera*. *Int. J. Biol. Macromol.* **2018**, *108*, 314–323. [CrossRef]

19. Rodrigues, J.A.; Vanderlei, E.S.; Silva, L.M.; Araújo, I.W.; Queiroz, I.N.; Paula, G.A.; Abreu, T.M.; Ribeiro, N.A.; Bezerra, M.M.; Chaves, H.V.; et al. Antinociceptive and anti-inflammatory activities of a sulfated polysaccharide isolated from the green seaweed *Caulerpa cupressoides*. *Pharmacol. Rep.* **2012**, *64*, 282–292. [CrossRef]

20. Carneiro, J.G.; Rodrigues, J.A.; de Sousa Oliveira Vanderlei, E.; Souza, R.B.; Quinderé, A.L.; Coura, C.O.; de Araújo, I.W.; Chaves, H.V.; Bezerra, M.M.; Benevides, N.M. Peripheral antinociception and anti-inflammatory effects of sulphated polysaccharides from the alga *Caulerpa mexicana*. *Basic Clin. Pharmacol. Toxicol.* **2014**, *115*, 335–342. [CrossRef]

21. Ribeiro, N.A.; Abreu, T.M.; Chaves, H.V.; Bezerra, M.M.; Monteiro, H.S.A.; Jorge, R.J.B.; Benevides, N.M.B. Sulfated polysaccharides isolated from the green seaweed *Caulerpa racemosa* plays antinociceptive and anti-inflammatory activities in a way dependent on HO-1 pathway activation. *Inflamm. Res.* **2014**, *63*, 569–580. [CrossRef] [PubMed]

22. Costa, L.S.; Fidelis, G.P.; Cordeiro, S.L.; Oliveira, R.M.; Sabry, D.A.; Câmara, R.B.; Nobre, L.T.; Costa, M.S.; Almeida-Lima, J.; Farias, E.H.; et al. Biological activities of sulfated polysaccharides from tropical seaweeds. *Biomed. Pharmacother.* **2010**, *64*, 21–28. [CrossRef] [PubMed]

23. Costa, M.S.S.P.; Costa, L.S.; Cordeiro, S.L.; Almeida-Lima, J.; Dantas-Santos, N.; Magalhães, K.D.; Sabry, D.A.; Albuquerque, I.R.L.; Pereira, M.R.; Leite, E.L.; et al. Evaluating the possible anticoagulant and antioxidant effects of sulfated polysaccharides from the tropical green alga *Caulerpa cupressoides* var. flabellata. *J. Appl. Phycol.* **2012**, *24*, 1159–1167. [CrossRef]

24. Barbosa, J.D.S.; Costa, M.S.S.P.; De Melo, L.F.M.; De Medeiros, M.J.C.; Pontes, D.D.L.; Scortecci, K.C.; Rocha, H.A.O. *In Vitro* immunostimulating activity of sulfated polysaccharides from *Caulerpa cupressoides* var. *Flabellata*. *Mar. Drugs* **2019**, *17*, 105. [CrossRef]

25. Soares, P.A.G.; Queiroz, I.N.L.; Pomin, V.H. NMR structural biology of sulfated glycans. *J. Biomol. Struct. Dyn.* **2017**, *35*, 1069–1084. [CrossRef]

26. Sabry, D.A.; Cordeiro, S.L.; Ferreira Silva, C.H.; Cunha Farias, E.H.; Sassaki, G.L.; Nader, H.B.; Oliveira Rocha, H.A. Pharmacological prospection and structural characterization of two purified sulfated and pyruvylated homogalactans from green algae *Codium isthmocladum*. *Carbohydr. Polym.* **2019**, *222*, 115010. [CrossRef]

27. Farias, E.H.C.; Pomin, V.H.; Valente, A.P.; Nader, H.B.; Rocha, H.A.O.; Mourão, P.A.S. A preponderantly 4-sulfated, 3-linked galactan from the green alga *Codium isthmocladum*. *Glycobiology* **2008**, *18*, 250–259. [CrossRef]

28. Bilan, M.I.; Vinogradova, E.V.; Shashkov, A.S.; Usov, A.I. Structure of a highly pyruvylated galactan sulfate from the Pacific green alga *Codium yezoense* (Bryopsidales, Chlorophyta). *Carbohydr. Res.* **2007**, *342*, 586–596. [CrossRef]

29. Arata, P.X.; Quintana, I.; Canelón, D.J.; Vera, B.E.; Compagnone, R.S.; Ciancia, M. Chemical structure and anticoagulant activity of highly pyruvylated sulfated galactans from tropical green seaweeds of the order *Bryopsidales*. *Carbohydr. Polym.* **2015**, *122*, 376–386. [CrossRef]

30. Fernández, P.V.; Raffo, M.P.; Alberghina, J.; Ciancia, M. Polysaccharides from the green seaweed *Codium decorticatum*: Structure and cell wall distribution. *Carbohydr. Polym.* **2015**, *117*, 836–844. [CrossRef]

31. Rocha, H.A.; Moraes, F.A.; Trindade, E.S.; Franco, C.R.; Torquato, R.J.; Veiga, S.S.; Valente, A.P.; Mourão, P.A.; Leite, E.L.; Nader, H.B.; et al. Structural and hemostatic activities of a sulfated galactofucan from the brown alga *Spatoglossum schröederi*. *J. Biol. Chem.* **2005**, *280*, 41278–41288. [CrossRef] [PubMed]

32. Bouwstra, J.B.; Kerékgyártó, J.; Kamerling, J.P.; Vliegenthart, J.F.G. ^{1}H- and ^{13}C-N.M.R. assignments for structural elements of xylose-containing *N*-linked oligosaccharides, using 1D- and 2D-N.M.R. experiments. *Carbohydr. Res.* **1989**, *186*, 39–49. [CrossRef]

33. Ogawa, K.; Yamaura, M.; Maruyama, I. Isolation and identification of 2-*O*-methyl-L-rhamnose and 3-*O*-methyl-L-rhamnose as constituents of an acidic polysaccharide of *Chlorella vulgaris*. *Biosci. Biotechnol. Biochem.* **1997**, *61*, 539–540. [CrossRef]

34. Panagiotopoulos, C.; Repeta, D.J.; Johnson, C.G. Characterization of methyl sugars, 3-deoxysugars and methyl deoxysugars in marine high molecular weight dissolved organic matter. *Org. Geochem.* **2007**, *38*, 884–896. [CrossRef]

35. Ciancia, M.; Alberghina, J.; Arata, P.X.; Benavides, H.; Leliaert, F.; Verbruggen, H.; Estevez, J.M. Characterization of cell wall polysaccharides of the coencocytic green seaweed *Bryopsis plumosa* (bryopsidaceae, chlorophyta) from the argentine coast. *J. Phycol.* **2012**, *48*, 326–335. [CrossRef]

36. Wynn, T.A.; Chawla, A.; Pollard, J.W. Macrophage biology in development, homeostasis and disease. *Nature* **2013**, *496*, 445–455. [CrossRef]

37. Oh, M.J.; Choi, H.D.; Ha, S.K.; Choi, I.; Park, H.Y. Immunomodulatory effects of polysaccharide fraction isolated from *Fagopyrum esculentum* on innate immune system. *Biochem. Biophys. Res. Commun.* **2018**, *496*, 1210–1216. [CrossRef]

38. Geng, L.; Hu, W.; Liu, Y.; Wang, J.; Zhang, Q. A heteropolysaccharide from *Saccharina japonica* with immunomodulatory effect on RAW 264.7 cells. *Carbohydr. Polym.* **2018**, *201*, 557–565. [CrossRef]

39. Qi, J.; Kim, S.M. Effects of the molecular weight and protein and sulfate content of *Chlorella ellipsoidea* polysaccharides on their immunomodulatory activity. *Int. J. Biol. Macromol.* **2018**, *107*, 70–77. [CrossRef]

40. Jiao, L.; Li, X.; Li, T.; Jiang, P.; Zhang, L.; Wu, M.; Zhang, L. Characterization and anti-tumor activity of alkali-extracted polysaccharide from *Enteromorpha intestinalis*. *Int. Immunopharmacol.* **2009**, *9*, 324–329. [CrossRef]

41. Cao, R.A.; Lee, Y.J.; You, S.G. Water soluble sulfated-fucans with immune-enhancing properties from *Ecklonia cava*. *Int. J. Biol. Macromol.* **2014**, *67*, 303–311. [CrossRef] [PubMed]

42. Cui, Y.; Liu, X.; Li, S.; Hao, L.; Du, J.; Gao, D.; Kang, Q.; Lu, J. Extraction, characterization and biological activity of sulfated polysaccharides from seaweed *Dictyopteris divaricata*. *Int. J. Biol. Macromol.* **2018**, *117*, 256–263. [CrossRef]

43. Liu, Q.M.; Xu, S.S.; Li, L.; Pan, T.M.; Shi, C.L.; Liu, H.; Cao, M.J.; Su, W.J.; Liu, G.M. In vitro and in vivo immunomodulatory activity of sulfated polysaccharide from *Porphyra haitanensis*. *Carbohydr. Polym.* **2017**, *165*, 189–196. [CrossRef] [PubMed]

44. Fang, Q.; Wang, J.F.; Zha, X.Q.; Cui, S.H.; Cao, L.; Luo, J.P. Immunomodulatory activity on macrophage of a purified polysaccharide extracted from *Laminaria japonica*. *Carbohydr. Polym.* **2015**, *134*, 66–73. [CrossRef] [PubMed]

45. Ferreira, S.S.; Passos, C.P.; Madureira, P.; Vilanova, M.; Coimbra, M.A. Structure-function relationships of immunostimulatory polysaccharides: A review. *Carbohydr. Polym.* **2015**, *132*, 378–396. [CrossRef]

46. Shemami, M.R.; Tabarsa, M.; You, S.G. Isolation and chemical characterization of a novel immunostimulating galactofucan from freshwater *Azolla filiculoides*. *Int. J. Biol. Macromol.* **2018**, *118*, 2082–2091. [CrossRef]

47. Leiro, J.M.; Castro, R.; Arranz, J.A.; Lamas, J. Immunomodulating activities of acidic sulphated polysaccharides obtained from the seaweed *Ulva rigida* C. Agardh. *Int. Immunopharmacol.* **2007**, *7*, 879–888. [CrossRef]

48. Borazjani, N.J.; Tabarsa, M.; You, S.; Rezaei, M. Purification, molecular properties, structural characterization, and immunomodulatory activities of water soluble polysaccharides from *Sargassum angustifolium*. *Int. J. Biol. Macromol.* **2018**, *109*, 793–802. [CrossRef]

49. Bahramzadeh, S.; Tabarsa, M.; You, S.G.; Li, C.; Bita, S. Purification, structural analysis and mechanism of murine macrophage cell activation by sulfated polysaccharides from *Cystoseira indica*. *Carbohydr. Polym.* **2019**, *205*, 261–270. [CrossRef]

50. Kohchi, C.; Inagawa, H.; Nishizawa, T.; Soma, G. ROS and innate immunity. *Anticancer Res.* **2009**, *29*, 817–821.

51. Deng, X.; Liu, Q.; Fu, Y.; Luo, X.; Hu, M.; Ma, F.; Wang, Q.; Lai, X.; Zhou, L. Effects of *Lycium barbarum* polysaccharides with different molecular weights on function of RAW264.7 macrophages. *Food Agric. Immunol.* **2018**, *29*, 808–820. [CrossRef]

52. Wang, Y.; Jiang, Z.; Kim, D.; Ueno, M.; Okimura, T.; Yamaguchi, K.; Oda, T. Stimulatory effect of the sulfated polysaccharide ascophyllan on the respiratory burst in RAW264.7 macrophages. *Int. J. Biol. Macromol.* **2013**, *52*, 164–169. [CrossRef] [PubMed]

53. Ren, Y.; Zheng, G.; You, L.; Wen, L.; Li, C.; Fu, X.; Zhou, L. Structural characterization and macrophage immunomodulatory activity of a polysaccharide isolated from *Gracilaria lemaneiformis*. *J. Funct. Foods* **2017**, *33*, 286–296. [CrossRef]

54. Choi, E.-M.; Kim, A.-J.; Kim, Y.-O.; Hwang, J.-K. Immunomodulating activity of arabinogalactan and fucoidan in vitro. *J. Med. Food* **2005**, *8*, 446–453. [CrossRef]

55. Chen, L.; Huang, G. The antiviral activity of polysaccharides and their derivatives. *Int. J. Biol. Macromol.* **2018**, *115*, 77–82. [CrossRef] [PubMed]

56. Pan, X.X.; Tao, J.H.; Jiang, S.; Zhu, Y.; Qian, D.W.; Duan, J.A. Characterization and immunomodulatory activity of polysaccharides from the stems and leaves of *Abelmoschus manihot* and a sulfated derivative. *Int. J. Biol. Macromol.* **2018**, *107*, 9–16. [CrossRef] [PubMed]

57. Yan, J.; Han, Z.; Qu, Y.; Yao, C.; Shen, D.; Tai, G.; Cheng, H.; Zhou, Y. Structure elucidation and immunomodulatory activity of a β-glucan derived from the fruiting bodies of *Amillariella mellea*. *Food Chem.* **2018**, *240*, 534–543. [CrossRef]

58. Yu, Y.; Shen, M.; Wang, Z.; Wang, Y.; Xie, M.; Xie, J. Sulfated polysaccharide from *Cyclocarya paliurus* enhances the immunomodulatory activity of macrophages. *Carbohydr. Polym.* **2017**, *174*, 669–676. [CrossRef]

59. Bi, D.; Yu, B.; Han, Q.; Lu, J.; White, W.L.; Lai, Q.; Cai, N.; Luo, W.; Gu, L.; Li, S.; et al. Immune activation of RAW264.7 macrophages by low molecular weight fucoidan extracted from new zealand *Undaria pinnatifida*. *J. Agric. Food Chem.* **2018**, *66*, 10721–10728. [CrossRef]

60. Farndale, R.; Buttle, D.; Barrett, A. Improved quantitation and discrimination of sulphated glycosaminoglycans by use of dimethylmethylene blue. *Biochim. Biophys. Acta Gen. Subj.* **1986**, *883*, 173–177. [CrossRef]

61. Dubois, M.; Gilles, K.A.; Hamilton, J.K.; Rebers, P.A.; Smith, F. Colorimetric method for determination of sugars and related substances. *Anal. Chem.* **1956**, *28*, 350–356. [CrossRef]

62. Dodgson, K.S.; Price, R.G. A note on the determination of the ester sulphate content of sulphated polysaccharides. *Biochem. J.* **1962**, *84*, 106–110. [CrossRef] [PubMed]

63. Bradford, M.M. A rapid and sensitive method for the quantitation of microgram quantities of protein utilizing the principle of protein-dye binding. *Anal. Biochem.* **1976**, *72*, 248–254. [CrossRef]

64. Sassaki, G.L.; Guerrini, M.; Serrato, R.V.; Santana Filho, A.P.; Carlotto, J.; Simas-Tosin, F.; Cipriani, T.R.; Iacomini, M.; Torri, G.; Gorin, P.A.J. Monosaccharide composition of glycans based on Q-HSQC NMR. *Carbohydr. Polym.* **2014**, *104*, 34–41. [CrossRef]

65. Mosmann, T. Rapid colorimetric assay for cellular growth and survival: Application to proliferation and cytotoxicity assays. *J. Immunol. Methods.* **1983**, *65*, 55–63. [CrossRef]

66. Green, L.C.; Wagner, D.A.; Glogowski, J.; Skipper, P.L.; Wishnok, J.S.; Tannenbaum, S.R. Analysis of nitrate, nitrite, and [15N] nitrate in biological fluids. *Anal. Biochem.* **1982**, *126*, 131–138. [CrossRef]

Chitosan-Gentamicin Conjugate Hydrogel Promoting Skin Scald Repair

Tingting Yan [1], Songzhi Kong [1,*], Qianqian Ouyang [1,2], Chengpeng Li [1,*], Tingting Hou [1], Yu Chen [3] and Sidong Li [1]

[1] Faculty of Chemistry and Environmental Science, Guangdong Ocean University, Zhanjiang 524088, China; 13922085100@163.com (T.Y.); ouyangqianqian0426@163.com (Q.O.); htt0415@126.com (T.H.); 13702737491@163.com (S.L.)

[2] College of Food Science and Technology, Yunnan Agricultural University, Kunming 650000, China

[3] School of Material Science and Engineering, Beijing Institute of Technology, Beijing 100081, China; bityuchen@bit.edu.cn

* Correspondence: kongsongzhi@126.com (S.K.); lcp0802@126.com (C.L.); Tel.: +(86)-759-2383-300 (S.K.); Fax: +(86)-759-2383-636 (S.K.)

Abstract: Our earlier research indicated that chitosan-gentamicin conjugate (CS-GT) possesses superior antimicrobial activity and good water solubility. To develop CS-GT-based scald dressings, the antibacterial properties of CS-GT were further studied, and the biosafety of CS-GT and the healing mechanism of CS-GT hydrogel was systematically explored in this article. It was found that cell viability shows a declined inclination with the prolonged culture time and the increased concentration of CS-GT. After three day's culture, the cell viability could still remain at 79.72% when CS-GT concentration was as high as 1000 μg/mL. On the other hand, the hemolysis rate of CS-GT was lower than 5% when its concentration is 800 μg/mL. Therefore CS-GT has good cytocompatibility and hemocompatibility. A wound-healing experiment has shown that the skin healing rate of CS-GT hydrogel was the highest at 99.61%, followed by the positive control (wet burn ointment) 94.98%, GT hydrogel 87.50%, and matrix 77.39%. The blank control group, however, possessed the lowest healing rate of 75.45%. Further analysis indicated that CS-GT hydrogel could promote the synthesis of total protein (TP) in skin granulation tissue, resulting in the enhanced hydroxyproline (HYP) content, which facilitated collagen fibrogenesis, reduced cytokine expression in an inflammatory response, and, ultimately, accelerated wound healing. To sum up, CS-GT hydrogel is a promising scald dressing.

Keywords: chitosan-gentamicin conjugate; antimicrobial; anti-inflammatory; scald repair

1. Introduction

Skin is the first line of human body defense against ambiance, featuring functions such as resisting microbial invasion, maintaining body fluid and water equilibrium, and regulating body temperature [1]. Upon scalding, the first line of defense is destroyed, and wound exudates such as protein and necrosed tissue prosper at the scald site, offering adequate high-nutrient substances for microbial growth and reproduction, which enables higher wound infection rates and is highly prone to an intense inflammatory response [2]. The inflammation phase of skin tissue regeneration is a crucial phase of normal wound healing, characterized by continuous infiltration of neutrophils, macrophages, and lymphocytes [3]. A few minutes after getting hurt, neutrophils arrive at the wound site and start action for several days, and they themselves are phagocytosed by tissue macrophages. Although the primary role of neutrophils is to kill bacteria, neutrophils are also a source of proinflammatory cytokines including interleukins 1α and β (IL-1α and IL-β) and tumor necrosis factor α (TNF-α) [4]. Providing the

earliest signal to inactivate fibroblasts and keratinocytes at the wound [5], these proinflammatory cytokines play a very important role in wound healing. Moreover, in the presence of microorganisms, free radicals and reactive oxygen species released at the wound site during this phase incur serious complications including infection [6], delayed healing process, and serious wound dehydration [7], while dehydration interrupts desirable moist healing environment and further postpones wound healing. Even though considerable progress has been made in burn care and treatment nowadays, infections are still an overarching risk of increased patient deaths [8]. Therefore, a desirable dressing for trauma repair should be nontoxic, non-adherent, capable of absorbing excessive exudate, and have a number of excellent properties such as efficient microbial resistance and biocompatibility.

In recent years, biomaterial-based wound dressings have been widely used, such as chitosan (CS) [9], polymeric nanofibers [10], collagen protein [11], and sodium alginate [12], among which CS is a cationic marine natural polysaccharide obtained from chitin after deacetylation of the *N*-acetyl glucosamine groups [13]. It is extensively applied in clinical practice due to the advantages of being self-biodegradable, biocompatible, non-antigenic, water absorbable, air and moisture permeable, non-toxic, and well adherent to skin without irritation [14]. In addition, studies in the past years have demonstrated that CS has certain antimicrobial activity, and in its dilute acid solution, free amino groups can be protonated such that CS carries positive charges. Then, the positively charged amino group can directly attack the negatively charged bacterial cell membrane via electrostatic attraction to disrupt the cell membrane to achieve a good antibacterial effect, which differs from target-specific interactions of conventional antibiotics and prevents drug resistance of bacteria from occurring to some extent [15–17]. By now, some CS-based wound dressing products have been developed in dosage forms of hydrogel [18,19], film [9], and sponge [20], among which hydrogel or hydrogel film is able to provide a moist environment to the wound, effectively preventing tissue dehydration and cell death, enhancing the migration of inflammatory cells and growth factors, facilitating air exchange and angiogenesis, serving as a microbial barrier, removing excessive exudate, and accelerating wound healing, among other merits, and thus has good application prospect [21–23].

Gentamicin (GT) is an aminoglycoside antibiotic with efficient antimicrobial activity, and, therefore, widely applied in the treatment of microbial infections, in particular, burn wounds [24]. If acting directly on skin, it will be difficult for GT to penetrate skin to deeper layers. Its systemic absorption is low probably due to its cationic nature, and therefore its efficacy mainly stems from a topical effect of the superficial layer of skin [25]. Nonetheless, GT can induce renal tubular necrosis and renal tubular congestion [26] and kill intra-auricular lymphocytes [27] to trigger certain nephrotoxicity and ototoxicity and is therefore limited in clinical application to some extent. In light of the toxic side effect of GT, many researchers treat GT by embedding [10,28] or fixing [29] to control GT release so that GT can act persistently. Alternatively, GT is delivered to a target site for specific binding to maintain prolonged action between the antibiotic and the target site by local delivery [30]. Based on this practice in combination with the above excellent properties of CS and application potential of CS gel formulation in wound repair, the present work intended to prepare a CS-GT hydrogel and further investigate its potential skin scald repair-promoting effect.

CS-GT has been successfully prepared in a previous study [31]. In this study, in order to investigate its potential scald healing-promoting effect, the antimicrobial activity of CS-GT was further studied, and the cytocompatibility and hemocompatibility of CS-GT were determined by cell viability assay and hemolysis assay.

2. Results and Discussion

2.1. Antibacterial Activity

A desirable wound dressing should have certain antimicrobial functions to minimize pathogens to reduce inflammatory response and tissue fluid exudation at the wound site and accelerate the healing process [32]. Figure 1 shows zones of inhibition of CS, GT, and CS-GT against *S. aureus* and *P. aeruginosa*,

respectively. CS samples were dissolved with 1% glacial acetic acid (HAc). As a result of adding dropwise 1% HAc alone onto paper discs (6.0 mm in diameter), zones of inhibition were all 6.0 mm in size, and, therefore, HAc solvent has no inhibitory effect against both test strains. Measurement of inhibition zones shows that diameters of the zones of inhibition of CS, GT, and CS-GT against *S. aureus* were 7.0 ± 1.0, 17.7 ± 1.2, and 20.0 ± 1.0 mm, respectively, and diameters of the zones of inhibition of CS, GT, and CS-GT against *P. aeruginosa* were 7.0 ± 1.0, 21.3 ± 0.6, and 20.3 ± 0.6 mm, respectively (Table 1). The results suggest that GT and CS-GT have comparable antibacterial activity against *P. aeruginosa*. However, these two samples have significant differences in the diameter of the zones of inhibition of *S. aureus* ($p < 0.05$). Compared with the results of CS, diameters of zones of inhibition of CS-GT against both test strains increased by 13.0 and 13.3 mm due to the introduction of GT, respectively, indicative of superior antimicrobial activity.
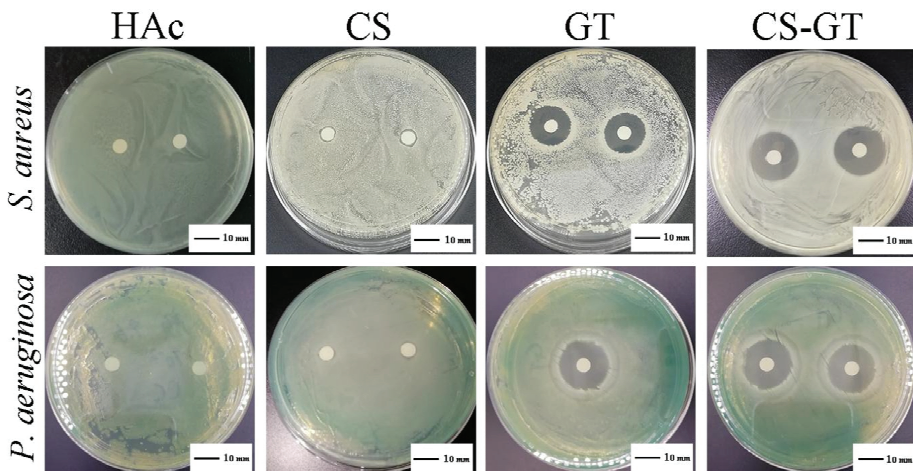
Figure 1. Zones of inhibition of glacial acetic acid (HAc), chitosan (CS), gentamicin (GT), and chitosan-gentamicin conjugate (CS-GT) against *S. aureus* and *P. aeruginosa*.

Table 1. Diameters of zones of inhibition in various groups (unit: mm, mean ± SD, $n = 3$). Note: versus CS group, * $p < 0.01$; versus GT group, # $p < 0.05$.

Test Strain	CS	GT	CS-GT
S. aureus	7.0 ± 1.0	17.7 ± 1.2 *	20.0 ± 1.0 *,#
P. aeruginosa	7.0 ± 1.0	21.3 ± 0.6 *	20.3 ± 0.6 *

2.2. Cell Viability

As shown by the results of the viability assay of L929 cells in the presence of CS-GT (Figure 2), cell viability decreased gradually with the increase of CS-GT concentration. After CS-GT and L929 cells were co-incubated for 1 and 2 days, CS-GT at a concentration of 100 µg/mL promoted cell growth to some extent, and cell viability values were 112.65% and 112.23%, respectively, indicating that CS-GT at this concentration is non-toxic to L929 cells. After CS-GT and L929 cells were co-incubated for 3 days, cell viability decreased to 90.79%, indicating that CS-GT at this concentration exhibited limited cell inhibition, possibly because cell proliferation via cell division led to higher cell density and competition among cells for nutrition ($p < 0.05$ compared to days 1 and 2) [33]. For CS-GT at a concentration of 200 µg/mL, cell viability values on days 1 and 2 were 101.68% and 100.44%, respectively, and no significant impact on cell growth was noted. On day 3, cell viability decreased to 86.73%, probably due to combined action of CS-GT and cell division and proliferation ($p < 0.05$ compared to days 1 and 2).

For CS-GT samples at concentrations between 300 and 1200 μg/mL, cell viability values on days 1 and 2 decreased in turn, respectively. However, at the same concentration, cell viability decreased less. On day 3, reduction in cell viability at each concentration was greater than those on days 1 and 2. At a concentration of 1200 μg/mL, cell viability decreased to 75.00%, the lowest one among cell viability values at all concentrations. According to ISO standard, after full action between a substance and cells, a concentration with cell viability above 75% is deemed not cytotoxic [34]. In summary, CS-GT samples at concentrations below 1200 μg/mL were non-toxic to L929 cells. In particular, at lower concentrations (e.g., 100 μg/mL) with action time not longer than 2 days, CS-GT promoted cell growth to some extent, indicating CS-GT has good cytocompatibility.
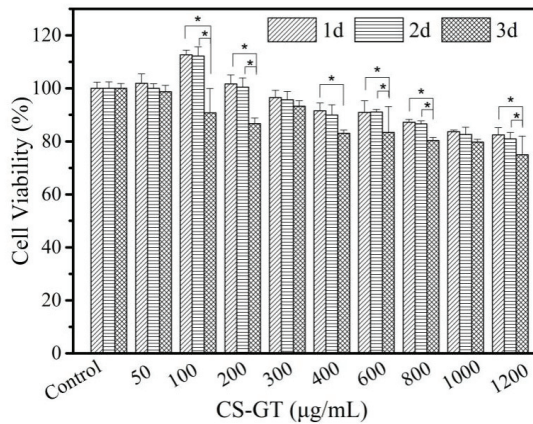
Figure 2. Cell viability of CS-GT (mean ± SD, * $p < 0.05$, $n = 6$).

L929 cells were treated with GT and CS-GT samples at a concentration of 100 μg/mL for 1, 2, and 3 days, respectively, and such cells were stained with AM/PI in these 3 consecutive days to observe the cell state (Figure 3). After reacting with cellular lactonase, calcein-AM emits green fluorescence and renders viable cells stained. Ethidium homodimer-1 binds to the DNA of dead or damaged cells, rendering dead cells stained red. Based on live/dead staining analysis, with the increase of culture time, a great number of normally-shaped green viable cells and a sequentially increased minor amount of red dead cells were observed in the control group. After L929 cells were treated with GT, more and more red dead cells were observed with the increase in incubation time. While the cells treated with CS-GT were basically normal in morphology, fewer red dead cells were observed, and the variability of cell staining versus time was similar to the case of the control group. Results of L929 cell viability (Figure 2) and observation of cell staining state further indicate that CS-GT is non-cytotoxic to L929 cells and has good cytocompatibility.
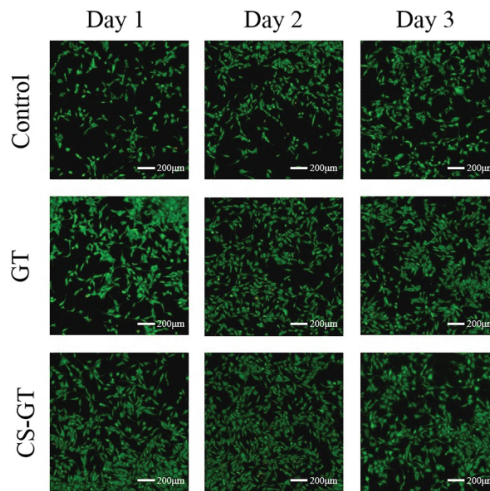
Figure 3. Live/dead staining analysis of cell compatibility of the sample. L929 cells in GT and CS-GT were stained after incubation for 1, 2, and 3 days.

2.3. Hemolysis Assay

Hemolysis assay can be used to evaluate material hemocompatibility as a hemolysis rate of ≤5% meets the hemolysis criterion for biomaterials [35]. Based on the hemolysis results of GT and CS-GT in Figure 4, the hemolysis rate of GT at a concentration of 100 μg/mL was lower than 5%, while the hemolysis rate of GT at a concentration of 200 μg/mL or above was higher than 5%. The hemolysis rate of CS-GT at a concentration of 800 μg/mL or below was lower than 5% (Figure 4a), indicating that CS-GT at the concentrations below 800 μg/mL has no hemolytic activity on red blood cells (RBCs) and is more hemocompatible than GT [36]. At the same concentrations, there was no significant difference in hemolysis rates between the two groups. As shown in Figure 4b, the content of cell-released hemoglobin increased with the increase of GT and CS-GT concentrations, and the higher the content of released hemoglobin, the stronger the hemolytic activity [37]. However, in general, at a concentration below 800 μg/mL, GT induced higher hemoglobin release than CS-GT, indicating that hemolytic activity of CS-GT was lower than that of GT. In addition, in order to further assess the hemolytic properties of GT and CS-GT, the morphology of RBCs treated with GT and CS-GT at 800 μg/mL was microscopically observed, and the results are shown in Figure 4c. After treatment with water, all RBCs were disrupted basically. Additionally, after treatment with PBS, RBCs were round-shaped and basically free of damage. As compared with PBS-treated RBCs, GT-treated RBCs exhibited more prominent damage and rupture in morphology, while only a minimal part of CS-GT-treated RBCs was damaged, without significant morphological variation in general. The above results indicate unanimously that the hemocompatibility of CS-GT is superior to GT.
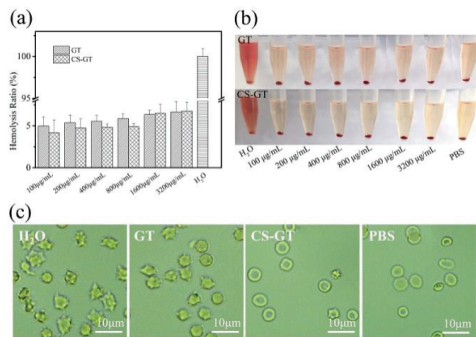
Figure 4. (**a**) Hemolysis rates of RBCs treated with GT and CS-GT, respectively; (**b**,**c**) images of RBCs treated with GT and CS-GT, respectively (mean ± SD, *n* = 3).

2.4. Wound Macroscopy and Healing Rates

Based on information on scald wound healing in each group at various time points in Figure 5, the scald wounds appeared subcircular and edematous, and their surfaces were softened and blanched on the day of modeling (Day 1). Over time, scald areas in each group turned smaller gradually, while the wound healing rate tended to increase (Table 2). Throughout the healing cycle, blank group and matrix group did not differ significantly in macroscopic wound change, and no significant difference in wound healing rate was noted in either group, indicating that the PVP matrix has no significant impact on wound healing. On day 7, the edema on the wound surface in each group began to resolve; however, in the case of the blank group, such edema was associated with certain tissue fluid exudation and purulent substance secretion and inflammatory response around the wound was more significant. On day 14, the peripheral scab of each scald wound in each group began to fall off, and the wound surface was dry without tissue fluid exudation and purulent substance secretion. The wound turned smaller without a distinct boundary with surrounding normal tissue, whereas effects on wound shrinkage in the positive control group, GT group, and CS-GT group were superior to those in the blank group and matrix group to a varied extent. On day 21, in the positive control group and CS-GT group, scald wound scabs basically fell off; however, a swelling phenomenon occurred in the positive control group where the scabs fell off. In the cases of the blank group, matrix group, and GT group, a minor amount of scabs were still attached to wound cores and appeared pale red.

A wound healing rate of 100% is a criterion for trauma repair. As shown in Table 2, throughout the healing cycle, the blank group and matrix group had no significant difference in wound healing rate, indicating that the matrix has no prominent action on wound healing. On day 3 after scalding, wound healing rates in the blank group were all negative, possibly because blank samples had no anti-inflammatory effect after scald wound modeling. When various proinflammatory cytokines were triggered, such wounds started to get inflamed and edematous, resulting in a larger wound area. On day 3, compared with the blank group, the GT and CS-GT groups exhibited significant wound healing effects, suggesting that GT and CS-GT exhibited stronger antimicrobial effects in the early phase of wound healing to reduce infection probability and shorten the inflammation phase so that the proliferation phase came in advance. On day 7 after trauma, wound healing rates in the blank group were the lowest, although wound healing rates in the positive control, GT, and CS-GT groups did not differ from those in the blank group significantly, which increased to a varying extent. The wound healing effects in the GT and CS-GT groups were the best, which was thought to be closely associated with the strong antibacterial activity of GT and CS-GT. On day 14, wound healing rates in the CS-GT group were 89.18% ± 11.75%, significantly different (*p* < 0.05) from those in the blank group (55.88% ± 7.07%). On day 21, in CS-GT group, the healing rates reached 99.61% ± 0.23% (*p* < 0.01 vs. blank group), and wounds were basically intact, while in the blank group, the healing rate was only

75.45% ± 2.17% and scabs did not fall off, which were congruent with the above macroscopic wound recovery. In the early phase of trauma, healing in the positive control group was slower than that in the CS-GT group. However, in the late phase of wound healing, the positive control sample had better trauma repair function, and wound healing rates on day 21 reached 94.98% ± 0.04%, only lower than those in CS-GT group. In contrast, GT had no trauma repair effect, and its healing effect in the late phase was inferior to that of CS-GT, with wound healing rates of only 87.50% ± 2.09% after 21 days of action. A synergic effect was observed to occur between CS and GT in the CS-GT group, and therefore in the late phase of trauma healing, the wound healing rates in the CS-GT group were significantly higher than those in the GT group.
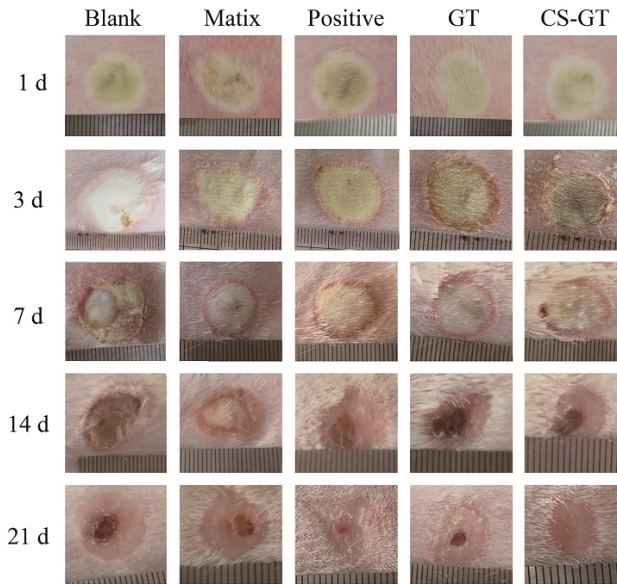
Figure 5. Different phases of wound healing in New Zealand rabbits treated with hydrogels.

Table 2. Wound healing rates (%) at different times in each group of scald wounds (mean ± SD, $n = 4$). Note: versus blank control group, * $p < 0.05$, ** $p < 0.01$.

Time/d	Blank	Matrix	Positive	GT	CS-GT
3	−6.67 ± 9.31	−1.81 ± 7.78	3.72 ± 2.10	20.12 ± 7.46 **	15.10 ± 8.82 *
7	11.88 ± 6.63	19.15 ± 10.03	24.68 ± 12.92	39.7 ± 5.24	31.57 ± 12.02
14	55.88 ± 7.07	58.26 ± 6.99	76.86 ± 6.34	66.24 ± 8.59	89.18 ± 11.75 *
21	75.45 ± 2.17	77.39 ± 0.67	94.98 ± 0.40*	87.50 ± 2.09 *	99.61 ± 0.23 **

2.5. Histological Observation

In order to further study the effects of the hydrogel on the regeneration of wound epidermis and dermis, skins of animals in each group were sampled on days 3, 7, 14, and 21, respectively, followed by hematoxylin and eosin (HE) staining to investigate wound tissue reepithelialization. As shown in Figure 6, on day 3 after scalding, epidermal layers in each group were seriously damaged, vesicles and inflammatory cell infiltration were visible in dermal layers, and dermal interstitium became loose. However, as compared with the blank group, inflammatory cell infiltration was milder in the GT and CS-GT groups. On day 7 after scalding, edema and many inflammatory cells were still present in the blank and matrix groups, and fewer inflammatory cells were observed in the

positive control group. In contrast, no epithelial regeneration was observed in all three groups. The inflammatory cell infiltration in the GT group was the mildest, whereas that in the CS-GT group was worse. In both groups, epithelial regeneration was observed. On day 14 after scalding, in addition to mild inflammatory cells, hyperkeratosis was also observed in the blank, matrix, and positive groups, while in the GT and CS-GT groups, complete epidermal regeneration was observed. On day 21 after scalding, scabs did not fall off completely, particularly in the blank group, and epidermal regeneration and angiogenesis, to some extent, were observed in other groups, especially in the CS-GT group, where connective tissue recombination was the best and previously unordered tight structure became more regular. In general, the skin healing process in the CS-GT hydrogel group was basically completed on day 21. The animals in CS-GT group had the thickest dermis, dense dermal mesenchyme, and spindle-shaped fibroblasts, indicative of optimal recovery.
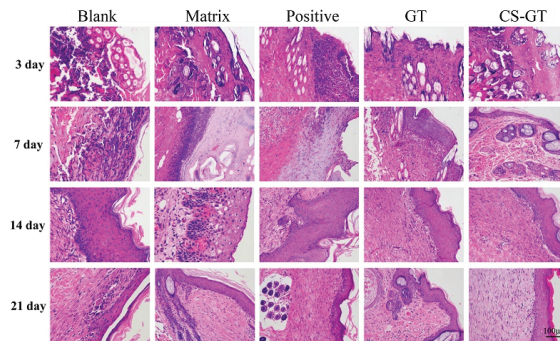
Figure 6. Hematoxylin and eosin (HE) staining images showing pathological changes of skin in various groups (200×).

The final tissue remodeling phase of trauma repair is tissue maturation and extracellular matrix deposition, mainly manifested as a gradual increase and recombination of collagen fibers [38]. Masson staining is classical staining of collagen fibers; in this study, skins at original scald sites in each group were sampled on day 21 for Masson staining to check collagen content wherein. As shown in Figure 7, compared with normal skin, the skin in the blank and matrix groups had fewer stained collagen fibers, which were sparsely and unorderly arranged. In contrast, in the positive control, GT, and CS-GT groups, the content of stained collagen in the skin increased significantly. Additionally, in the case of the CS-GT group, collagen fibers in the skin were orderly arranged with more uniform density.
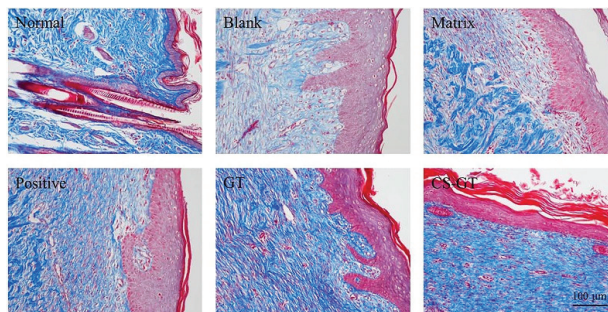

Figure 7. Masson staining on Day 21 postinjury (200×).

In addition, Image-pro plus software was used to quantitate the collagen fiber content (expressed as mean optical density) in a Masson plot. As shown in Figure 8, the collagen fiber contents of skin

in the matrix group were comparable to those in the blank group, indicating that the PVP matrix has no significant impact on collagen fibrogenesis in the scald-skin healing process. In CS-GT group, the collagen fiber content in the skin was close to the level in normal skin, which was significantly different from those in the blank group ($p < 0.05$). The results of the positive control and GT groups were intermediate between those of the blank group and normal skin. Therefore, it can be found that the scald-skin healing effect in the CS-GT group was superior and the efficacy was most significant.
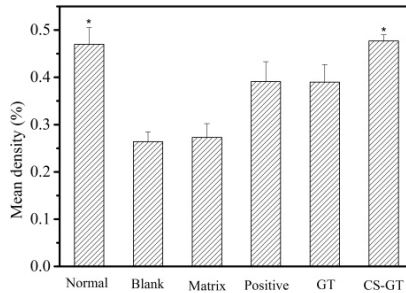
Figure 8. Mean density values of collagen in scald wound in various groups (mean ± SD, $n = 4$). Note: versus blank control group, * $p < 0.05$.

2.6. TP and HYP Contents in Granulation Tissue

After a skin trauma, protein in granulation tissue will be substantially hydrolyzed, enabling the growth of a great number of bacteria at the wound, which will affect the epidermal formation and further wound healing rate. TP is the content of all proteins during the growth of granulation tissue on the wound surface. As shown in Figure 9, the content of TP in skin wound granulation tissue in each group increased gradually over time. Throughout the study cycle, the TP level in the skin in the blank group was basically consistent with that in the matrix group, without significant difference, indicating that PVP has no significant impact on TP content in tissue. On day 3 after scalding, compared with the TP content in the blank group, the TP contents in the positive control, GT, and CS-GT groups increased to some extent, among which the GT group had the highest TP content. On day 7, there was a trend similar to that on day 3. However, for the CS-GT hydrogel group relative to that in the blank group, the increase in TP content was significantly different ($p < 0.05$). From days 14 to 21, variations in TP content in the blank group were smaller, whereas an increase in TP in other groups was significant. On day 21, the TP content in CS-GT group was the highest with a significant difference from that in the blank group ($p < 0.01$). In summary, compared with GT alone, CS-GT was more capable of accelerating protein synthesis in wound granulation tissue.
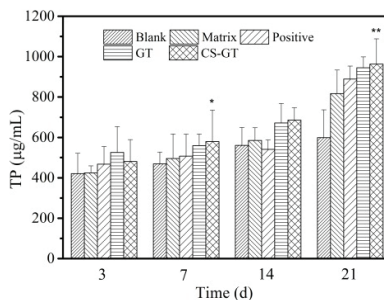

Figure 9. Total protein (TP) contents of wounds in various groups (mean ± SD, $n = 4$). Note: versus blank control group, * $p < 0.05$, ** $p < 0.01$.

During wound healing, connective tissue mainly consists of fibroblasts and collagen, and collagen content has an immediate impact on the wound repair process. HYP is a precursor amino acid of collagen synthesis and the HYP content of granulation tissue represents the collagen level; therefore, a study on HYP content enables further reflection of wound healing [39]. Based on variations in HYP content in various groups (Figure 10), on day 3 after scalding, as compared with normal skin, scalding led to a significant decrease in HYP content in skin wound tissue. From days 3 to 21, HYP content in wound tissue in each group increased gradually, among which, HYP content in CS-GT group at various time intervals was higher than those in the blank, matrix, and positive groups. The HYP content in the CS-GT group on days 7 and 21 exhibited significant differences from that in the blank group ($p < 0.05$). Additionally, from day 7 on, HYP contents in both the GT and CS-GT groups were close to that in normal skin. The above findings indicate that CS-GT hydrogel is able to effectively promote HYP synthesis in traumatic tissue and accelerate collagen synthesis and accumulation so as to provide a material basis for expediting wound healing.
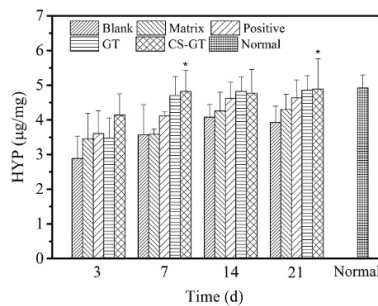

Figure 10. Hydroxyproline (HYP) contents of wounds in various groups (mean ± SD, $n = 4$). Note: versus blank control group, * $p < 0.05$.

2.7. Expression of Proinflammatory Factors

After skin damage, the damaged tissue will undergo a slow-onset persistent inflammatory response focusing on the release of pro-inflammatory factors TNF-α and IL-6, among which, TNF-α is capable of stimulating vascular endothelial cells to regulate cell metabolism within an organism [40], while IL-6 has an immediate impact on the growth of fibroblast and endothelial cells [41]. However, the persistent presence of excessively high levels of TNF-α and IL-6 in tissues would enhance the toxicity of inflammatory cells and induction capacity of related inflammatory mediators, and eventually, leading to damage and necrosis of more tissue cells [42].

Based on the levels of TNF-α and IL-6 in wound tissue in various groups (Figure 11), throughout wound healing, the levels of TNF-α and IL-6 in skin tissue in the blank group did not differ significantly from those in matrix group, indicating that PVP matrix has no significant impact on the inflammatory response of wound tissue. From days 3 to 21 after scalding, the IL-6 levels in wound tissue in various groups tended largely to decrease gradually over time and were all higher than the level (Normal) in normal skin. In particular, in the early phase (days 3 and 7), the IL-6 levels in the skin in the GT and CS-GT groups decreased significantly, suggesting that the test article has a good inhibitory effect against early inflammation. On day 21, only during the study cycle, the TNF-α level in the CS-GT group was significantly lower than that in the blank group and close to the level in normal skin, and such levels in all the other groups did not differ significantly from the level in the blank group. Therefore, CS-GT hydrogel is superior to that of positive control, and GT can alleviate the local inflammatory response of a wound to accelerate scald wound healing.
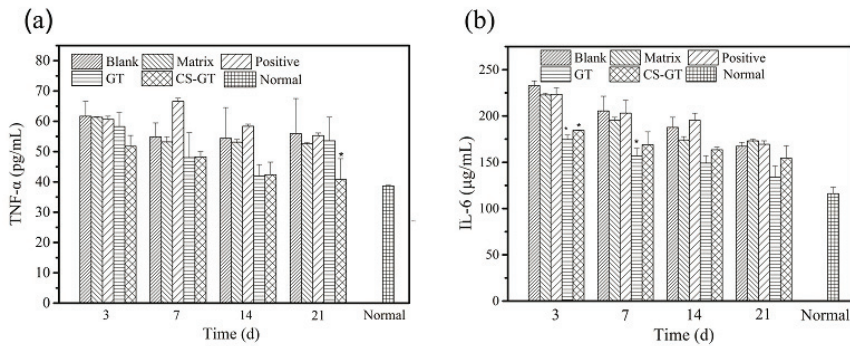
Figure 11. Levels of TNF-α (**a**) and IL-6 (**b**) in wounds in various groups (mean ± SD, $n = 4$). Note: versus blank control group, * $p < 0.05$.

3. Materials and Methods

3.1. Experimental Materials

Chitosan (544kDa, degree of deacetylation 86.7%, Nantong Xingcheng Biological Products Factory, Qingdao, China), gentamicin sulfate (AR, Aladdin Reagent Company, Shanghai, China), polyvinylpyrrolidone (medical grade, Shanghai Aladdin Reagent Company, Shanghai, China), wet burn ointment (Shantou Meibao Pharmaceutical Co., Ltd., Shantou, China), Interleukin IL-6 ELISA Kit (rabbit-IL-6, Nanjing Jiancheng Biotechnology Research Institute, Nanjing, China), Tumor Necrosis Factor TNF-α ELISA Kit (rabbit-TNF, Nanjing Jiancheng Biotechnology Research Institute, Nanjing, China), TP Kit (A045-3, Nanjing Jiancheng Bioengineering Research Institute, Nanjing, China), HYP Kit (A030-2, Nanjing Jiancheng Bioengineering Research Institute, Nanjing, China), and Calcein-AM/PI Live Cell/Dead Cell Double Staining Kit (500T, Shanghai Ye Sheng Biotechnology Co., Ltd., Shanghai, China).

Benchtop super temperature control scalder (YSL-5Q, Beijing ZhongshiDichuang Technology Development Co., Ltd., Beijing, China), microplate reader (DNM-9602, Beijing Prolong New Technology Co., Ltd., Beijing, China), inverted microscope (ECLIPSE Ti, Nikon, Tokyo, Japan), and portable high-speed disperser (S10, Ningbo Xinzhi Co., Ltd., Ningbo, China).

3.2. Experimental Materials

Sixteen New Zealand rabbits (half male and half female, conventional grade) weighing 2000 ± 20 g before modeling were provided by Guangdong Medical Laboratory Animal Center. The laboratory animal production license number is SCXK (Guangdong) 2014-0035, and the laboratory animal quality certificate number is 44411000004907. The rabbits were individually housed with free access to water and food under the following conditions: 25 °C temperature, 40–70% humidity, and 12 h light/12 h dark cycles. Experimental study on scald repair of CS-GT hydrogels after one week of adaptive breeding. Animal experiments were undertaken according to guidelines set by the Experimental Animal Center of Guangdong Ocean University (Guangdong, China) for the care and use of laboratory animals (SYXK (Yue) 2014-0053). This study was approved by the Animal Ethics Committee of Guangdong Ocean University.

3.3. Preparation of CS-GT Hydrogel

To fabricate CS-GT hydrogel, 8 g of PVP was firstly dissolved in 32 g of distilled water, which was then mixed with 20 g CS-GT aqueous solution containing 5 g of CS-GT [31] and 40 g glycerin under magnetic stirring till a homogeneous solution was obtained. GT hydrogel was prepared using the same method, where 5 g GT was introduced to replace the 5 g CS-GT. For comparison, the matrix was also prepared based on the same procedures without CS-GT and GT loaded.

3.4. In Vitro Antibacterial Assay

As *S. aureus* and *P. aeruginosa* often exist in patient exudate and are important pathogenic strains causing infections in burn/scald patients [43]. These two strains were chosen in this study as indicator microorganisms, followed by antimicrobial assay of CS-GT via diameter of zone of inhibition [44] according to the following procedure: 100 μL of bacterial suspension (1×10^8 CFU/mL) was evenly plated onto NB agar plate, and a sterile paper disc (6.0 mm in diameter, sterilized by autoclaving) was placed on the agar surface, onto which a test sample was then added dropwise. After the sample was incubated at 37 °C for 24 h, the diameter of the zone of inhibition was determined. The solvent of 1% HAc, CS-GT, and GT was distilled water, while the solvent of CS was 1% HAc. The concentration of all samples was 1 mg/mL. GT's graft rate was 22.1%, as reported in our previous research [31].

3.5. In Vitro Cytotoxicity Study

In this study, MTT assay was used to determine the effect of CS-GT on the viability of human skin fibroblasts (L929) so as to evaluate it in vitro cytotoxicity. A normal control group (Control) and test groups of CS-GT at various concentrations (100, 200, 300, 400, 600, 800, 1000, and 1200 μg/mL, respectively) were set up. Cells in good growth state were selected, and after adjustment of cell concentration, they were seeded onto a 96-well culture plate at a plating density of 5×10^3 cells/well (100 μL per well, 6 replicate wells per group); then, the plate was put into a cell incubator (37 °C, 5% CO_2) and incubated for 24 h. After the culture medium was pipetted off, blank medium and DMEM medium for CS-GT at varied concentrations were added to the wells (100 μL/well), respectively, and the plate was put into the incubator again for further culturing. Cell viability assay was performed for each group by MTT after every 1 day of culture for 3 consecutive days to study the effects of CS-GT in varying action time on L929 viability [45]. The absorbance at 570 nm was measured by an RT-2100C microplate reader.

Cell viability was calculated using the following formula:

$$Cell\ viability(\%) = \frac{OD_{test\ well} - OD_{blank\ well}}{OD_{control\ well} - OD_{blank\ well}} \times 100\%$$

In addition, in order to have a more straightforward observation of the compatibility of the test sample with L929 cells, the cells in this study were stained using a Calcein-AM/PI Double Stain Kit to observe cell viability state [46]. Cell suspension was prepared with 1× assay buffer with density ranging from (1×10^5) to (1×10^6) cells/mL. Then, such cell suspension was divided into two aliquots, into which CS-GT (100 μg/mL, 50 μL) and GT (100 μg/mL, 50 μL) were added, respectively, followed by incubation for 24, 48, and 72 h, respectively. Then, 100 μL of staining working solution was added into 200 μL of each part of cell suspension, mixed well, incubated at 37 °C for 15 min, and stained; then, cell morphology and staining status were observed using an inverted fluorescence microscope.

3.6. Hemolysis Assay

According to the literature [36], the hemolysis rate of CS-GT was determined as follows: 3 mL of rat blood was centrifuged at 2000 rpm for 15 min to isolate RBCs from serum, and then the above RBC sediment was washed with 1× PB buffer three times until a clear supernatant was observed. Next, the RBC sediment was diluted with PBS to a concentration of 2% (*v/v*) for later use, while RBCs incubated with deionized water and PBS were used as the positive and negative controls, respectively. GT and CS-GT solutions at various concentrations (100, 200, 400, 800, 1600, and 3200 μg/mL) were added into the above 2% RBC suspension, respectively. RBS suspension samples prepared as above were incubated at 37 °C for 1 h and then centrifuged at 2000 rpm for 15 min; the image of each centrifuged

sample was captured with a digital camera, and absorbance of each supernatant was measured at 540 nm with a plate reader. The hemolysis rates were calculated using the following formula:

$$H\% = \frac{H_1 - H_0}{H_{100} - H_0} \times 100\%$$

where H_0, H_1, and H_{100} are absorbance values of the negative control (PBS), test sample, and positive control (H_2O), respectively.

In addition, GT-treated RBCs and CS-GT-treated RBCs at a concentration of 800 μg/mL were microscopically examined as follows for any morphological change: After incubation at 37 °C for 1 h, the RBC solutions were centrifuged at 20,000 rpm for 20 min. The supernatants were photographed using a digital camera. The collected RBC pellets were diluted in PBS, dispensed onto clean glass slides, covered with a coverslip, and then photographed by using a microscope equipped with a digital camera.

3.7. In Vivo Animal Test

Twenty-four hours before the experiment, each New Zealand rabbit was dehaired using 10% sodium sulfide, then, the dehaired area was immediately cleaned with lukewarm water and the rabbits housed in a single cage. Briefly, 3% pentobarbital sodium (30 mg/kg) was injected via ear vein to anesthetize the New Zealand rabbit and 75% ethanol was used to disinfect the skin of dorsal hair loss area, then, 5 scald wounds of 1.5 cm² in area were created laterally at points 2 cm away from the dorsal midline of the rabbit by using a scalding apparatus. The scalding conditions were described as follows: probe temperature, 100 °C; working pressure, 1000 g; probe-to-skin contact time, 6 s. Each animal was self-controlled, and 5 wounds of each rabbit correspond to the blank group, matrix group, positive control group, GT group, and CS-GT group, respectively, as shown in Figure 12.
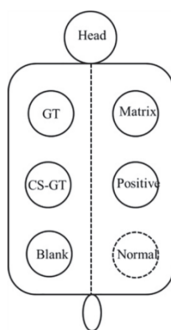

Figure 12. Correspondence of groups to scald wounds.

After modeling, scald wounds exhibited typical scald features: pale opalescent appearance and dry surface. In the case of the blank group, no treatment was performed after successful modeling. In the case of matrix group, the scald was daily treated by applying PVP hydrogel, once in the morning and once in the evening (about 1 g/dose) for 21 consecutive days starting on day 1 after modeling. In the cases of the positive control, GT, and CS-GT groups, moist exposed burn repair ointment (MEBO), GT hydrogel, and CS-GT hydrogel were applied, respectively, in the same manner as in the case of the matrix group. On the day of modeling and upon dressing change each time, size, color, exudate, scab formation, and scab falloff of each wound were inspected, photographed, and documented. On days 3, 7, 14, and 21, variations in wound area were determined as follows to evaluate wound healing: wound closure was monitored by imaging with a digital camera and a scale bar, and wound

area was quantitated by Photoshop so that pixel area was calculated from wound contour plotted by a blinded observer. Then, wound healing rate *M* was calculated using the following formula:

$$M\% = \frac{M_0 - M_1}{M_0} \times 100\%$$

where M_0 is the initial wound area, and M_1 is wound area at a time point.

3.8. Histological Observation

In histological examination, on days 3, 7, 14, and 21 after scalding, 4 test animals in each group were euthanized, respectively, and a full layer of skin tissue of about 1.5 cm^2 in area around each original scald site was immediately incised as a sample. A small patch of skin sample incised from the center of the scald was fixed in 4% paraformaldehyde (PFA) for histology and collagen deposition examination (Masson staining method), while the remaining skin tissue samples were used for subsequent monitoring of biochemical parameters. The above tissue samples, which had been fixed with 4% PFA for 24 h, were embedded in paraffin and then cut with paraffin microtome (CUT 4050, Micro Tec, Inc., Walldorf, Germany) in a direction longitudinal to the tissue, followed by staining with HE and modified Masson trichrome staining kit (Beijing Leagene Biotechnology Co., Ltd., Beijing, China), respectively. Thereafter, the regeneration of epidermis and dermis, and the level and distribution of collagen fibers in each skin sample were examined via an optical microscope (DMI3000B, Leica).

3.9. Determination of TP Content and Proinflammatory Cytokine Levels

The desired amount of each remaining skin tissue sample was accurately weighed, mixed with normal saline at a ratio of weight (g): volume (mL) = 1:9, and mechanically homogenized in an ice water bath. The resulting homogenate was cryogenically centrifuged to isolate supernatant, and content of TP and levels of proinflammatory cytokines (TNF-α and IL-6) in tissue in the supernatant were determined as per kit operating procedure.

3.10. Determination of HYP

Take an appropriate amount of the remaining fresh skin tissue samples from each of the above groups, accurately weighed them, and then measured the content of HYP according to the kit method.

3.11. Statistical Analysis

The data were processed with SPSS 17.0 software and were analyzed using independent-samples *t*-tests. Numerical data are expressed as means ± SD, and the differences among groups were analyzed using a one-way analysis of variance. $P < 0.05$ was used to indicate statistical significance.

4. Conclusions

This study demonstrates that CS-GT has efficient antimicrobial properties, as evidenced by viability assay and hemolysis assay of L929 cells that CS-GT is not cytotoxic and has good cytocompatibility and hemocompatibility. With CS-GT as an active repair component and PVP as the matrix, CS-GT hydrogel was prepared. The application of this hydrogel enabled quicker scald healing and shorter healing time in animals. Biochemical analysis shows that by facilitating the synthesis of TP and HYP in granulation tissue, CS-GT hydrogel promoted collagen fibrosis while reducing cytokine levels in an inflammatory response, and thereby accelerated wound healing. All these results demonstrate that CS-GT hydrogel is a promising efficient novel scald repair dressing.

References

1. Wells, A.; Nuschke, A.; Yates, C.C. Skin tissue repair: Matrix microenvironmental influences. *Matrix Biol.* **2016**, *49*, 25–36. [CrossRef]

2. Singh, N.P.; Rani, M.; Gupta, K.; Sagar, T.; Kaur, I.R. Changing trends in antimicrobial susceptibility pattern of bacterial isolates in a burn unit. *Burns* **2017**, *43*, 1083–1087. [CrossRef] [PubMed]

3. Ross, R.B.E. Wound healing and collagen formation. II. Fine structure inexperimental scurvy. *J. Cell Biol.* **1962**, *12*, 533–551. [CrossRef]

4. Wang, Z.; Zhang, H.; Han, J.; Xing, H.; Wu, M.C.; Yang, T. Deadly Sins of Antibiotic Abuse in China. *Infect. Cont. Hosp. Epidemiol.* **2017**, *38*, 758–759. [CrossRef]

5. Nishio, N.; Okawa, Y.; Sakurai, H.; Isobe, K. Neutrophil depletion delays wound repair in aged mice. *Age* **2008**, *30*, 11–19. [CrossRef]

6. Rashaan, Z.M.; Krijnen, P.; Kwa, K.A.A.; van der Vlies, C.H.; Schipper, I.B.; Breederveld, R.S. Flaminal(R) versus Flamazine(R) in the treatment of partial thickness burns: A randomized controlled trial on clinical effectiveness and scar quality (FLAM study). *Wound Repair Regen.* **2019**, *27*, 257–267. [CrossRef] [PubMed]

7. Patel, S.; Srivastava, S.; Singh, M.R.; Singh, D. Preparation and optimization of chitosan-gelatin films for sustained delivery of lupeol for wound healing. *Int. J. Biol. Macromol.* **2018**, *107*, 1888–1897. [CrossRef] [PubMed]

8. Sahu, S.A.; Agrawal, K.; Patel, P.K. Scald burn, a preventable injury: Analysis of 4306 patients from a major tertiary care center. *Burns* **2016**, *42*, 1844–1849. [CrossRef]

9. Bano, I.; Arshad, M.; Yasin, T.; Ghauri, M.A. Preparation, characterization and evaluation of glycerol plasticized chitosan/PVA blends for burn wounds. *Int. J. Biol. Macromol.* **2019**, *124*, 155–162. [CrossRef]

10. Guadalupe, E.; Ramos, D.; Shelke, N.B.; James, R.; Gibney, C.; Kumbar, S.G. Bioactive polymeric nanofiber matrices for skin regeneration. *J. Appl. Polym. Sci.* **2015**, *132*, 1–10. [CrossRef]

11. Hu, S.; Cai, X.; Qu, X.; Yu, B.; Yan, C.; Yang, J.; Li, F.; Zheng, Y.; Shi, X. Preparation of biocompatible wound dressings with long-term antimicrobial activity through covalent bonding of antibiotic agents to natural polymers. *Int. J. Biolog. Macromol.* **2019**, *123*, 1320–1330. [CrossRef] [PubMed]

12. Hajiali, H.; Summa, M.; Russo, D.; Armirotti, A.; Brunetti, V.; Bertorelli, R.; Athanassiou, A.; Mele, E. Alginate–lavender nanofibers with antibacterial and anti-inflammatory activity to effectively promote burn healing. *J. Mater. Chem. B* **2016**, *4*, 1686–1695. [CrossRef] [PubMed]

13. Gao, Y.; Zhang, X.; Jin, X. Preparation and Properties of Minocycline-Loaded Carboxymethyl Chitosan Gel/Alginate Nonwovens Composite Wound Dressings. *Mar. Drugs* **2019**, *17*, 575. [CrossRef] [PubMed]

14. Sajomsang, W.; Gonil, P.; Tantayanon, S. Antibacterial activity of quaternary ammonium chitosan containing mono or disaccharide moieties: Preparation and characterization. *Int. J. Biol. Macromol.* **2009**, *44*, 419–427. [CrossRef]

15. Aranaz, I.; Mengíbar, M.; Harris, R.; Paños, I.; Miralles, B.; Acosta, N.; Galed, G.; Heras, Á. Functional Characterization of Chitin and Chitosan. *Curr. Chem. Biolog.* **2009**, *3*, 203–230.

16. Cazón, P.; Velazquez, G.; Ramírez, J.A.; Vázquez, M. Polysaccharide-based films and coatings for food packaging: A review. *Food Hydrocoll.* **2017**, *68*, 136–148. [CrossRef]

17. Chabala, L.F.G.; Cuartas, C.E.E.; Lopez, M.E.L. Release Behavior and Antibacterial Activity of Chitosan/Alginate Blends with Aloe vera and Silver Nanoparticles. *Mar. Drugs* **2017**, *15*, 1–13.

18. Xia, G.; Liu, Y.; Tian, M.; Gao, P.; Bao, Z.; Bai, X.; Yu, X.; Lang, X.; Hu, S.; Chen, X. Nanoparticles/thermosensitive hydrogel reinforced with chitin whiskers as a wound dressing for treating chronic wounds. *J. Mater. Chem. B* **2017**, *5*, 3172–3185. [CrossRef]

19. Joraholmen, M.W.; Bhargava, A.; Julin, K.; Johannessen, M.; Skalko-Basnet, N. The Antimicrobial Properties of Chitosan Can be Tailored by Formulation. *Mar. Drugs* **2020**, *18*, 96. [CrossRef]

20. Wang, C.; Luo, W.; Li, P.; Li, S.; Yang, Z.; Hu, Z.; Liu, Y.; Ao, N. Preparation and evaluation of chitosan/alginate porous microspheres/Bletillastriata polysaccharide composite hemostatic sponges. *Carbohyd. Polym.* **2017**, *174*, 432–442. [CrossRef]

21. Rudyardjo, D.I.; Wijayanto, S. The synthesis and characterization of hydrogel chitosan-alginate with the addition of plasticizer lauric acid for wound dressing application. *J. Phys. Conf. Ser.* **2017**, *853*, 1–7. [CrossRef]

22. Ito, T.; Fraser, I.P.; Yeo, Y.; Highley, C.B.; Bellas, E.; Kohane, D.S. Anti-inflammatory function of an in situ cross-linkable conjugate hydrogel of hyaluronic acid and dexamethasone. *Biomaterials* **2007**, *28*, 1778–1786. [CrossRef]

23. Luo, Y.; Diao, H.; Xia, S.; Dong, L.; Chen, J.; Zhang, J. A physiologically active polysaccharide hydrogel promotes wound healing. *J. Biomed. Mater. Res. A* **2010**, *94*, 193–204. [CrossRef] [PubMed]

24. Chang, H.I.; Perrie, Y.; Coombes, A.G.A. Delivery of the antibiotic gentamicin sulphate from precipitation cast matrices of polycaprolactone. *J. Control. Release* **2006**, *110*, 414–421. [CrossRef] [PubMed]

25. Iannuccelli, V.; Maretti, E.; Bellini, A.; Malferrari, D.; Ori, G.; Montorsi, M.; Bondi, M.; Truzzi, E.; Leo, E. Organo-modified bentonite for gentamicin topical application: Interlayer structure and *in vivo* skin permeation. *Appl. Clay Sci.* **2018**, *158*, 158–168. [CrossRef]

26. Balakumar, P.; Rohilla, A.; Thangathirupathi, A. Gentamicin-induced nephrotoxicity: Do we have a promising therapeutic approach to blunt it? *Pharmacol. Res.* **2010**, *62*, 179–186. [CrossRef]

27. Forge, A.; Li, L. Apoptotic death of hair cells in mammalian vestibular sensory epithelia. *Hearing Res.* **2000**, *139*, 97–115. [CrossRef]

28. Ji, J.; Hao, S.; Wu, D.; Huang, R.; Xu, Y. Preparation, characterization and in vitro release of chitosan nanoparticles loaded with gentamicin and salicylic acid. *Carbohyd. Polym.* **2011**, *85*, 803–808. [CrossRef]

29. Monteiro, N.; Martins, M.; Martins, A.; Fonseca, N.A.; Moreira, J.N.; Reis, R.L.; Neves, N.M. Antibacterial activity of chitosan nanofiber meshes with liposomes immobilized releasing gentamicin. *Acta Biomater.* **2015**, *18*, 196–205. [CrossRef]

30. Zalavras, C.G.; Patzakis, M.J.; Holtom, P. Local Antibiotic Therapy in the Treatment of Open Fractures and Osteomyelitis. *Clin. Orthop. Relat. Res.* **2004**, 86–93. [CrossRef]

31. Yan, T.; Li, C.; Ouyang, Q.; Zhang, D.; Zhong, Q.; Li, P.; Li, S.; Yang, Z.; Wang, T.; Zhao, Q. Synthesis of gentamicin-grafted-chitosan with improved solubility and antibacterial activity. *React. Funct. Polym.* **2019**, *137*, 38–45. [CrossRef]

32. Xue, H.; Hu, L.; Xiong, Y.; Zhu, X.; Wei, C.; Cao, F.; Zhou, W.; Sun, Y.; Endo, Y.; Liu, M.; et al. Quaternized chitosan-Matrigel-polyacrylamide hydrogels as wound dressing for wound repair and regeneration. *Carbohyd. Polym.* **2019**, *226*, 115302. [CrossRef] [PubMed]

33. Goushbolagh, N.A.; Keshavarz, M.; Zare, M.H.; Bahreyni-Toosi, M.H.; Kargar, M.; Farhood, B. Photosensitizer effects of MWCNTs-COOH particles on CT26 fibroblastic cells exposed to laser irradiation. *Artif. Cells Nanomed. Biotechnol.* **2019**, *47*, 1326–1334. [CrossRef] [PubMed]

34. Roy, A.; Joshi, M.; Butola, B.S.; Ghosh, S. Evaluation of biological and cytocompatible properties in nano silver-clay based polyethylene nanocomposites. *J. Hazard. Mater.* **2019**, *384*, 121309. [CrossRef] [PubMed]

35. Huang, Y.; Ding, X.; Qi, Y.; Yu, B.; Xu, F.J. Reduction-responsive multifunctional hyperbranchedpolyaminoglycosides with excellent antibacterial activity, biocompatibility and gene transfection capability. *Biomaterials* **2016**, *106*, 134–143. [CrossRef] [PubMed]

36. Zheng, C.; Liu, C.; Chen, H.; Wang, N.; Liu, X.; Sun, G.; Qiao, W. Effective wound dressing based on Poly (vinyl alcohol)/Dextran-aldehyde composite hydrogel. *Int. J. Biol. Macromol.* **2019**, *132*, 1098–1105. [CrossRef]

37. Liu, J.Y.; Li, Y.; Hu, Y.; Cheng, G.; Ye, E.; Shen, C.; Xu, F.J. Hemostatic porous sponges of cross-linked hyaluronic acid/cationized dextran by one self-foaming process. *Mater. Sci. Eng. C Mater. Biol. Appl.* **2018**, *83*, 160–168. [CrossRef]

38. Kulshrestha, S.; Chawla, R.; Alam, M.T.; Adhikari, J.S.; Basu, M. Efficacy and dermal toxicity analysis of Sildenafil citrate based topical hydrogel formulation against traumatic wounds. *Biomed. Pharmacother.* **2019**, *112*, 128571. [CrossRef]

39. Liang, Y.; Zhao, X.; Hu, T.; Chen, B.; Yin, Z.; Ma, P.X.; Guo, B. Adhesive Hemostatic Conducting Injectable Composite Hydrogels with Sustained Drug Release and Photothermal Antibacterial Activity to Promote Full-Thickness Skin Regeneration During Wound Healing. *Small* **2019**, *15*, 1–17. [CrossRef]

40. Strassberg, S.S.; Cristea, I.A.; Qian, D.; Parton, L.A. Single nucleotide polymorphisms of tumor necrosis factor-alpha and the susceptibility to bronchopulmonary dysplasia. *Pediatr. Pulm.* **2007**, *42*, 29–36. [CrossRef]

41. Huusko, J.M.; Karjalainen, M.K.; Mahlman, M.; Haataja, R.; Kari, M.A.; Andersson, S.; Toldi, G.; Tammela, O.; Rämet, M. A study of genes encoding cytokines (IL6, IL10, TNF), cytokine receptors (IL6R, IL6ST), and glucocorticoid receptor (NR3C1) and susceptibility to bronchopulmonary dysplasia. *BMC Medical Genet.* **2014**, *15*, 1–9. [CrossRef] [PubMed]

42. Prasad, R.; Kapoor, R.; Srivastava, R.; Mishra, O.P.; Singh, T.B. Cerebrospinal fluid TNF-alpha, IL-6, and IL-8 in children with bacterial meningitis. *Pediatr. Neurol.* **2014**, *50*, 60–65. [CrossRef] [PubMed]

43. Pujji, O.J.S.; Nakarmi, K.K.; Shrestha, B.; Rai, S.M.; Jeffery, S.L.A. The Bacteriological Profile of Burn Wound Infections at a Tertiary Burns Center in Nepal. *J. Burn. Care. Res.* **2019**, *40*, 838–845. [CrossRef] [PubMed]

44. Wang, X.; Deng, A.; Cao, W.; Li, Q.; Wang, L.; Zhou, J.; Hu, B.; Xing, X. Synthesis of chitosan/poly (ethylene glycol)-modified magnetic nanoparticles for antibiotic delivery and their enhanced anti-biofilm activity in the presence of magnetic field. *J. Mater. Sci.* **2018**, *53*, 6433–6449. [CrossRef]

45. Feng, C.; Li, J.; Wu, G.S.; Mu, Y.Z.; Kong, M.; Jiang, C.Q.; Cheng, X.J.; Liu, Y.; Chen, X.G. Chitosan-Coated Diatom Silica as Hemostatic Agent for Hemorrhage Control. *ACS Appl. Mater. Interfaces* **2016**, *8*, 34234–34243. [CrossRef]

46. Zhu, M.; Liu, P.; Shi, H.; Tian, Y.; Ju, X.; Jiang, S.; Li, Z.; Wu, M.; Niu, Z. Balancing antimicrobial activity with biological safety: Bifunctional chitosan derivative for the repair of wounds with Gram-positive bacterial infections. *J. Mater. Chem. B* **2018**, *6*, 3884–3893. [CrossRef]